

REFERENCE USE ONLY

**FAA-77-13**  
REPORT NO. FAA-RD-77-85

LASER DOPPLER VELOCIMETER  
MEASUREMENTS OF B-747 WAKE  
VORTEX CHARACTERISTICS

M. R. Brashears  
A. D. Zalay

LOCKHEED MISSILES & SPACE COMPANY, INC.  
HUNTSVILLE RESEARCH & ENGINEERING CENTER  
4800 Bradford Drive  
Huntsville AL 35807



SEPTEMBER 1977  
FINAL REPORT

DOCUMENT IS AVAILABLE TO THE U.S. PUBLIC  
THROUGH THE NATIONAL TECHNICAL  
INFORMATION SERVICE, SPRINGFIELD,  
VIRGINIA 22161

Prepared for  
U.S. DEPARTMENT OF TRANSPORTATION  
FEDERAL AVIATION ADMINISTRATION  
Systems Research and Development Service  
Washington DC 20591

NOTICE

This document is disseminated under the sponsorship of the Department of Transportation in the interest of information exchange. The United States Government assumes no liability for its contents or use thereof.

NOTICE

The United States Government does not endorse products or manufacturers. Trade or manufacturers' names appear herein solely because they are considered essential to the object of this report.

Technical Report Documentation Page

1. Report No. <b>FAA-RD-77-85</b>		2. Government Accession No.		3. Recipient's Catalog No.	
4. Title and Subtitle <b>LASER DOPPLER VELOCIMETER MEASUREMENTS OF B-747 WAKE VORTEX CHARACTERISTICS</b>				5. Report Date <b>September 1977</b>	
7. Author(s) <b>M. R. Brashears and A. D. Zalay</b>				6. Performing Organization Code	
9. Performing Organization Name and Address <b>Lockheed Missiles &amp; Space Company, Inc.* Huntsville Research &amp; Engineering Center 4800 Bradford Drive Huntsville AL 35807</b>				8. Performing Organization Report No. <b>DOT-TSC-FAA-77-13 LMSC-HREC-TR D496975</b>	
12. Sponsoring Agency Name and Address <b>U. S. Department of Transportation Federal Aviation Administration Systems Research and Development Service Washington DC 20590</b>				10. Work Unit No. (TRAIS) <b>FA705/R7126</b>	
15. Supplementary Notes <b>*Under Contract to: U. S. Department of Transportation Transportation Systems Center Kendall Square Cambridge MA 02142</b>				11. Contract or Grant No. <b>DOT-TSC-1145</b>	
16. Abstract <p>To determine the behavior of the wake vortices of a B-747 at low altitudes and to measure the vortex-decay process behind the B-747 as a function of altitude above ground, flap and spoiler settings, and different flight configurations, a B-747 aircraft flew 54 passes at low level over a ground-based laser Doppler velocimeter (LDV) system. From the LDV measurements, the location and flow field of the wake vortices and the general vortex roll-up, transport, and decay trends were obtained. Results of the study indicated that the deployment of spoilers and flaps enhanced the decay of the vortex peak tangential velocity in the near wake while aircraft altitude, glide slope, and landing gear deployment had little effect. The report discusses the LDV wake vortex measurements including the instrumentation used, the experimental test sequence, the results of the wake measurements in terms of the vortex roll-up, transport, and decay trends, and a comparison of the wake vortex characteristics for different configurations.</p>				13. Type of Report and Period Covered <b>Final Report Nov. 1975 - Jan. 1977</b>	
17. Key Words <b>Aircraft Wakes, Trailing Vortex, Wake Vortices, Laser Doppler Velocimetry</b>				14. Sponsoring Agency Code	
18. Distribution Statement <b>DOCUMENT IS AVAILABLE TO THE U.S. PUBLIC THROUGH THE NATIONAL TECHNICAL INFORMATION SERVICE, SPRINGFIELD, VIRGINIA 22161</b>					
19. Security Classif. (of this report) <b>Unclassified</b>		20. Security Classif. (of this page) <b>Unclassified</b>		21. No. of Pages <b>224</b>	
				22. Price	

## PREFACE

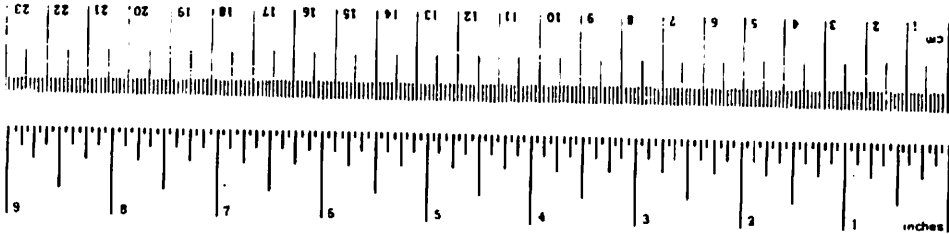
The laser Doppler velocimeter measurements of wake vortex characteristics described in this report were carried out by Lockheed Missiles & Space Company, Inc., Huntsville Research & Engineering Center working in conjunction with AeroVironment, Inc., under the "Wake Decay near the Ground" program sponsored by the U.S. Department of Transportation. Lockheed-Huntsville's role in the program consisted of operating the Lockheed Mobile laser Doppler velocimeter system and collecting measurements of vortex characteristics with the system and processing and analyzing the measurements to determine the dominant vortex decay characteristics.

The following Lockheed-Huntsville personnel made significant contributions to this effort: C. E. Craven, B. B. Edwards, J. L. Jetton, A. J. Jordan, M. C. Krause, T. R. Lawrence, and K. R. Shrider. The authors are grateful to the Optics Branch at NASA-Marshall Space Flight Center for making their filter bank and signal processor available for this study and to J. W. Bilbro and H. B. Jeffreys at NASA-MSFC and to Bill Keenum, Earl Lucas, and Rick Bynum at Computer Sciences Corporation for processing the measurements obtained with the NASA-MSFC filter bank and signal processor. The authors are grateful to Dr. J. N. Hallock, TSC Contracting Officer's Technical Monitor, and to Dr. D. C. Burnham, staff scientist at TSC, for their technical contributions and able assistance during the performance of this contract.

# METRIC CONVERSION FACTORS

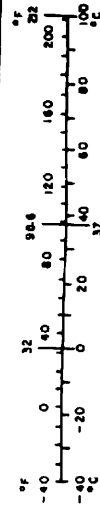
## Approximate Conversions to Metric Measures

Symbol	When You Know	Multiply by	To Find	Symbol
	<b>LENGTH</b>			
in	inches	2.5	centimeters	cm
ft	feet	30	centimeters	cm
yd	yards	0.9	meters	m
mi	miles	1.6	kilometers	km
	<b>AREA</b>			
m <sup>2</sup>	square inches	6.5	square centimeters	cm <sup>2</sup>
ft <sup>2</sup>	square feet	0.09	square meters	m <sup>2</sup>
yd <sup>2</sup>	square yards	0.8	square meters	m <sup>2</sup>
mi <sup>2</sup>	square miles	2.6	square kilometers	km <sup>2</sup>
	acres	0.4	hectares	ha
	<b>MASS (weight)</b>			
oz	ounces	28	grams	g
lb	pounds	0.45	kilograms	kg
	short tons (2000 lb)	0.9	tonnes	t
	<b>VOLUME</b>			
teaspoon	teaspoons	5	milliliters	ml
tablespoon	tablespoons	15	milliliters	ml
fluid ounce	fluid ounces	30	milliliters	ml
cup	cups	0.24	liters	l
pint	pints	0.47	liters	l
quart	quarts	0.95	liters	l
gallon	gallons	3.8	liters	l
ft <sup>3</sup>	cubic feet	0.03	cubic meters	m <sup>3</sup>
yd <sup>3</sup>	cubic yards	0.76	cubic meters	m <sup>3</sup>
	<b>TEMPERATURE (exact)</b>			
°F	Fahrenheit temperature	5/9 (after subtracting 32)	Celsius temperature	°C



## Approximate Conversions from Metric Measures

Symbol	When You Know	Multiply by	To Find	Symbol
	<b>LENGTH</b>			
mm	millimeters	0.04	inches	in
cm	centimeters	0.4	inches	in
m	meters	3.3	feet	ft
m	meters	1.1	yards	yd
km	kilometers	0.6	miles	mi
	<b>AREA</b>			
cm <sup>2</sup>	square centimeters	0.16	square inches	in <sup>2</sup>
m <sup>2</sup>	square meters	1.2	square yards	yd <sup>2</sup>
km <sup>2</sup>	square kilometers	0.4	square miles	mi <sup>2</sup>
ha	hectares (10,000 m <sup>2</sup> )	2.5	acres	acres
	<b>MASS (weight)</b>			
g	grams	0.036	ounces	oz
kg	kilograms	2.2	pounds	lb
t	tonnes (1000 kg)	1.1	short tons	short tons
	<b>VOLUME</b>			
ml	milliliters	0.03	fluid ounces	fl oz
l	liters	2.1	pints	pt
l	liters	1.06	quarts	qt
m <sup>3</sup>	cubic meters	0.26	gallons	gal
m <sup>3</sup>	cubic meters	36	cubic feet	ft <sup>3</sup>
m <sup>3</sup>	cubic meters	1.3	cubic yards	yd <sup>3</sup>
	<b>TEMPERATURE (exact)</b>			
°C	Celsius temperature	9/5 (then add 32)	Fahrenheit temperature	°F



## CONTENTS

<u>Section</u>		<u>Page</u>
	PREFACE	
1	INTRODUCTION	1
2	INSTRUMENTATION	3
	2.1 Laser Doppler Velocimeter System	3
	2.1.1 Arc-Scan Mode of Operation	12
	2.1.2 Finger Scan Mode of Operation	14
	2.2 Data Processing	17
3	DESCRIPTION OF EXPERIMENTAL TESTS	21
	3.1 Flight Test Program	21
	3.2 Operation of Laser Doppler Velocimeter Remote Sensor	23
	3.2.1 Calibration	23
	3.2.2 Wake Surveys	23
4	RESULTS OF WAKE VORTEX MEASUREMENTS	28
	4.1 Vortex Roll-Up	28
	4.1.1 Initial Spanwise Downwash Distribution	28
	4.1.2 Vortex Pair Characteristics	60
	4.1.3 Multiple Vortex Characteristics	64
	4.2 Vortex Transport	68
	4.2.1 Near Wake Vortex Tracks	68
	4.2.2 Far Wake Vortex Tracks	68
	4.2.2.1 Low-Speed Data	71
	4.2.2.2 High-Speed Data	71
	4.3 Vortex Decay	76
	4.3.1 Decay of Vortex Rotational Velocity	81
	4.3.2 Core Radius Time History	83
	4.3.3 Circulation Decay	83
	4.3.4 Comparison of Vortex Decay Trends for Different Flight Configurations	89

<u>Section</u>		<u>Page</u>
5	CONCLUSIONS	94
	REFERENCES	95
 <u>Appendix</u>		
A	External Logs for Rosamond Tests	A-1
B	Sample Output from Vortex Azimuth Display and Vortex Tracker Program for Rosamond Flyby 25	B-1
C	Sample Output from NASA-MSFC LDV Data Processing Routines for Rosamond Flyby 47	C-1
D	Wake Vortex Tracks Computed from Low-Speed Measurements	D-1
E	Wake Vortex Tracks Computer from High-Speed Measurements	E-1
F	Time History of Vortex Rotational Velocity	F-1
G	Time History of Vortex Circulation	G-1
H	Report of Inventions	H-1

#### LIST OF TABLE

<u>Table</u>		<u>Page</u>
1	Summary of B-747 Flight Parameters	24

#### LIST OF ILLUSTRATIONS

1	Lockheed LDV System Monitoring Wake Vortex Generated by a B-747 Aircraft at the Rosamond California, Test Site	4
2	Component Configuration of the Lockheed Laser Doppler Velocimeter	6
3	View Through Side Window of Laser Doppler Velocimeter Depicting Scanning Optics (Note relection of telescope primary mirror in elevation scanning mirror)	7
4	Interior View of Laser Doppler Velocimeter Van Looking Forward (Depicted in foreground is elevation scanning mirror on left and laser on right. Teleprinter in right rear.)	8

LIST OF ILLUSTRATIONS (Continued)

<u>Figure</u>		<u>Page</u>
5	Interior View of Laser Doppler Velocimeter Van (Display and scanner controls in first rack, computer in second rack, digital tape unit aft, and optics package on right.)	9
6	Definition of Laser Doppler Velocimeter Output Signature	11
7	Geometry for Arc Scanning for Rosamond Wake Vortex Tests	13
8	Magnitude of Characteristic LDV Velocity Component Observed During One Finger - Scan Sweep	16
9	Data Processing Sequence Carried Out for the Rosamond Wake Decay Measurements	18
10	Spoiler and Flap Arrangement on B-747 Aircraft	22
11	Location of Lockheed LDV During the Rosamond Wake Vortex Measurements	26
12	Overhead Arc Scan Configuration Illustrated for Rosamond Flyby 11	27
13	$ V_{pk} $ as a Function of Lateral Distance for Rosamond B-747 Flyby 8	29
14	$ V_{pk} $ as a Function of Lateral Distance for Rosamond B-747 Flyby 11	36
15	$ V_{pk} $ as a Function of Lateral Distance for Rosamond B-747 Flyby 12	45
16	$ V_{pk} $ as a Function of Lateral Distance for Rosamond B-747 Flyby 13	52
17	Magnitude of Line-of-Sight Velocity Component for Rosamond B-747 Flyby 11 at $t \sim 2$ sec, Assuming a Fully Rolled-Up Vortex Pair	61
18	Magnitude of Wake Vortex Velocity Distribution with 0 Spoilers	63
19	Circulation as a Function of Radius for 0 Spoiler Flight Configuration	65
20	Magnitude of Line-of-Sight Velocity Component for Rosamond B-747 Flyby 11 at $t \sim 2$ sec, Assuming Multiple Wake Vortices	67



LIST OF ILLUSTRATIONS (Concluded)

<u>Figure</u>		<u>Page</u>
21	Vortex Descent as a Function of Downstream Distance for Flybys with 30/30 Flaps, 0 Spoilers	69
22	Vortex Spacing as a Function of Downstream Distance for Flybys with 30/30 Flaps, 0 Spoilers	70
23	Comparison of Photographic and LDV Measurements for Rosamond B-747 Flyby 27	72
24	Comparison of Photographic and LDV Measurements for Rosamond B-747 Flyby 28	77
25	Decay of Magnitude of Wake Vortex Rotational Velocity Component for Flyby 44	82
26	$ V_{pk} $ as a Function of Time for Flyby 27 Using Photographic Tracks to Locate the Vortex Center	84
27	$ V_{pk} $ as a Function of Time for Flyby 28 Using Photographic Tracks to Locate the Vortex Center	85
28	Vortex Core Radius as a Function of Time for Flyby 27	86
29	Vortex Core Radius as a Function of Time for Flyby 28	87
30	Vortex Core Radius as a Function of Time for Flyby 44	88
31	Comparison of Magnitude of Wake Vortex Rotational Velocity for B-747 Flybys With and Without Spoilers	90
32	Comparison of Magnitude of Wake Vortex Rotational Velocity Component for B-747 With and Without Flaps	91
33	Comparison of Magnitude of Wake Vortex Rotational Velocity Component for B-747 With and Without Gear Down	92
34	Comparison of Magnitude of Wake Vortex Rotational Velocity Component for B-747 in Level Flight and in Descending Flight	93

## 1. INTRODUCTION

Wake vortex transport and decay parameters near the ground are important factors in determining safe aircraft separation distances for terminal areas. For an operational Wake Vortex Avoidance System (WVAS), a knowledge of the location and intensity of wake vortices near the terminal area is necessary to determine the minimum-delay safe spacings. Under light cross-wind conditions, a wake vortex can remain in the approach corridor, and the minimum aircraft separation distance is dictated primarily by the wake decay process near the ground. Therefore, an important consideration in determining safe aircraft separations is the decay of the wake vortex near the ground. While numerous vortex decay theories have been proposed, there are little full-scale experimental data available for comparison. Experimental vortex decay data near the ground are also lacking for aerodynamic wake minimization concepts where variations in aircraft geometry are used to tailor the wake vortex flow. Flight tests by NASA have shown that certain flap and spoiler settings can reduce the imposed rolling moments on following aircraft (in the near wake); however, wake vortex measurements near the ground for full-scale aircraft with different wake minimization concepts are needed. Thus, for both wake vortex avoidance and wake vortex minimization techniques, a knowledge of the vortex-rollup, transport, and decay characteristics near the ground is important.

To determine the behavior of aircraft wake vortices at low altitudes, a flight test program was conducted by DOT/NASA. The primary goal of the test program was to measure the wake vortex decay process behind a conventional jumbo jet as a function of altitude above ground, flap and spoiler settings, and different flight configurations. To isolate the influence of aircraft and flight parameters on the wake decay process, the flight tests were conducted at the Rosamond Dry Lake test area in California during the

early morning hours when calm atmospheric conditions prevailed. The Rosamond wake decay measurements were sought to quantify the effect of burst, link and viscous decay parameters on the wake vortex dissipation process. The wake decay measurements were also sought to demonstrate the effectiveness of recently developed vortex minimization concepts. In addition to the wake decay measurements, the flight tests were also focused on measuring the wake vortex rollup and transport phenomena in ground plane proximity.

The Rosamond flight tests involved airborne and ground-based meteorological sensors, an acoustic Doppler system, a mobile laser Doppler velocimeter, a flow visualization using smoke and balloons. In this report the measurements obtained with the laser Doppler velocimeter system (LDV) are discussed including: (1) the initial downwash field; (2) the lateral and horizontal transport of the coherent wake vortex; and (3) the decay of the vortex flow in terms of the time history of the circulation, peak tangential velocity, and the diffusion of the viscous core radius. While the application of LDV techniques for the study of wake vortex flows is not novel, this is the first time, to our knowledge, that the details of the vortex formation and decay process have been extracted for a full-scale aircraft using an LDV system. In addition to providing detailed wake measurements for comparison with available theoretical and empirical models, the results show the influence of changes in flap, spoiler, and landing gear settings on the wake characteristics.

The report discusses the LDV wake vortex measurements including the instrumentation used, the experimental test sequence, and the results of the wake measurements in terms of the vortex-rollup, transport, and decay trends, and a comparison of the wake vortex decay characteristics for different configurations. A brief discussion of the LDV wind measurements is given followed by the overall conclusions and recommendations.

## 2. INSTRUMENTATION

The wake vortex and atmospheric wind measurements were carried out by means of a scanning LDV system contained in a mobile van. Preliminary processing of the data was carried out with a SEL computer aboard the van. Reduction and analysis of the vortex and wind signatures were carried out by off-line processing software using a Univac 1108 and a PDP11 computer. A description of the instrumentation and the data processing methods for the Rosamond tests is given in terms of the LDV system configuration and the data processing techniques used.

### 2.1 Laser Doppler Velocimeter System

The Lockheed-Huntsville LDV was used to obtain wake vortex measurements during the Rosamond flight tests. A photograph of the van-mounted LDV system is given in Fig. 1. The wake measurements were accomplished as follows: (1) the wake generated by the aircraft was scanned by the CO<sub>2</sub> laser; (2) the radiation backscattered from the aerosol in the wake was collected; (3) the radiation was photomixed with a portion of the transmitted beam on a photodetector; and (4) the intensity and Doppler shift frequency of the signal were displayed.

The difference in frequency between the transmitted and backscattered signal generated at the photodetector, the Doppler shift frequency, is a measure of the aerosol's absolute line-of-sight velocity within the laser focal volume

$$\left| \bar{v} \right| = \frac{\lambda \Delta f}{2 \cos \gamma}, \quad (1)$$

where  $\left| \bar{v} \right|$  is the magnitude of the velocity component in the region being sensed,  $\lambda$  is the laser radiation wavelength (10.6 $\mu$ m),  $\Delta f$  is the Doppler shift,

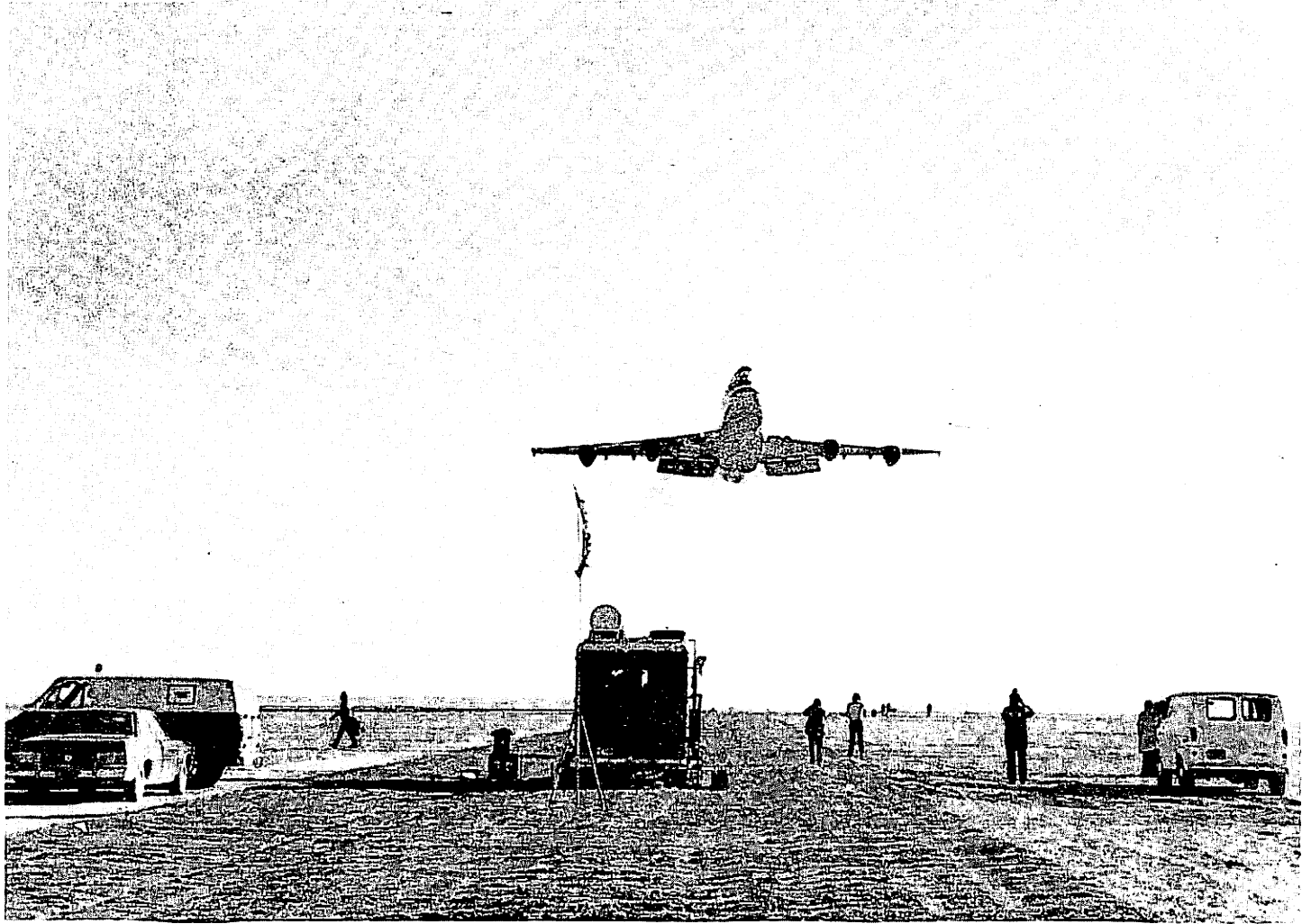


Fig. 1 - Lockheed LDV System Monitoring Wake Vortex Generated by a B-747 Aircraft at the Rosamond, California, Test Site

## 2. INSTRUMENTATION

The wake vortex and atmospheric wind measurements were carried out by means of a scanning LDV system contained in a mobile van. Preliminary processing of the data was carried out with a SEL computer aboard the van. Reduction and analysis of the vortex and wind signatures were carried out by off-line processing software using a Univac 1108 and a PDP11 computer. A description of the instrumentation and the data processing methods for the Rosamond tests is given in terms of the LDV system configuration and the data processing techniques used.

### 2.1 Laser Doppler Velocimeter System

The Lockheed-Huntsville LDV was used to obtain wake vortex measurements during the Rosamond flight tests. A photograph of the van-mounted LDV system is given in Fig. 1. The wake measurements were accomplished as follows: (1) the wake generated by the aircraft was scanned by the CO<sub>2</sub> laser; (2) the radiation backscattered from the aerosol in the wake was collected; (3) the radiation was photomixed with a portion of the transmitted beam on a photodetector; and (4) the intensity and Doppler shift frequency of the signal were displayed.

The difference in frequency between the transmitted and backscattered signal generated at the photodetector, the Doppler shift frequency, is a measure of the aerosol's absolute line-of-sight velocity within the laser focal volume

$$\left| \bar{V} \right| = \frac{\lambda \Delta f}{2 \cos \gamma} , \quad (1)$$

where  $\left| \bar{V} \right|$  is the magnitude of the velocity component in the region being sensed,  $\lambda$  is the laser radiation wavelength (10.6 $\mu$ m),  $\Delta f$  is the Doppler shift,

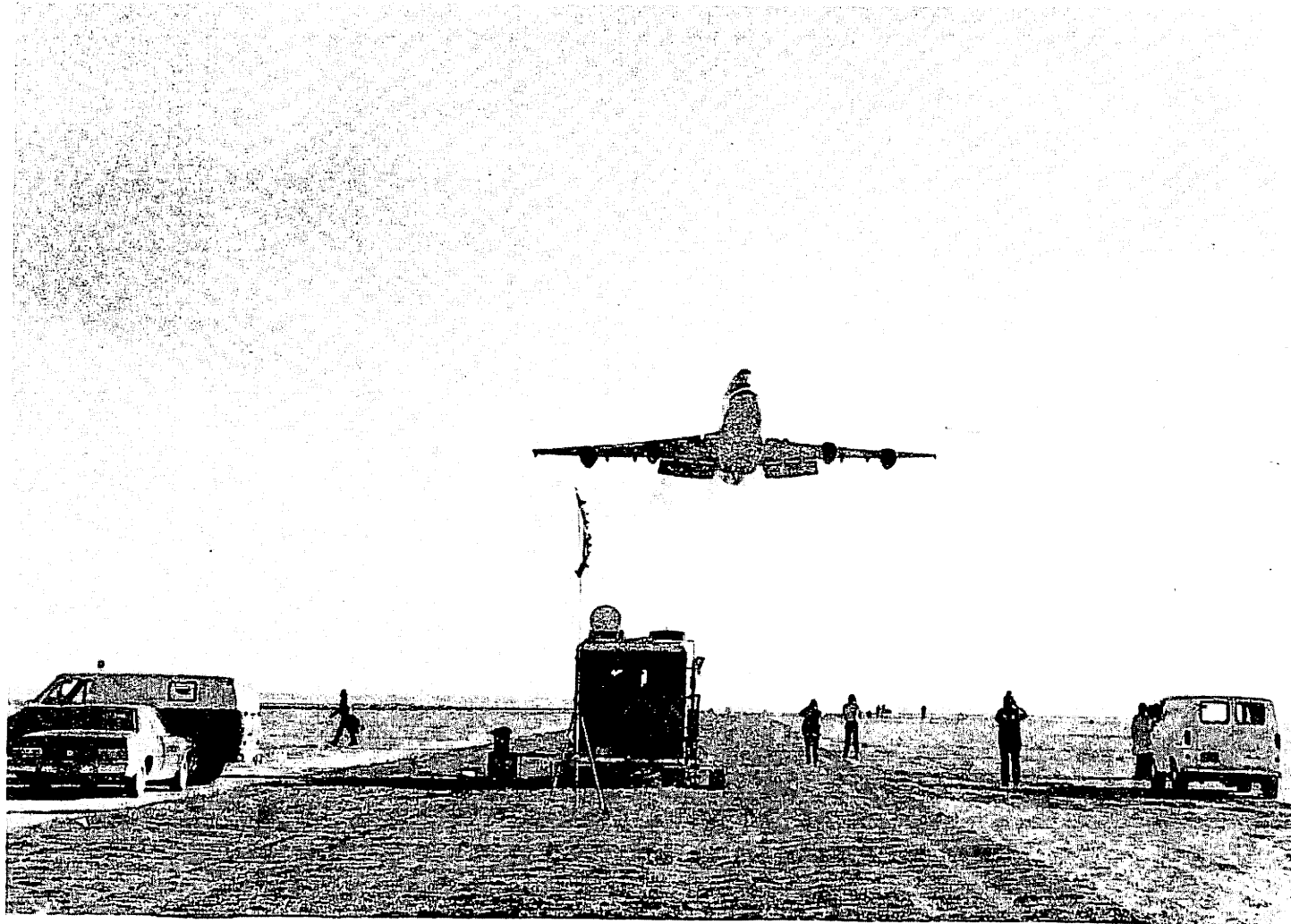


Fig. 1 - Lockheed LDV System Monitoring Wake Vortex Generated by a B-747 Aircraft  
at the Rosamond, California, Test Site

and  $\gamma$  is the angle subtended by the velocity vector and the optic system line of sight. From Eq. (1), it is noted that the Doppler shift is a direct and absolute measure of aerosol velocity component and a frequency shift of 188 kHz corresponds to a 1 m/sec magnitude line-of-sight velocity.

A sketch of the optical and electronic equipment for measuring the intensity and frequency spectrum of the coherent backscatter from the focal volume is shown in Fig. 2, and described in more detail in Refs. 1, 2, and 3. Photographs of the optical and electronic equipment for measuring the aerosol backscatter are shown in Figs. 3, 4, and 5.

The Lockheed LDV system used in the Rosamond wake vortex tests monitors the magnitude of the velocity component of ambient atmospheric particulate matter within its instantaneous sensing volume. The pertinent operating characteristics of the LDV are summarized as follows:

#### Performance

1. Threshold of Magnitude of Velocity Component: 0.5 m/sec
2. Range of Magnitude of Velocity Component: 0.5 to 28 m/sec

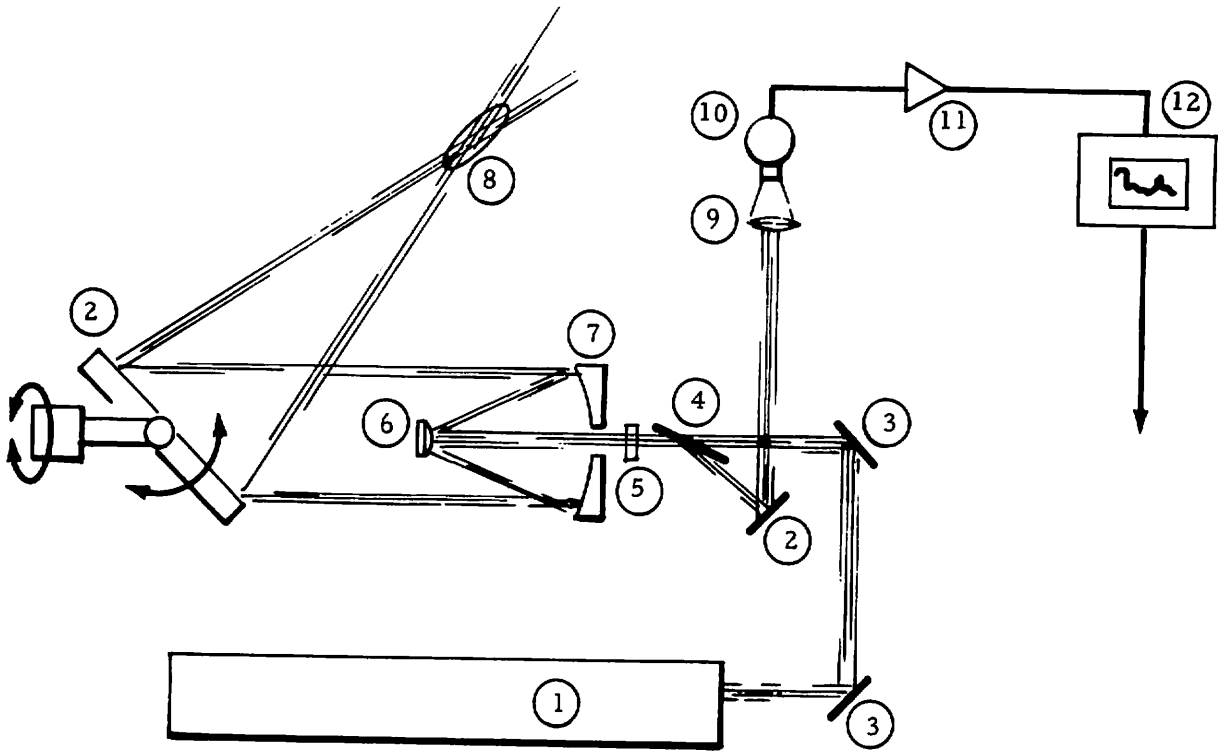
#### Sample Rate

1. Low Data Rate: 70 Hz
2. High Data Rate: 500 Hz (using the NASA filter bank processor).

#### Spatial Resolution

1. Range Accuracy:  $\pm 0.4$  m at 30 m,  $\pm 44$  m at 300 m
2. Elevation Angle Accuracy:  $\pm 0.25$  deg.





- |                         |                     |
|-------------------------|---------------------|
| ① CO <sub>2</sub> Laser | ⑦ Primary Mirror    |
| ② Mirror                | ⑧ Focal Volume      |
| ③ Mirror                | ⑨ Lens              |
| ④ Brewster Window       | ⑩ Photodetector     |
| ⑤ Quarter Wave Plate    | ⑪ Preamplifier      |
| ⑥ Secondary Mirror      | ⑫ Spectrum Analyzer |

Fig. 2 - Component Configuration of the Lockheed Laser Doppler Velocimeter

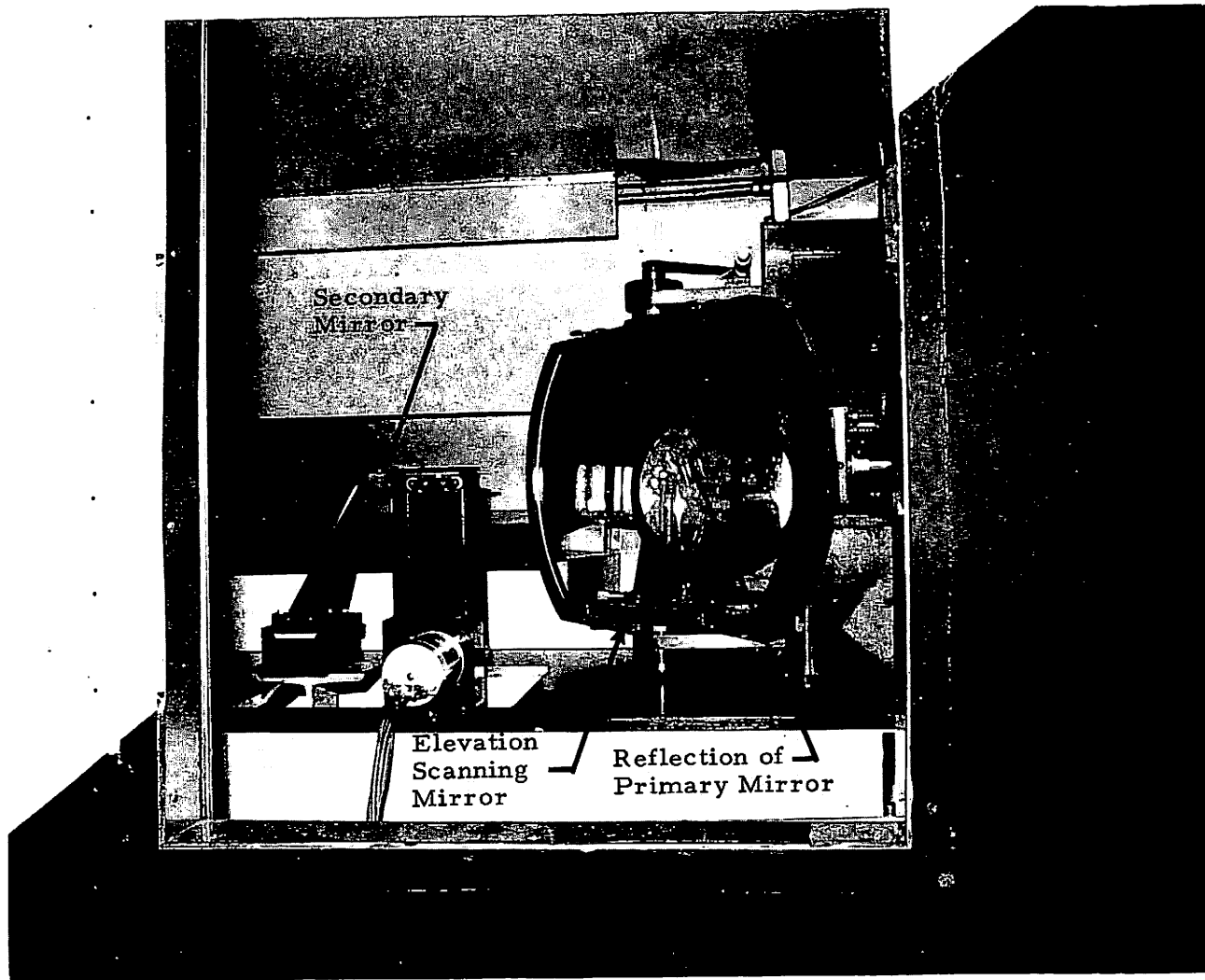


Fig. 3 - View Through Side Window of Laser Doppler Velocimeter Depicting Scanning Optics (Note reflection of telescope primary mirror in elevation scanning mirror)

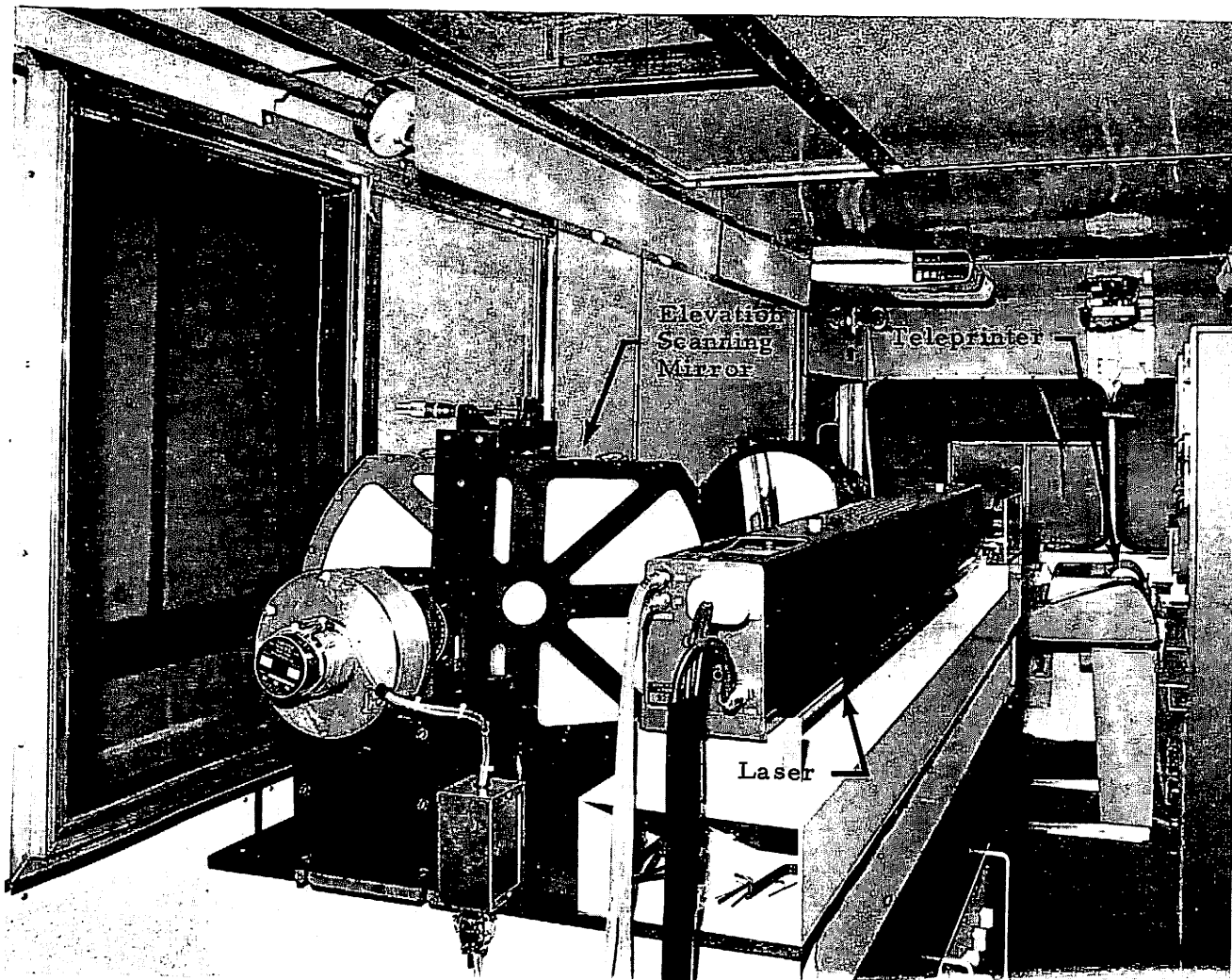


Fig. 4 - Interior View of Laser Doppler Velocimeter Van Looking Forward (Depicted in foreground is elevation scanning mirror on left and laser on right. Teleprinter in right rear.)

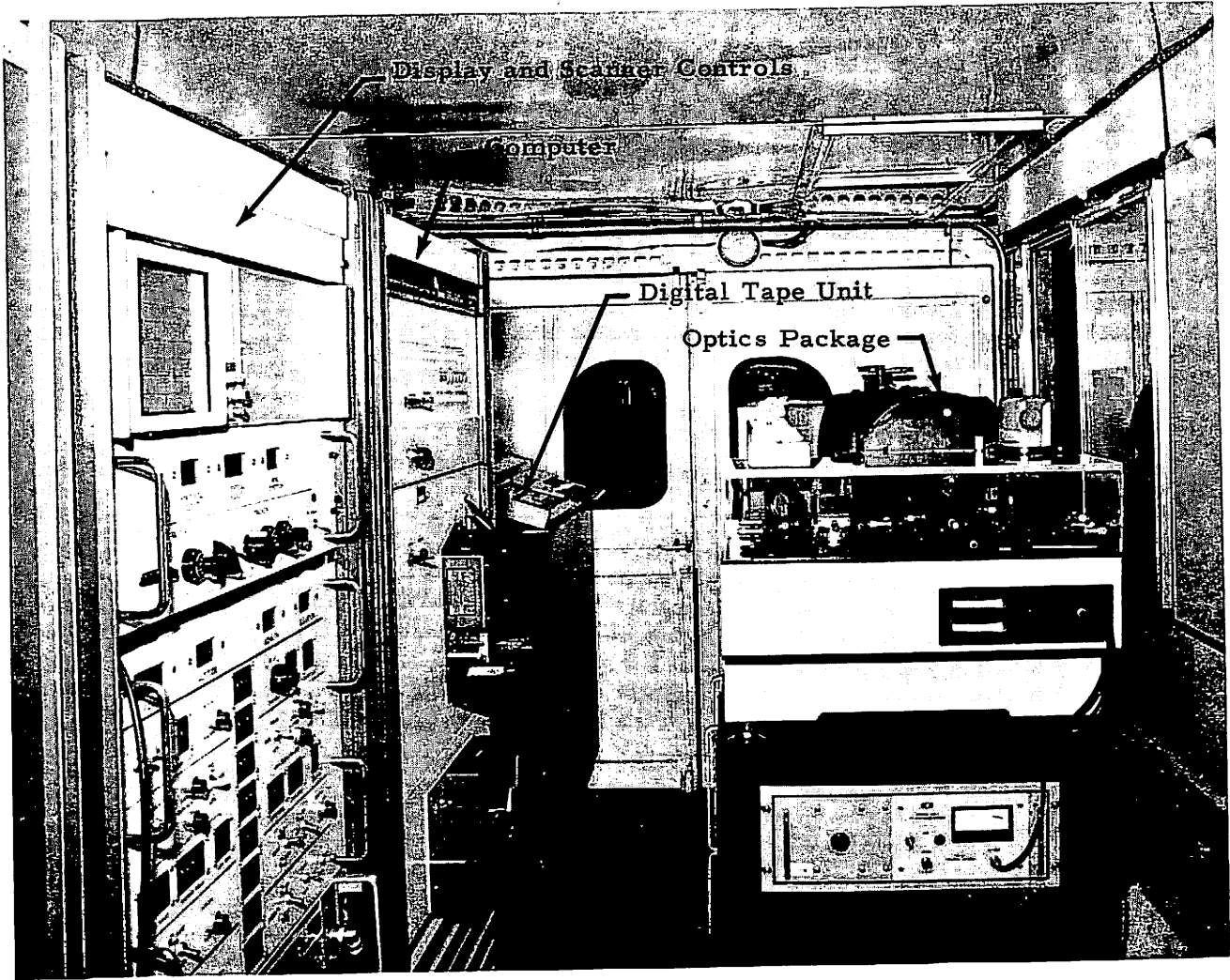


Fig. 5 - Interior View of Laser Doppler Velocimeter Van (Display and scanner controls in first rack, computer in second rack, digital tape unit aft, and optics package on right.)

### Scan Modes

1. Range or Line Scan
2. Elevation
3. Altitude
4. Azimuth
5. Horizontal Wind
6. Vertical Wind
7. Wind Direction
8. Line-of-Sight Velocity Component

The characteristic output signal from the LDV system is an intensity versus frequency spectrum illustrated in Fig. 6. The output parameters  $V_{pk}$  and  $V_{ms}$  are indicative of the magnitude of the velocity component in the LDV focal volume corresponding to the fastest particle (or particles) above the amplitude threshold and the particle (or particles) having the highest backscatter, respectively. The bandwidth,  $N$ , is a measure of the range of particle velocities in the focal volume. Intensity and frequency thresholds are applied to the signal, as shown, to eliminate noise and to improve the resolution of the system. For example, in the vortex tracking mode the frequency threshold of the LDV is set relatively high to filter out the low-frequency signal associated with the ambient wind.

The velocity resolution of the LDV is determined by the signal-to-noise ratio characteristics of the system as well as the atmospheric aerosol particle-size distribution. During the Rosamond tests, no difficulty was encountered detecting the high velocity regions, as high as 28 m/sec, associated with the wake vortex phenomena. The very low ambient winds, on the order of 1 to 2 m/sec, were also detected by the LDV at Rosamond which were above the system's threshold of 0.5 m/sec.

The spatial resolution of the LDV is determined by the size of the laser beam sensing volume where the beam is focused. The extent of the laser Doppler system sensing volume is a function of range which is shown in the following table ( $\Delta r = 9.84 \times 10^{-4} (m^{-1}) R^2$ ) obtained from calibration measurements (Ref. 4).

$V_{pk}$  = Magnitude of velocity component of highest channel above amplitude threshold  
 $V_{ms}$  = Magnitude of velocity component of the channel having the peak signal

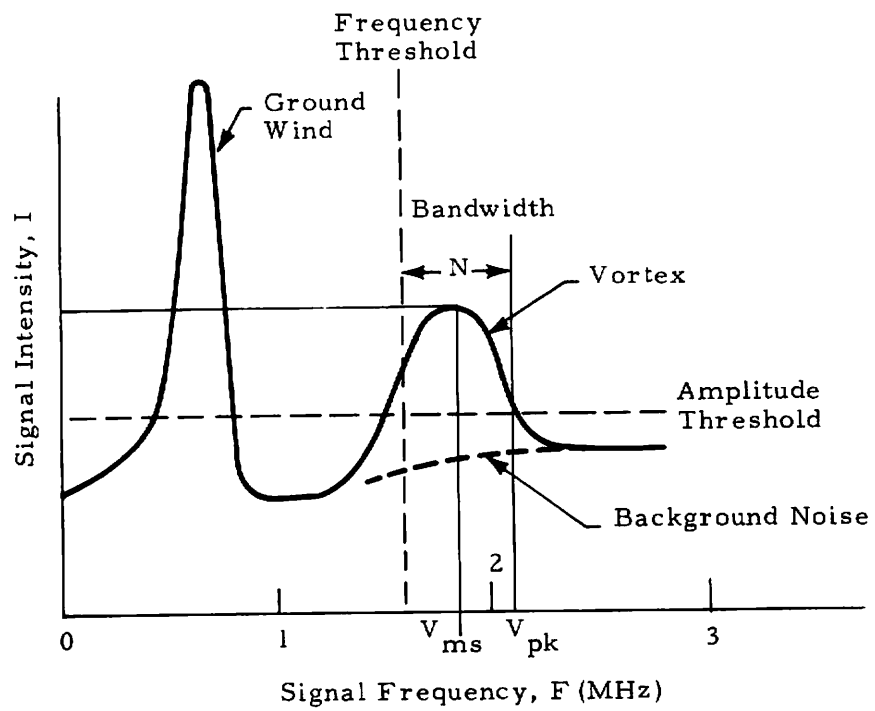


Fig.6 - Definition of Laser Doppler Velocimeter Output Signature

Range to Focus, R(m)	Sensing Volume Length (Half Power Value) $\Delta r$ (m)
76	5.68
100	9.84
152	22.73

For example, if the LDV system is tracking wake vortices at a range of 60 m, a needle-shaped volume of the vortex 3.54 m long and 4 mm in diameter is sampled. During the Rosamond tests, the typical vortex range was 60 m so that the spatial resolution due to the spreading of the focal volume was 3.54 m.

In addition to the finite focal volume, the sampling rate of the LDV plays an important role in determining the overall resolution of the system. During the Rosamond tests, measurements were obtained at two data rates, at 70 and 500 Hz. The lower data rate was achieved with a scanning spectrum analyzer and the higher data rate with a filter bank provided by NASA-MSFC. Since the spatial resolution of the flow is a function of the selected data rate and scan mode, the resolution must be considered separately for each type of operation; the arc scan, finger scan, and LDV modes.

### 2.1.1 Arc-Scan Mode of Operation

In the arc-scan mode, the LDV interrogates the vortex wake at a fixed range along an arc normal to the aircraft flight path. As shown in Fig. 7, the sensing volume is moved between two elevation limits (the typical cone angle is  $2\alpha = 30$  deg) at a fixed rate (the typical scan rate is 0.5 Hz) while the vortex drifts past the scanned arc. Thus, the arc scan measurements indicate the spanwise downwash distribution in the wake of the aircraft, provided that vortex range is sufficiently close to the selected scan range.

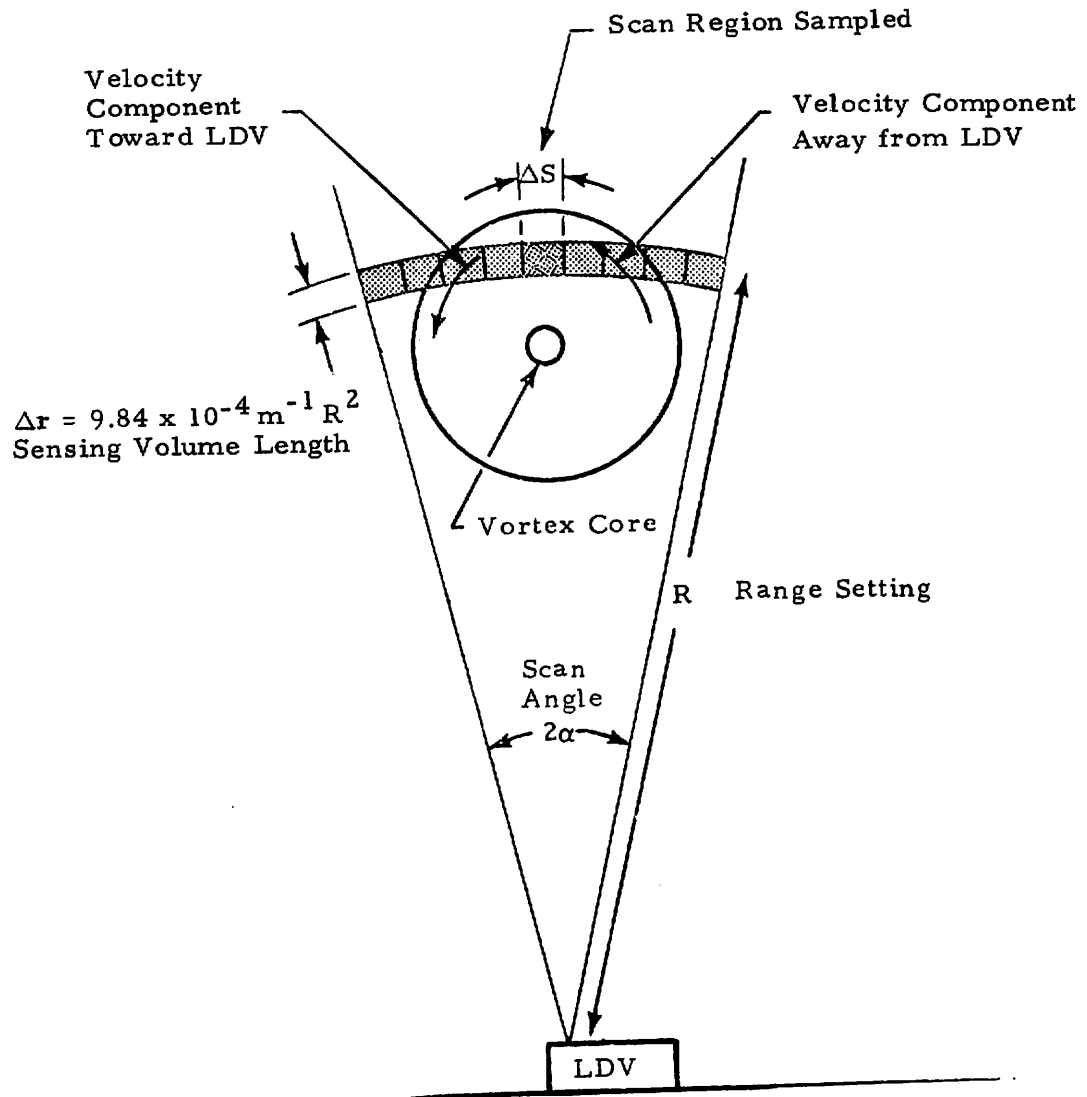


Fig. 7 - Geometry for Arc Scanning for Rosamond Wake Vortex Tests



During one arc scan of the vortex wake, the vortex flow field is sampled at discrete evenly spaced intervals along the arc as shown in Fig. 7. The separation between successive sample points,  $\Delta S$ , based on the sampling rate  $f$ , range  $R$ , and cone angle  $2\alpha$  is given by

$$\frac{\Delta S}{R} = \frac{2\pi}{360^\circ} \frac{2\alpha/\text{sec}}{f}, \quad (2)$$

where  $2\alpha/\text{sec}$  is the elevation angle scan rate at a frequency of 0.5 Hz. For a typical arc scan wake vortex measurement at Rosamond,  $f = 500$  and  $70$  Hz,  $R = 60$  m and  $2\alpha = 30$  deg, so that the wake vortex flow field is sampled every 0.06 and 0.4 m at the high- and low-data rates, respectively. Since the range of vortex core diameters measured for a B-747 aircraft is 0.3 to 2 m based on tower flybys (Ref. 5), the sampling rate of the LDV system is sufficient to obtain several cuts through the vortex core along the arc (or essentially in the spanwise direction), particularly at the high data rate.

The drift of the wake vortex affects the resolution of the vortex measurements in the vertical direction. During a single scan frame, the vortex is translated by an amount depending on the cross-wind velocity and on the mutual induction of the complete vortex field. Since the tests were conducted during the early morning hours, cross winds were generally negligible and the primary motion of the wake vortex was in the downward direction. Assuming a typical vortex descent rate of 2 m/sec, and a typical scan rate of 0.5 Hz, this implies that a spanwise traverse of the wake vortex is taken every 2 m in the vertical plane in the arc-scan mode. Based on these values, it is noted that the LDV arc-scan technique can observe the detailed characteristics of the wake vortex phenomena which are larger in extent than 0.06 and 2 m in the horizontal and vertical directions, respectively.

### 2.1.2 Finger-Scan Mode of Operation

During the Rosamond flight tests, 56% of the LDV wake vortex measurements were conducted using the finger-scan mode. In the finger-scan mode, both the range and elevation of the laser beam were varied simultaneously and

linearly with time, producing a multiple lobe scan pattern with the laser beam as shown in Fig. 8. The settings and sampling rates for the finger-scan mode are given in Appendix A.

The distance between sample points for the finger-scan mode is higher than for the previous arc-scan mode. From Appendix A, it is noted that the typical range scan excursion for the finger scan mode is 105 m, and the normal range rate is 3.5 Hz. It follows that the beam-scan velocity is 735 m/sec. Because the LDV measurements were sampled every 2 and 14.3 msec at the low and high data rates, the wake vortex flow field is measured at every 1.5 and 10.5 m increment in range, respectively. Thus, the finger scan mode can interrogate a large cross-sectional area rapidly, and this is ideal for vortex tracking. In addition, the LDV finger scan measurements contain essential information regarding the wake vortex phenomena.

The characteristic line-of-sight component as a function of range and elevation angle during one finger-scan sweep is shown in Fig. 8. A pair of double-peak patterns is noted in the line-of-sight velocity profile as a function of elevation angle. The maximum values occur at the elevation angles where the line of sight is tangent to the viscous core radius of the vortex. Thus, the mean elevation angle of the local maxima in the  $V_{pk}$  vs  $\theta$  curve yields the elevation angle of the wake vortex,  $\theta_{vortex} = (\theta_1 + \theta_2)/2$ . Similarly, the difference between the two elevation angles is a measure of the vortex viscous core radius,  $r_{vortex} = R_1 \left| \tan \frac{\theta_1 - \theta_2}{2} \right|$ . The peak tangential velocity and core circulation of the vortex is given by  $V_{pk\ vortex} = (V_{pk\ \theta_1} + V_{pk\ \theta_2})/2$  and  $\Gamma_{vortex} = 2\pi R_{vortex} V_{pk\ vortex}$ , assuming circular symmetry. The peak line-of-sight component at the two edges of the vortex,  $V_{pk\ \theta_1}$  and  $V_{pk\ \theta_2}$  are not necessarily equal due to a contribution by the other vortex and the ambient winds. The range of the vortex,  $R_1$ , is given by the local maximum in the line-of-sight component at the two edges of the in the bottom of Fig. 8, and is not affected by the ambient winds. Based on the characteristic LDV signature observed for one scan, it is noted

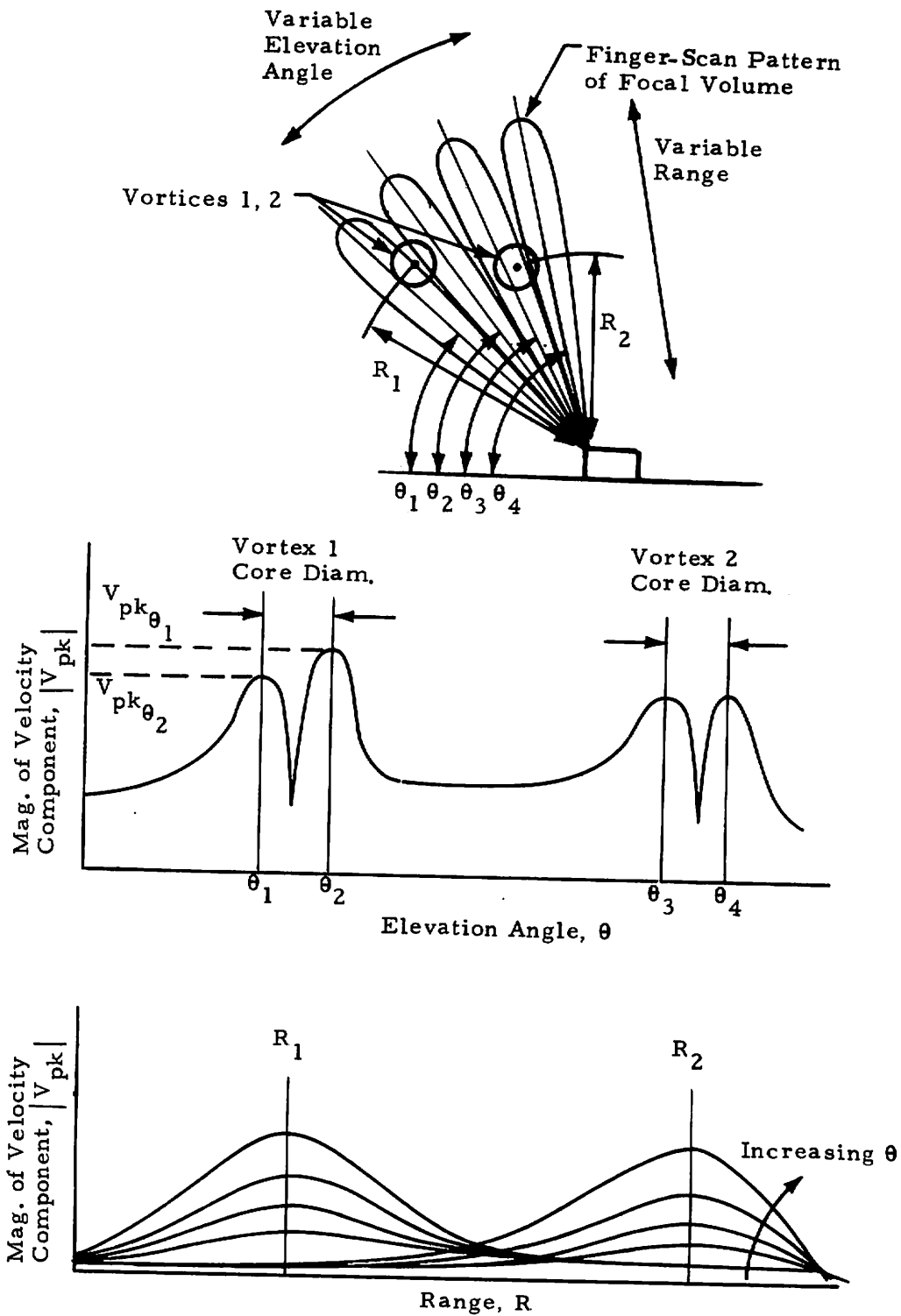


Fig. 8 - Magnitude of Characteristic LDV Velocity Component Observed During One Finger-Scan Sweep

that several successive finger scans contain the essential decay history of the wake vortices, provided that at least two sample points are obtained for each vortex, one upwash and one downwash measurement, where the line of sight is tangent to the viscous core and the mean vortex range is within the LDV focal volume.

## 2.2 DATA PROCESSING

The output from the LDV system consisting of the coherent backscatter intensity versus frequency from the focal volume as well as the location of the focal volume in space was processed to yield the aircraft downwash field and the wake vortex characteristics. Reduction and analysis of the LDV measurements were carried out as follows: (1) the low-speed signal was digitized and stored on magnetic tape by the onboard SEL computer and subsequently processed off-line on a Univac 1108 computer, and (2) the high-speed data were both digitized and processed off-line on a Univac 1108 computer and the vortex tracks computed on a PDP 11 computer. A flow chart of the data processing sequence used for the Rosamond wake decay study is shown in Fig. 9. The software system for processing the low-speed and high-speed LDV data is described in more detail in Refs. 4 and 6, respectively.

The high-speed processor utilized the raw range and elevation signal, while the low-speed processor used the raw range and commanded elevation signal to determine the location of the LDV focal volume. As a result, the magnitude of the velocity component versus elevation angle measured with the high-speed processor showed scatter due to the  $\pm 0.25$  deg elevation angle resolution. In addition, noise was present in the elevation angle versus time distribution from the high-speed data characterized by a square wave with a frequency of 14 Hz and an amplitude of 0.7 deg. This was believed to be a symptom of a processing or decode problem. The normal scatter in the elevation angle was not noticeable at the low data rate, but the low-speed data did show a finite lag in the scan pattern. A time lag of approximately 0.3 sec, and a corresponding lag in the position of the LDV focal volume depending on the selected scan rate was observed. The lag in the system resulted from the difference between commanded versus actual angular position of the scanning mirror.

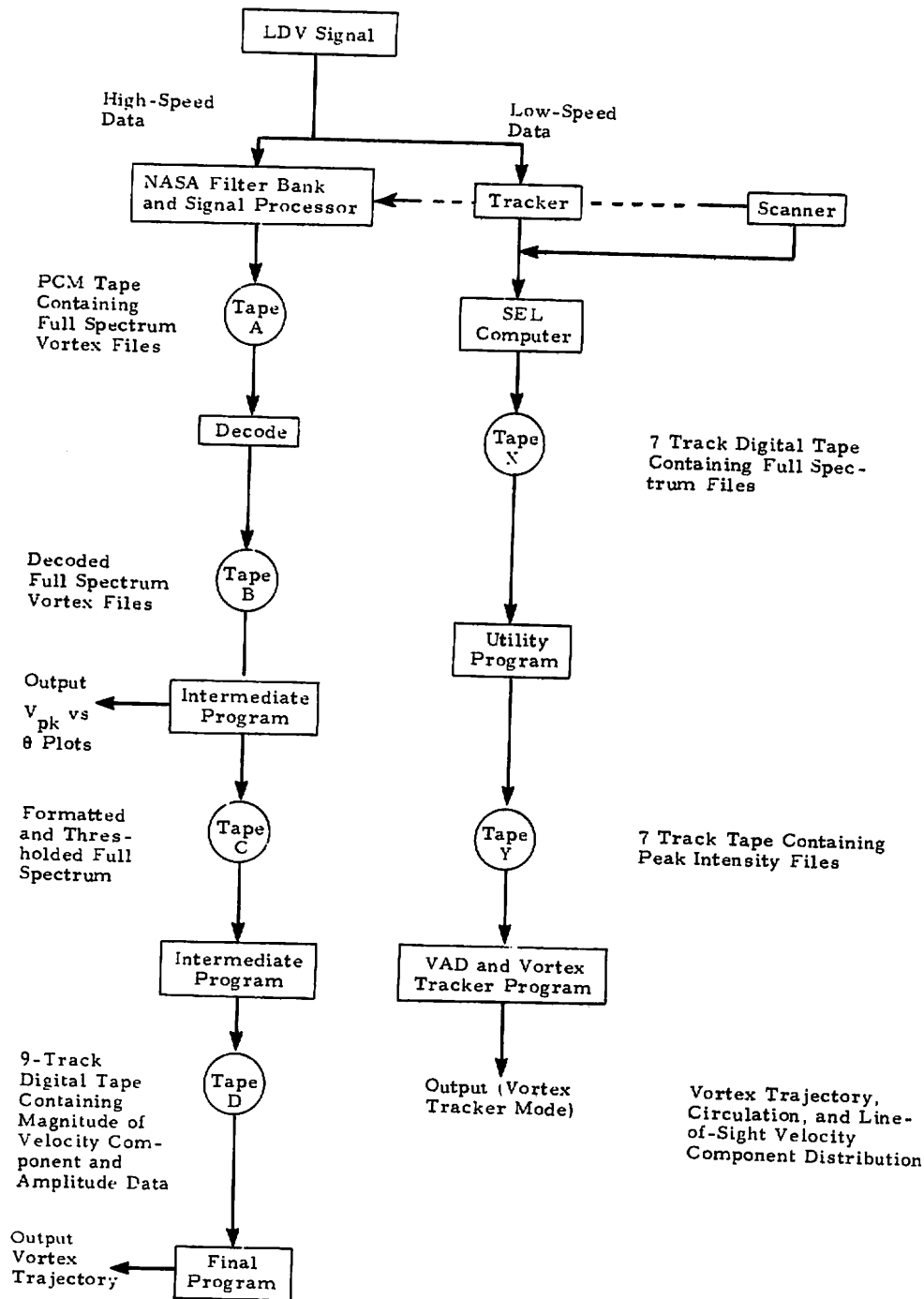


Fig. 9 - Data Processing Sequence Carried Out for the Rosamond Wake Decay Measurements

The manner in which the wake vortex measurements were processed from both the high-speed and low-speed data is summarized as follows. The frequencies and amplitudes associated with the laser Doppler signal were sampled at fixed intervals. The spectrum was recorded if it was above the frequency and amplitude threshold settings (Fig. 6). The amplitude and frequency threshold settings for the Rosamond tests are given in the log sheets in Appendix A. From the array of recorded frequency and intensity points, the magnitude of the line-of-sight velocity component was computed, and the vortex parameters including location and velocity distribution were determined.

To compute the wake vortex transport and decay characteristics from the low-speed line-of-sight velocity component magnitude, the Rosamond measurements were analyzed using the "Velocity Azimuth Display and Vortex Track Program" (Ref. 5). Based on previous experience with the program, the following parameters were selected for the analysis of the Rosamond data:

INTVEL = 2	Flag INTVEL = 1, Velocity oriented vortex determination INTVEL = 2, Intensity oriented vortex determination
NPSUF = 4	Sufficient number of points to determine vortex position
APERCT = 0.1	Fraction of points below the maximum velocity or intensity points
BPERCT = 0.1	Fraction of points within the correlation circle where Q is at least APERCT fraction of the maximum Q (Q is velocity or intensity as determined by INTVEL)
RPERCT = 0.3	Fraction of number of points in correlation circle used for determining vortex 1 (required for determination of vortex 2)
RPERCT = 0.3	Fraction of aircraft wing span used for correlation radius
EPERCT = 2.0	Fraction of correlation radius from vortex 1 for excluding initial point of vortex 2
NOISEF = 0	Noise floor
ADJI = 0.0	Intensity adjustment (fraction of noise floor added to total intensity).

A sample output from the VAD and Vortex Track Program is presented in Appendix B. The intermediate sorting parameters used in determining the location of the vortex core region are also given in the printouts along with "scatter plots" indicating the line-of-sight velocity magnitudes. From the typical line-of-sight velocity magnitude illustrated in Appendix B, the time history of the vortex wake was determined for many of the flybys.

In parallel with the low-speed data acquisition and processing, the LDV signal was also fed into the high-speed NASA-MSFC data processing system as illustrated in Fig. 9. The high-speed data processing technique is similar to the low-speed technique described earlier, and is described in detail in Ref. 6. A sample output from the NASA-MSFC LDV data processing routines is shown in Appendix C, including the listing of the magnitude of the raw line-of-sight velocity component, the plot of  $|v_{pk}|$  versus elevation angle, and plots of the vortex trajectory.

### 3. DESCRIPTION OF EXPERIMENTAL TESTS

A two-day test sequence was carried out to determine the wake vortex characteristics of a B-747 aircraft as a function of spoiler, flap, and landing gear settings, altitude above ground, and glideslope. The test consisted of 54 low level passes during the early morning hours over the LDV system deployed at Rosamond Dry Lake near Edwards AFB, California, on 2 and 3 December 1975.

#### 3.1 FLIGHT TEST PROGRAM

The aircraft used for the tests was a Boeing 747-123 aircraft. A plan view of the aircraft showing the details of the flap and spoiler configurations is presented in Fig. 10.

Aircraft configuration varied from run to run, with dominant emphasis on as close to a normal landing configuration as operating conditions would allow. The clean configuration was also studied, and special flap and spoiler configurations were investigated for vortex alleviation effectiveness. The Boeing 747 flew at 30 to 250 m above the ground level of 700 m MSL. Runs were made in level flight as well as in descending and climbing flight. Descents were at about 250 m/min. A lift coefficient of approximately 1.4 was used for all flaps-down runs.

Of the 54 runs, 35 (or about 65%) were made with the inboard flaps lowered 30 deg and the outboard flaps lowered 30 deg (denoted 30/30); eight (approximately 15%) with 10/10 flaps; and five (approximately 9%) with flaps retracted. The remaining six runs had the inboard flaps lowered 30 deg and the outboard flaps lowered 1 deg, to test the effects of this configuration



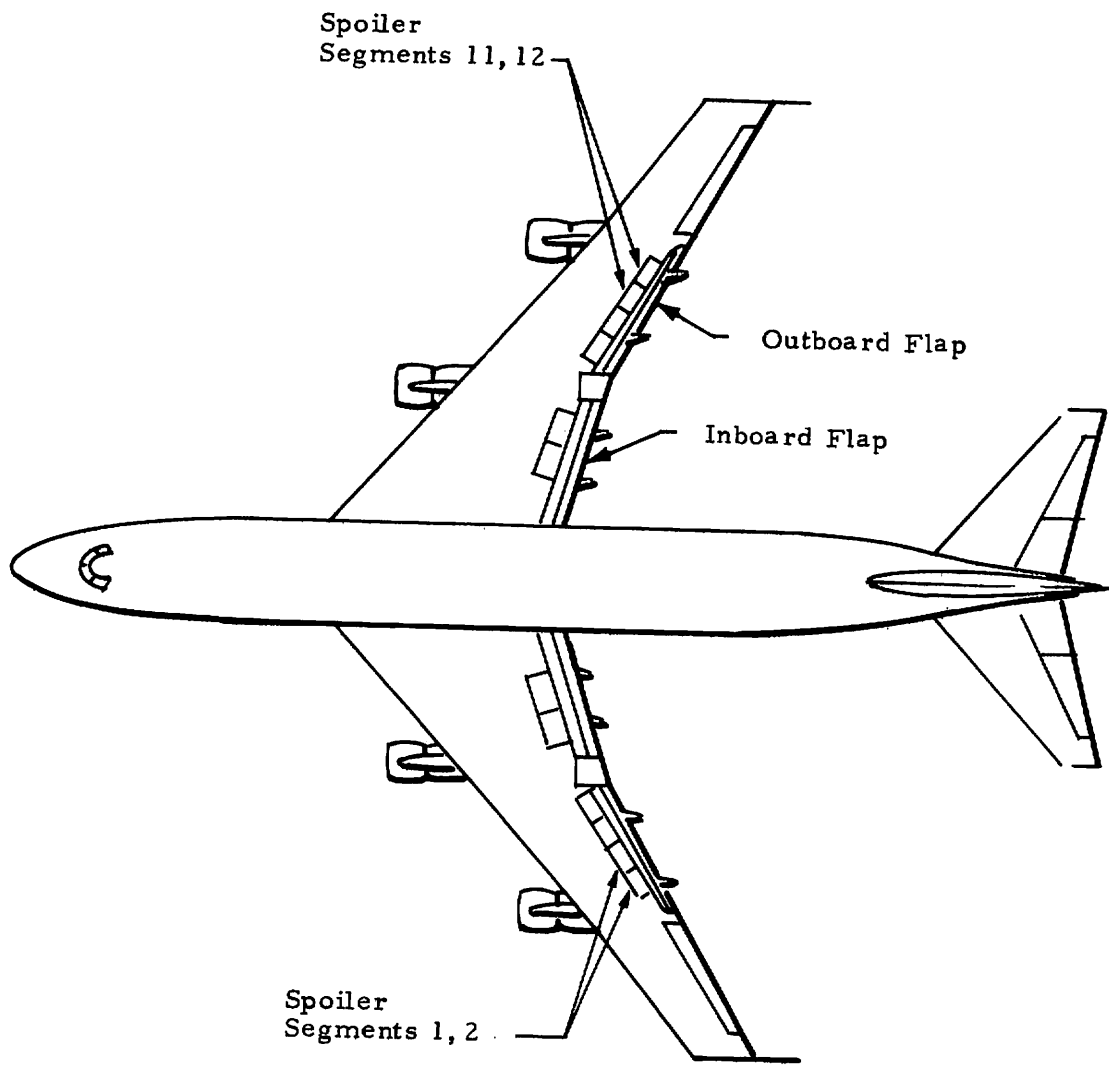


Fig. 10 - Spoiler and Flap Arrangement on B-747 Aircraft

on vortex alleviation. For each flap setting, runs were conducted with the gear down or retracted, and some had spoilers deployed (the extension angle was always 41 deg) in addition to the flap. A summary of the aircraft altitude, speed, weight, and flap, landing gear, and spoiler settings for each of the flybys is given in Table 1.

### 3.2 OPERATION OF LASER DOPPLER VELOCIMETER REMOTE SENSOR

The LDV system was set up and calibrated at the Rosamond test site prior to conducting the actual wake surveys. A discussion of the calibration procedure and the conduct of the wake vortex surveys is summarized below.

#### 3.2.1 Calibration

During the set-up process, the optical bench was leveled with the external van jacks using a bubble level for reference (estimated accuracy of  $\pm 0.5$  deg). For the second day of the tests, the scanner was offset 45 deg using a tri-square for reference (estimated accuracy of  $\pm 0.5$  deg). Prior to the actual wake surveys, the elevation and azimuth angle readouts from the LDV were calibrated. The calibration involved pointing the optical system at the sun and comparing the observed elevation and azimuth angle readouts with those given in the ephemeris. The results indicated that a -3 deg and  $\pm 139$  deg correction should be applied to the raw elevation and azimuth readouts from the LDV, respectively.

During the Rosamond tests, the range resolution and signal-to-noise ratio characteristics of the LDV were not recalibrated. The range and signal-to-noise ratio calibrations taken a few months earlier and documented in Ref. 4 were assumed to be representative of the systems overall performance.

#### 3.2.2 Wake Surveys

During the Rosamond wake decay tests, 53 aircraft flybys were recorded with the LDV system (flyby 36 was lost due to a loss in electrical power). The test conditions and the LDV scan, range, and elevation settings for the

**Table 1**  
**SUMMARY OF B-747 FLIGHT PARAMETERS**

<u>Flyby No.</u>	<u>Altitude (m AGL)</u>	<u>IAS (knots)</u>	<u>Weight (kg/1000)</u>	<u>Flap (deg)</u>	<u>Spoilers Deployed</u>	<u>Thrust (EPR)</u>	<u>Gear</u>
1	56	146	255				
2	62	146	252	30/30	0	1.25	Down
3	68	145	250	30/30	0	1.21	Down
4	65	145	249	30/30	0	1.25	Down
5	122	144	248	30/30	0	1.22	Down
6	122	144	247	30/30	0	1.22	Down
7	244	143	245	30/30	0	1.23	Down
8	244	143	244	30/30	0	1.23	Down
9	61	143	236	30/30	0	1.20	Down
10	122	143	235	30/30	1, 2, 11, 12	1.26	Down
11	183	142	234	30/30	1, 2, 11, 12	1.26	Down
12	244	142	232	30/30	1, 2, 11, 12	1.25	Down
13	64	142	230	30/30	1, 2, 11, 12	1.25	Down
14	65	138	228	30/30	1, 2, 11, 12	1.24	Down
15	61	138	227	30/30	1, 2, 11, 12	1.20	Down
16	61	138	226	30/30	1, 2, 11, 12	1.20	Down
17	30	141	222	30/30	1, 2, 11, 12	1.18	Down
18	37	141	218	30/1	0	1.19	Down
19	38	141	216	30/1	0	1.18	Down
20	67	139	215	30/1	0	1.18	Up
21	64	139	213	30/1	0	1.18	Down
22	91	139	212	30/1	0	1.16	Up
23	122	148	250	30/30	0	1.23	Down
24	122	220	259	30/30	0	1.24	Down
25	122	147	258	0/0	0	1.03	Up
26	122	215	256	30/30	0	1.24	Down
27	67 (LDG)	146	255	0/0	0	1.06	Up
28	66	146	254	30/30	0	1.20	Down
29	72 (LDG)	146	252	30/30	0	1.20	Down
30	66	145	251	30/30	0	1.14	Down
31	107 (TO)	156	243	30/30	0	1.24	Down
32	65	156	242	10/10	0	1.38	Up
33	57 (TO)	156	241	10/10	0	1.11	Up
34	59	143	240	10/10	0	1.36	Up
35	63	142	239	10/10	0	1.15	Up
36	68	142	238	30/30	0	1.20	Down
37	67	141	237	30/30	0	1.20	Up
38	61	141	236	30/30	0	1.21	Down
39	47 (TO)	151	230	30/30	0	1.22	Up
40	46 (TO)	151	228	10/10	1, 2, 11, 12	1.35	Up
41	48 (TO)	150	227	10/10	0	1.36	Up
42	54 (TO)	150	226	10/10	1, 2, 11, 12	1.36	Up
43	61	138	225	10/10	0	1.40	Up
44	63 (LDG)	138	224	30/30	0	1.24	Down
45	50 (LDG)	138	223	30/30	0	1.12	Down
46	37	137	222	30/30	0	1.16	Down
47	91	135	215	30/30	0	1.24	Down
48	91	135	214	30/30	0	1.15	Down
49	37	134	213	30/30	1, 2, 11, 12	1.20	Down
50	91 (LDG)	134	210	30/30	1, 2, 11, 12	1.20	Down
51	122	200	209	30/30	0	1.11	Down
52	122	200	208	0/0	0	1.11	Down
53	122	133	207	0/0	0	1.03	Up
54	122	200	206	30/30	0	1.22	Down
					0	1.05	Up

**LDG:** Aircraft descending along imaginary glideslope.

**TO:** Aircraft ascending as in actual takeoff.

Rosamond tests are summarized in the log sheets given in Appendix A, while a list of the flight parameters is given in Table 1. Primarily, those flybys have been processed from the wake measurements where flow visualization and photographic data (photographs were taken of vortices at 1 sec increments) were available for comparison with the LDV measurements.

To maximize the amount of data collected regarding wake vortex trajectories, velocity profiles, and decay rates, the LDV was operated in different scan modes including: arc-scan and, finger-scan configurations. The wake vortex surveys were conducted in the following manner.

On the first test day, the LDV was located directly under the flight path (Fig. 11) and scanned arcs in a plane perpendicular to the flight path (Fig. 12) with a complete scan every 2 sec. Scans were at a fixed range until the vortex passed through the scan arc, at which time the sensor range was lowered and remained fixed again until the vortex descended through the new range. The objective of the overhead arc scan measurements was the measurement of the initial downwash field and the wake vortex roll-up process.

On the second test day, the LDV was moved 60 m north of the flight path (Fig. 11) and scanned simultaneously in elevation and range (finger-scan mode) at a frequency of 0.2 Hz, and 2 to 2.5 Hz, respectively. The objective of the finger scan measurements was to track the location of the vortex pair and to observe the vortex decay rates. The coordinated variations in range and elevation settings for the finger scan mode were selected on the basis of the aircraft wake vortex parameters. In addition, during the last sorties, the azimuth angle was changed during the run to 90- and 180-deg angles to scan both down the vortex (axially) and to follow the vortex drift away from the LDV.

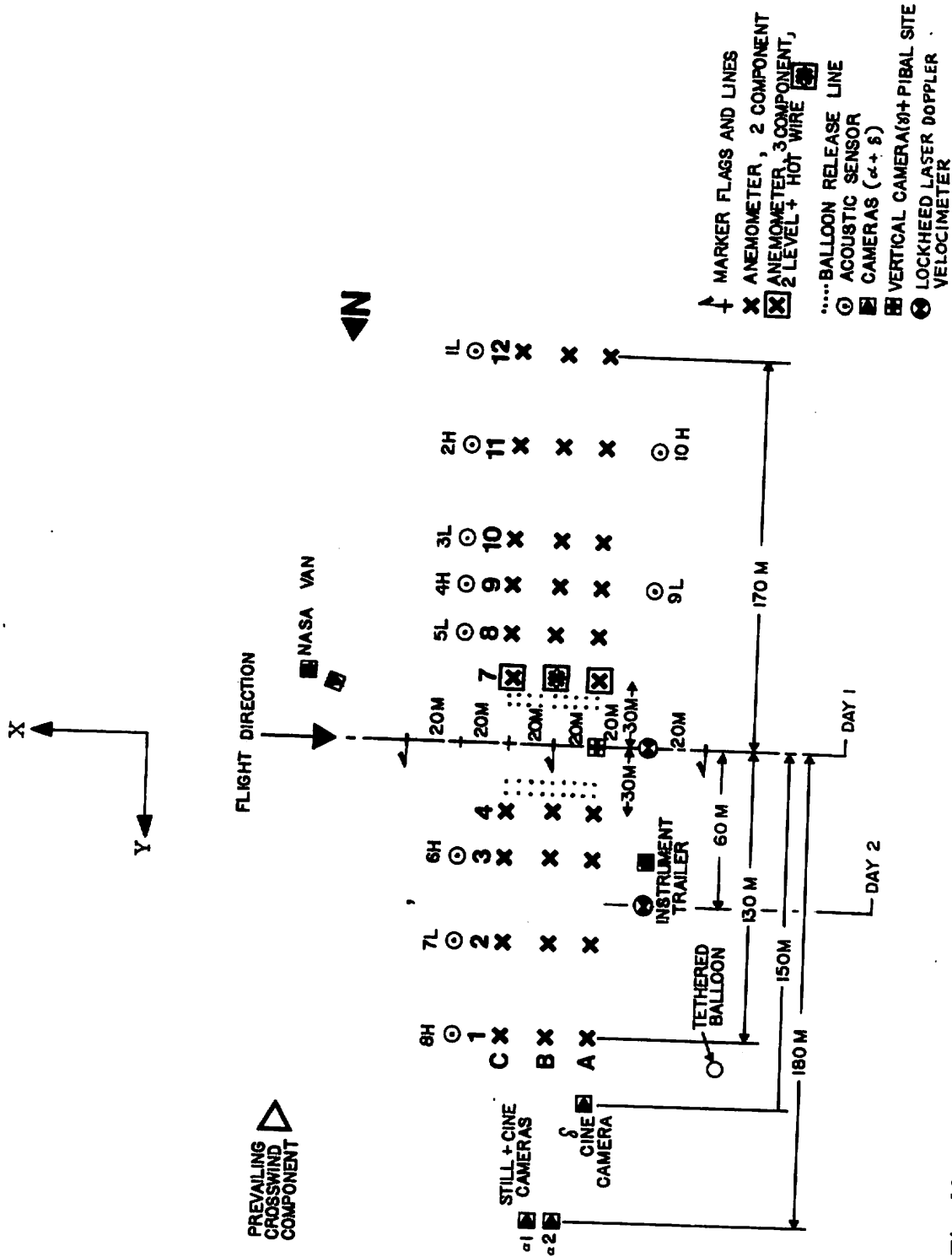


Fig. 11 - Location of Lockheed LDV During the Rosamond Wake Vortex Measurements

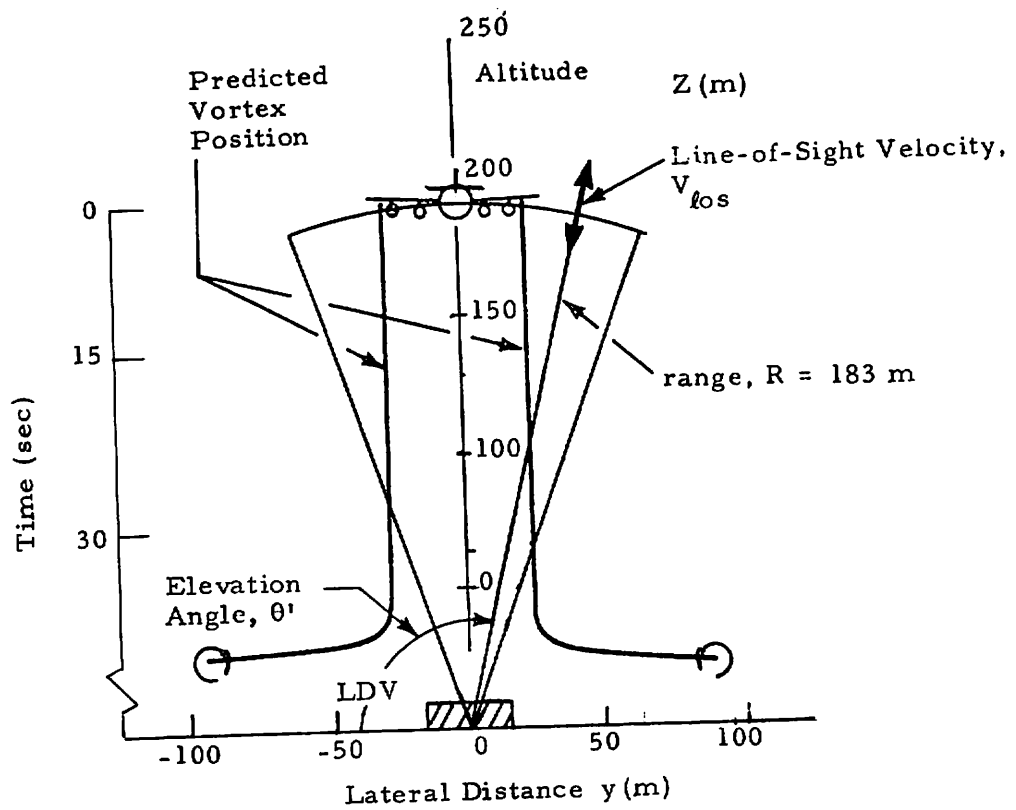


Fig. 12 - Overhead Arc Scan Configuration Illustrated for Rosamond Flyby 11

## 4. RESULTS OF WAKE VORTEX MEASUREMENTS

The LDV measurements obtained during the Rosamond tests have been analyzed to determine the dominant characteristics of the B-747 wake. In the following discussion, the observed wake vortex characteristics are described including the vortex roll-up, vortex transport, and vortex decay parameters.

### 4.1 VORTEX ROLL-UP

To determine the vortex roll-up parameters, the downwash field behind the B-747 aircraft was measured with the LDV operated in a constant-range arc-scan mode. In the typical arc-scan configuration, illustrated earlier in Fig. 13, the magnitude of the line-of-sight velocity component observed by the LDV was essentially a measure of the spanwise downwash distribution in the aircraft nearwake. Thus, from the magnitude of the LDV line-of-sight velocity distribution in the near wake the downwash and vortex formation and roll-up characteristics were determined.

#### 4.1.1 Initial Spanwise Downwash Distribution

The magnitude of the peak line-of-sight velocity component,  $|V_{pk}|$  (m/sec), from the high-speed data is shown as a function of lateral distance,  $y$ (m), in Figs. 13 through 16 for flybys 8, 11, 12, and 13, respectively, over the time interval  $t = 0$  to 8 sec. Each scan is defined as the period between two successive elevation angle reversals and is approximately 1 sec in duration. Occasionally, some overlapping occurs between successive scans due to limitations in the processing software. Therefore, successive scans shown in Figs. 13 through 16 do not always have the same starting and ending limits, and, as a result, the lateral scales can be different. The direction and mid-time of each scan is indicated in the figures. The lateral distance,  $y$ , was computed directly from the raw range,  $R$ , and raw elevation angle

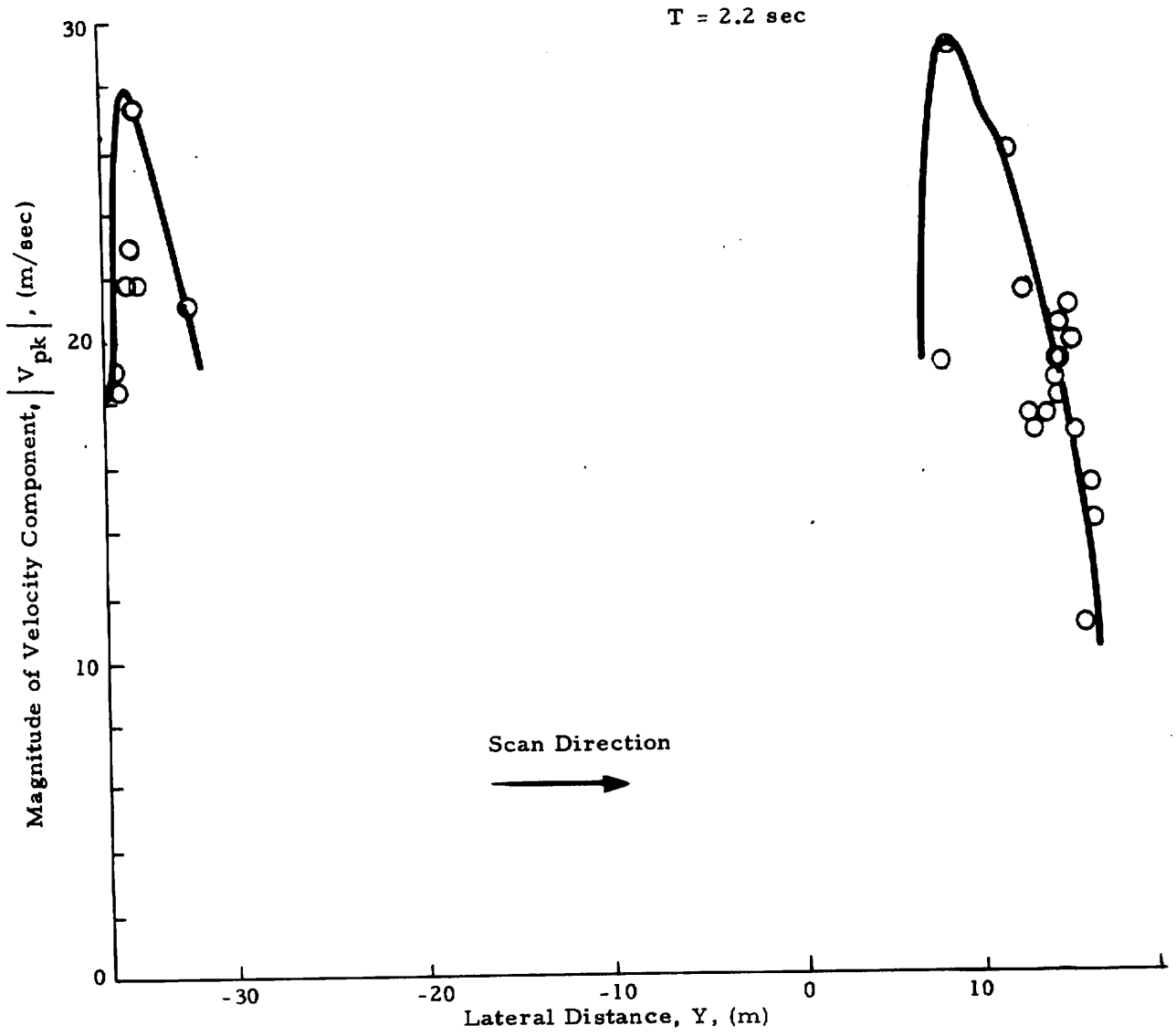


Fig. 13 -  $|V_{pk}|$  as a Function of Lateral Distance for Rosamond B-747 Flyby 8



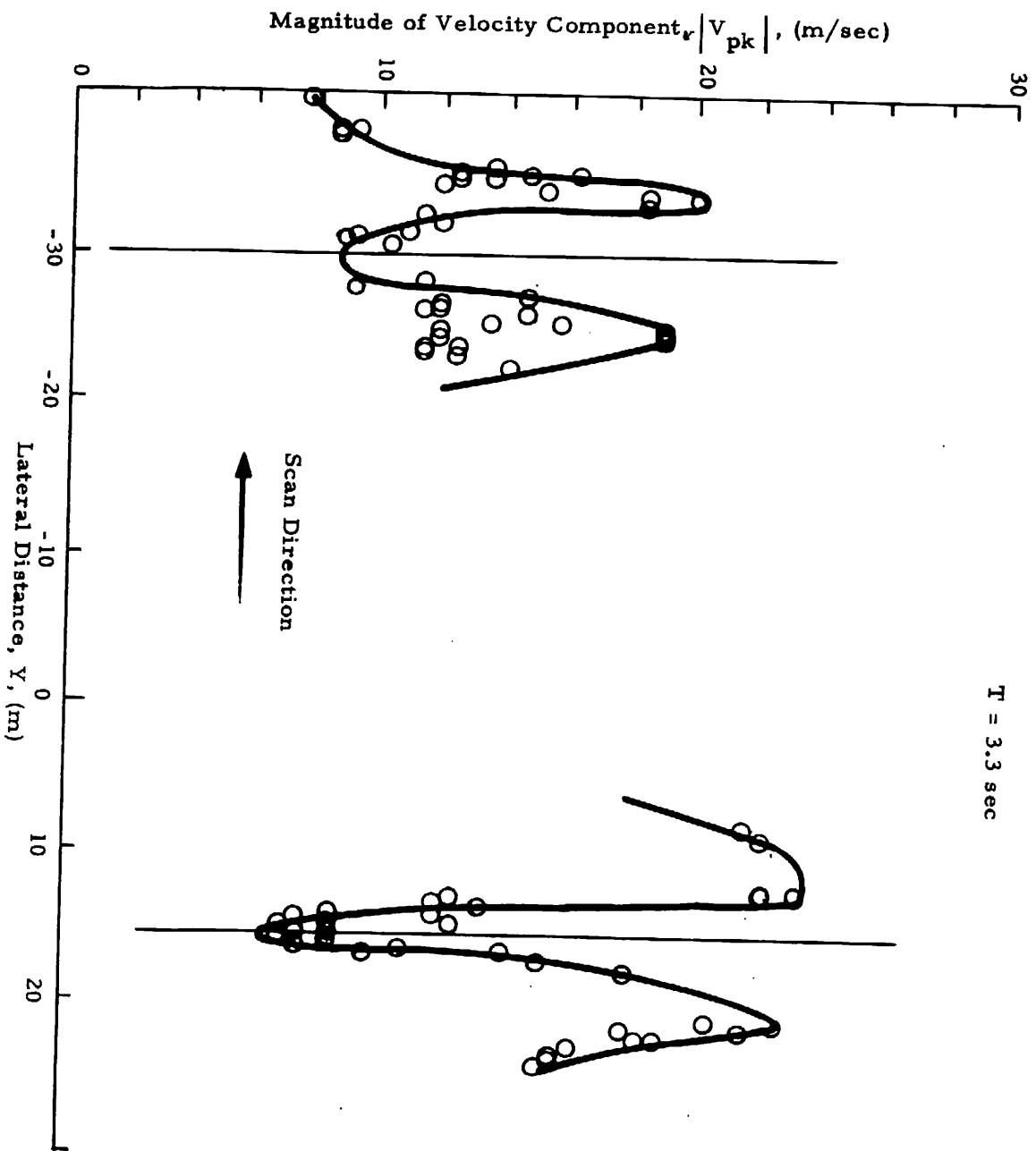


Fig. 13 (Continued)

T = 4.2 sec

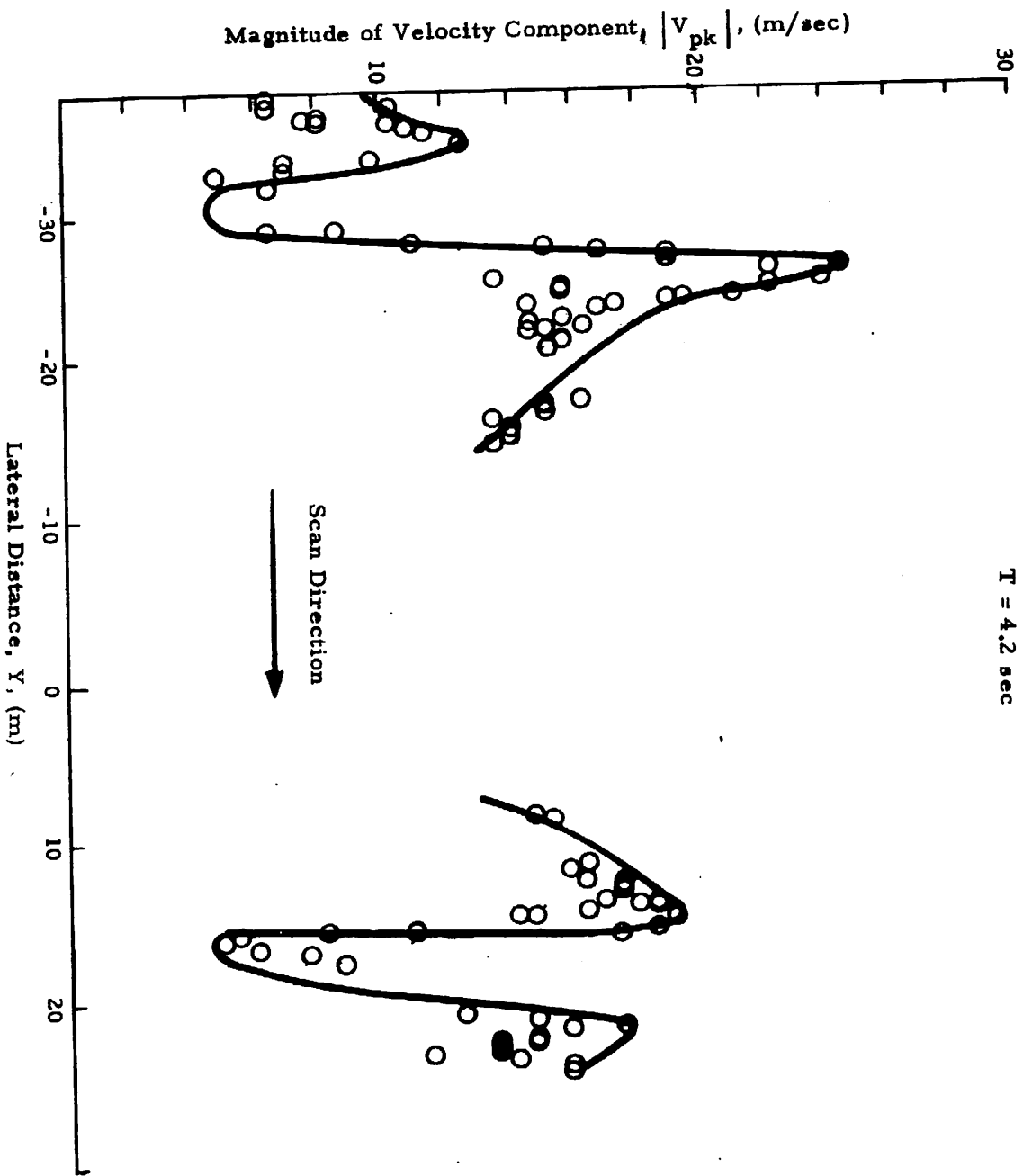


Fig. 13 (Continued)

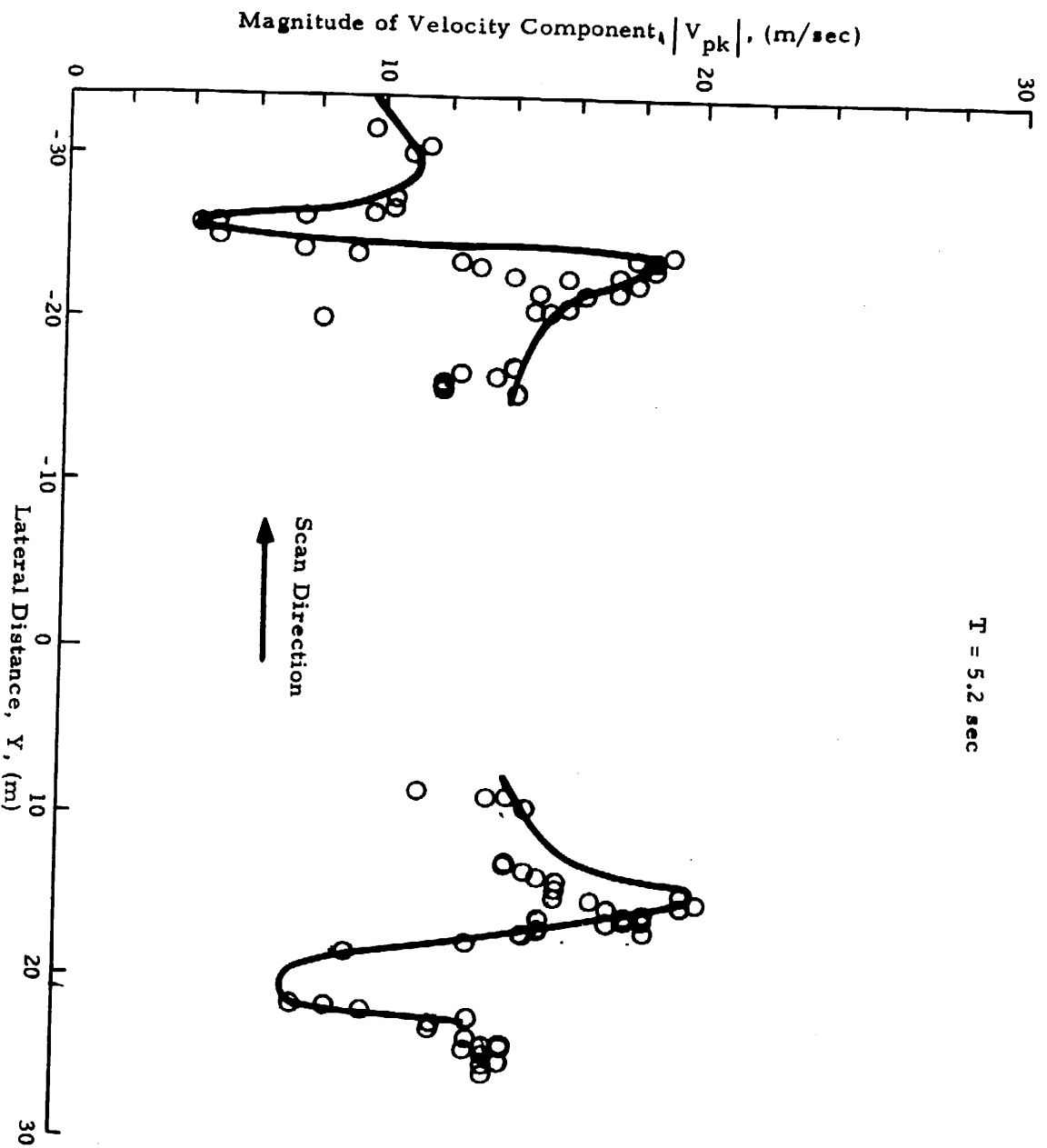


Fig. 13 (Continued)

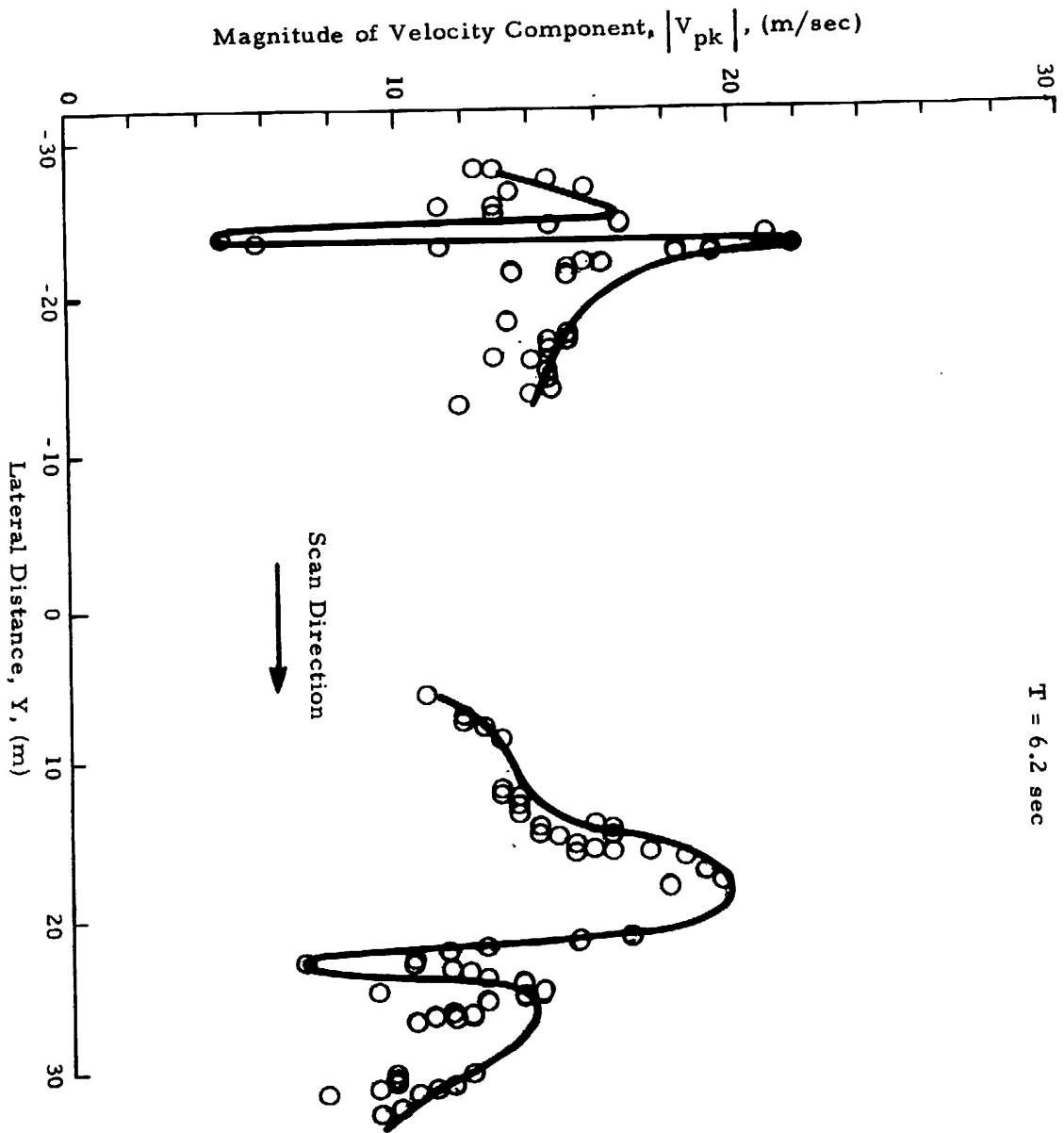


Fig. 13 (Continued)

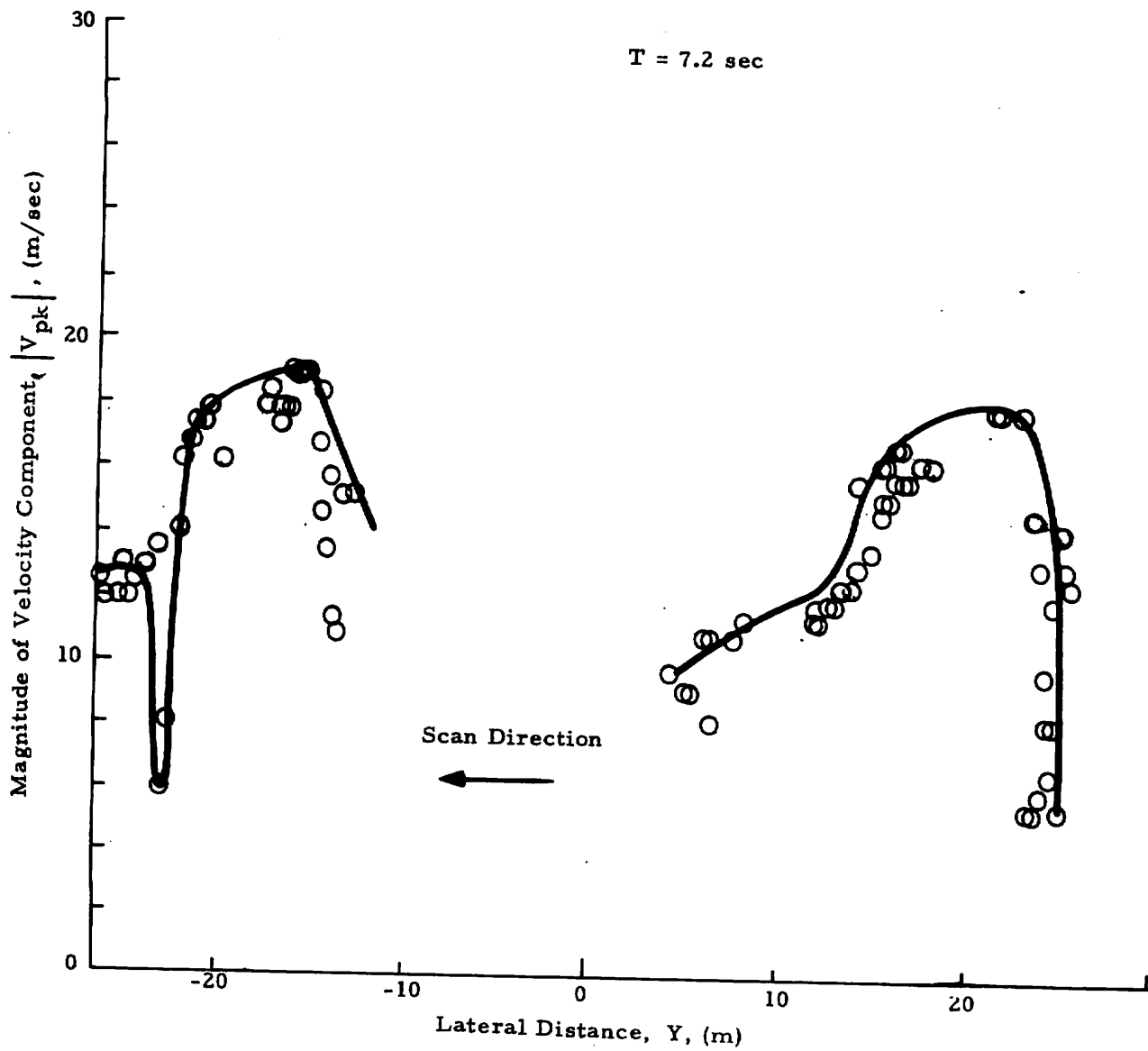


Fig. 13 (Continued)

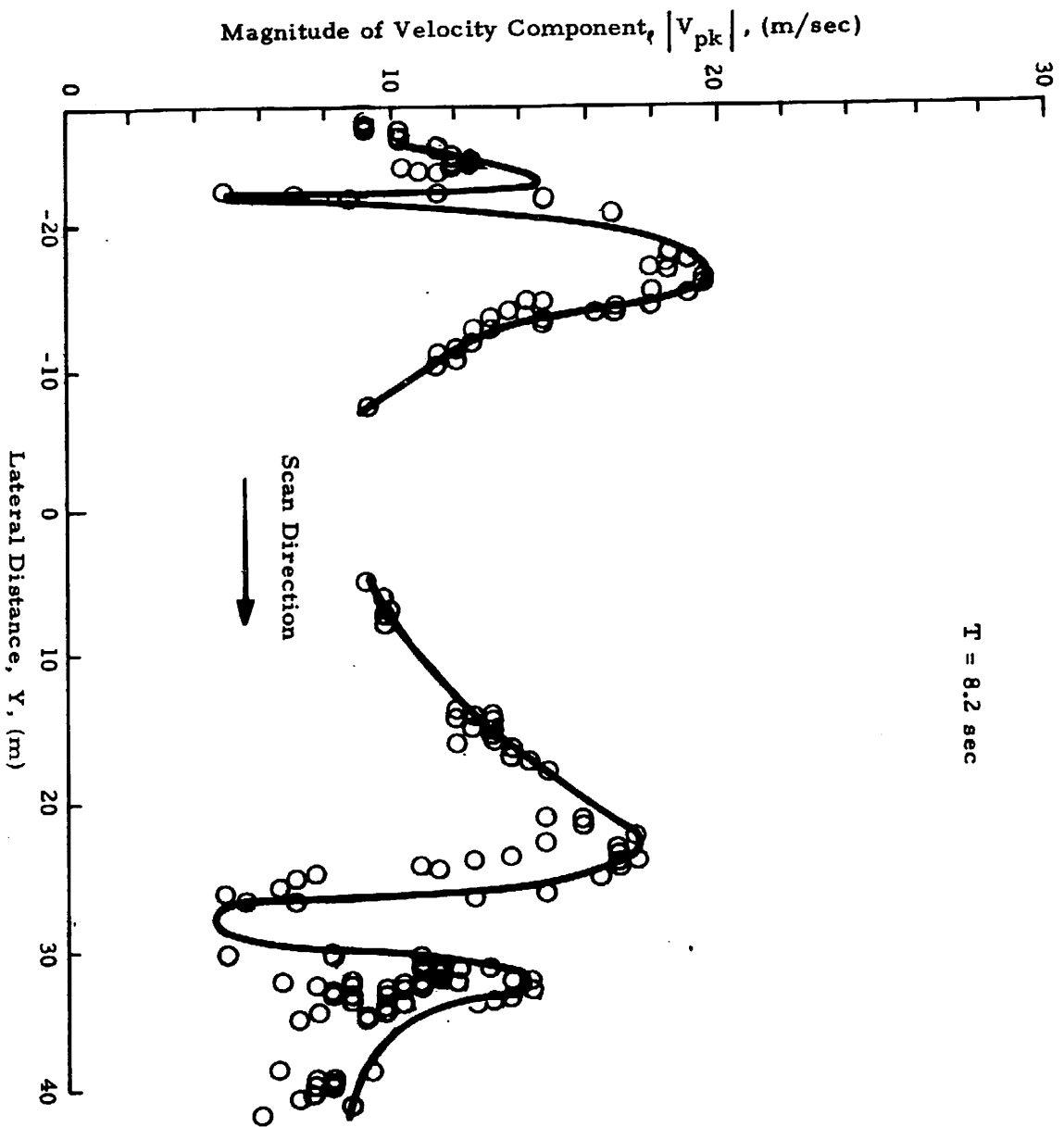


Fig. 13 (Concluded)

T = 1.5 sec

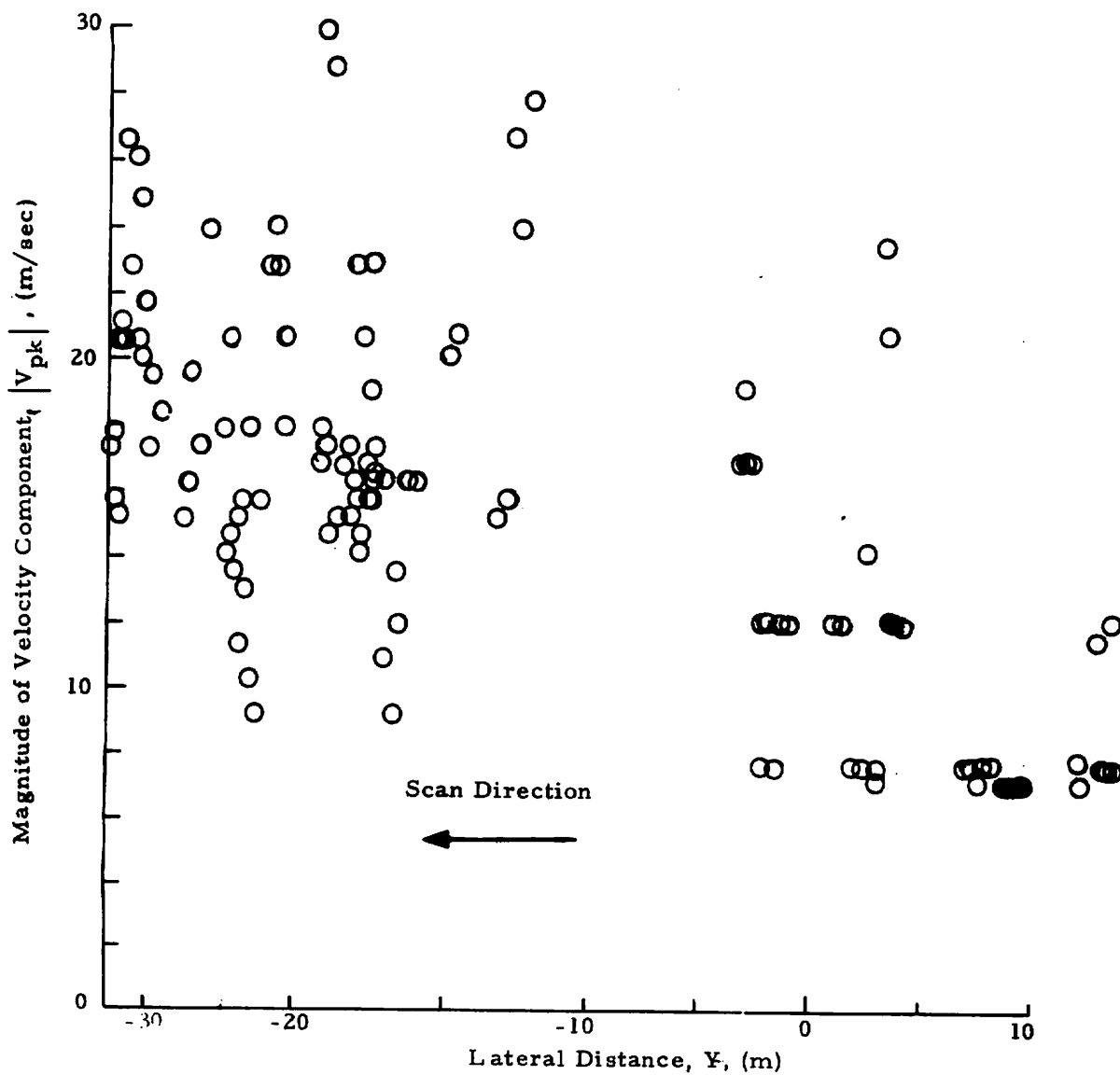


Fig.14-  $|V_{pk}|$  as a Function of Lateral Distance for Rosamond B-747 Flyby 11

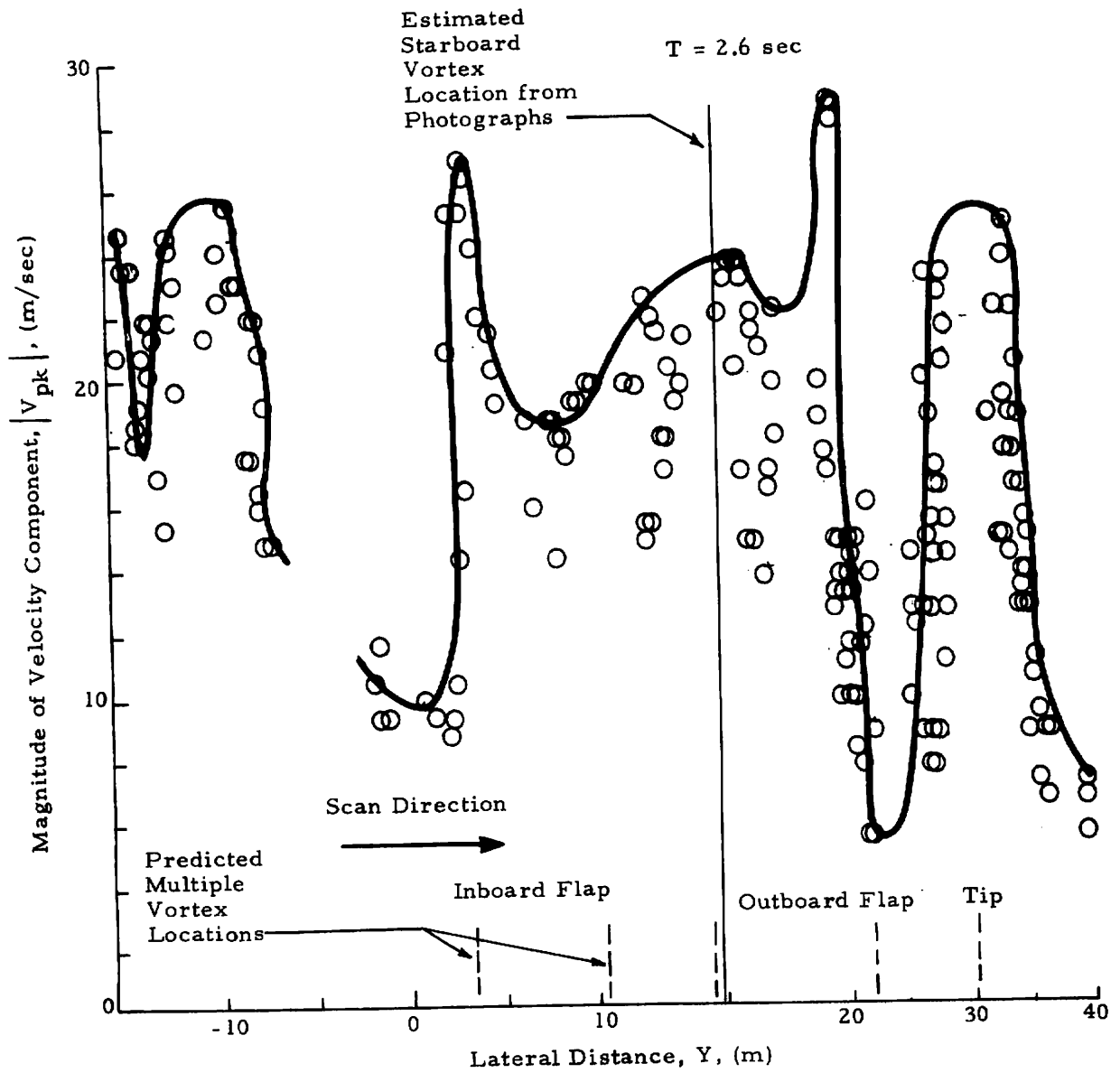


Fig. 14(Continued)



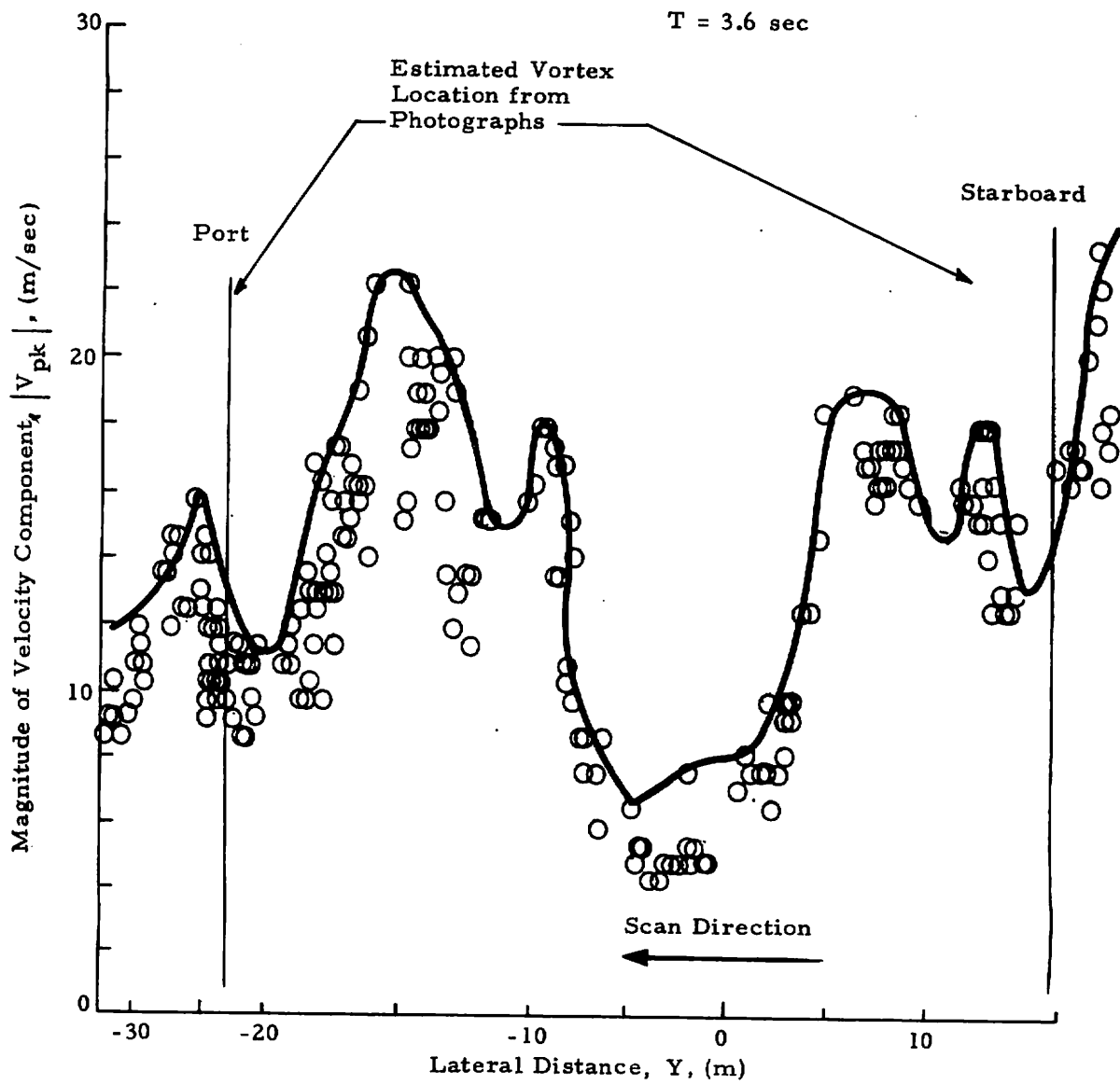


Fig.14 (Continued)

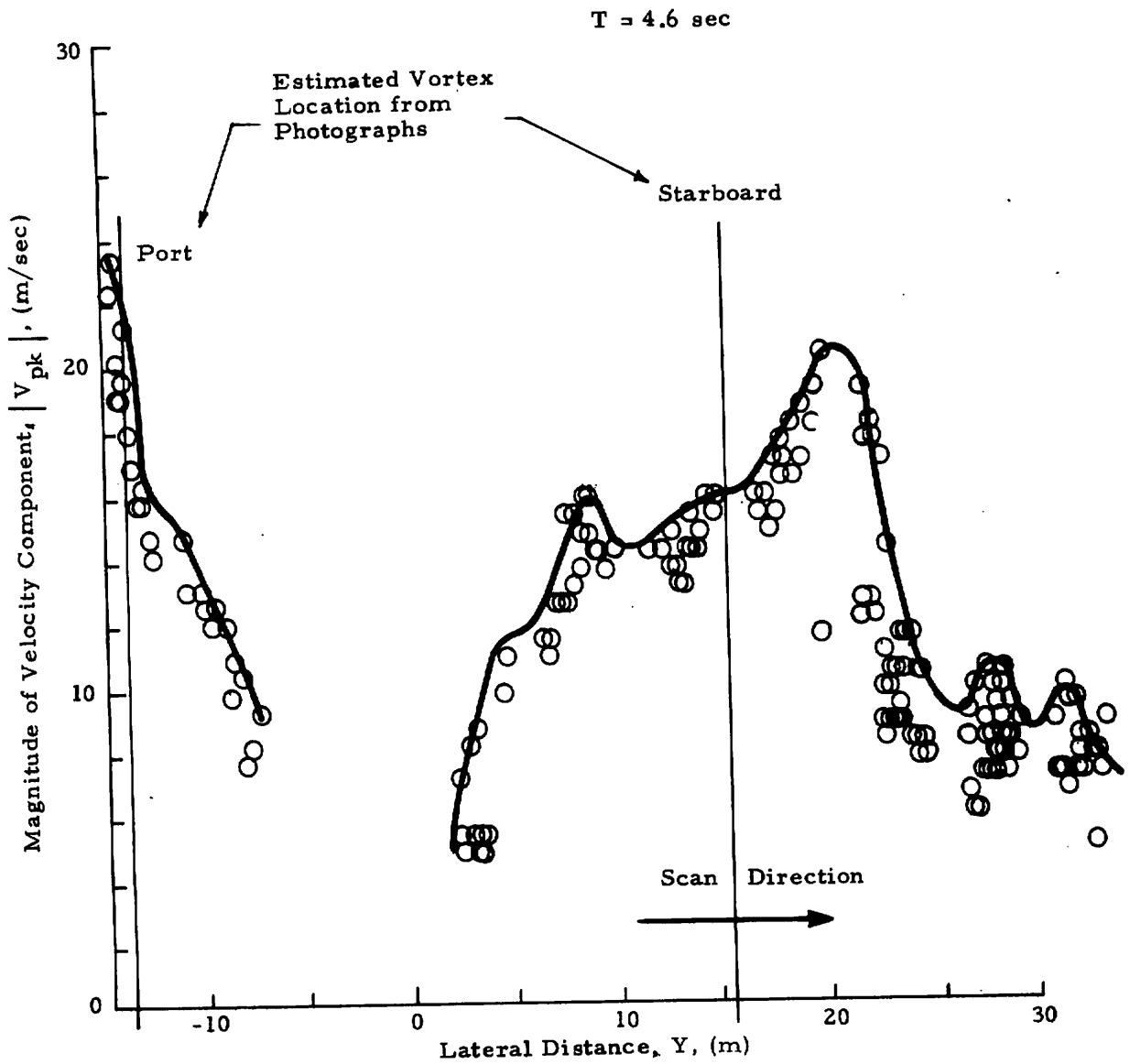


Fig. 14 (Continued)

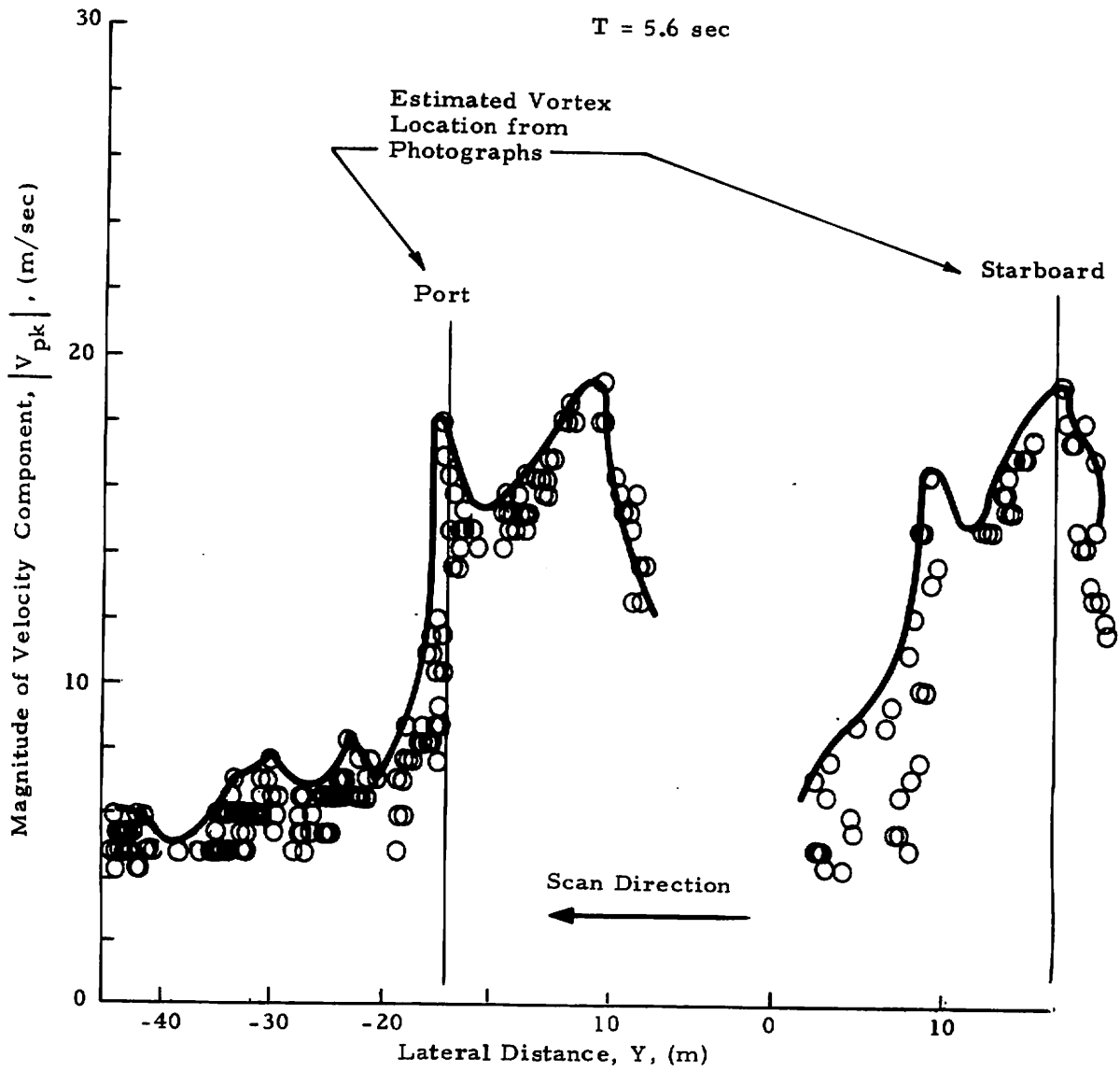


Fig. 14 (Continued)

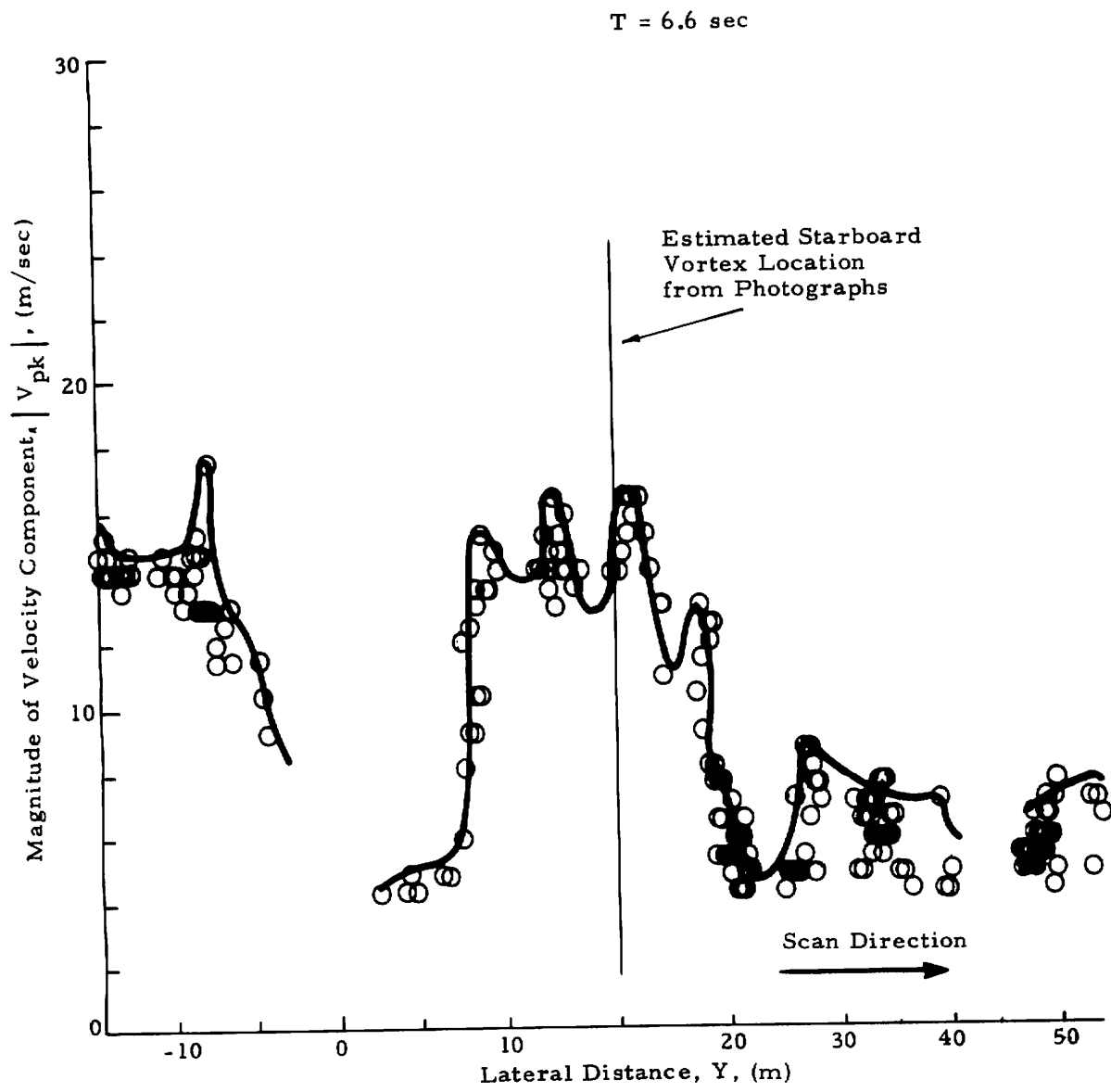


Fig. 14 (Continued)

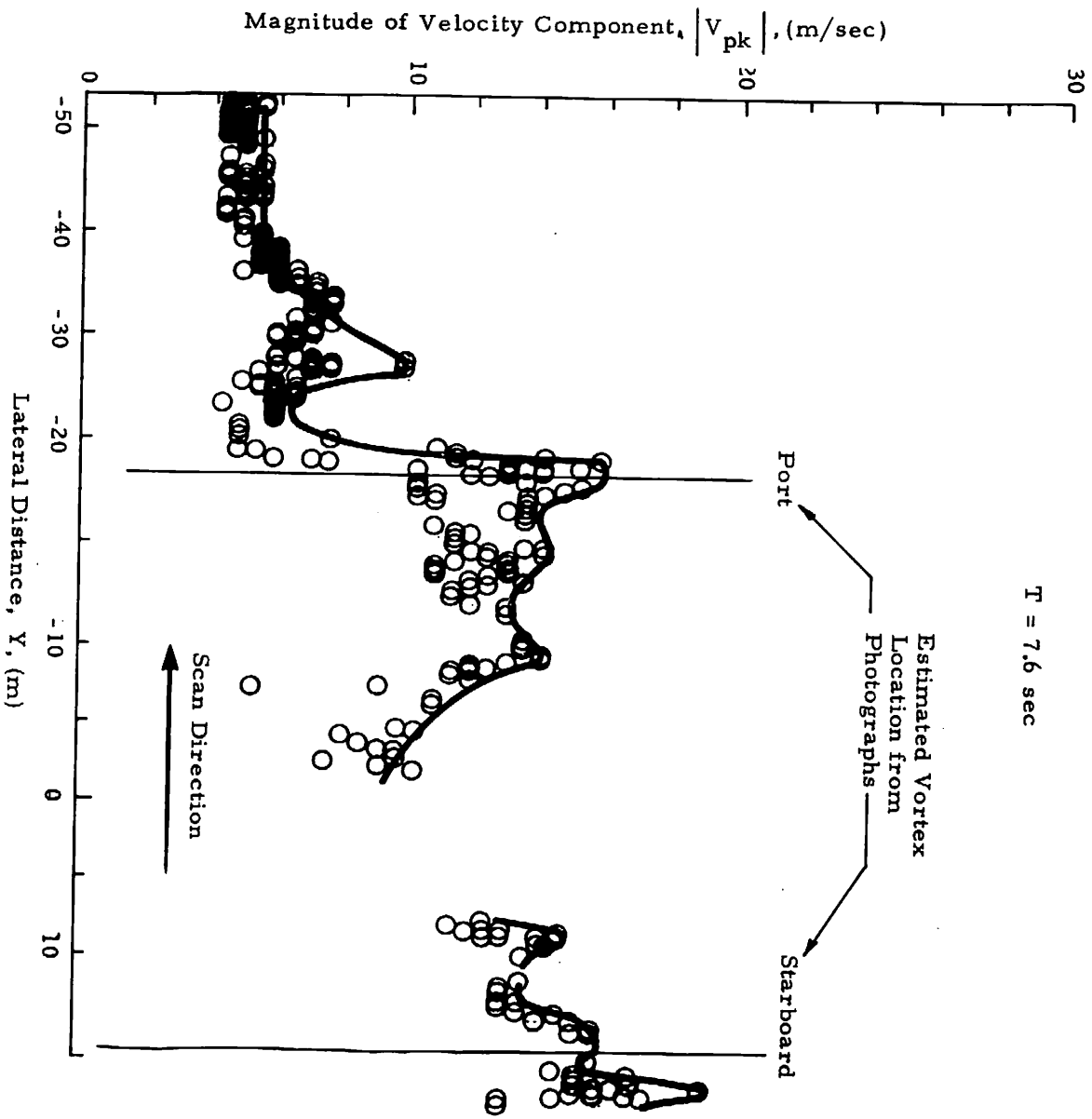


Fig. 14 (Continued)

T = 8.7 sec

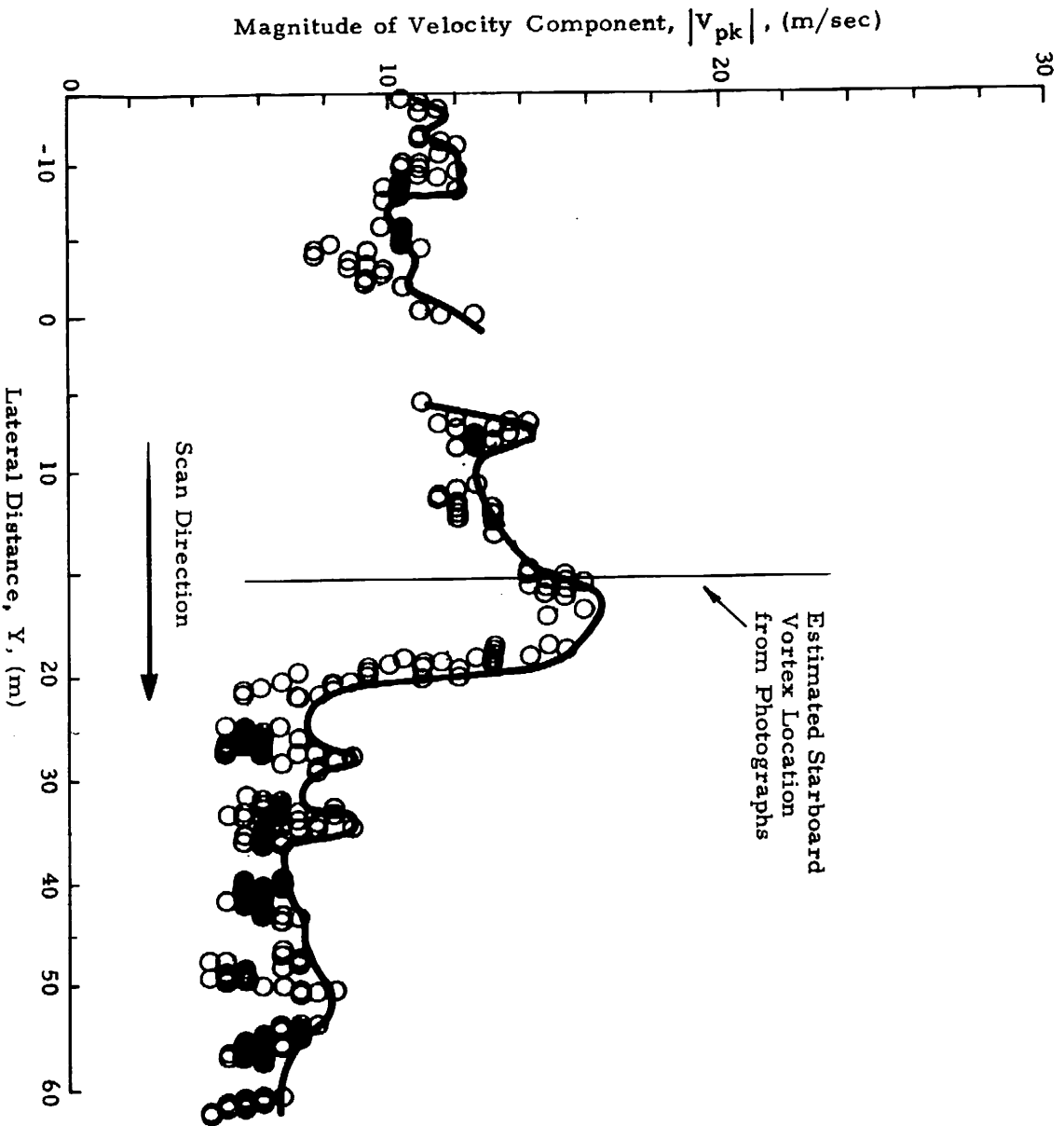


Fig. 14 (Continued)

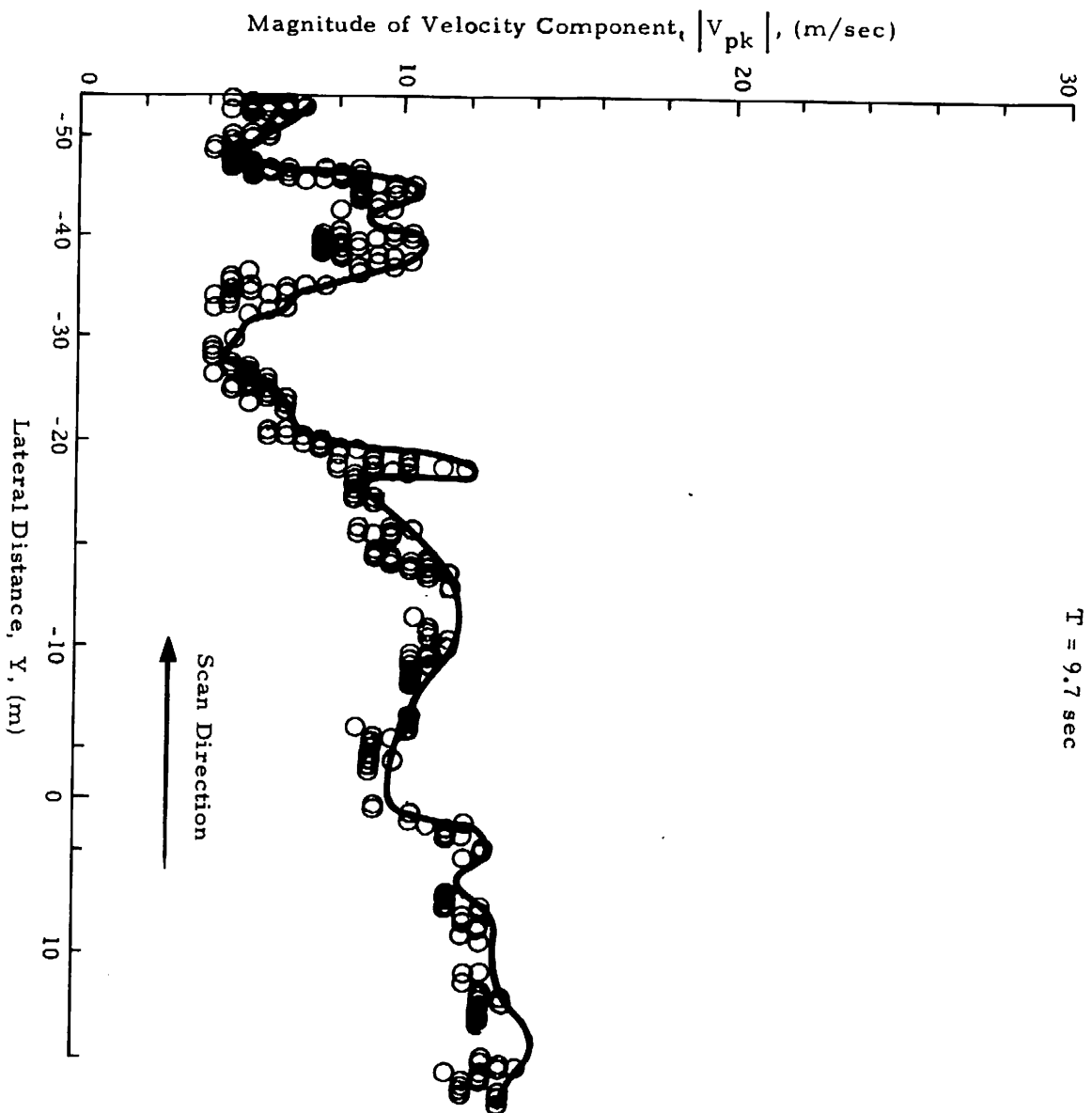


Fig. 14 (Concluded)

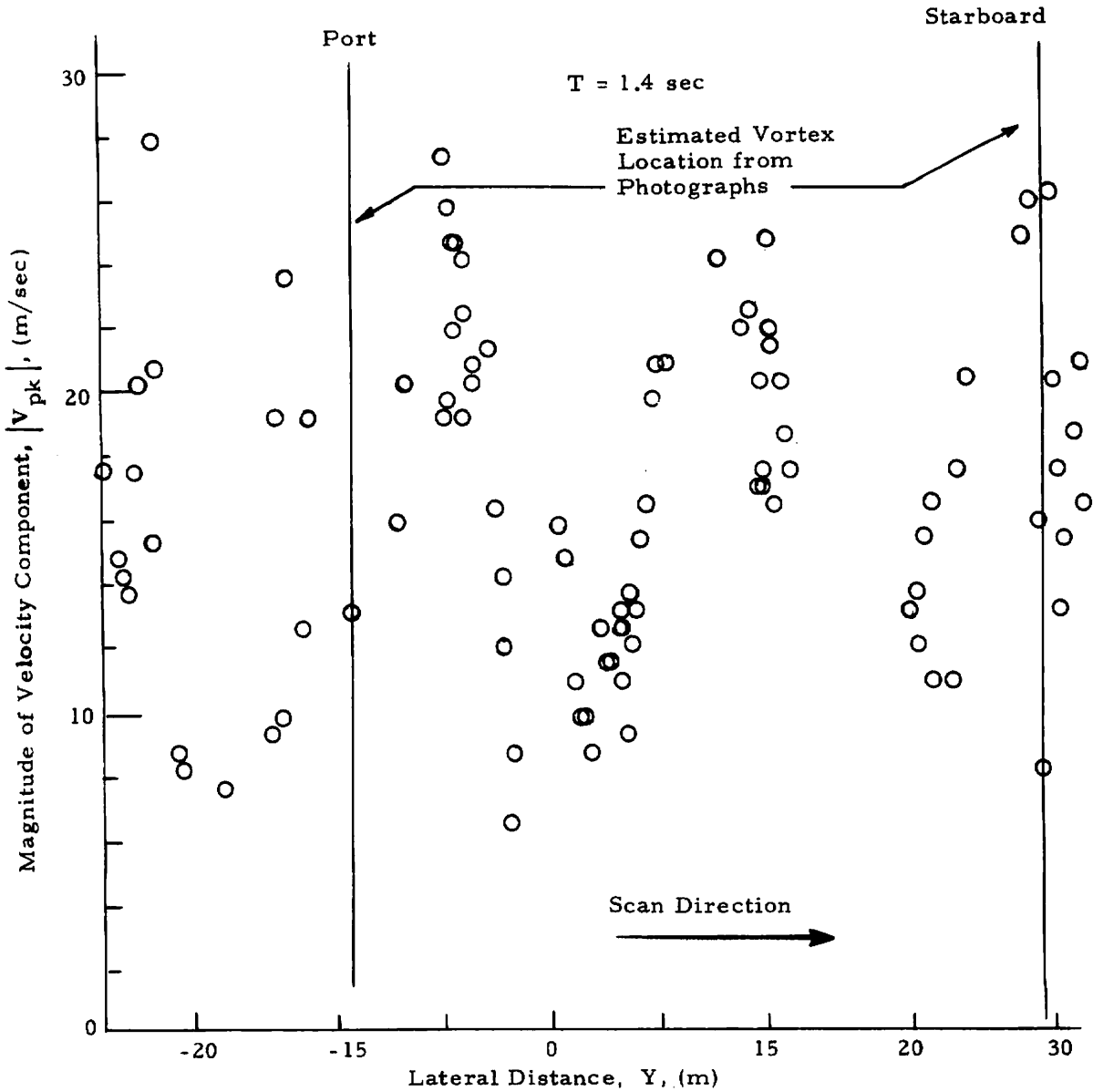


Fig. 15 -  $|V_{pk}|$  as a Function of Lateral Distance for Rosamond B-747 Flyby 12



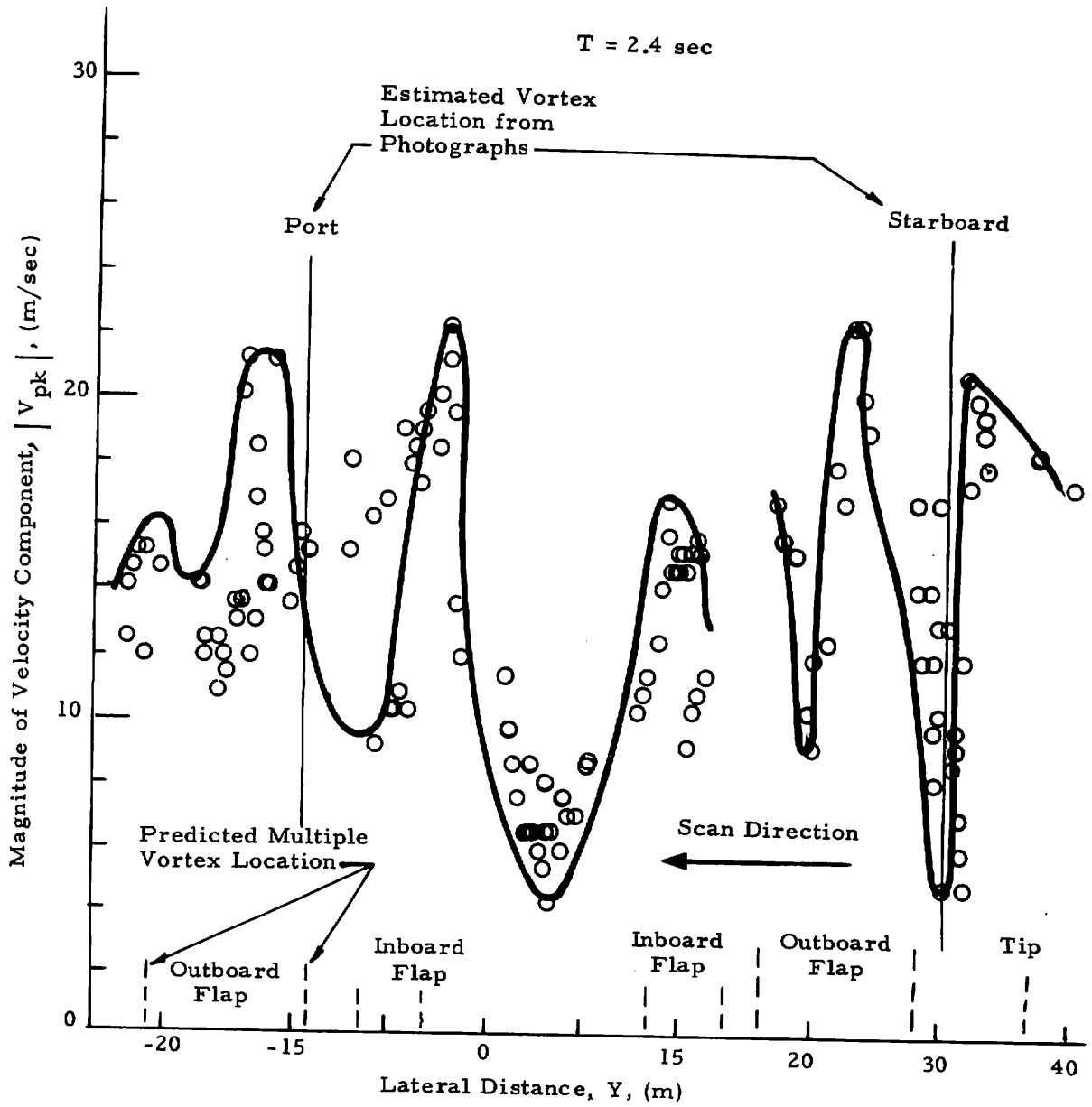


Fig. 15 (Continued)

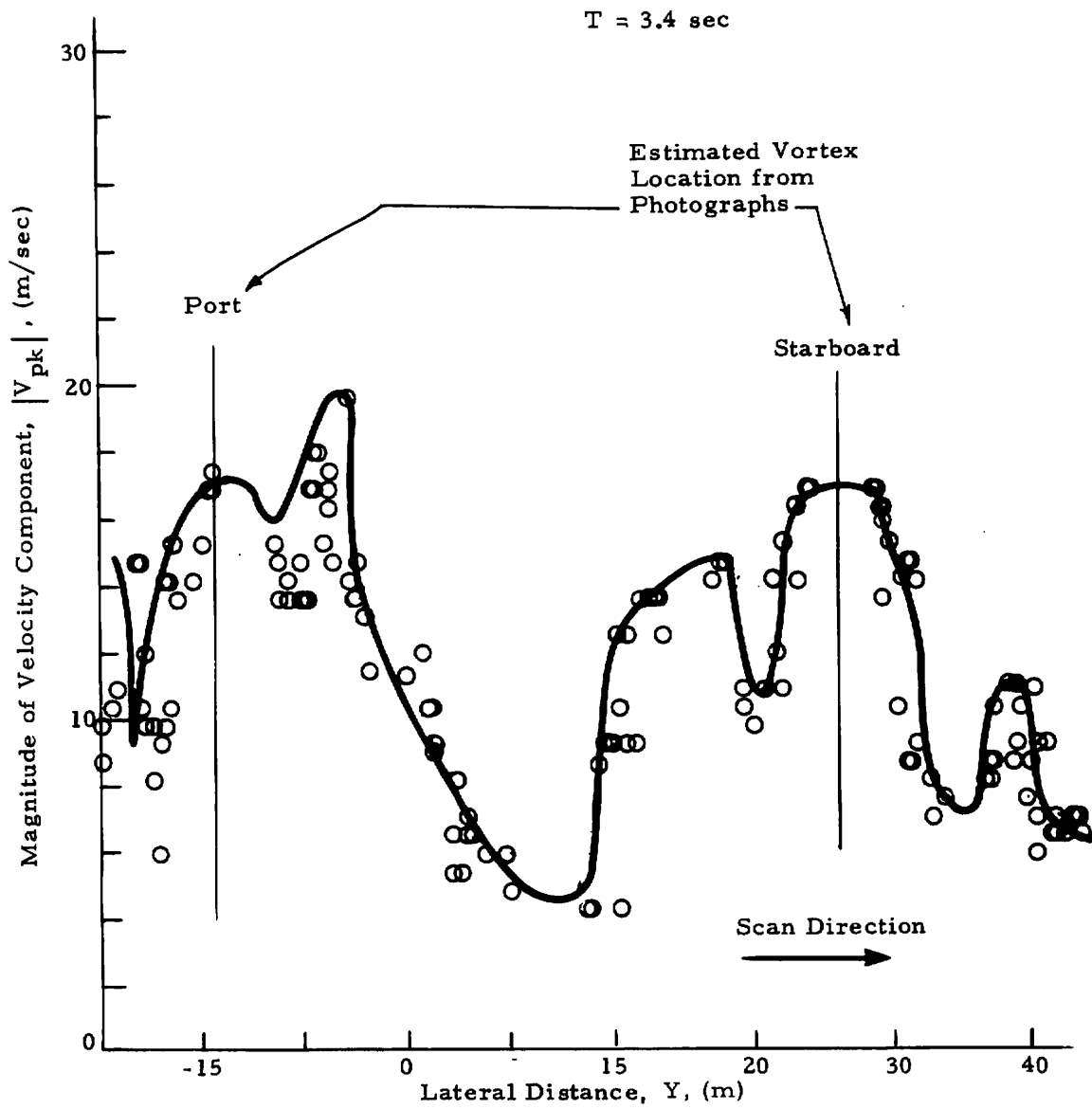


Fig. 15 (Continued)

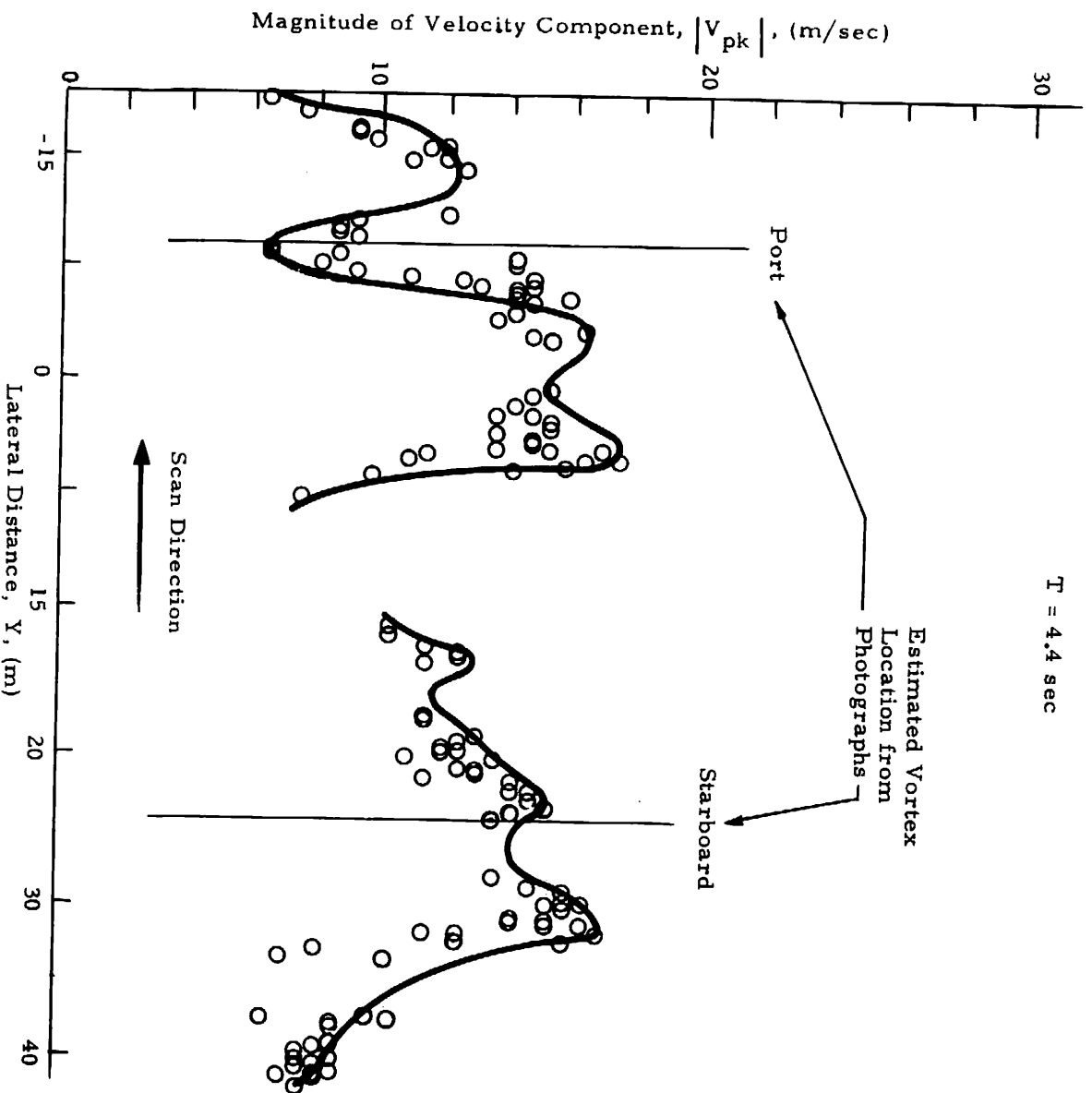


Fig. 15 (Continued)

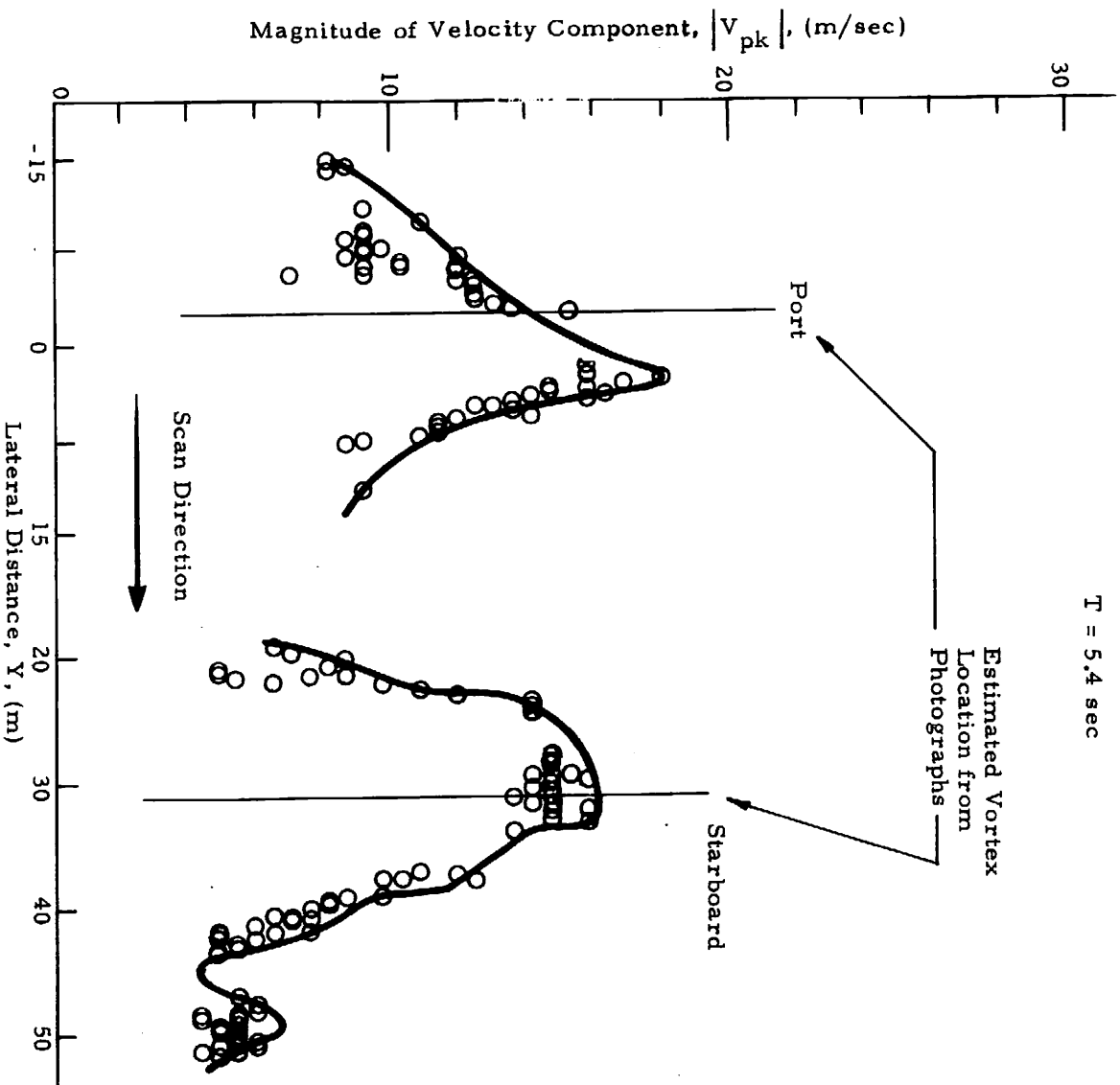


Fig. 15 (Continued)

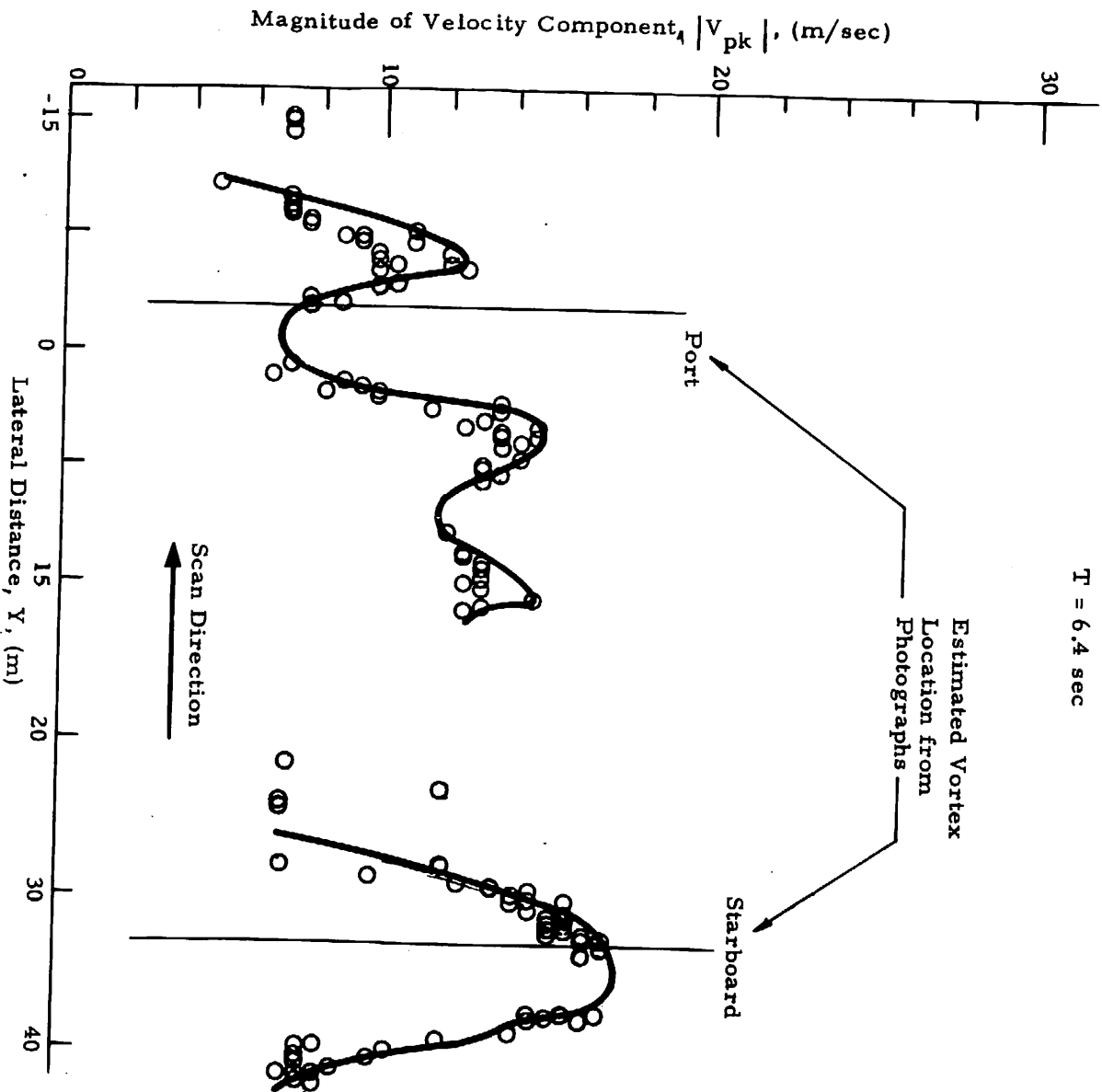


Fig. 15 (Continued)

T = 8.5 sec

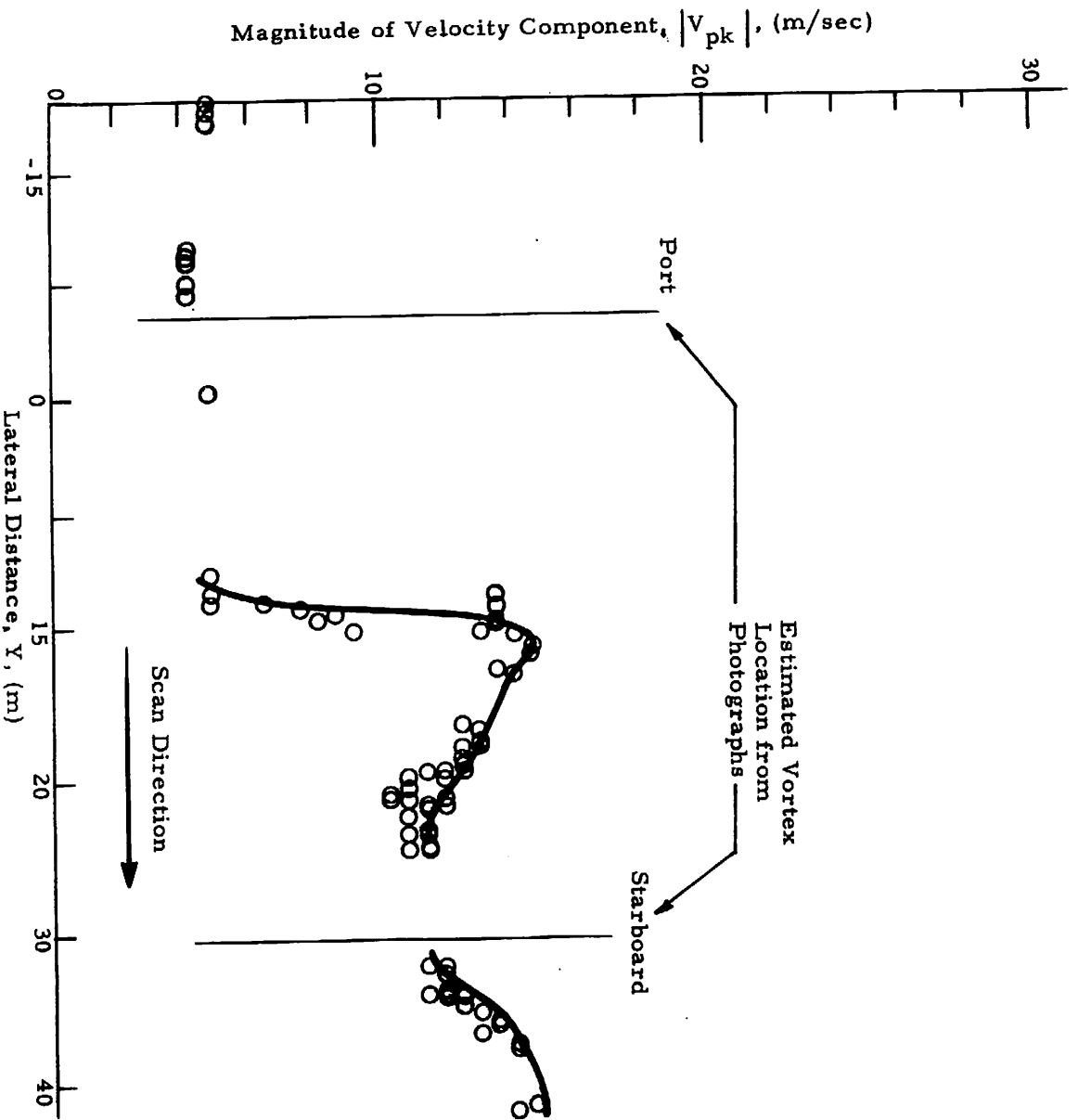


Fig. 15 (Concluded)

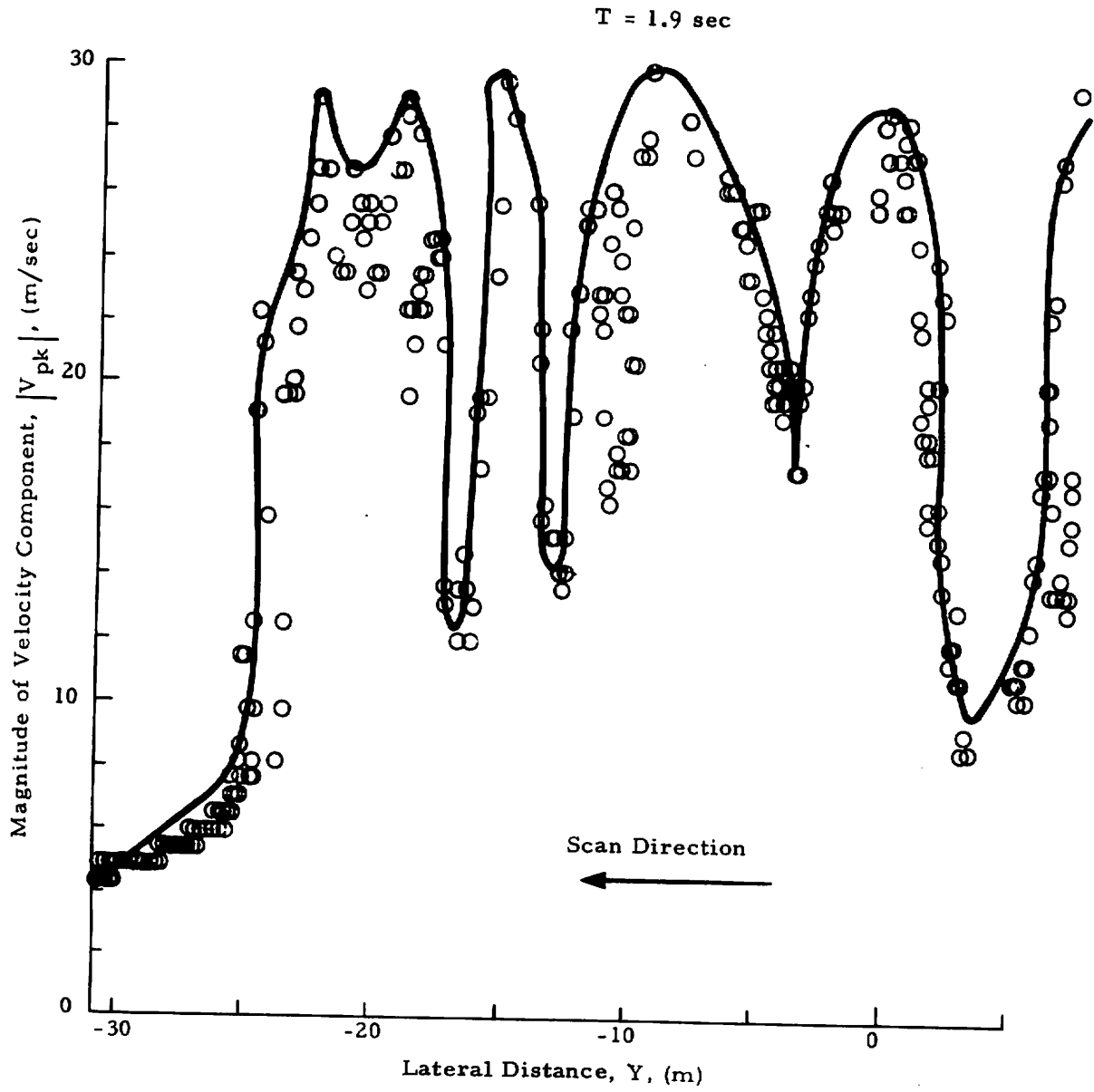


Fig. 16 -  $|V_{pk}|$  as a Function of Lateral Distance for Rosamond B-747 Flyby 13

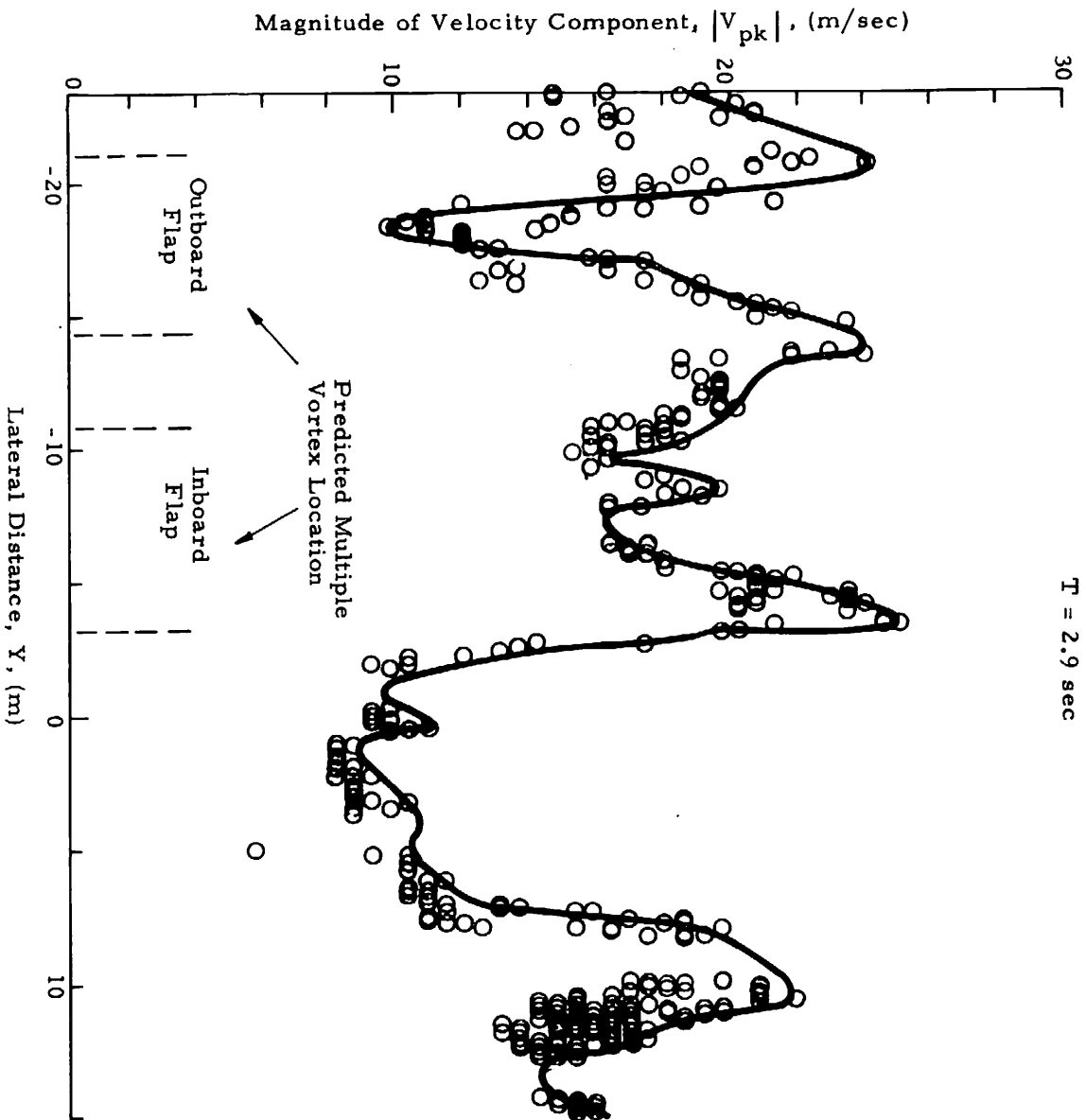


Fig. 16 (Continued)



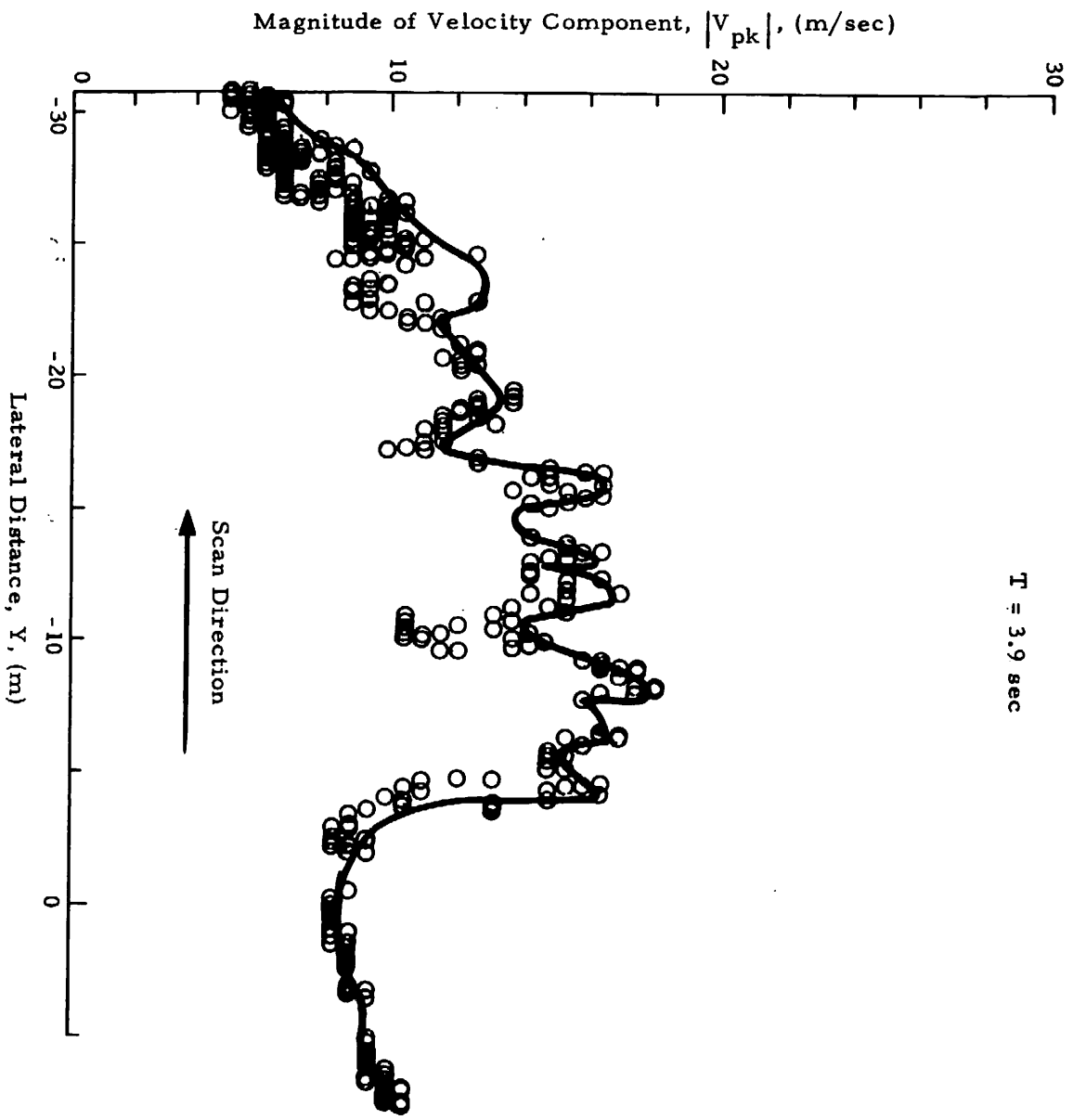


Fig. 16 (Continued)

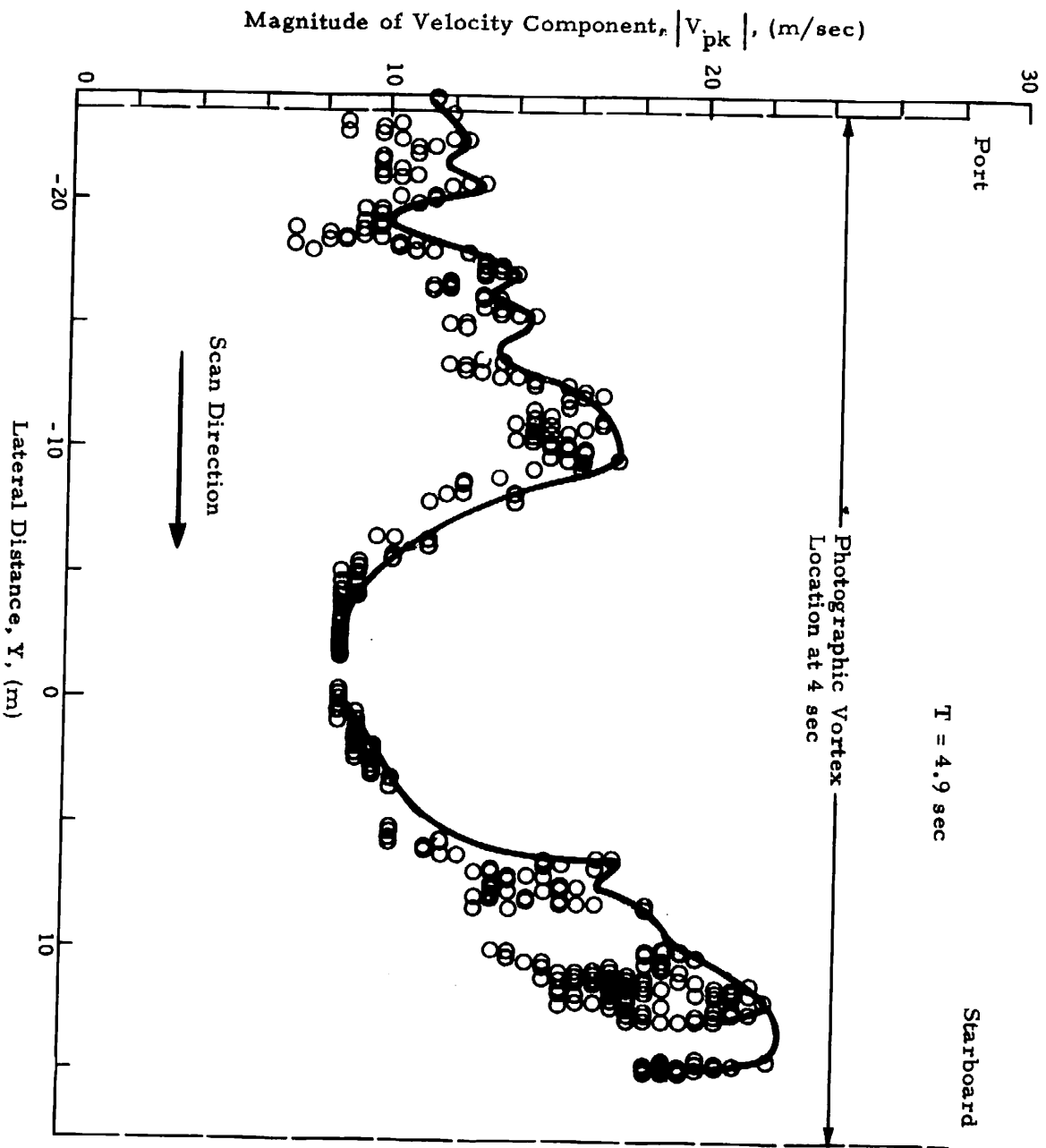


Fig. 16 (Continued)

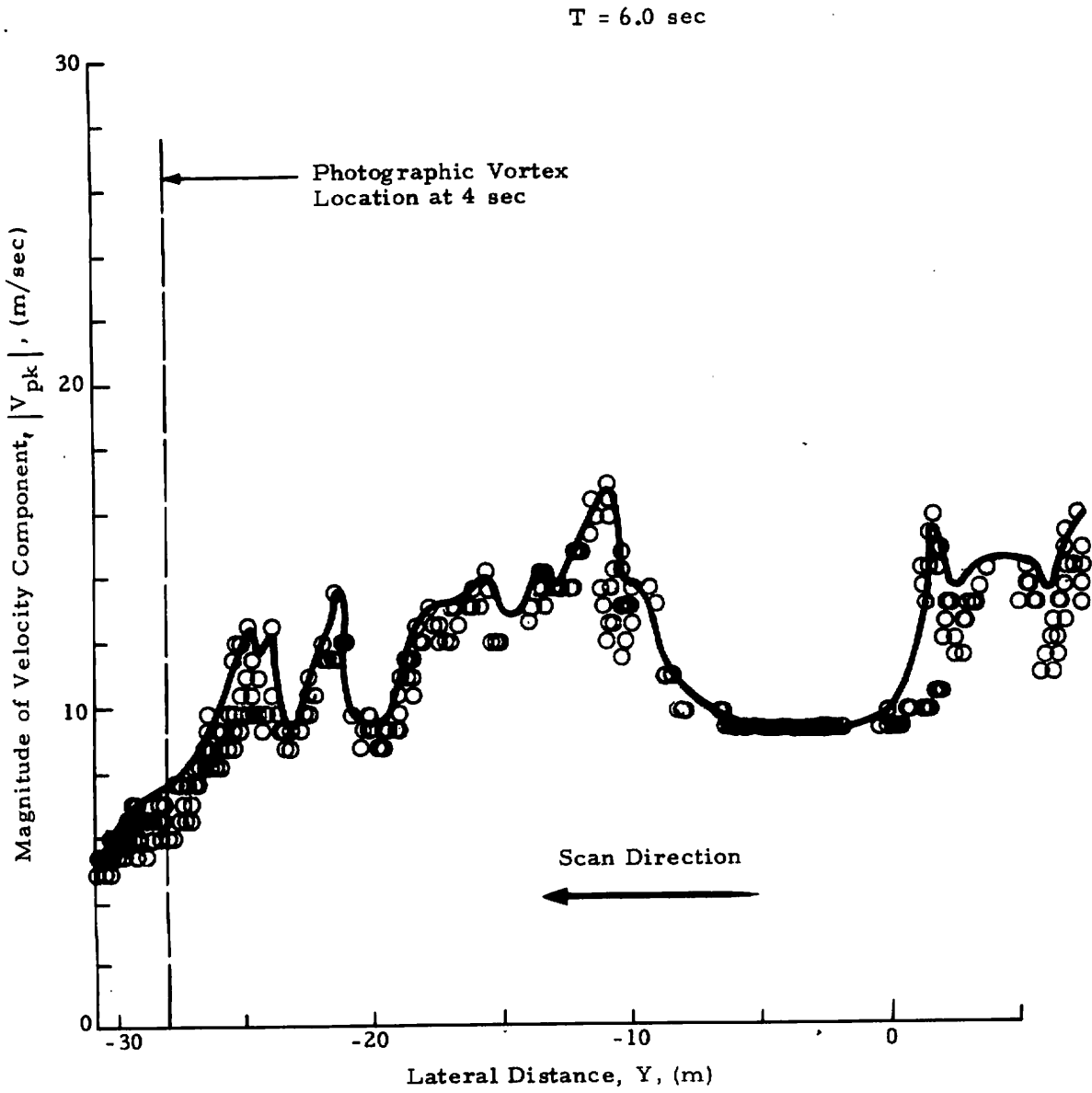


Fig.16 (Continued)

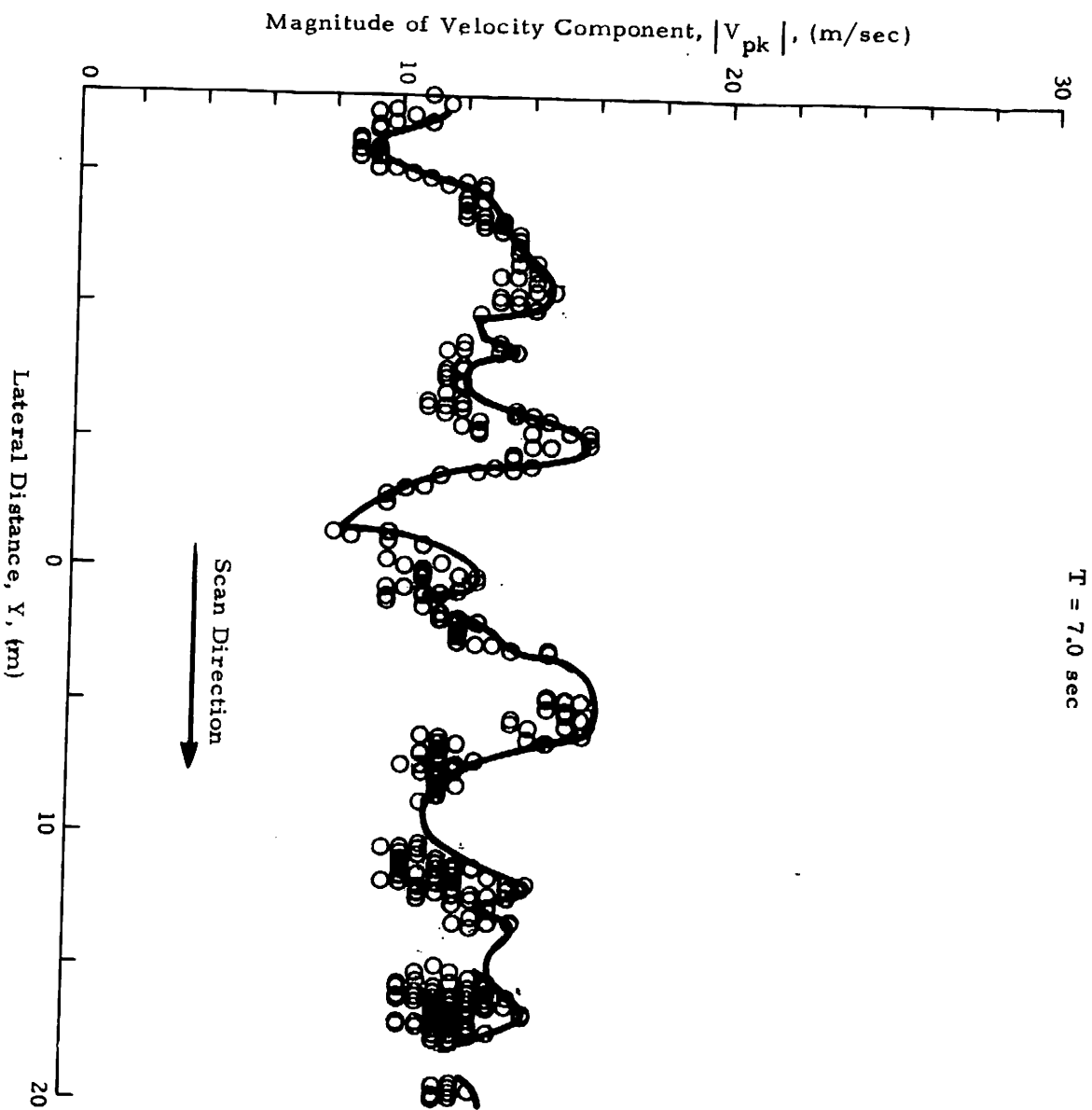


Fig. 16 (Continued)

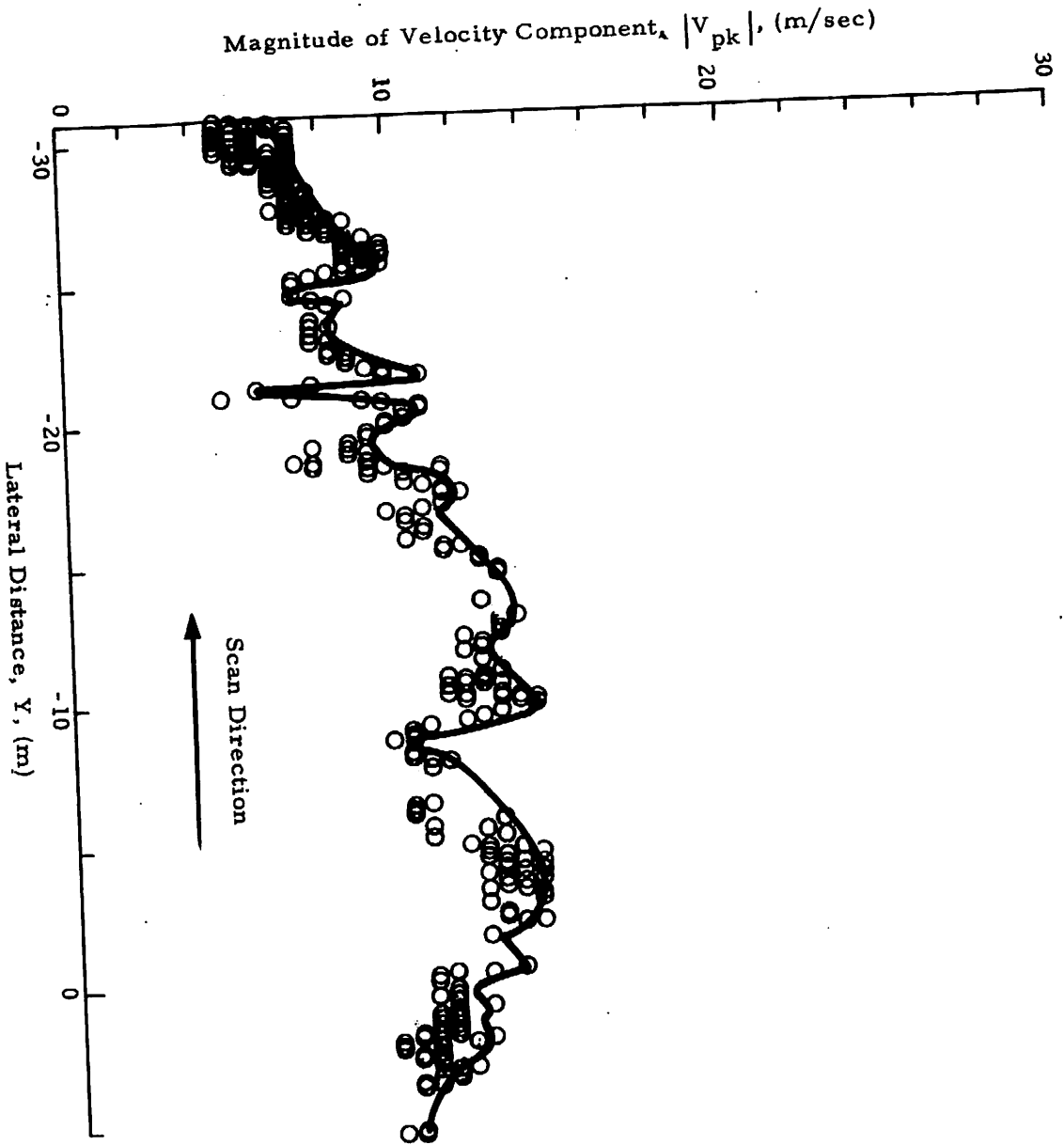


Fig. 16 (Concluded)

measurements,  $\theta$ , where  $y = -R \cos\theta$ . This resulted in a nonlinear lateral scale at extended distances from the flight path centerline.

To illustrate the maximum downwash or upwash velocities in the aircraft near wake, the highest values of  $|V_{pk}|$  occurring over 1 deg increments were faired by a smooth curve. The solid lines in the plots represent a faired curve through the highest LDV measurements given by the circles. Since the arc-scan measurements were made at an initial range equal or somewhat less than the airplane height, and since the maximum descent rate of the trailing vortices was on the order of 2 m/sec, the wake vortex remained essentially in the focal volume of the LDV system over the time period of 0 to 8 sec. Thus, the solid lines shown in Figs. 13 through 16 are indicative of the peak velocities observed with the LDV system in the aircraft near wake.

Available measurements of vortex lateral position obtained from a triangulation of simultaneous photographs or estimated from overhead photographs are also shown in Figs. 13, 14, and 15.

The spanwise downwash distribution for flyby 8, the 0-spoiler configuration, shows a well defined double-peak signature in most of the plots shown in Fig. 13 which is suggestive of a coherent vortex. For example, in Fig. 13 at  $t = 2.2$  sec, two broad peaks are observed separated by a spacing of 0.76 wingspan. The lack of signature in the inboard regions may be attributed to the lack of high velocities or aerosols near the flight path centerline. The two broad peaks become more well defined at later times ( $t = 3.3$  to 8.2 sec), showing a double-peak signature characteristic of the rotational velocity profile of a viscous vortex. The lateral separation and the maximum speed for the two double-peak signatures do not change significantly over this time range.

In contrast to the coherent wake structure observed earlier for the 0-spoiler configuration (Fig. 13), the downwash field for flybys 11, 12 and 13, where the two outer spoilers were deployed, shows a broad high amplitude region composed of narrower closely spaced peaks. This is suggestive of multiple

vortices and an incomplete vortex roll-up phase. These measurements indicate that the deployment of spoilers has a marked effect on the near-wake structure, tending to retard the early formation of a coherent trailing vortex pair. Analysis of the downwash field shown in Figs. 13 through 16 has been carried out to determine the basic characteristics of single and multiple vortices such as location, circulation strength, and the magnitude of the velocity component.

#### 4.1.2 Vortex Pair Characteristics

For the 0-spoiler configuration, the spanwise downwash distribution in the wake shows a well defined double-peak signature (Fig. 13). A double-peak signature is predicted theoretically when a vortex pair is interrogated in the arc-scan mode. For example, the magnitude of the line-of-sight velocity component for Rosamond flyby 11 at  $t \sim 2$  sec assuming a fully rolled-up vortex pair is shown in Fig. 17. The magnitude of the line-of-sight velocity generated by a distribution of  $N$  line vortices with the LDV located at the origin is given by

$$|V_{\ell os}| = \frac{1}{2\pi} \sum_{n=1}^N \Gamma_n \frac{[(Y_n - Y_o) X_o + (X_o - X_n) Y_o]}{[(X_o - X_n)^2 + (Y_o - Y_n)^2] [X_n^2 + Y_n^2]^{1/2}} \quad (3)$$

where  $(X_o, Y_o)$  is the location of the centroid of the focal volume, and  $(X_n, Y_n)$  and  $\Gamma_n$  are the coordinate and circulation strength of the  $n^{\text{th}}$  vortex, respectively.

In Fig. 17, the magnitude of the computed line-of-sight velocity is shown for a pair of line vortices with spacing  $b' = Kb = 41.8$  m and circulation strength  $\Gamma = U_{\infty} \bar{c} C_L / 2K = 606 \text{ m}^2/\text{sec}$  where the spanwise loading coefficient, wingspan, flight velocity, mean chord, and lift coefficient are taken to be  $K = 0.7$ ,  $b = 59.7$  m,  $U = 72.5 \text{ m/sec}$ ,  $\bar{c} = 8.3$  m,  $C_L = 1.41$ . The vortex pair was assumed to be located at an altitude of 180 m and the selected arc scan range was 183 m. The magnitude of the computed line-of-sight velocity for the vortex pair shows the characteristic double peak signatures noted earlier in the LDV measurements. The magnitude of the peak velocity is determined by the separation distance between

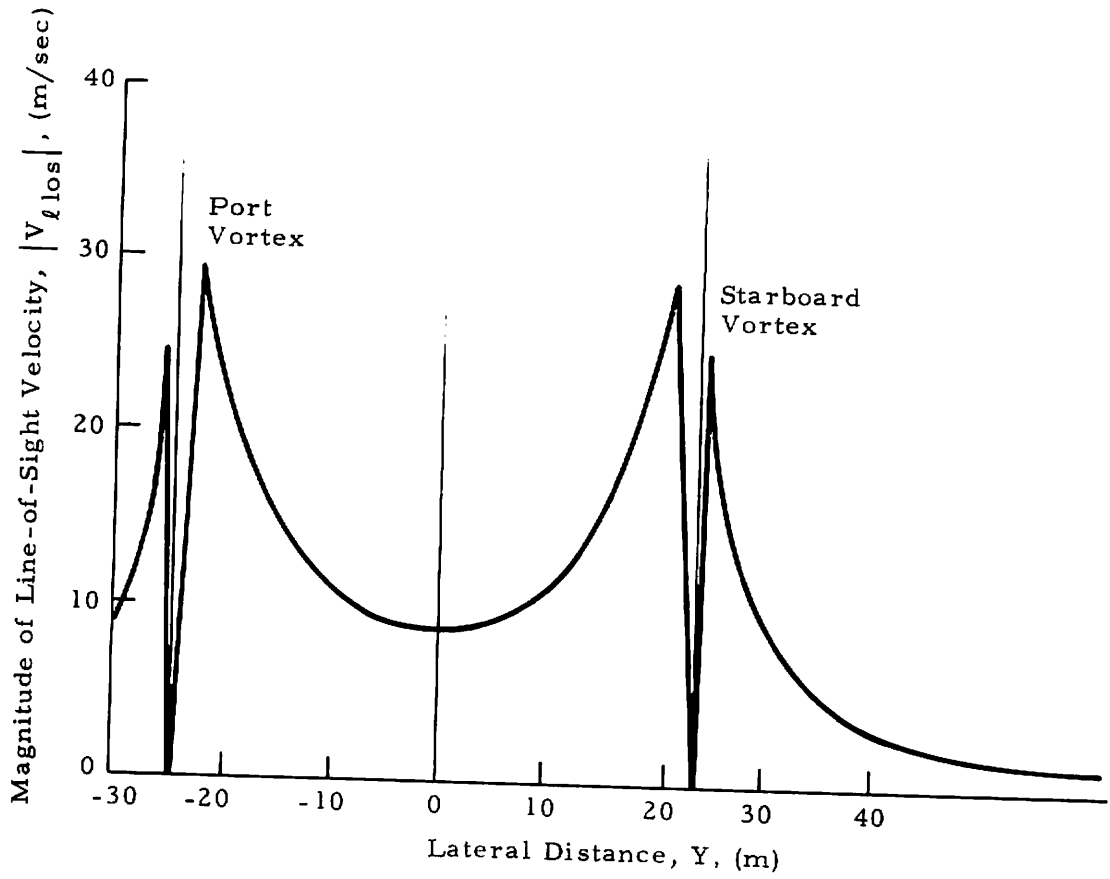


Fig. 17 - Magnitude of Line-of-Sight Velocity Component for Rosamond B-747 Flyby 11 at  $t \sim 2$  sec, Computed Assuming a Fully Rolled-Up Vortex Pair



the vortex pair and the scan arc. The slight asymmetry in the double peaks results from the velocity contribution of the adjoining vortex, the scan geometry, and the decrease in the contribution of the vortex rotational velocity along the line of sight at extended lateral distances from the centerline.

Note the two double-peak patterns in the  $V_{\text{LOS}}$  distribution in Fig. 17 at  $y = \pm 23$  m which correspond to the approximate location of the two vortices. As the vortex pair is traversed by the arc-scan pattern, the peak tangential velocity, resolved about the line of sight, is observed giving rise to the closely spaced double peaks. When the vortex center is intersected exactly by the arc scan, the location of the peaks is a measure of the vortex position, the magnitude of the peaks is indicative of the magnitude of the peak tangential velocity in the core, and the lateral separation between the peaks is a measure of the vortex core diameter. If the vortex is below (or above) the arc-scan, as shown in the sample simulation in Fig. 17, the vortex position is bounded by the lateral location of the two peaks, the magnitude of the two peaks is less than the peak tangential velocity, and the lateral separation between the two peaks is a function of the separation distance between the vortex and the scan arc.

The magnitude of the predicted line-of-sight velocity shown in Fig. 17 agrees with the trends shown by the 0-spoiler flyby (Fig. 13), while the 1, 2, 11, and 12-spoiler flybys (Figs. 14 to 16) are noticeably different. Since the LDV signature for flyby 8 is suggestive of a coherent vortex pair, it is useful to make a more detailed analysis of this case. From the seven scans shown in Fig. 13 the earliest scan showing the two double peak signatures was selected ( $t = 3.3$  sec); the minimum points were used to determine the lateral position of the port vortex (vortex altitude was assumed to be the scan range  $R = 240$  m), and the peak velocity magnitudes observed by the LDV for the port vortex were plotted as a function of radius about the vortex center in Fig. 18. For comparison, the magnitude of the velocity for a potential line vortex and a turbulent viscous vortex are also shown in Fig. 18 matched to the experimentally measured core circulation and core velocity.

LDV Measurements of Port Vortex, Flyby 8

Time = 3.3 sec

Core Radius = 4.5 m

Circulation =  $565 \text{ m}^2/\text{sec}$

○ Starboard Scan

□ Port Scan

Theory

— Hoffman & Joubert Model (Ref.7)

- - -  $1/r$  Field for Line Vortex with Circulation  $\Gamma = 565 \text{ m}^2/\text{sec}$

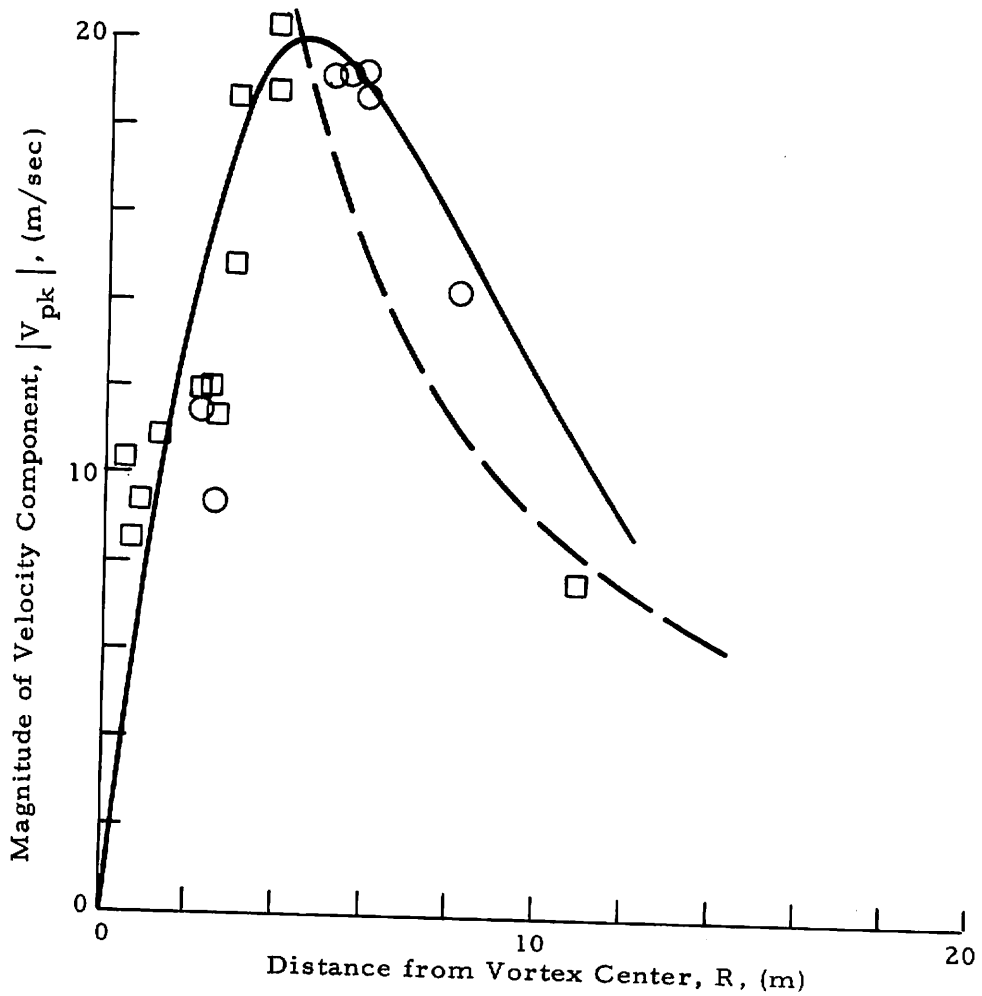


Fig. 18 - Magnitude of Wake Vortex Velocity Distribution with 0 Spoilers

The results in Fig. 18 indicate that the velocity distribution observed with the LDV is in general agreement with the theoretical model of Hoffman and Joubert near the core region of the vortex. In the outer flow region, the experimental velocity distribution decreases more rapidly than the theoretical logarithmic circulation model and approaches the  $1/r$  profile. However, sufficient scatter exists in the LDV data points to make a detailed comparison difficult, and agreement with other theoretical models is possible.

The circulation distribution derived from the vortex velocity distribution is shown in Fig. 19. Note that essentially all of the circulation is contained within the viscous core region of radius  $r_c = 4.5$  m and of circulation  $\Gamma_c = 565$  m<sup>2</sup>/sec. This suggests that the vortex roll-up process is complete for the 0-spoiler configuration at  $t = 3.3$  sec. In comparison, the predicted vortex circulation strength for this flyby is  $\Gamma = \frac{1}{2} U_\infty \bar{c} C_L / K = 565$  m<sup>2</sup>/sec, where the flight velocity, mean wing chord, lift coefficient and spanwise loading coefficient, are given by  $U_\infty = 73.6$  m/sec,  $\bar{c} = 8.3$  m,  $C_L = 1.41$ ,  $K = 0.762$ . The value of  $K$  was selected on the basis of the observed separation between the vortex pair. The circulation distribution predicted from the turbulent viscous vortex model using the observed core parameters is also shown in Fig. 19 where

$$\Gamma = \Gamma_c 1.83 (r/r_c)^2,$$

$$\Gamma = \Gamma_c [1 + 2.14 \log_{10} (r/r_c)],$$

in the inner and outer core regions, respectively.

#### 4.1.3 Multiple Vortex Characteristics

The spanwise downwash distributions for the 1, 2, 11, and 12-spoiler configurations (Figs. 14 to 16) showed multiple closely spaced peaks which did not resemble the velocity distribution predicted for a coherent trailing vortex pair (Fig. 17). Since the multiple high-velocity peaks in the near-wake downwash field are found in multiple vortex wakes; and the 1, 2, 11, and 12-spoiler configurations (flybys 11, 12, and 13) have been analyzed to identify possible multiple vortex characteristics.

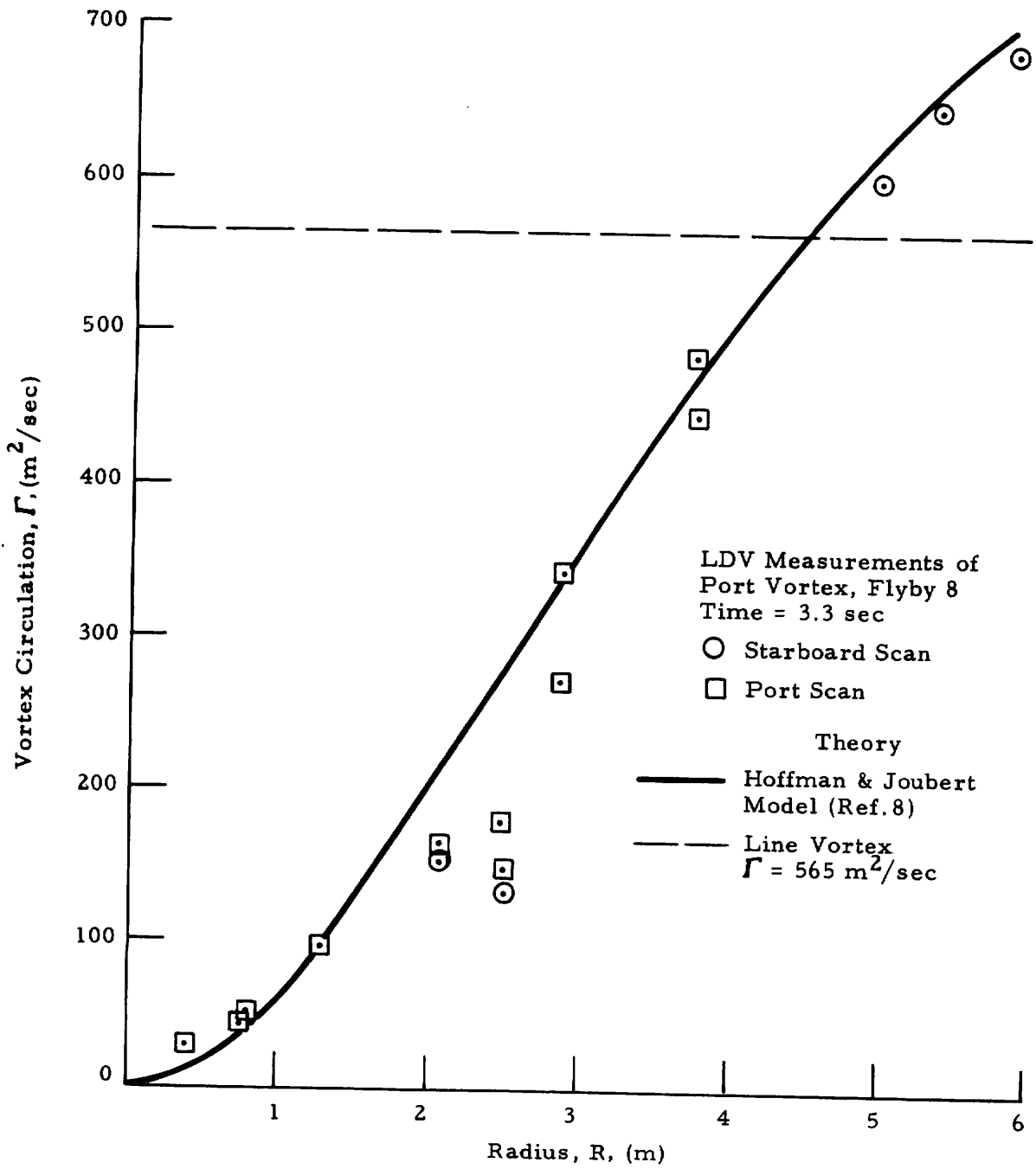


Fig. 19 - Circulation as a Function of Radius for 0 Spoiler Flight Configuration

The magnitude line-of-sight velocity component predicted for a B-747 aircraft assuming the multiple vortices are shed from the inboard and outboard flaps and wing tips is presented in Fig. 20. The strength and lateral spacing of the multiple vortices given on the top of Fig. 20 were calculated from the modified Betz roll-up technique (Ref. 9) and the altitude of the vortices was 180 m, and the arc scan range was 183 m. From the magnitudes of the velocity shown in Fig. 20 it is noted that the multiple vortices generate multiple peaks of varying magnitudes with the zero points occurring near the vortex locations. Assuming the LDV arc scan intersects the centers of the multiple vortices, the spacing and magnitudes of the multiple peaks can be used to deduce the location, strength, and magnitude of the peak velocity component of the wake vortices.

As an example, consider the profile shown in Fig. 14. Note that for the 1.5-sec plot high velocity magnitudes are recorded, but the peaks are scattered and it is difficult to distinguish the location of the multiple vortices suggested in Fig. 20. At 2.6 sec the multiple peaks in Fig. 14 are more ordered and resemble the line-of-sight velocity magnitudes predicted by the multiple vortex model. For example, the starboard vortex occupies a broad region spanning from approximately 3 to 40 m from the centerline, and the zero points occur at  $y \sim 0, 10, 15, 22,$  and  $30$  m at  $t = 2.6$  sec in Fig. 14. The superimposed predicted multiple vortex locations are at  $y = 3, 10.4, 14, 21.3,$  and  $29.6$  m (Fig. 20). Thus, the broad multiple peak regions in flyby 11 contain to some extent the multiple vortex peaks predicted from theory. A similar trend can be noted for the other 1, 2, 11, and 12-spoiler cases. In Fig. 15 at  $t = 2.4$  sec, the zero points on the starboard side are located at  $y \sim 0, 17, 25,$  and  $32$  m, and in Fig. 18 at  $t = 2.9$  sec, the zero points on the port side occur at  $y \sim 0, 5, 10$  and  $18$  m. Comparing all three 1, 2, 11, and 12 spoiler runs, it is observed that minimums occur in the downwash velocity profile repeatedly for lateral spacings of  $y \sim 0, 10, 15,$  and  $25$  m from the wake centerline.

These results suggest that three or four merged vortices are present in the near wake for each semispan. A more detailed analysis of the LDV measurements may establish the strength and core radii of these vortices.

$\Gamma_1 = 62.3 \text{ m}^2/\text{sec}$ ,  $\Gamma_2 = 433.5 \text{ m}^2/\text{sec}$ ,  $\Gamma_3 = -158.4 \text{ m}^2/\text{sec}$ ,  $\Gamma_4 = 298 \text{ m}^2/\text{sec}$ ,  $\Gamma_5 = -16.2 \text{ m}^2/\text{sec}$   
 $\Gamma_6 = -62.3 \text{ m}^2/\text{sec}$ ,  $\Gamma_7 = -433.5 \text{ m}^2/\text{sec}$ ,  $\Gamma_8 = 158.4 \text{ m}^2/\text{sec}$ ,  $\Gamma_9 = -298 \text{ m}^2/\text{sec}$ ,  $\Gamma_{10} = 16.2 \text{ m}^2/\text{sec}$   
 $y_1 = 29.6 \text{ m}$ ,  $x_1 = 180 \text{ m}$ ,  $y_2 = 21.3 \text{ m}$ ,  $x_2 = 180 \text{ m}$ ,  $y_3 = 14 \text{ m}$ ,  $x_3 = 180 \text{ m}$ ,  $y_4 = 10.4 \text{ m}$ ,  $x_4 = 180 \text{ m}$ ,  
 $y_5 = 3 \text{ m}$ ,  $x_5 = 180 \text{ m}$ ,  $y_6 = -29.6 \text{ m}$ ,  $x_6 = 180 \text{ m}$ ,  $y_7 = -21.3 \text{ m}$ ,  $x_7 = 180 \text{ m}$ ,  $y_8 = -14 \text{ m}$ ,  $x_8 = 180 \text{ m}$ ,  
 $y_9 = -10.4 \text{ m}$ ,  $x_9 = 180 \text{ m}$ ,  $y_{10} = -3 \text{ m}$ ,  $x_{10} = 180 \text{ m}$   
 (Subscripts 1-5 Starboard Vortices, 6-10 Port Vortices)

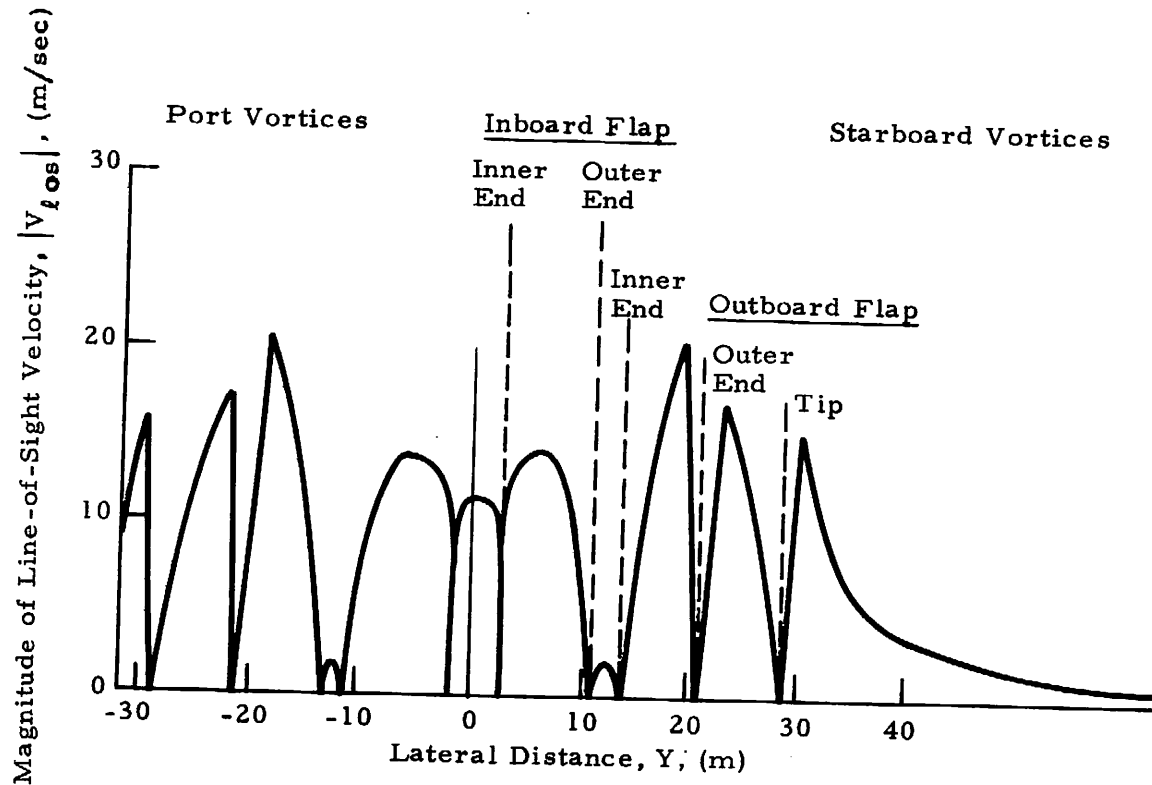


Fig. 20 - Magnitude of Line-of-Sight Velocity Component for Rosamond B-747  
 Flyby 11 at  $t \sim 2$  sec, Computed Assuming Multiple Wake Vortices

However, the LDV measurements have shown that multiple vortices exist in the near wake of the B-747 aircraft when spoilers are deployed, whereas a coherent rolled-up trailing vortex pair exists in the near wake for 0 spoilers.

## 4.2 VORTEX TRANSPORT

The line-of-sight velocity measurements obtained by the LDV in the wake of the B-747 aircraft in the finger-scan mode have been processed to yield the altitude and lateral position of the vortices, and have been compared with photographic and theoretical wake trajectories. The following analysis of the vortex transport characteristics includes the early near-wake flow as well as the subsequent far-wake transport process.

### 4.2.1 Near-Wake Vortex Tracks

From the Rosamond wake measurements, those flybys where photographic measurements of the near-wake trajectory were available for comparison with the LDV tracks have been selected. The near wake was assumed to be the region within 20 spans downstream of the aircraft,  $x/b \leq 20$ .

The lateral versus horizontal wake vortex location 5 to 10 sec after aircraft passage is shown in Figs. 21 and 22. The LDV and photographic measurements indicate that the center of the wake vortex pair is located at approximately 80% semispan and descends at  $\sim 1.5$  m/sec over the 4 to 10 sec interval. However, as much as a 15% scatter in the vortex lateral location and 50% scatter in the descent rate can be noted in the initial vortex trajectories which may be associated with uncertainties in the airplane location or may be due to the different flight configurations. The photographic measurements shown in Figs. 21 and 22 are in general agreement with the LDV trends.

### 4.2.2 Far Wake Vortex Tracks

The line-of-sight velocity measurements obtained with the LDV system in the finger-scan mode have been processed with the VAD and Vortex Track Program and the  $I_{pk}$  program to determine the far-wake vortex trajectories.

Solid Symbols Photo, Open  
 Symbols LDV Measurements

Flyby	Aircraft Alt. (m)
○ 27	67
◇ 28	66
△ 30	66

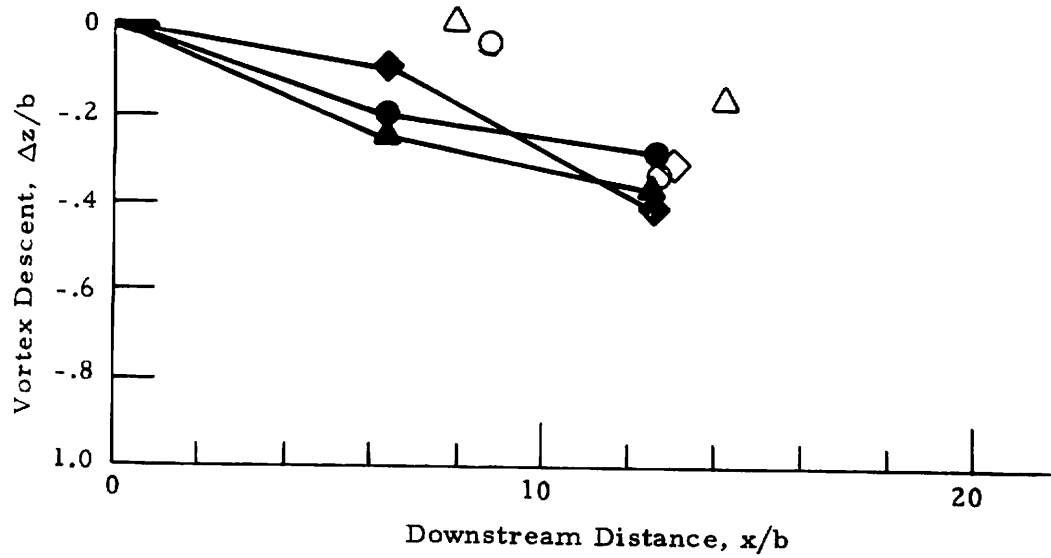


Fig. 21 - Vortex Descent as a Function of Downstream Distance  
 for Flybys with 30/30 Flaps, 0 Spoilers



Solid Symbols Photo, Open  
Symbols LDV Measurements

Flyby

○ 27

◇ 28

△ 30

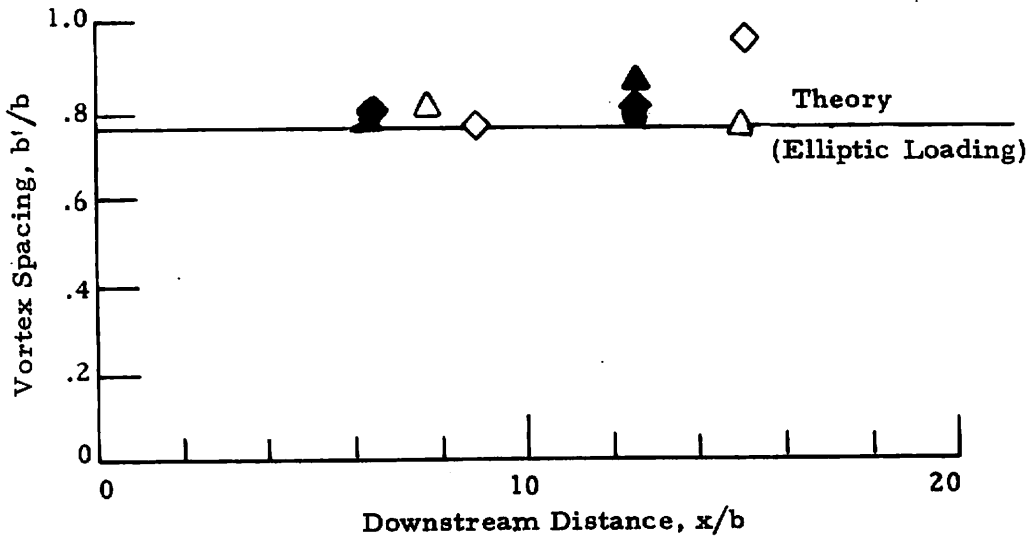


Fig. 22 - Vortex Spacing as a Function of Downstream Distance  
for Flybys with 30/30 Flaps, 0 Spoilers

The regions of the maximum backscatter intensity were used to locate the vortex core region. The wake vortex tracks from the Rosamond tests include the results from the low-speed data and high-speed data.

#### 4.2.2.1 Low-Speed Data

The wake vortex trajectories from the low-speed LDV measurements are presented in Appendix D. From the wake vortex trajectories presented in Appendix D, the following wake transport characteristics can be noted: (1) the wake vortex descends nearly vertically with very little horizontal motion; (2) the initial descent rate over the period 0 through 20 sec after aircraft passage is in general agreement with the prediction; and (3) the wake descent diminishes after 20 sec and the vortex tends to remain at a constant altitude in ground effect. In addition to the above trends, some scatter is noted in the location of the vortices. Since both the photographic and LDV tracks show the vortex wandering in lateral position and altitude, particularly at late times, this is believed to be the effect of random atmospheric winds and gusts. However, in some cases, a large scatter is noted in the LDV vortex tracks which is not seen in the corresponding photographic measurements. This has been investigated using the high-speed data since accurate determination of the vortex position is a prerequisite in determining other relevant parameters such as the decay of the vortex rotational velocity and circulation strength.

#### 4.2.2.2 High-Speed Data

The wake vortex tracks computed from the high-speed LDV data using the  $I_{pk}$  algorithm are given in Appendix E for flybys 27, 28, 44, 47, 48, and 49. The vertical and lateral vortex trajectories computed from the high-speed data show the same trends as the low-speed tracks discussed earlier.

Comparison of the high-speed wake vortex measurements with the observed photographic vortex position is shown in the  $V_{pk}$  versus elevation angle curves in Figs. 23 and 24. With the exception of any dominant low

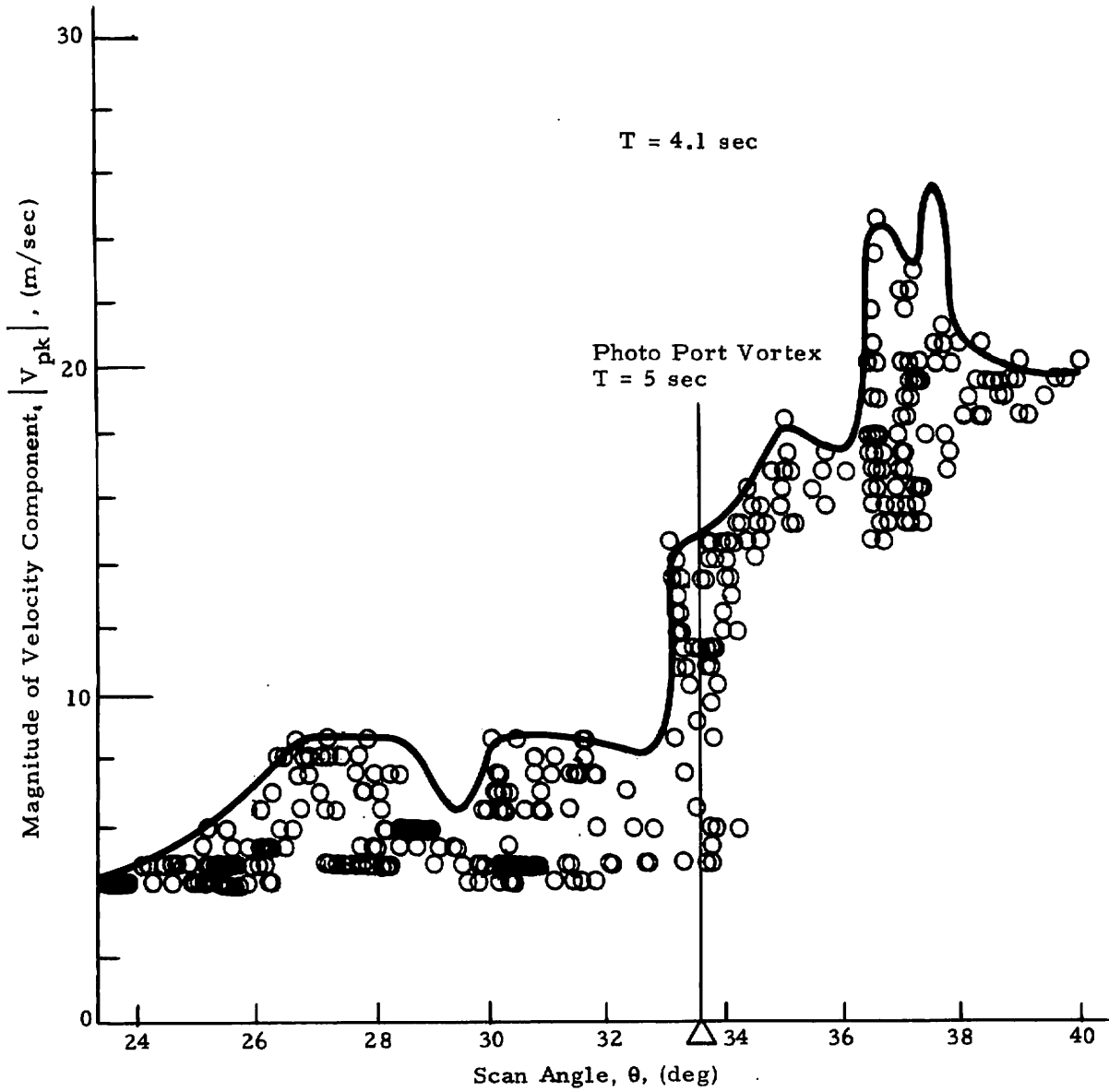


Fig. 23 - Comparison of Photographic and LDV Measurements for Rosamond B-747 Flyby 27

Flyby 27  
T = 6.6 sec

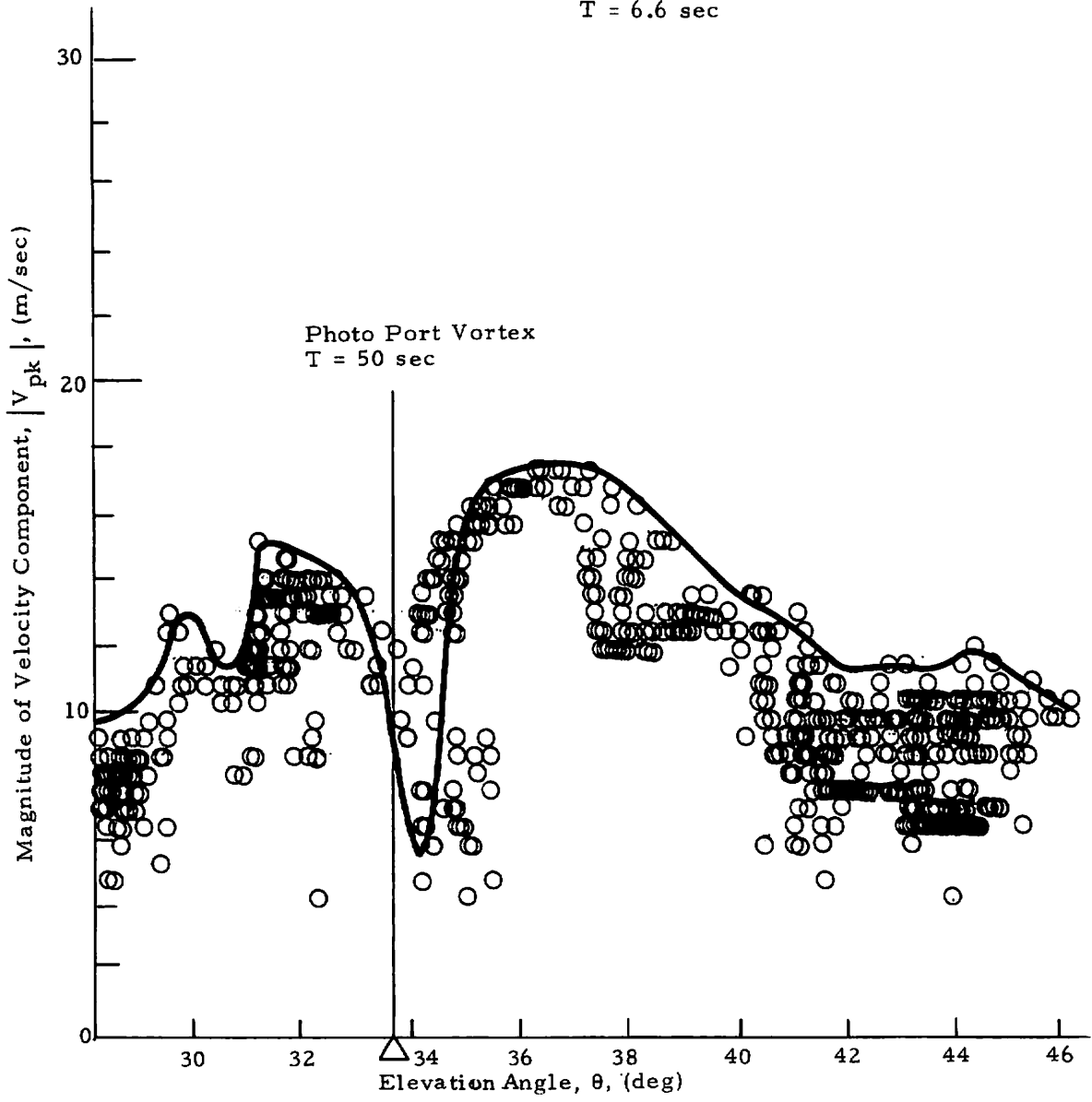


Fig. 23 (Continued)

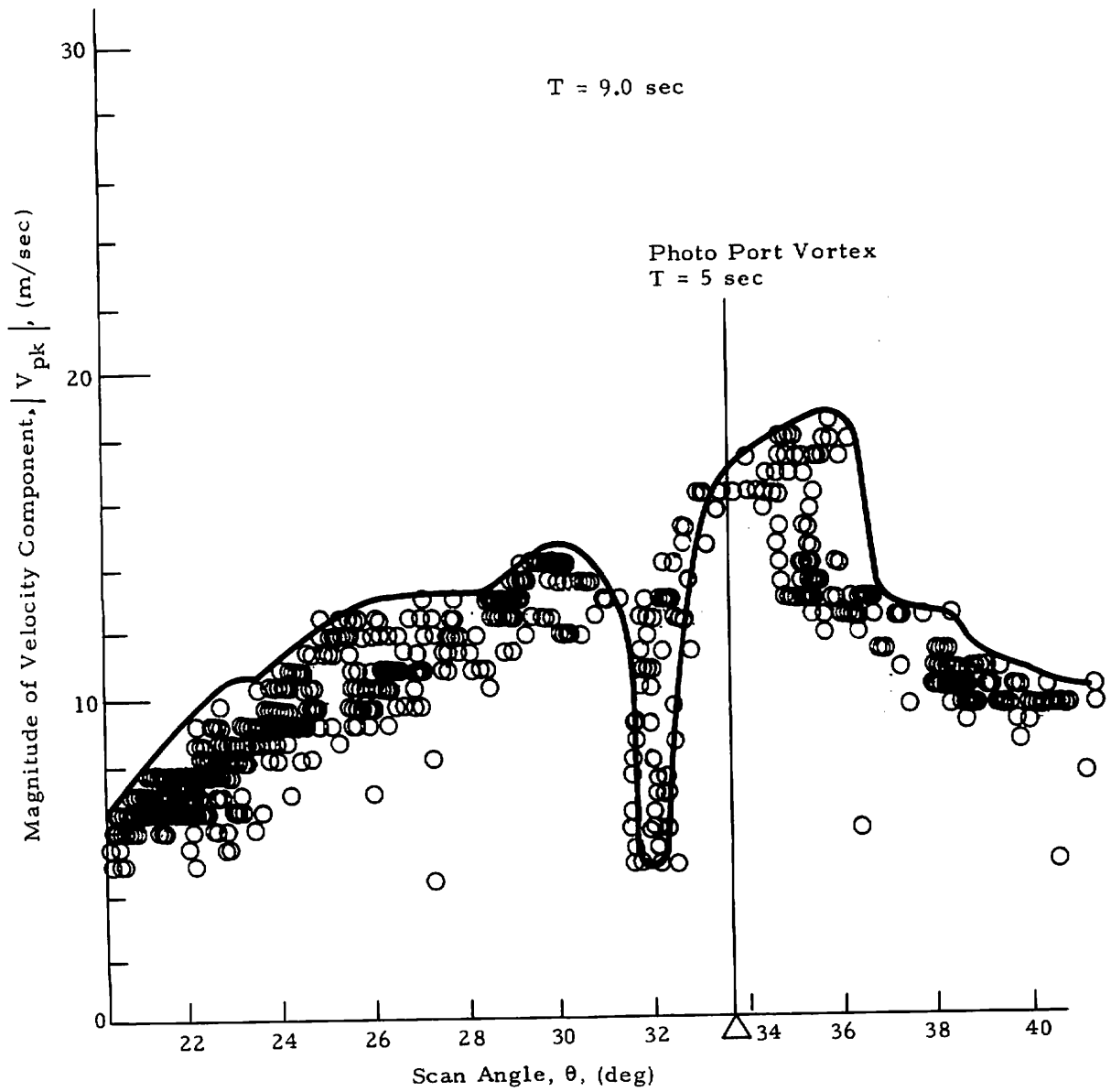


Fig. 23 (Continued)

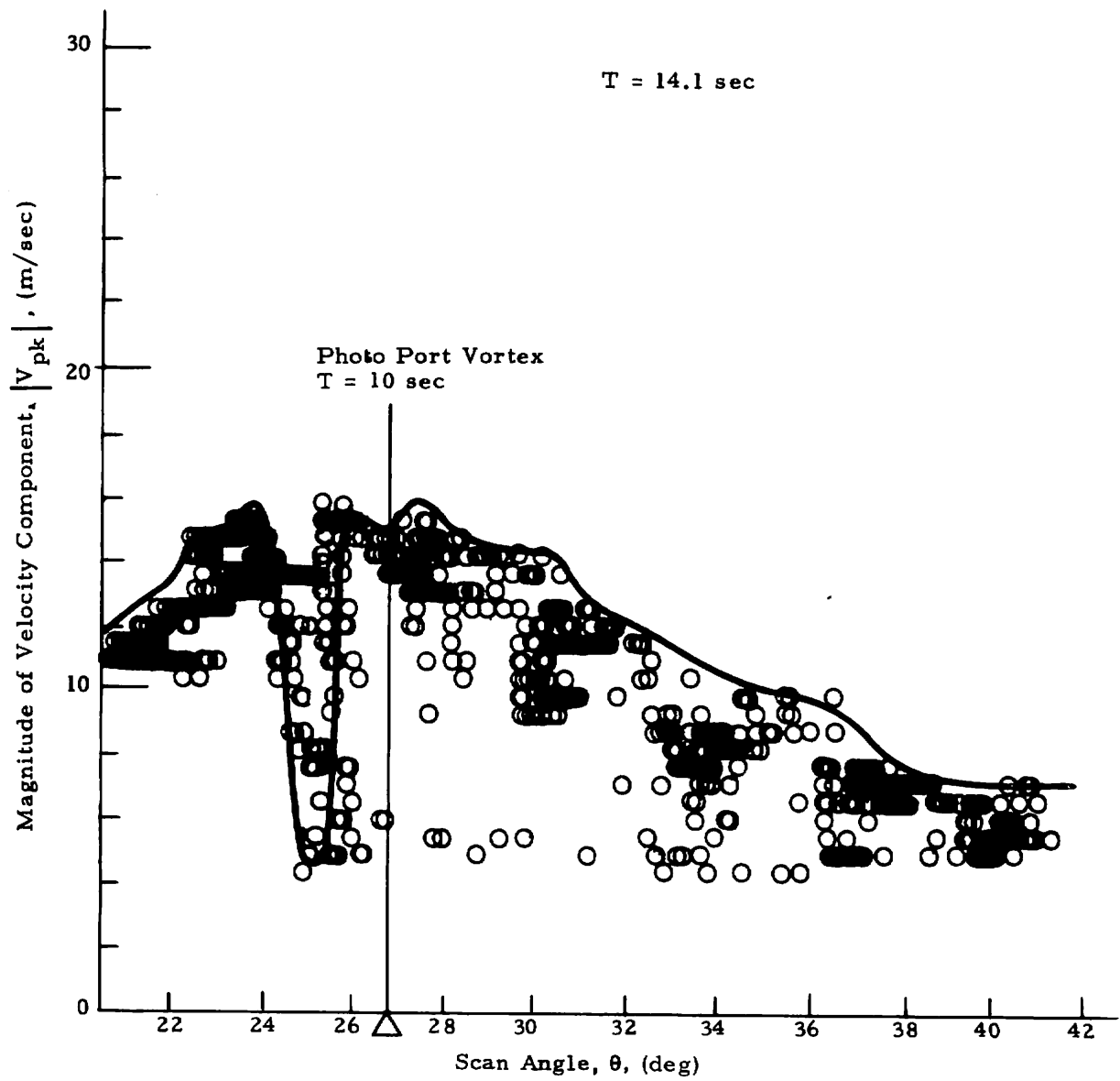


Fig.23 (Concluded)

magnitude spikes, the solid line in the plots connects the maximum values of  $|V_{pk}|$  observed by the LDV in the finger scan mode for one scan between the two elevation angle limits (i.e., it represents the maximum value of  $|V_{pk}|$  for many finger-scan lobes). Since the LDV is scanned rapidly in range (3.5 Hz) and slowly in elevation angle (0.2 Hz), the peaks in the  $|V_{pk}|$  versus elevation-angle curves indicate the elevation angle at which the maximum line-of-sight velocity is observed by the LDV system. Thus, when a vortex is interrogated by the LDV system, two maxima occur in the  $|V_{pk}|$  versus elevation angle at those angles where the line of sight is tangent to the vortex core and a minimum occurs at the mid-elevation angle, or in other words, a double-peak signature results. The low magnitude spike bounded by the high amplitude peaks marks the vortex core, and here, the minimum  $|V_{pk}|$  points are connected. For a number of LDV measurements, this double-peak signature can be clearly recognized; for example, at  $t = 6.6, 9.0$  and  $14.1$  sec for flyby 23 (Fig. 27) and at  $t = 4.2$  and  $14.2$  sec for flyby 28 (Fig. 24). In addition, the elevation angle at which these double-peak patterns occur is often within a few degrees of the vortex elevation angle measured photographically.

While the photographic and LDV measurements agree well for some scans in terms of the location of the vortex signature, for other scans, the scatter in elevation angle is as high as 6 deg (Fig. 24,  $t = 5$  and  $9$  sec). It is possible that the core diameter of the vortex is small, and the scan pattern misses the peak-tangential velocity regions. It is also possible that the photographic measurements may be subjected to some errors, or that the smoke does not mark the exact vortex location accurately. Lastly, the error may be a result of anomalies in the determination and processing of the LDV elevation angle.

#### 4.3 VORTEX DECAY

Information regarding the decay of wake vortices such as the time history of the peak tangential velocity, circulation and viscous core radius is contained in the line-of-sight velocity magnitudes measured by the LDV system.

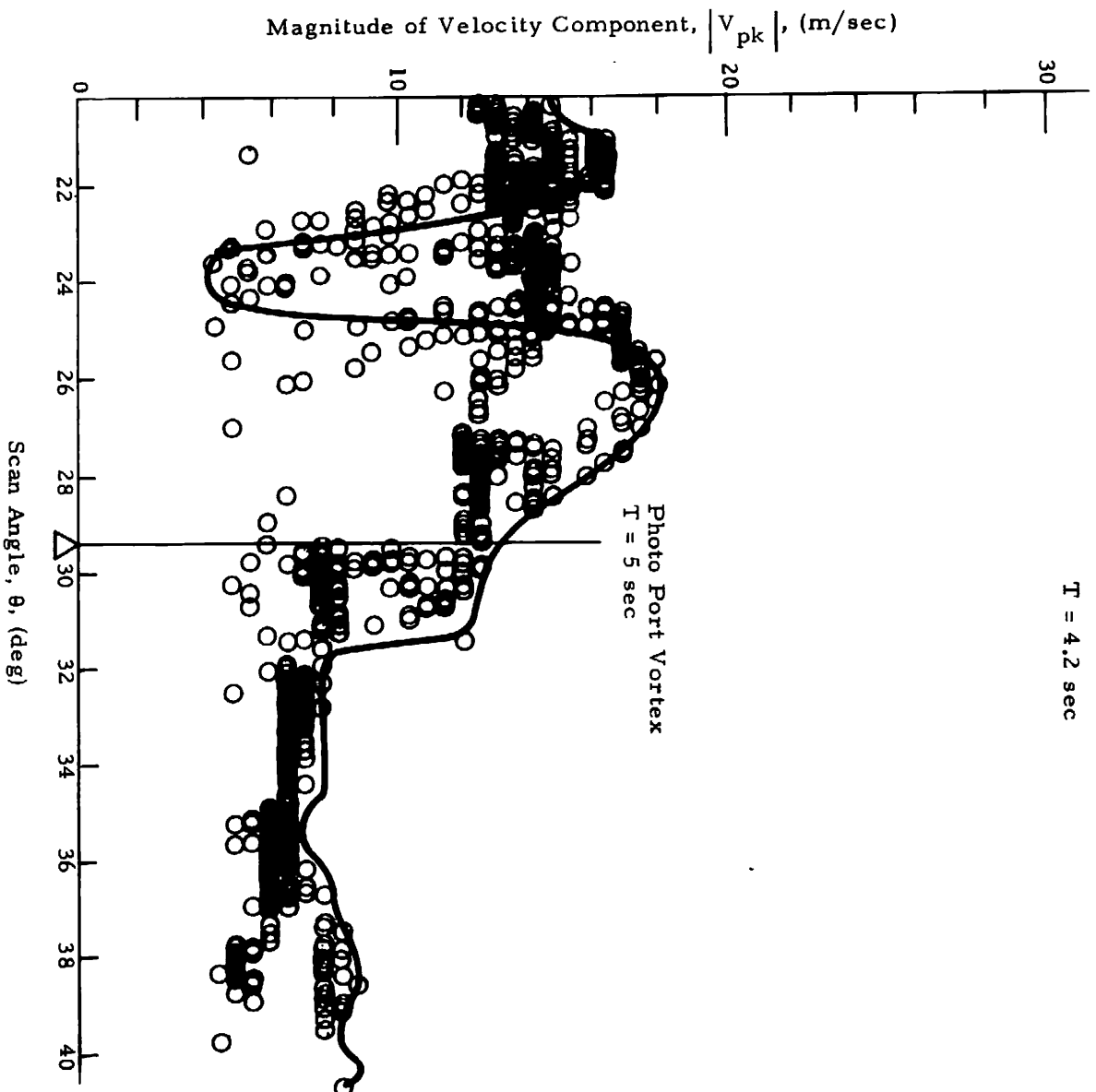


Fig. 24 - Comparison of Photographic and LDV Measurements  
for Rosamond B-747 Flyby 28



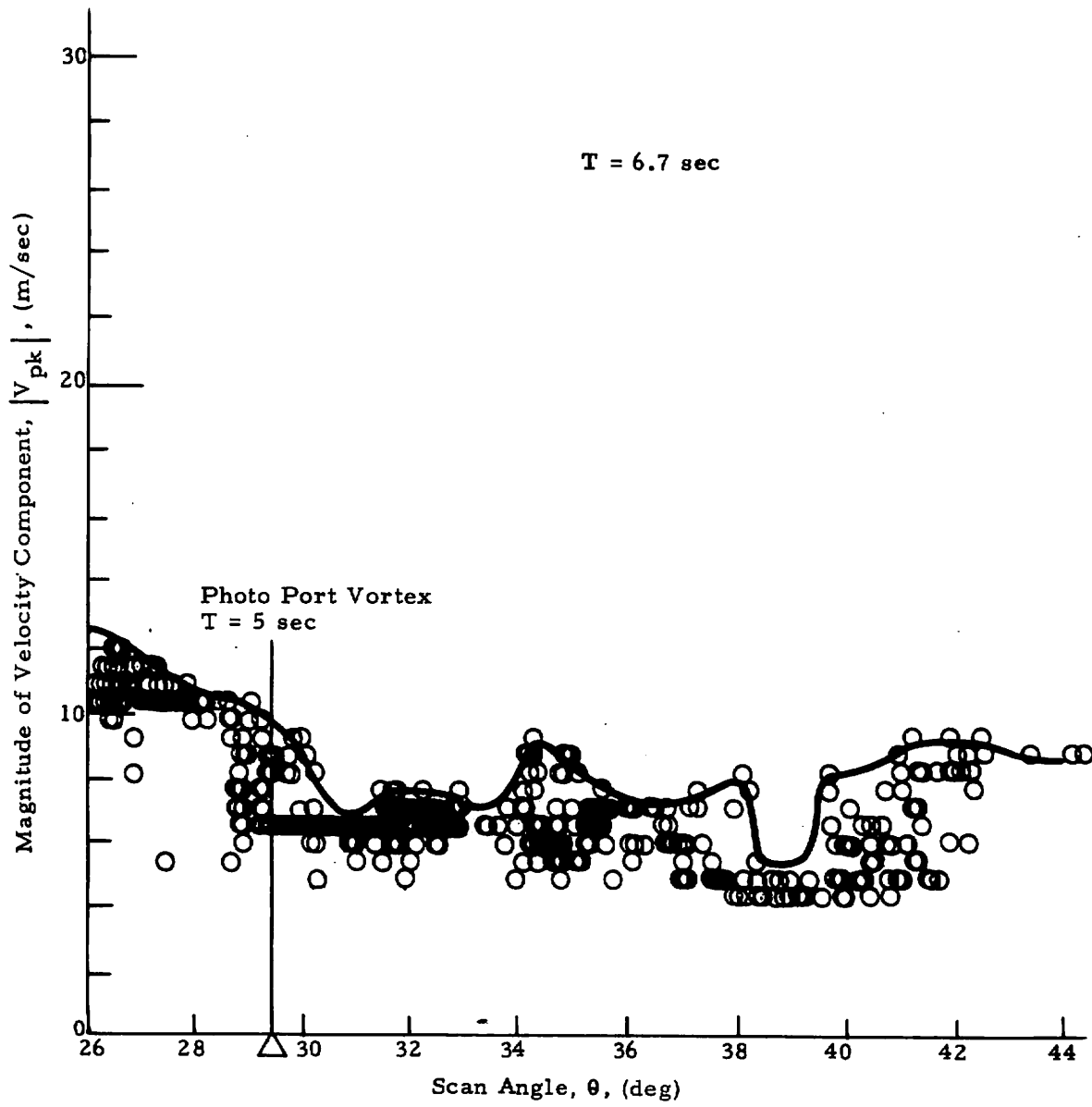


Fig. 24 (Continued)

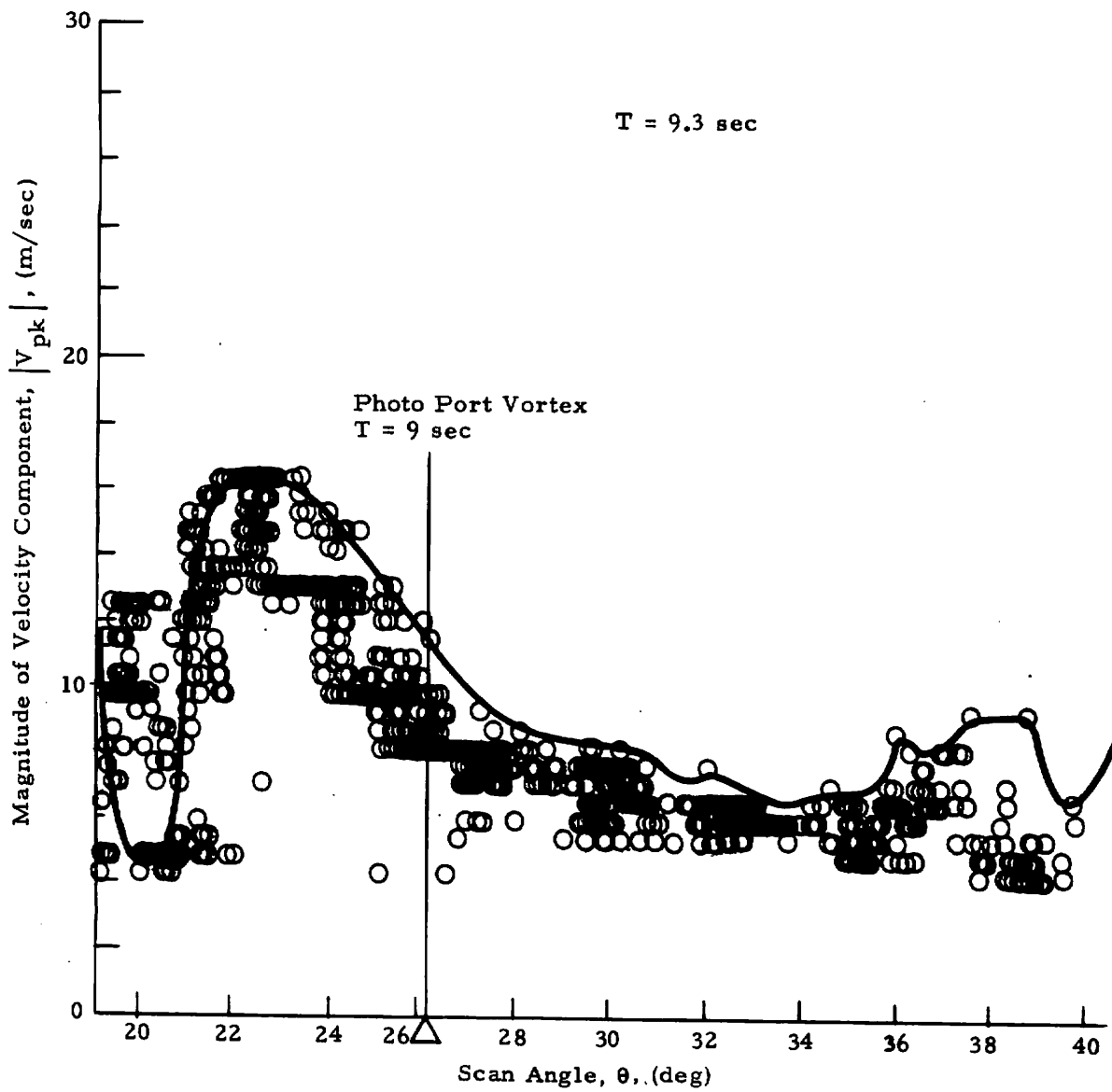


Fig. 24 (Continued)

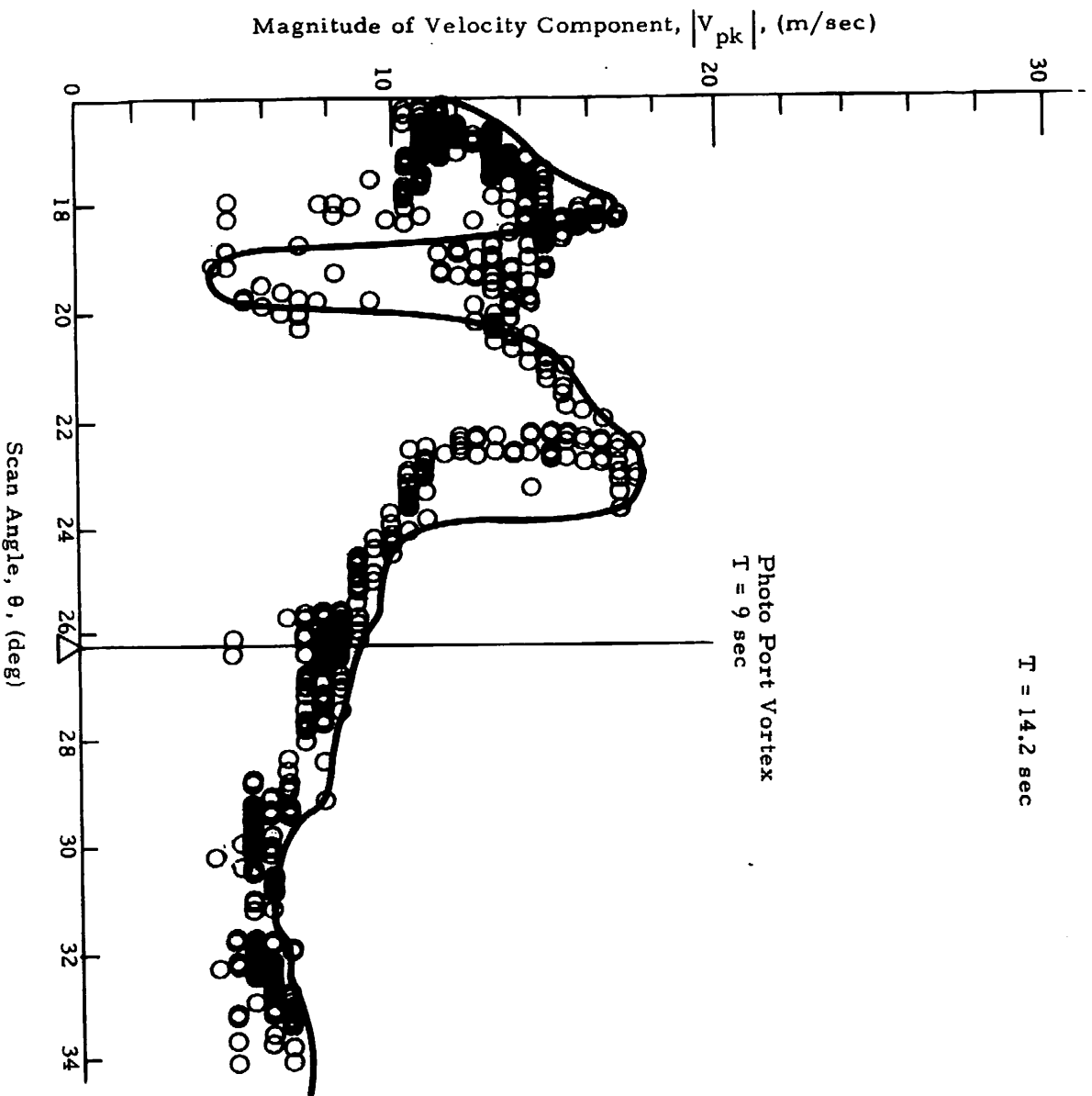


Fig. 24 (Concluded)

#### 4.3.1 Decay of Vortex Rotational Velocity

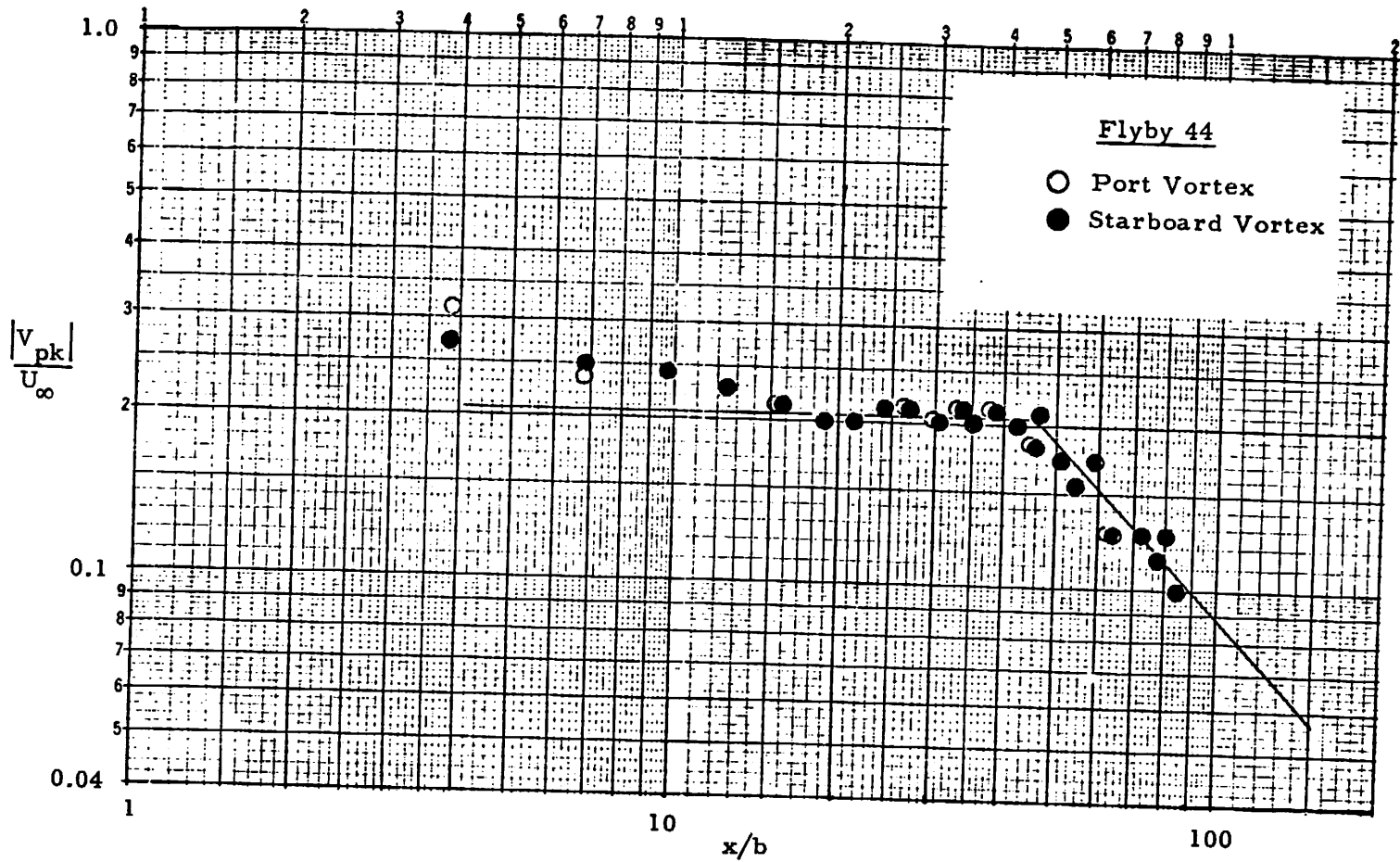
To determine the decay of the wake vortex rotational velocity from the LDV line-of-sight velocity magnitudes, two basic methods were used to pick out the maximum tangential velocity of the vortex:

- a. Selection of the maximum value of  $|V_{pk}|$  (or  $|V_{ms}|$ ) occurring during each scan between minimum and maximum elevation settings.
- b. Selection of the maximum value of  $|V_{pk}|$  occurring within  $\pm 3$  deg of the known elevation angle of the vortex.

For both techniques, the maximum value of  $|V_{pk}|$  is a good measure of the magnitude of the peak tangential velocity of the vortex if the LDV line of sight is tangent at some point with the circular core region of the vortex, and the vortex range falls within the focal volume. However, in the first approach, the  $|V_{pk}|$  time history becomes meaningless if the vortex drifts out of the scan area. To eliminate this uncertainty, in the second approach, other information, i.e., photographic vortex position, is used to establish the approximate location of the vortices. These regions are then searched for the maximum  $|V_{pk}|$  values which are associated with the vortex phenomena.

The  $|V_{pk}|$  and  $|V_{ms}|$  time histories determined using the first technique are shown in Appendix F. A bandwidth criterion of  $N \geq 2$  was used in the analysis to filter out random high-frequency noise (i.e., at least two of the 100 frequency bins had to be activated for the data to be used). A sample of the results, presented in Fig. 25, indicates that the wake vortex rotational velocity is nearly constant approximately 50 spans downstream of the aircraft followed by  $1/\text{time}$  decay. Some scatter which may be associated with the uncertainty in vortex location may be noted in the velocity decay curve.

Using the photographic vortex tracks to determine the approximate vortex location (the second technique above), the  $|V_{pk}|$  time history has been



82

Fig. 25 - Decay of Magnitude of Wake Vortex Rotational Velocity Component for Flyby 44

recomputed for flybys 27 and 28 and is presented in Figs. 26 and 27. The results shown in Figs. 26 and 27 also indicate a nearly constant magnitude of the vortex velocity component within 50 spans downstream of the aircraft. Less scatter occurs in  $|V_{pk}|$  versus time plots when the photographic tracks are used to establish the vortex center. Unfortunately, photographic measurements were not available at late times to establish the final vortex decay process.

#### 4.3.2 Core Radius Time History

The vortex core radius was determined from the observed variations in  $|V_{pk}|$  with range and elevation angle according to the technique discussed earlier in Section 2.1.2. The computed vortex core radius time history for flybys 27, 28, and 44 is given in Figs. 28, 29, and 30, respectively. Photographic vortex tracks were compared with LDV  $|V_{pk}|$  distributions to compute the core radius time history in Figs. 28 and 29, while the predicted vortex tracks were used to compute the core radius time history in Fig. 30. The LDV wake vortex measurements show that the vortex core radius is approximately constant in the aircraft near wake. The observed core radius ranges from 1 to 4 m, and the mean core radius is approximately 2 m.

#### 4.3.3 Circulation Decay

The circulation time history was computed from the observed LDV line-of-sight velocity distribution using: (1) the vortex tracks from the low-speed data, and (2) the photographic tracks to determine the vortex location. In the first technique, the circulation was determined from the average moment of the line-of-sight velocity components within a correlation radius of the computer vortex center. In the second technique, the circulation was computed from the moment of the two maximum  $|V_{pk}|$  values adjacent to the center of the vortex as outlined earlier in Section 2.1.2, and the photographic vortex tracks were used to determine the vortex location. It was found that this technique was very sensitive to errors in core radius.

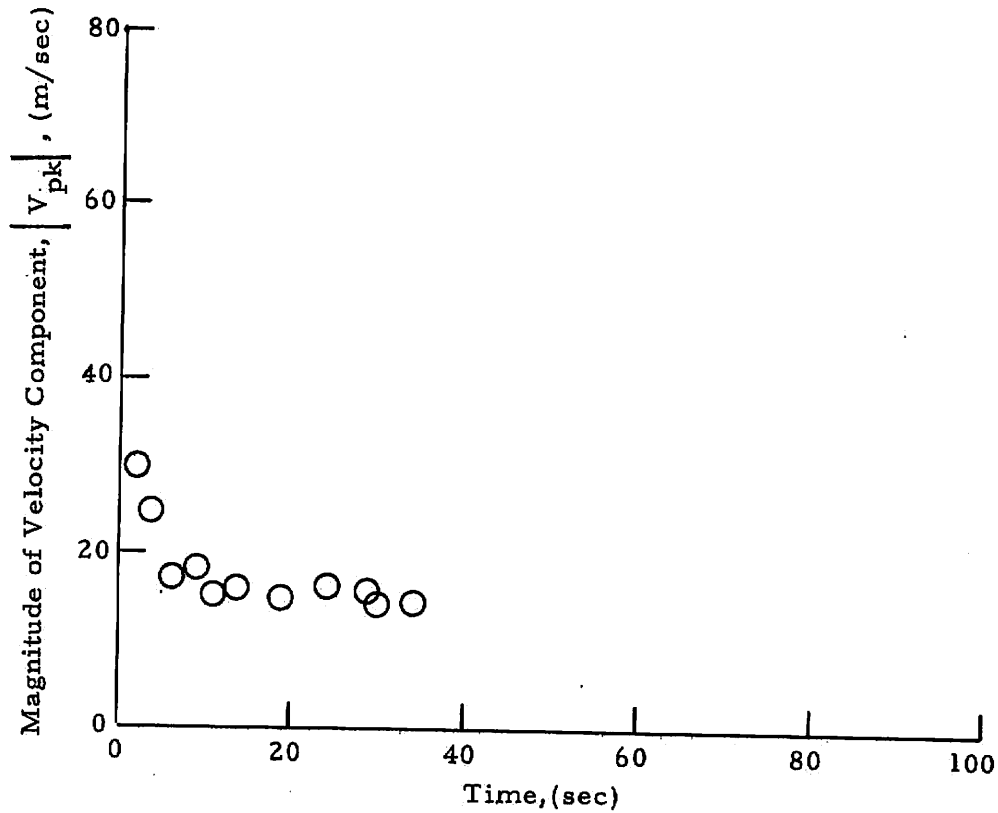


Fig. 26 -  $|V_{pk}|$  as a Function of Time for Flyby 27 Using Photographic Tracks to Locate the Vortex Center

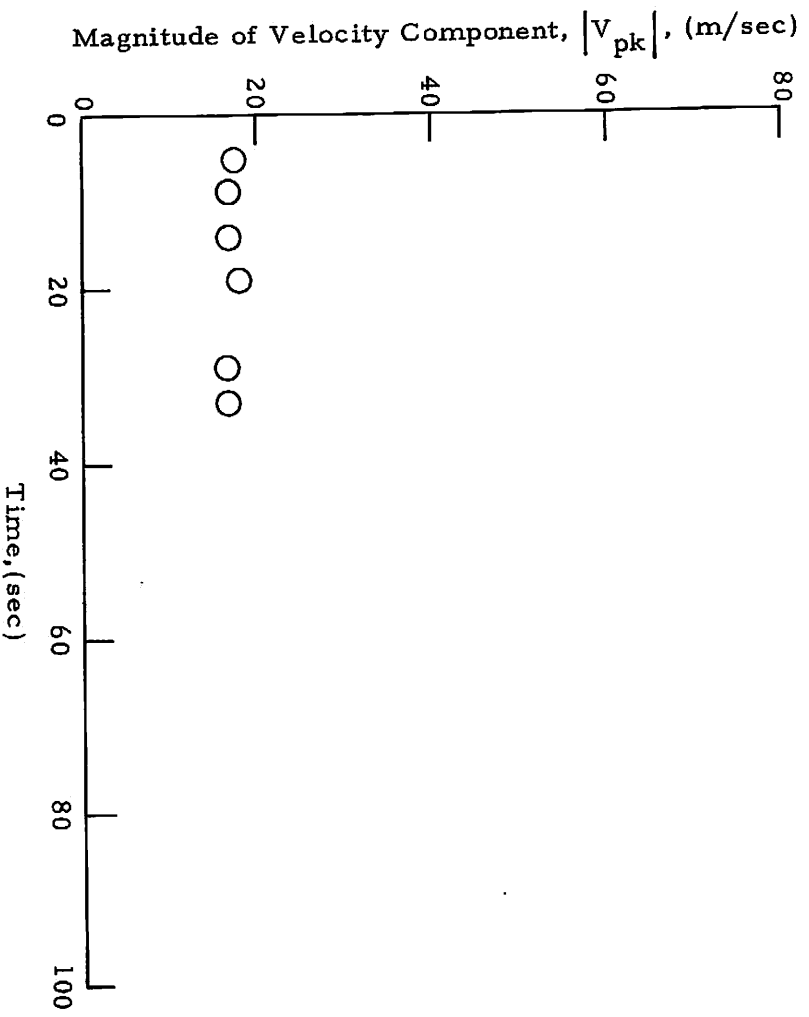


Fig. 27 -  $|V_{pk}|$  as a Function of Time for Flyby 28 Using Photo-  
graphic Tracks to Locate the Vortex Center



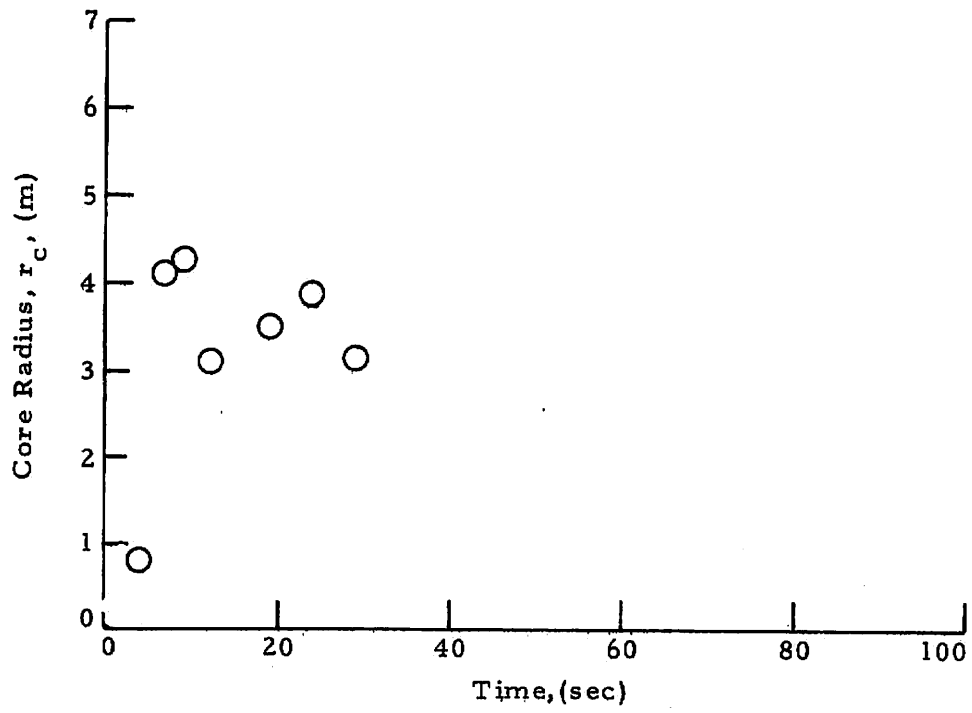


Fig. 28 - Vortex Core Radius as a Function of Time for Flyby 27

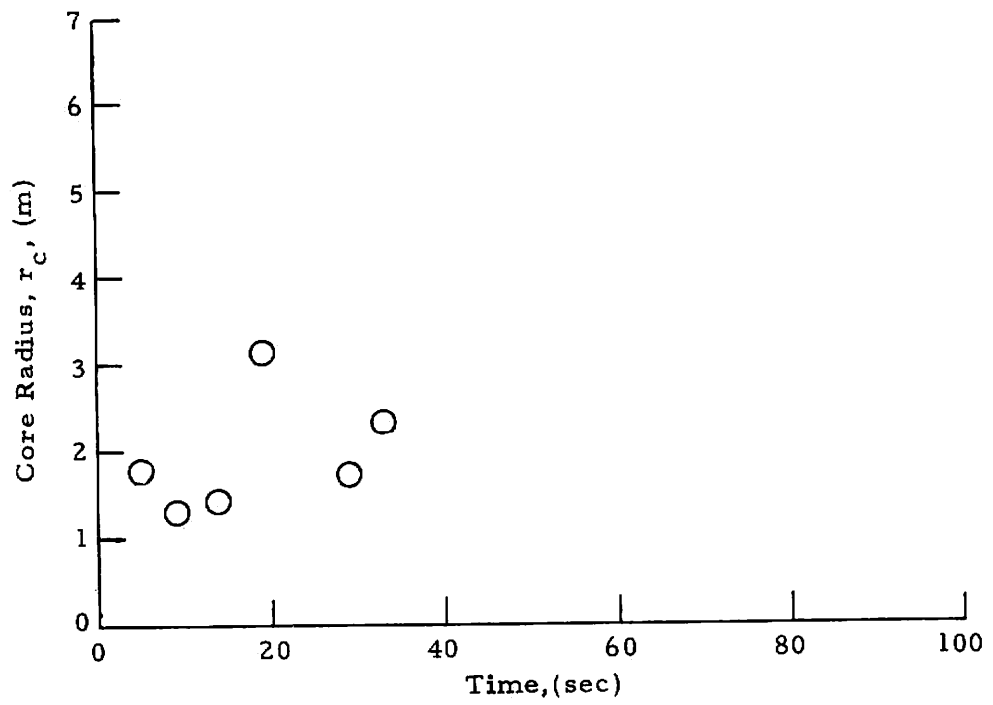


Fig. 29 - Vortex Core Radius as a Function of Time for Flyby 28

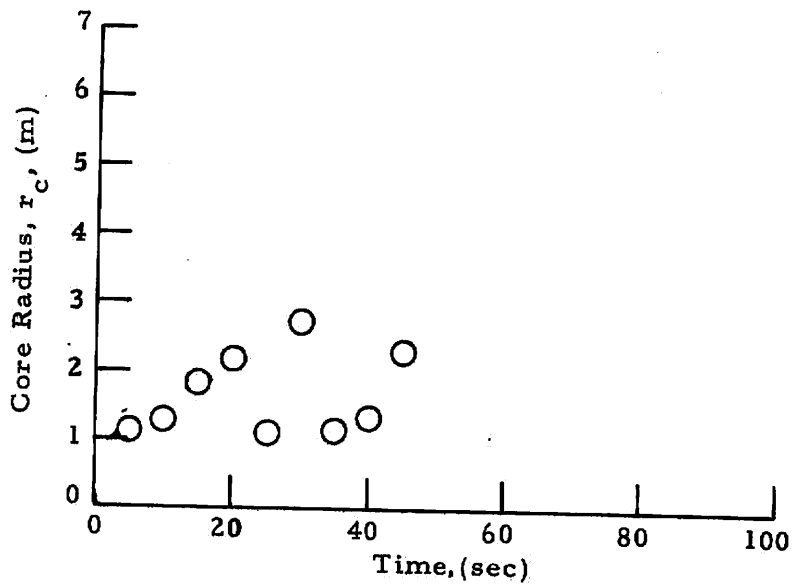


Fig. 30 - Vortex Core Radius as a Function of Time for Flyby 44

The circulation time history computed from the low-speed data vortex tracks is shown in Appendix G. The computed circulation is shown from 20 sec to the time of the last measurement. At periods earlier than a few sec, circulations are not shown since the vortex may not be fully rolled up. The general circulation decay trend is similar to the velocity decay trends noted earlier - relatively small decay initially followed by rapid decay in the far wake. More scatter is evident in the circulation distributions than the velocity or core radius distributions presented earlier because the circulation involves the product of the scatter of the previous two measurements. To reduce this scatter, the circulation has been recomputed using the photographic vortex tracks to define the vortex center more closely.

#### 4.3.4 Comparison of Vortex Decay Trends for Different Flight Configurations

To determine the vortex decay trends for different flight configurations, the time history of the vortex rotational velocity, circulation, and core radius presented earlier can be cross correlated. The decay of the wake vortex rotational velocity for different spoiler and flap and landing gear settings and flight paths is compared in Figs. 31 through 34, respectively. These results indicate that the deployment of spoilers decreases the vortex rotational velocity in the near wake while flap and landing gear settings and aircraft flight path angle do not appear to have a significant effect. However, care must be used in interpreting the above results since for some of the runs the wake vortices drifted out of the field of view (see Appendix D).

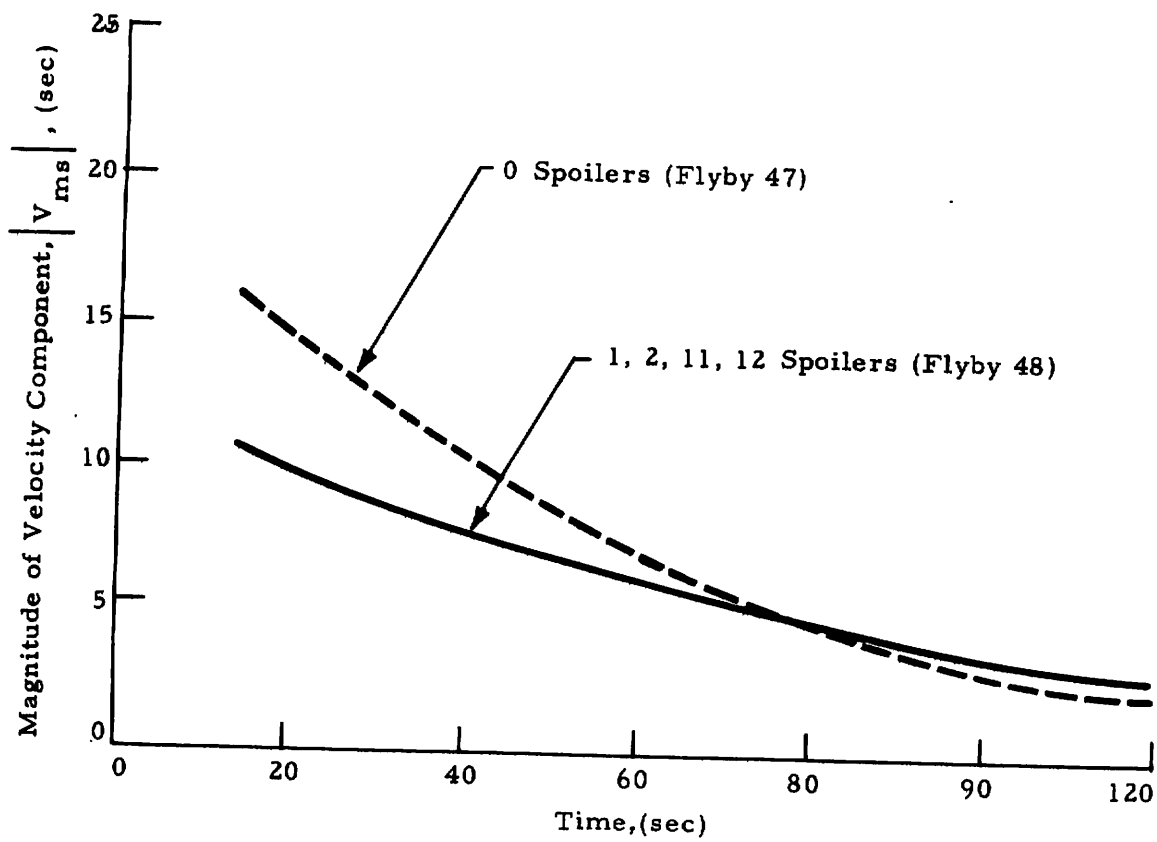


Fig. 31 - Comparison of Magnitude of Wake Vortex Rotational Velocity Component for B-747 Flybys With and Without Spoilers

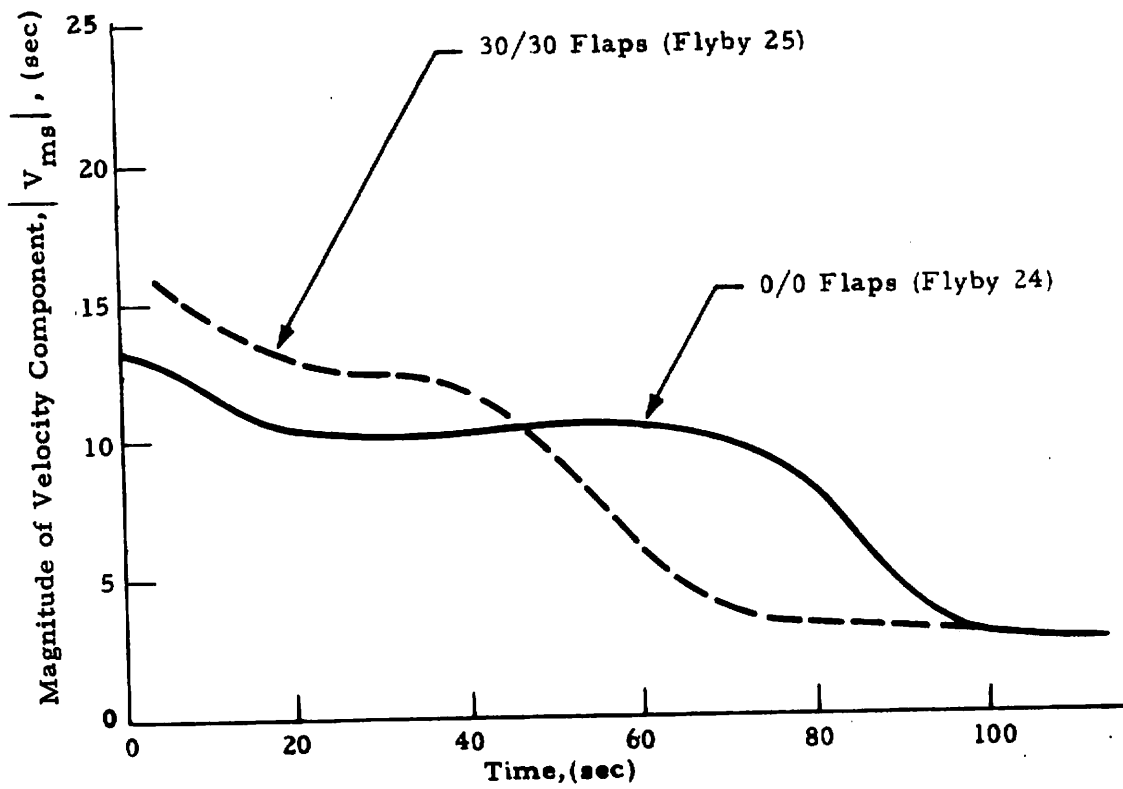


Fig. 32 - Comparison of Magnitude of Wake Vortex Rotational Velocity Component for B-747 Flyby With and Without Flaps

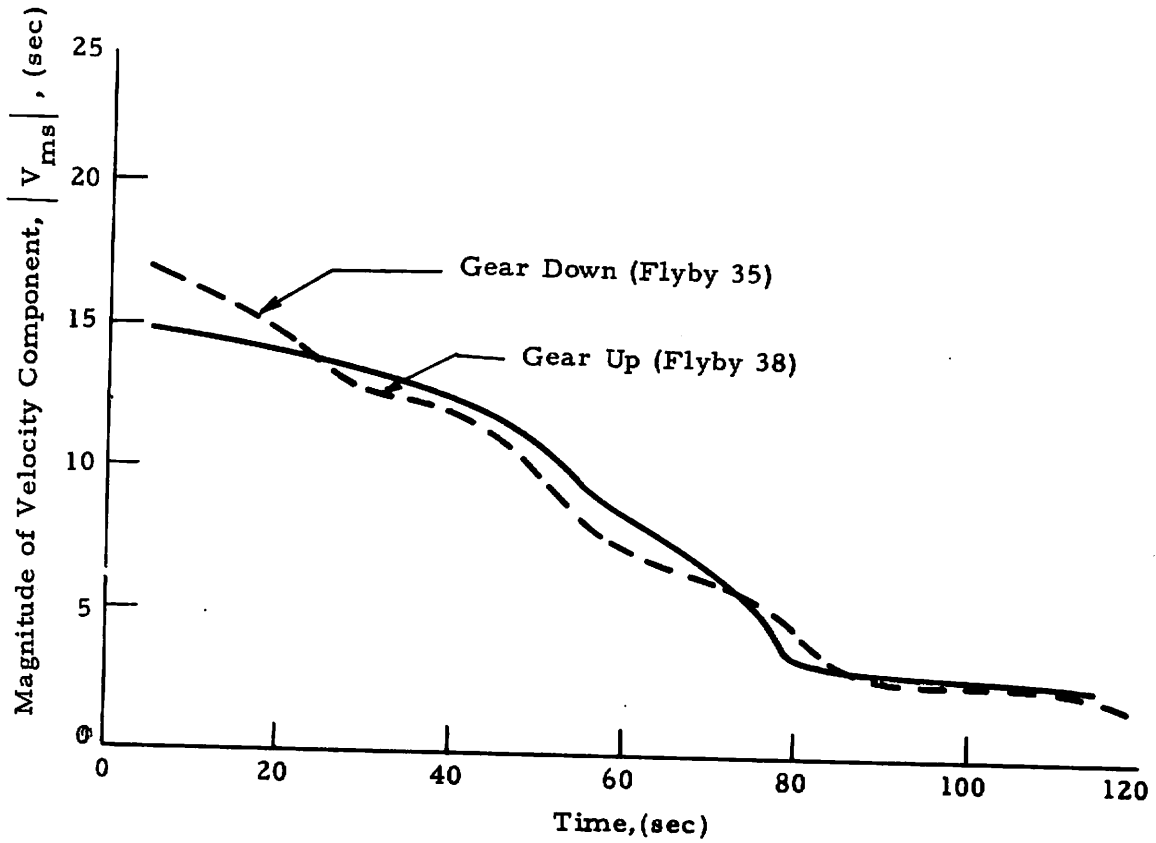


Fig. 33 - Comparison of Magnitude of Wake Vortex Rotational Velocity Component for B-747 Flybys With and Without Gear Down

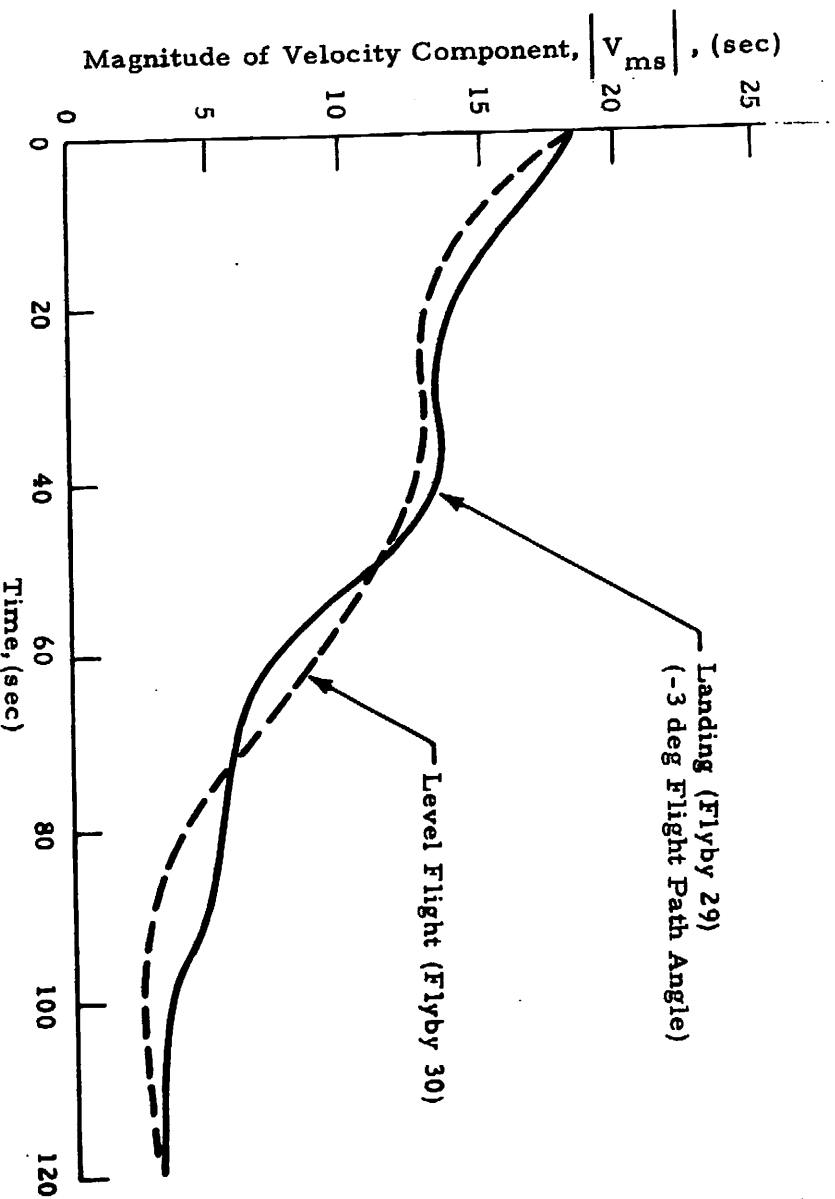


Fig. 34 - Comparison of Magnitude of Wake Vortex Rotational Velocity Component for B-747 in Level Flight and in Descending Flight



## 5. CONCLUSIONS

Laser Doppler velocimeter measurements of the wake vortex characteristics of a B-747 aircraft in various configurations have shown the following trends.

### 5.1 FOR VORTEX FORMATION:

- a. The rollup of the vortex sheet occurred rapidly within a few spans downstream of the aircraft.
- b. The observed location, spacing, and strength of the multiple vortices were in general agreement with theoretical rollup calculations.
- c. The peak tangential velocity and circulation of the merged vortices remained nearly constant in the near wake.
- d. The B-747 spoilers affected the vortices, producing vortices with large cores.

### 5.2 FOR VORTEX TRANSPORT:

- a. The wake vortices descended vertically with little horizontal motion.

### 5.3 FOR VORTEX DECAY:

- a. A decrease in the peak tangential velocity and circulation and an increase in the core radius was observed in the far wake.
- b. Deployment of spoilers and flaps enhanced the vortex peak tangential velocity decay process in the near wake.

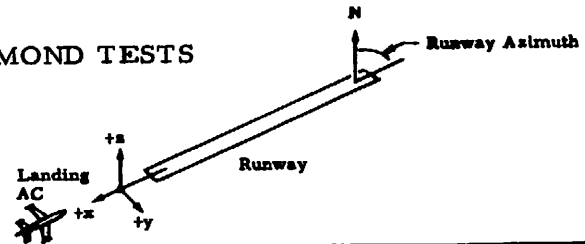
## REFERENCES

1. Krause, M. C., L. K. Morrison, C. E. Craven, N. A. Logan and T. R. Lawrence, "Development of Theory and Experiments to Improve Understanding of Laser Doppler Systems - Final Report," LMSC-HREC TR D306632, Lockheed Missiles & Space Company, Huntsville, Ala., June 1973.
2. Wilson, D. J., M. C. Krause, E. W. Coffey, C-C. Huang, B. B. Edwards, C. E. Craven, K. R. Shrider, J. L. Jetton and L. K. Morrison, "Development and Testing of Laser Doppler System Components for Wake Vortex Monitoring - Volume I - Scanner Development, Laboratory and Field Testing and System Modeling," LMSC-HREC TR D390159-I, Lockheed Missiles & Space Company, Huntsville, Ala., August 1974.
3. Lawrence, T. R. et al., "Application of a Laser Velocimeter for Remote Wind Velocity and Turbulence Measurements," Proceedings of the International Conference on Aerospace and Aeronautical Meteorology, 22-26 May 1972, Washington, D. C., The American Meteorological Society.
4. Brashears, M. R., T. R. Lawrence and A. D. Zalay, "Mobile Laser Doppler System Check Out and Calibration," FAA-RD-77-48, Lockheed Missiles & Space Company, Huntsville, Ala., September 1976.
5. Garodz, L. J., D. M. Lawrence and N. J. Miller, "Measurement of the Trailing Vortex Systems of Large Transport Aircraft, Using Tower Fly-by and Flow Visualization," FAA-RD-75-127, NAFEC, Atlanta City, N. J., January 1976.
6. Bilbro, J. W., H. B. Jeffreys, E. A. Weaver, R. M. Huffaker, G. D. Craig, R. W. George, and P. J. Marrero, "Laser Doppler Velocimeter Wake Tests," FAA-RD-76-11 (also NASA TM X 64988), March 1976.
7. Hoffman, E. R., and P. M. Joubert, "Turbulent Line Vortices," J. Fluid Mech., Vol. 16, Part 3, July 1963, p. 395.
8. Snedeker, R. S., and A. J. Bilanin, "Analysis of the Vortex Wakes of the Boeing 727, Lockheed L-1011, McDonnell Douglas DC-10, and Boeing 747 Aircraft," ARAP Report No. 245, July 1975.
9. Brashears, M. R., N. A. Logan, S. J. Robertson, K. R. Shrider, and C. D. Walters, "Analysis of Predicted Aircraft Wake Vortex Transport and Comparison with Experiment," FAA-RD-74-74, Lockheed Missiles & Space Company, Huntsville, Ala., April 1974.

## Appendix A

### EXTERNAL LOGS FOR ROSAMOND TESTS

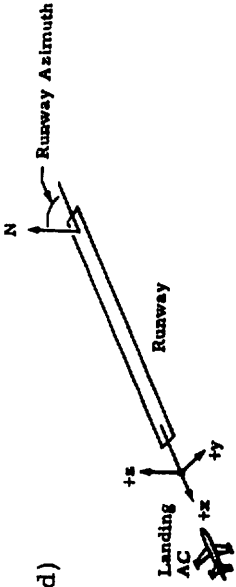
Location: Rosamond Air Base Van X Position: \_\_\_\_\_ Runway Azimuth: \_\_\_\_\_  
 Date: 12/2/5 - Day 1 Ref. Pt. \_\_\_\_\_  
 Sheet 1 of 2 Van Y Position: \_\_\_\_\_ Mirror Azimuth \_\_\_\_\_  
 Ref. Pt. Center of RW for Switch \_\_\_\_\_



A-1

Run ID		Spectrum Analyser						Scanner						Computer		Time		Estimated Wind Azimuth (from)	azimuth 42° is normal to runway. Comments
No.	AC Type or VAD	B. W. (kHz)	Log Lin	Freq. Span (MHz)			Rate (msec)	Range			Elevation			Tape No.	No. Records	Start	Stop		
				Min.	f <sub>c</sub>	Max.		Max.	Min.	Rate	Max.	Min.	Rate						
1	VAD	10	LW	0	2cm.	.5	1							DK701		6:45:00	6:49:30	est. from North	alt. of 31, 46, 61, 76, 91, 122, 244, 488 at 1 Rev/alt.
2	VAD															6:50:00	6:59:00		same alt.
3	AC 1	30		1	0	2		57			63 <sup>±15</sup>	3	.1kg			7:04:04	7:06:06		
4	AC 2	100		1		6							.5kg			7:04:37	7:11:25		
5	AC 3															7:15:04	7:17:07		
6	AC 4			0	1cm	5		60								7:20:49	7:22:53		
7	AC 5							118			63	20				7:25:56	7:27:40		Time mark on supt; not heard going 5-10° past 90°
8	AC 6	30						118			63	03				7:31:07	7:33:25		Run stop-comp. halt; Gen-fail; Precipiter run number still No. 6
9	AC 7										63	30				7:35:53	7:37:42		
10	AC 8							240			63	21				7:40:39	7:42:44		azimuth 180° + 42° (± 222°)
11	VAD	10		0		.5	1									7:50:00	7:58:00		Same alt. as run 1. Sync. clock 07:58:00 Ovr. clock 07:58:05
12	AC 9	30		0	1/2cm	5		58			63	03	.5			8:12:49	8:15:37		222° azimuth
13	AC 10							120			63	15				8:18:08	8:19:54		
14	AC 11							183			63	25				8:23:37	8:25:39		
15	AC 12							240			62	35				8:27:31	8:31:11		
16	AC 13							57			62	03				8:35:07	8:36:34		
17	AC 14							57								8:40:34	8:41:50		Precisely in middle / Analog tape run out for 1st min (or longer) - this run.
18	AC 15							57								8:46:04	8:48:19		Range 58 m; Az. at 42°; Amplitude threshold not changed.
19	AC 16							68								8:51:07	8:53:14		
20	VAD	10		0	1.3cm	.5										8:58:00	9:01:02	est. from North	same alt. as run 1.
21	AC 17	30		0	.6cm	5		35			62	03				9:32:12	9:33:32		Az. 42°. Corrected time code this run.
22	AC 17A															9:37:44	9:38:58		is part of previous run (run 17)
23	AC 18															9:42:16	9:43:08		

# Appendix A (Continued)



Location: NEWBY  
 Date: 12/2/75  
 Sheet 2 of 2

Van X Position: \_\_\_\_\_  
 Ref. Pt. \_\_\_\_\_

Van Y Position: \_\_\_\_\_  
 Ref. Pt. \_\_\_\_\_

Center of RW \_\_\_\_\_

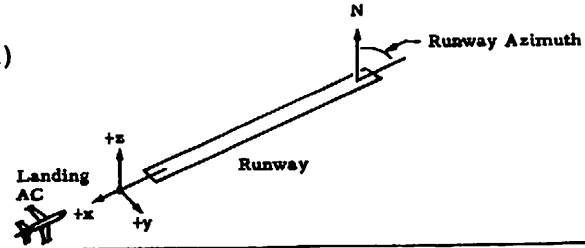
Runway Azimuth: \_\_\_\_\_

Mirror Azimuth for Switch \_\_\_\_\_

Run ID	Spectrum Analyzer				Scanner			Computer		Time		Estimated Wind Azimuth (from)	Comments	
	No.	AC Type or VAD	B.W. (kHz)	Log Lin	Freq. Span (MHz)	Rate (msec)	Range	Elevation	Tape No.	No. Records	Start			Stop
				Min.	Max.	Min.	Max.	Min.	Rate					
24	AC 19	30		0	5	63	63	03			7:46:21	7:48:12		
25	AC 20					63					7:49:08	7:52:38		
26	AC 21					90					7:55:08	9:57:53		Good low, vertics over run - high vol. this
27	AC 22													* 4 SA HPD
28	VAD	10		0	.5						11:12			same as, as run 2.
														* NOTE: 3rd SRTIE aborted due to hydraulic problem on 2nd

Appendix A (Continued)

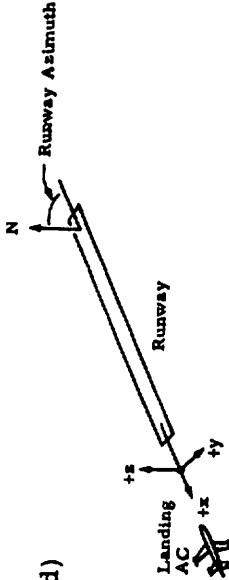
Location: Rosemead Dry Lake Van X Position: \_\_\_\_\_  
 Date: 12/3/75 - Day 2 Ref. Pt. \_\_\_\_\_  
 Sheet 1 of 2 Van Y Position: \_\_\_\_\_  
 Ref. Pt. 200' N of RW Mirror Azimuth for Switch \_\_\_\_\_



A-3

Run ID		Spectrum Analyzer						Scanner						Computer		Time		Estimated Wind Azimuth (from)	Comments
No.	AC Type or VAD	B. W. (kHz)	Log Lin	Freq. Span (MHz)			Rate (msec)	Range			Elevation			Tape No.	No. Records	Start	Stop		
				Min.	f <sub>c</sub>	Max.		Max.	Min.	Rate	Max.	Min.	Rate						
1	VAD	10	lw	0	2cm	.5	1							DE02		6:29	6:35	est. from south	alt. of 31, 46, 61, 76, 91, 122, 244, 488 at 1 rev./alt.
2	AC 23	30		0	1cm	5	1	140	35	3.5	63	10	.2			6:55:06	6:57:03		processor run no. not updated for run 3 (AC run 24)
3	AC 24															6:59:04	7:01:12		
4	AC 25															7:03:32	7:05:38		
5	AC 26															7:07:47	7:10:00		
6	AC 27										45	17				7:12:33	7:14:41		
7	AC 28										40	17				7:16:50	7:18:58		
8	AC 29															7:21:23	7:23:37		
9	AC 30										45	17				7:25:17	7:27:18		
10	VAD	10		0	2cm	.5										7:31	7:37		alt. same as run 1.
11	AC 31	30		0	.8cm	5		140	35	3.5	45	17	.2			7:56:09	7:58:30		pilot came in at 350 ft. instead of 200.
12	AC 32															8:00:47	8:04:11		elev. scanner screwed up prior to this run but scanned
13	AC 33										55	30				8:06:09	8:08:36		to work ok. before run started.
14	AC 34															8:11:02	8:12:04		Run AC 33: pilot came in at 210 ft. Alt.
15	AC 35															8:15:44	8:17:59		Mel switch run no. in processor to 34
16	AC 36															8:18:47	8:22:08		during runs.
17	AC 37															8:25:37	8:27:17		Run AC 35: Analog tape run not this run.
18	AC 38															8:30:30	8:32:35		Run AC 36: Lost CPU power during run 36. Plug to mainframe pulled out, inserted at 8:22:30. Also, our time "mark" and AV "mark" not synchronous for run 36.
19	VAD	10		0	15cm	.5										8:34	8:46		alt. same as run 1.

# Appendix A (Concluded)



Location: \_\_\_\_\_  
 Date: 12/5/75 - day ?  
 Sheet ? of ?  
 Van X Position: \_\_\_\_\_  
 Ref. Pt. \_\_\_\_\_  
 Van Y Position: \_\_\_\_\_  
 Ref. Pt. \_\_\_\_\_  
 Runway Azimuth: \_\_\_\_\_  
 Mirror Azimuth for Switch: \_\_\_\_\_  
 200' N of RW

Run ID	Spectrum Analyzer				Scanner				Computer		Time		Estimated Wind Azimuth (from)	Comments	
	No.	AC Type or VAD	B.W. (kHz)	Log Lin	Freq. Span (MHz)	Rate (msec)	Range	Elevation	Tape No.	No. Records	Start	Stop			
		Min.	Max.	Min.	Max.	Min.	Max.	Min.	Rate						
20	AC 39	30	30	0	5	35	35	55	23			9:01:11	9:02:31	SW	
21	AC 40											9:06:52	9:08:57	N.W.	
22	AC 41											9:12:30	9:14:34		
23	AC 42											9:18:06	9:20:26		
24	AC 43					35	35					9:23:17	9:26:31		
25	AC 44					35	35					9:28:40	9:30:55		
26	AC 45											9:33:37	9:36:46		
27	AC 46					35	35					9:39:09	9:42:11		
28	VAD	10		0	5							9:44	9:52		off, same as Run 1. (sketch 1)
29	AC 47	30		0	5	35	35	63	23			10:10:30	10:13:11		
30	AC 48											10:15:13	10:17:17		10:10 Freq used, both vertical dir. +, +x, +y, dust screen, +x, +y, dust screen, +x, +y, dust screen.
31	AC 49											10:20:16	10:23:10		
32	AC 50					35	35					10:24:19	10:27:44		Rotated scan 180° @ 10:25:17
33	AC 51											10:31:31	10:33:18		Rotated scan 90° @ 10:30:46 (off)
34	AC 52											10:33:57	10:36:26		Rotated scan ground 90° @ 10:35:00
35	AC 53											10:37:50	10:41:50		Rotated scan off 90° @ 10:38:58, 10:40:00 @ 10:39:55
36	AC 54											10:41:57	10:44:56		Rotated scan off 90° @ 10:43:27
37	VAD	10		0	5							10:49:00	10:52:15		NOTE: AC Run 53, picked up vertical @ 10:51:16 after 1st rotation, off, same as Run 1. (sketch 1)

NOTES: TIME CHECK & END OF SET 4  
 CLEAR TIME 10:46:13  
 AU TIME 10:48:10  
 Range checked after runs O.K.

## Appendix B

### SAMPLE OUTPUT FROM VELOCITY AZIMUTH DISPLAY AND VORTEX TRACKER PROGRAM FOR ROSAMOND FLYBY 25

Page B-2 indicates the relative intensity (INTENSITY) and  $V_{ms}$  (SPEED (ft/sec)) of the LDV signal as a function of time and space for one sweep between the minimum and maximum elevation-angle setting in the finger-scan mode. A list of the data sorted according to INTENSITY is given on page B-3 followed by the list of the values selected for determining the vortex location on page B-4. A "scatter plot" showing the location of the intensity points in units of ft and their relative magnitude (on a scale of A to 0) is given on page B-5 along with the selected center of the two correlation circles (labeled Z) and the centroid of the correlation circles (the vortex locations labeled P and S for port and starboard, respectively). On page B-6, the points used in determining the vortex location are listed. The data are printed out on pages B-7 through B-12 and B-13 through B-17 for two other sample scans during flyby 25. A summary of the port and starboard locations from each of the scans is given on pages B-18 through B-20. The vortex trajectories are displayed on the last two pages of Appendix B, including time versus lateral displacement of the vortices (page B-21) and time versus vertical location as a function of time (page B-22).

TIME OF SWEEP START = 3.272 SEC.  
 TIME OF SWEEP END = 4.841 SEC.  
 MID TIME OF SWEEP = 4.056 SEC.

IP	TIME	RANGE	ANGLE	YP	ZP	DELTA TIME	C WIND	SPEED	IFREQ	INTENSITY
1	3.272	386.2	62.6	22.1	349.7	.784	.00	15.65	18	254
2	3.287	359.2	62.3	33.2	325.7	.769	.00	13.04	15	190
3	3.302	326.9	62.0	46.3	295.5	.754	.00	16.52	19	158
4	3.317	293.8	61.8	61.0	265.2	.740	.00	18.26	21	200
5	3.332	259.7	61.6	76.3	235.4	.725	.00	19.13	22	112
6	3.451	267.6	59.5	64.4	237.4	.605	.00	23.47	27	126
7	3.466	291.0	59.3	51.6	257.3	.590	.00	13.04	15	126
8	3.496	350.1	58.8	18.4	306.4	.560	.00	16.52	19	124
9	3.511	380.4	58.6	1.6	331.6	.545	.00	13.91	16	128
10	3.541	437.9	58.1	-31.6	378.4	.515	.00	27.82	32	124
11	3.795	319.1	53.9	12.0	264.2	.261	.00	20.87	24	126
12	3.810	341.7	53.6	-2.8	281.9	.247	.00	8.69	10	148
13	3.825	376.4	53.4	-24.6	309.1	.232	.00	16.52	19	158
14	3.855	432.6	52.9	-61.2	351.9	.202	.00	29.56	34	126
15	3.869	434.6	52.5	-64.4	351.2	.187	.00	35.65	41	124
16	3.884	418.5	52.3	-55.7	338.3	.172	.00	23.47	27	144
17	3.899	391.2	52.1	-40.1	315.2	.157	.00	26.95	31	166
18	3.914	360.5	51.8	-22.8	290.4	.142	.00	39.99	46	112
19	3.929	331.7	51.5	-6.4	266.7	.127	.00	35.65	41	126
20	3.944	310.2	51.4	6.3	249.4	.112	.00	10.43	12	126
21	3.959	274.4	51.2	27.9	220.7	.097	.00	15.65	18	120
22	3.974	240.0	51.0	48.8	193.4	.082	.00	16.52	19	128
23	4.079	262.2	49.1	28.3	205.1	-.022	.00	46.95	54	184
24	4.094	292.1	48.9	8.0	227.1	-.037	.00	46.08	53	220
25	4.109	322.0	48.6	-13.1	248.4	-.052	.00	50.43	58	256
26	4.123	348.1	48.3	-31.6	266.9	-.067	.00	42.60	49	256
27	4.138	375.3	48.1	-50.5	286.4	-.082	.00	36.52	42	192
28	4.153	402.2	47.9	-69.5	305.4	-.097	.00	30.43	35	280
29	4.168	434.0	47.7	-91.9	328.2	-.112	.00	26.08	30	318
30	4.183	438.8	47.4	-97.2	329.2	-.127	.00	13.04	15	320
31	4.198	425.8	47.2	-89.4	319.1	-.142	.00	9.56	11	190
32	4.213	401.4	47.0	-73.9	300.2	-.157	.00	9.56	11	192
33	4.228	371.4	46.7	-54.6	277.4	-.172	.00	29.56	34	222
34	4.243	348.9	46.6	-39.9	260.4	-.187	.00	7.82	9	320
35	4.258	308.0	46.1	-13.5	229.2	-.202	.00	33.04	38	164
36	4.273	277.6	45.9	7.0	206.5	-.217	.00	24.34	28	168
37	4.467	393.9	42.8	-89.2	274.4	-.411	.00	17.39	20	158
38	4.482	420.7	42.6	-109.9	291.5	-.426	.00	20.87	24	128
39	4.497	438.9	42.3	-124.5	302.5	-.441	.00	16.52	19	174
40	4.512	427.5	42.0	-117.9	292.2	-.456	.00	17.39	20	128
41	4.527	406.9	41.8	-103.5	278.2	-.471	.00	16.52	19	192
42	4.781	384.1	37.6	-104.4	241.9	-.725	.00	8.69	10	128
43	4.796	409.6	37.4	-125.5	255.7	-.740	.00	8.69	10	118
44	4.811	437.7	37.2	-148.8	271.1	-.754	.00	9.56	11	196
45	4.826	435.6	36.8	-148.9	267.2	-.769	.00	8.69	10	190
46	4.841	414.7	36.6	-133.0	254.1	-.784	.00	8.69	10	174

ORDER	VELOCITY	INTENSITY
1	25	30
2	23	34
3	24	29
4	26	28
5	18	1

B-2



6	27	25
7	15	26
8	19	33
9	35	24
10	28	4
11	14	44
12	33	27
13	10	32
14	17	41
15	29	2
16	36	31
17	6	45
18	16	23
19	11	39
20	38	46
21	5	36
22	4	17
23	37	35
24	40	3
25	3	13
26	8	37
27	13	12
28	22	16
29	39	9
30	41	22
31	1	38
32	21	40
33	9	42
34	2	6
35	7	7
36	30	11
37	20	14
38	31	19
39	32	20
40	44	8
41	12	10
42	42	15
43	43	21
44	45	43
45	46	5
46	34	18

	I1	I13	N1	N2	R2
30	29	29	2	2	30.15
30	28	28	3	3	1355.06
30	32	32	4	4	1405.40
30	41	41	5	5	2727.48
30	31	31	6	6	171.75
30	39	39	7	7	1492.69
30	17	17	8	8	3453.66
30	37	37	9	9	3134.18
30	16	16	10	10	1796.11
30	38	38	11	11	1633.05
30	40	40	12	12	1798.91
30	14	14	13	13	1782.36
30	15	15	14	14	1556.26

KV = 1	JJJ = 30	YC = -81.6	ZC = 316.6		
	11	113	N1	N2	R2
	24	23	2	2	897.96
	24	36	3	3	425.12
	24	35	4	4	463.56
	24	12	5	5	3123.12
	24	22	6	6	2803.32
	24	6	7	7	3296.32
	24	7	8	8	2819.10
	24	11	9	9	1438.20
	24	19	10	10	1772.64
	24	20	11	11	499.09
	24	21	12	12	440.48
KV = 2	JJJ = 24	YC = 15.2	ZC = 229.4		



NPHV = 4	KD = 244	RANGE =	293.44	ANGLE =	45.62	NSAMPL = 10	RANGEI =	296.59	RANGE =	265.09
NPHV = 5	KD = 256	RANGE =	351.49	ANGLE =	48.62	NSAMPL = 11	RANGEI =	347.77	RANGE =	381.56
NPHV = 6	KD = 258	RANGE =	407.88	ANGLE =	49.05	NSAMPL = 13	RANGEI =	403.87	RANGE =	434.71
NPHV = 7	KD = 259	RANGE =	435.10	ANGLE =	49.43	NSAMPL = 13	RANGEI =	434.71	RANGE =	437.66
NPHV = 8	KD = 240	RANGE =	435.54	ANGLE =	49.62	NSAMPL = 12	RANGEI =	437.66	RANGE =	419.95
NPHV = 9	KD = 261	RANGE =	416.27	ANGLE =	49.83	NSAMPL = 14	RANGEI =	419.95	RANGE =	393.70
NPHV = 10	KD = 264	RANGE =	332.55	ANGLE =	50.62	NSAMPL = 12	RANGEI =	336.29	RANGE =	305.12
NPHV = 11	KD = 275	RANGE =	291.67	ANGLE =	53.30	NSAMPL = 26	RANGEI =	283.14	RANGE =	315.94
NPHV = 12	KD = 277	RANGE =	345.14	ANGLE =	53.82	NSAMPL = 10	RANGEI =	341.86	RANGE =	374.67
NPHV = 13	KD = 278	RANGE =	381.86	ANGLE =	54.06	NSAMPL = 30	RANGEI =	374.67	RANGE =	398.62
NPHV = 14	KD = 279	RANGE =	408.18	ANGLE =	54.33	NSAMPL = 32	RANGEI =	398.62	RANGE =	428.48
NPHV = 15	KD = 280	RANGE =	438.03	ANGLE =	54.73	NSAMPL = 32	RANGEI =	428.48	RANGE =	428.48
NPHV = 16	KD = 1	RANGE =	435.45	ANGLE =	54.87	NSAMPL = 35	RANGEI =	440.62	RANGE =	428.48
NPHV = 17	KD = 2	RANGE =	416.75	ANGLE =	55.07	NSAMPL = 37	RANGEI =	428.48	RANGE =	428.48
NPHV = 18	KD = 3	RANGE =	390.35	ANGLE =	55.28	NSAMPL = 41	RANGEI =	428.48	RANGE =	428.48
NPHV = 19	KD = 4	RANGE =	360.89	ANGLE =	55.57	NSAMPL = 42	RANGEI =	401.25	RANGE =	401.25
NPHV = 20	KD = 5	RANGE =	329.96	ANGLE =	55.88	NSAMPL = 39	RANGEI =	374.67	RANGE =	374.67
NPHV = 21	KD = 6	RANGE =	-297.67	ANGLE =	56.09	NSAMPL = 43	RANGEI =	341.86	RANGE =	341.86
NPHV = 22	KD = 7	RANGE =	272.57	ANGLE =	56.24	NSAMPL = 43	RANGEI =	311.35	RANGE =	311.35
NPHV = 23	KD = 17	RANGE =	287.93	ANGLE =	56.24	NSAMPL = 21	RANGEI =	279.53	RANGE =	279.53
NPHV = 24	KD = 18	RANGE =	320.95	ANGLE =	58.54	NSAMPL = 35	RANGEI =	276.90	RANGE =	246.39
NPHV = 25	KD = 19	RANGE =	351.24	ANGLE =	58.89	NSAMPL = 45	RANGEI =	308.40	RANGE =	308.40
NPHV = 26	KD = 20	RANGE =	375.79	ANGLE =	59.09	NSAMPL = 47	RANGEI =	336.29	RANGE =	336.29
NPHV = 27	KD = 21	RANGE =	405.09	ANGLE =	59.26	NSAMPL = 30	RANGEI =	368.11	RANGE =	368.11
NPHV = 28	KD = 22	RANGE =	430.70	ANGLE =	59.48	NSAMPL = 39	RANGEI =	393.70	RANGE =	393.70
NPHV = 29	KD = 23	RANGE =	436.37	ANGLE =	59.78	NSAMPL = 44	RANGEI =	422.90	RANGE =	422.90
NPHV = 30	KD = 24	RANGE =	419.37	ANGLE =	60.07	NSAMPL = 35	RANGEI =	440.62	RANGE =	440.62
NPHV = 31	KD = 25	RANGE =	395.17	ANGLE =	60.27	NSAMPL = 37	RANGEI =	428.48	RANGE =	428.48
NPHV = 32	KD = 26	RANGE =	370.74	ANGLE =	60.48	NSAMPL = 39	RANGEI =	403.87	RANGE =	403.87
NPHV = 33	KD = 27	RANGE =	339.06	ANGLE =	60.74	NSAMPL = 34	RANGEI =	381.56	RANGE =	381.56
NPHV = 34	KD = 28	RANGE =	305.17	ANGLE =	61.07	NSAMPL = 35	RANGEI =	349.74	RANGE =	349.74
NPHV = 35	KD = 29	RANGE =	273.09	ANGLE =	61.28	NSAMPL = 42	RANGEI =	319.23	RANGE =	319.23
		RANGE =		ANGLE =	61.48	NSAMPL = 39	RANGEI =	285.76	RANGE =	285.76
		RANGE =		ANGLE =			RANGEI =		RANGE =	253.28

IP	TIME OF SWEEP START	23.516 SEC.	ANGLE	YP	ZP	DELTA TIME	C WIND	SPEED	IFREQ	INTENSITY
1	23.516	378.9	36.8	-103.2	234.1	7.99	.00	7.82	9	148
2	23.770	392.6	40.8	-97.1	263.7	5.45	.00	13.04	15	144
3	23.799	440.0	41.2	-130.8	297.1	5.15	.00	9.56	11	128
4	23.844	381.9	42.0	-83.7	262.7	4.71	.00	13.04	15	112
5	23.889	288.2	42.8	-114.4	203.0	4.26	.00	18.26	21	126
6	24.024	273.4	45.1	6.9	200.5	2.91	.00	23.47	27	126
7	24.053	333.0	45.5	-33.3	244.4	2.61	.00	26.08	30	208
8	24.068	361.0	45.9	-51.4	266.1	2.47	.00	28.69	33	128
9	24.083	392.0	46.1	-72.0	289.1	2.32	.00	31.30	36	188
10	24.098	416.2	46.3	-87.7	307.7	2.17	.00	26.95	31	158
11	24.113	437.7	46.6	-100.8	324.9	2.02	.00	39.99	46	348
12	24.128	432.2	46.9	-95.5	322.3	1.87	.00	23.47	27	318
13	24.143	405.5	47.1	-76.1	304.0	1.72	.00	39.12	45	256
14	24.158	381.2	47.3	-58.6	287.1	1.57	.00	33.91	39	152
15	24.173	353.0	47.6	-38.2	267.4	1.42	.00	35.65	41	156
16	24.188	324.6	47.9	-17.8	247.7	1.27	.00	26.95	31	128
17	24.203	297.1	48.0	1.3	227.9	1.12	.00	13.04	15	128
18	24.237	267.1	50.3	29.2	212.4	.92	.00	25.21	29	126
19	24.352	299.5	50.5	9.4	238.0	.83	.00	35.65	41	126
20	24.367	327.3	50.7	-7.2	260.4	.72	.00	28.69	33	136
21	24.382	348.5	51.0	-19.2	277.9	.67	.00	12.17	19	172
22	24.397	381.6	51.2	-38.9	304.5	.62	.00	16.52	20	200
23	24.412	412.0	51.5	-56.7	329.2	.57	.00	27.82	32	256
24	24.427	436.5	51.7	-70.4	349.7	.51	.00	26.95	31	256
25	24.442	435.1	52.1	-67.5	350.7	.47	.00	26.95	31	192
26	24.457	414.8	52.3	-53.9	335.0	.42	.00	26.08	30	358
27	24.472	389.6	52.5	-37.4	315.9	.37	.00	23.47	27	254
28	24.487	364.3	52.6	-21.0	296.4	.32	.00	21.74	25	160
29	24.502	333.5	52.9	-11.2	273.0	.27	.00	19.13	22	232
30	24.517	301.9	53.2	19.4	248.9	.22	.00	20.00	23	192
31	24.531	266.4	53.5	41.4	221.0	.17	.00	23.47	27	224
32	24.546	234.3	53.6	61.1	195.7	.12	.00	18.26	21	126
33	24.561	225.3	53.7	71.5	192.1	.11	.00	18.26	21	166
34	24.576	259.4	53.8	52.9	220.4	.10	.00	22.60	26	118
35	24.591	283.5	54.0	39.9	241.0	.09	.00	10.43	12	136
36	24.606	317.0	54.2	21.9	269.3	.08	.00	13.91	16	172
37	24.621	375.5	54.4	-7.6	319.9	.07	.00	17.39	20	352
38	24.636	402.2	54.6	-21.2	342.9	.06	.00	16.52	19	128
39	24.651	430.7	54.8	-35.6	367.5	.05	.00	15.65	18	192
40	24.666	424.1	54.9	-48.3	364.4	.04	.00	13.91	16	200
41	24.681	397.1	54.9	-62.6	342.4	.03	.00	14.78	17	238
42	24.696	372.9	54.9	-78.3	322.4	.02	.00	11.30	13	112
43	24.711	341.0	54.9	-95.1	296.4	.01	.00	13.91	16	126
44	24.726	310.4	54.9	-114.4	271.4	.00	.00	14.78	17	126
45	24.741	278.4	54.9	-126.6	244.7	.00	.00	14.78	17	124
46	24.756	247.7	54.9	-141.4	222.4	.00	.00	13.04	15	176
47	24.771	217.7	54.9	-156.7	196.0	.00	.00	13.04	15	160
48	24.786	188.2	54.9	-173.0	173.0	.00	.00	12.17	14	126
49	24.801	159.7	54.9	-191.2	151.2	.00	.00	12.17	14	126
50	24.816	131.2	54.9	-210.8	131.2	.00	.00	10.43	12	190
51	24.831	102.7	54.9	-231.9	112.7	.00	.00	8.77	11	152
52	24.846	74.2	54.9	-254.2	94.2	.00	.00	7.11	10	126
53	24.861	45.7	54.9	-277.7	75.7	.00	.00	5.45	9	190

ORDER	VELOCITY	INTENSITY	54	25.069	441.8	62.3	-5.6	398.0	-.754	.00	14.78	17	158
1	11	26	55	25.099	401.7	62.8	16.4	364.3	-.784	.00	18.26	21	190
2	13	37	56	25.114	376.6	62.8	27.6	341.8	-.799	.00	20.87	24	126
3	15	11											
4	19	12											
5	14	49											
6	9	13											
7	8	23											
8	20	24											
9	23	27											
10	10	41											
11	16	29											
12	24	31											
13	25	7											
14	7	22											
15	26	40											
16	18	21											
17	17	6											
18	12	30											
19	27	39											
20	31	50											
21	34	53											
22	28	55											
23	56	9											
24	30	46											
25	49	36											
26	29	28											
27	47	47											
28	5	10											
29	32	54											
30	33	15											
31	50	14											
32	55	51											
33	37	1											
34	22	2											
35	38	20											
36	51	35											
37	39	3											
38	52	8											
39	41	16											
40	44	17											
41	53	19											
42	41	17											
43	54	38											
44	40	5											
45	43	6											
46	45	18											
47	47	2											
48	48	4											
49	49	17											
50	46	44											
51	51	21											
52	45	48											
	48	56											

53 44 45  
 54 35 34  
 55 3 4  
 56 1 42

N1	N2	R2
11	113	
26	37	2373.59
26	11	2301.73
26	12	1895.58
26	13	1455.54
26	23	41.24
26	24	487.28
26	27	637.40
26	41	1761.82
26	22	1155.79
26	40	1518.96
26	25	414.05
26	39	1389.61
26	9	2415.77
26	28	2556.46
26	10	1891.43
26	14	2324.26
26	38	1133.88
26	42	3215.43
26	42	-60.4

N1 = 1  
 JJJ = 26  
 YC = 323.2

N1	N2	R2
11	113	
31	30	1260.20
31	46	3191.45
31	36	2711.50
31	47	1280.65
31	35	402.96
31	17	1655.47
31	19	1310.45
31	5	3104.77
31	6	1611.90
31	18	221.90
31	32	1029.38
31	33	1742.47
31	44	2559.26
31	48	1410.64
31	45	749.01
31	34	133.03
31	34	37.2

N1 = 2  
 JJJ = 31  
 YC = 225.8





MPHV= 4	KD= 279	RANGEP=	249.61	ANGLEP=	61.74	NSAMPL= 20	RANGEI=	256.54	RANGEN=	221.78
MPHV= 5	KD= 280	RANGEP=	214.83	ANGLEP=	61.54	NSAMPL= 20	RANGEI=	221.78	RANGEN=	221.78
MPHV= 6	KD= 5	RANGEP=	209.80	ANGLEP=	60.37	NSAMPL= 14	RANGEI=	205.71	RANGEN=	237.20
MPHV= 7	KD= 6	RANGEP=	245.00	ANGLEP=	60.10	NSAMPL= 23	RANGEI=	237.20	RANGEN=	289.69
MPHV= 8	KD= 7	RANGEP=	278.56	ANGLEP=	59.73	NSAMPL= 33	RANGEI=	269.69	RANGEN=	296.59
MPHV= 9	KD= 8	RANGEP=	305.63	ANGLEP=	59.54	NSAMPL= 33	RANGEI=	296.59	RANGEN=	327.76
MPHV= 10	KD= 9	RANGEP=	335.79	ANGLEP=	59.34	NSAMPL= 31	RANGEI=	327.76	RANGEN=	353.67
MPHV= 11	KD= 10	RANGEP=	361.82	ANGLEP=	59.09	NSAMPL= 29	RANGEI=	353.67	RANGEN=	383.86
MPHV= 12	KD= 11	RANGEP=	391.95	ANGLEP=	58.74	NSAMPL= 27	RANGEI=	383.86	RANGEN=	411.75
MPHV= 13	KD= 12	RANGEP=	420.04	ANGLEP=	58.54	NSAMPL= 32	RANGEI=	411.75	RANGEN=	437.66
MPHV= 14	KD= 15	RANGEP=	403.30	ANGLEP=	57.73	NSAMPL= 33	RANGEI=	411.75	RANGEN=	464.15
MPHV= 15	KD= 16	RANGEP=	376.45	ANGLEP=	57.53	NSAMPL= 34	RANGEI=	386.15	RANGEN=	487.61
MPHV= 16	KD= 17	RANGEP=	347.46	ANGLEP=	57.33	NSAMPL= 27	RANGEI=	357.61	RANGEN=	517.28
MPHV= 17	KD= 18	RANGEP=	318.99	ANGLEP=	57.15	NSAMPL= 27	RANGEI=	327.76	RANGEN=	549.81
MPHV= 18	KD= 19	RANGEP=	283.56	ANGLEP=	56.86	NSAMPL= 35	RANGEI=	295.28	RANGEN=	582.69
MPHV= 19	KD= 20	RANGEP=	250.89	ANGLEP=	56.54	NSAMPL= 32	RANGEI=	261.81	RANGEN=	615.81
MPHV= 20	KD= 21	RANGEP=	217.85	ANGLEP=	56.34	NSAMPL= 30	RANGEI=	227.69	RANGEN=	648.88
MPHV= 21	KD= 26	RANGEP=	207.05	ANGLEP=	55.15	NSAMPL= 24	RANGEI=	199.80	RANGEN=	681.99
MPHV= 22	KD= 27	RANGEP=	240.91	ANGLEP=	54.87	NSAMPL= 32	RANGEI=	229.99	RANGEN=	714.11
MPHV= 23	KD= 28	RANGEP=	269.99	ANGLEP=	54.55	NSAMPL= 23	RANGEI=	264.11	RANGEN=	747.70
MPHV= 24	KD= 30	RANGEP=	300.20	ANGLEP=	54.34	NSAMPL= 32	RANGEI=	289.70	RANGEN=	780.51
MPHV= 25	KD= 31	RANGEP=	330.09	ANGLEP=	54.14	NSAMPL= 30	RANGEI=	322.51	RANGEN=	813.77
MPHV= 26	KD= 32	RANGEP=	358.24	ANGLEP=	53.88	NSAMPL= 31	RANGEI=	347.77	RANGEN=	846.56
MPHV= 27	KD= 33	RANGEP=	388.25	ANGLEP=	53.54	NSAMPL= 25	RANGEI=	381.56	RANGEN=	879.87
MPHV= 28	KD= 34	RANGEP=	411.58	ANGLEP=	53.14	NSAMPL= 31	RANGEI=	403.87	RANGEN=	912.71
MPHV= 29	KD= 35	RANGEP=	434.71	ANGLEP=	52.69	NSAMPL= 28	RANGEI=	417.32	RANGEN=	945.08
MPHV= 30	KD= 37	RANGEP=	409.47	ANGLEP=	52.69	NSAMPL= 28	RANGEI=	391.08	RANGEN=	977.81
MPHV= 31	KD= 38	RANGEP=	384.00	ANGLEP=	52.34	NSAMPL= 26	RANGEI=	365.81	RANGEN=	1010.65
MPHV= 32	KD= 39	RANGEP=	357.71	ANGLEP=	52.15	NSAMPL= 26	RANGEI=	334.65	RANGEN=	1043.17
MPHV= 33	KD= 40	RANGEP=	326.20	ANGLEP=	51.95	NSAMPL= 26	RANGEI=	302.17	RANGEN=	1075.69
MPHV= 34	KD= 41	RANGEP=	293.72	ANGLEP=	51.70	NSAMPL= 26	RANGEI=	269.69	RANGEN=	1108.22
MPHV= 35	KD= 42	RANGEP=	260.98	ANGLEP=	51.35	NSAMPL= 26	RANGEI=	236.22	RANGEN=	1140.88
MPHV= 36	KD= 43	RANGEP=	228.27	ANGLEP=	51.15	NSAMPL= 17	RANGEI=	203.43	RANGEN=	1173.55
MPHV= 37	KD= 49	RANGEP=	229.23	ANGLEP=	49.73	NSAMPL= 24	RANGEI=	170.69	RANGEN=	1206.22
MPHV= 38	KD= 50	RANGEP=	263.43	ANGLEP=	49.35	NSAMPL= 23	RANGEI=	137.94	RANGEN=	1238.91
MPHV= 39	KD= 51	RANGEP=	290.68	ANGLEP=	49.15	NSAMPL= 23	RANGEI=	105.19	RANGEN=	1271.60
MPHV= 40	KD= 52	RANGEP=	321.53	ANGLEP=	48.95	NSAMPL= 18	RANGEI=	72.44	RANGEN=	1304.29
MPHV= 41	KD= 53	RANGEP=	346.42	ANGLEP=	48.76	NSAMPL= 20	RANGEI=	39.69	RANGEN=	1336.98
MPHV= 42	KD= 54	RANGEP=	379.46	ANGLEP=	48.52	NSAMPL= 20	RANGEI=	6.94	RANGEN=	1369.67
MPHV= 43	KD= 55	RANGEP=	406.17	ANGLEP=	48.15	NSAMPL= 23	RANGEI=	25.19	RANGEN=	1402.36
MPHV= 44	KD= 59	RANGEP=	392.37	ANGLEP=	47.17	NSAMPL= 17	RANGEI=	34.44	RANGEN=	1435.05
MPHV= 45	KD= 60	RANGEP=	369.50	ANGLEP=	46.97	NSAMPL= 15	RANGEI=	3.19	RANGEN=	1467.74
MPHV= 46	KD= 61	RANGEP=	334.73	ANGLEP=	46.76	NSAMPL= 18	RANGEI=	2.94	RANGEN=	1500.43
MPHV= 47	KD= 62	RANGEP=	304.25	ANGLEP=	46.54	NSAMPL= 16	RANGEI=	2.69	RANGEN=	1533.12
MPHV= 48	KD= 63	RANGEP=	270.77	ANGLEP=	46.17	NSAMPL= 15	RANGEI=	2.44	RANGEN=	1565.81
MPHV= 49	KD= 64	RANGEP=	238.08	ANGLEP=	45.97	NSAMPL= 16	RANGEI=	2.19	RANGEN=	1598.50
MPHV= 50	KD= 65	RANGEP=	204.57	ANGLEP=	45.77	NSAMPL= 16	RANGEI=	1.94	RANGEN=	1631.19
MPHV= 51	KD= 69	RANGEP=	191.67	ANGLEP=	44.76	NSAMPL= 20	RANGEI=	1.69	RANGEN=	1663.88
MPHV= 52	KD= 70	RANGEP=	223.48	ANGLEP=	44.32	NSAMPL= 19	RANGEI=	1.44	RANGEN=	1696.57
MPHV= 53	KD= 71	RANGEP=	256.67	ANGLEP=	44.32	NSAMPL= 15	RANGEI=	1.19	RANGEN=	1729.26
MPHV= 54	KD= 72	RANGEP=	284.06	ANGLEP=	43.97	NSAMPL= 15	RANGEI=	0.94	RANGEN=	1761.95
MPHV= 55	KD= 73	RANGEP=	315.03	ANGLEP=	43.57	NSAMPL= 20	RANGEI=	0.69	RANGEN=	1794.64
MPHV= 56	KD= 74	RANGEP=	341.40	ANGLEP=	43.57	NSAMPL= 15	RANGEI=	0.44	RANGEN=	1827.33
MPHV= 57	KD= 75	RANGEP=	375.07	ANGLEP=	43.32	NSAMPL= 20	RANGEI=	0.19	RANGEN=	1860.02
MPHV= 58	KD= 76	RANGEP=	399.81	ANGLEP=	42.96	NSAMPL= 19	RANGEI=	0.19	RANGEN=	1892.71
MPHV= 59	KD= 77	RANGEP=	428.81	ANGLEP=	42.76	NSAMPL= 20	RANGEI=	0.19	RANGEN=	1925.40
MPHV= 60	KD= 78	RANGEP=	437.37	ANGLEP=	42.54	NSAMPL= 22	RANGEI=	0.19	RANGEN=	1958.09

"PHV= 61	KD= 79	RANGEP=	420.44	ANGLEP=	42.34	NSAMPL= 22	RANGEL=	425.85	RANGEN=	401.28
"PHV= 62	KD= 80	RANGEP=	395.97	ANGLEP=	42.10	NSAMPL= 24	RANGEL=	401.25	RANGEN=	379.27
"PHV= 63	KD= 81	RANGEP=	372.07	ANGLEP=	41.76	NSAMPL= 20	RANGEL=	379.27	RANGEN=	347.77
"PHV= 64	KD= 82	RANGEP=	342.03	ANGLEP=	41.56	NSAMPL= 19	RANGEL=	347.77	RANGEN=	317.59
"PHV= 65	KD= 83	RANGEP=	311.36	ANGLEP=	41.36	NSAMPL= 18	RANGEL=	317.59	RANGEN=	283.14
"PHV= 66	KD= 84	RANGEP=	276.57	ANGLEP=	41.12	NSAMPL= 20	RANGEL=	283.14	RANGEN=	250.33
"PHV= 67	KD= 85	RANGEP=	243.91	ANGLEP=	40.76	NSAMPL= 19	RANGEL=	250.33	RANGEN=	216.54
"PHV= 68	KD= 86	RANGEP=	212.85	ANGLEP=	40.58	NSAMPL= 11	RANGEL=	216.54	RANGEN=	183.07
"PHV= 69	KD= 92	RANGEP=	252.79	ANGLEP=	39.08	NSAMPL= 30	RANGEL=	274.61	RANGEN=	274.61
"PHV= 70	KD= 93	RANGEP=	282.60	ANGLEP=	38.74	NSAMPL= 29	RANGEL=	243.44	RANGEN=	302.17
"PHV= 71	KD= 94	RANGEP=	311.42	ANGLEP=	38.54	NSAMPL= 30	RANGEL=	274.61	RANGEN=	333.01
"PHV= 72	KD= 95	RANGEP=	342.53	ANGLEP=	38.33	NSAMPL= 33	RANGEL=	302.17	RANGEN=	361.88
"PHV= 73	KD= 96	RANGEP=	372.10	ANGLEP=	38.13	NSAMPL= 35	RANGEL=	333.01	RANGEN=	391.08
"PHV= 74	KD= 97	RANGEP=	401.05	ANGLEP=	37.85	NSAMPL= 38	RANGEL=	361.88	RANGEN=	417.32
"PHV= 75	KD= 98	RANGEP=	423.38	ANGLEP=	37.55	NSAMPL= 38	RANGEL=	391.08	RANGEN=	440.62
"PHV= 76	KD= 99	RANGEP=	434.25	ANGLEP=	37.33	NSAMPL= 26	RANGEL=	417.32	RANGEN=	440.62
"PHV= 77	KD= 100	RANGEP=	419.57	ANGLEP=	37.11	NSAMPL= 46	RANGEL=	428.48	RANGEN=	409.12
"PHV= 78	KD= 101	RANGEP=	399.77	ANGLEP=	36.85	NSAMPL= 46	RANGEL=	409.12	RANGEN=	383.86
"PHV= 79	KD= 102	RANGEP=	371.18	ANGLEP=	36.52	NSAMPL= 37	RANGEL=	428.48	RANGEN=	353.67
"PHV= 80	KD= 103	RANGEP=	349.54	ANGLEP=	36.37	NSAMPL= 42	RANGEL=	409.12	RANGEN=	324.15
"PHV= 81	KD= 105	RANGEP=	279.09	ANGLEP=	35.87	NSAMPL= 14	RANGEL=	353.67	RANGEN=	287.55
"PHV= 82	KD= 112	RANGEP=	219.44	ANGLEP=	34.11	NSAMPL= 33	RANGEL=	289.70	RANGEN=	236.22
"PHV= 83	KD= 113	RANGEP=	239.47	ANGLEP=	34.11	NSAMPL= 45	RANGEL=	205.71	RANGEN=	268.70
"PHV= 84	KD= 114	RANGEP=	280.13	ANGLEP=	33.98	NSAMPL= 10	RANGEL=	236.22	RANGEN=	268.70
"PHV= 85	KD= 115	RANGEP=	308.70	ANGLEP=	33.63	NSAMPL= 43	RANGEL=	268.70	RANGEN=	295.28
"PHV= 86	KD= 116	RANGEP=	336.66	ANGLEP=	33.31	NSAMPL= 44	RANGEL=	295.28	RANGEN=	325.79
"PHV= 87	KD= 117	RANGEP=	365.04	ANGLEP=	33.12	NSAMPL= 39	RANGEL=	325.79	RANGEN=	353.67
"PHV= 88	KD= 118	RANGEP=	391.53	ANGLEP=	32.93	NSAMPL= 35	RANGEL=	353.67	RANGEN=	386.15
"PHV= 89	KD= 119	RANGEP=	420.04	ANGLEP=	32.72	NSAMPL= 21	RANGEL=	386.15	RANGEN=	411.75
"PHV= 90	KD= 120	RANGEP=	436.69	ANGLEP=	32.34	NSAMPL= 32	RANGEL=	411.75	RANGEN=	437.66
"PHV= 91	KD= 121	RANGEP=	428.20	ANGLEP=	32.13	NSAMPL= 33	RANGEL=	437.66	RANGEN=	434.71
"PHV= 92	KD= 122	RANGEP=	409.48	ANGLEP=	31.94	NSAMPL= 32	RANGEL=	434.71	RANGEN=	414.37
"PHV= 93	KD= 124	RANGEP=	356.35	ANGLEP=	31.72	NSAMPL= 21	RANGEL=	414.37	RANGEN=	391.08
"PHV= 94	KD= 126	RANGEP=	292.69	ANGLEP=	31.17	NSAMPL= 17	RANGEL=	361.88	RANGEN=	329.40
"PHV= 95	KD= 136	RANGEP=	408.19	ANGLEP=	30.78	NSAMPL= 12	RANGEL=	296.59	RANGEN=	264.11
"PHV= 96	KD= 140	RANGEP=	435.18	ANGLEP=	28.17	NSAMPL= 13	RANGEL=	288.39	RANGEN=	322.51
"PHV= 97	KD= 141	RANGEP=	435.01	ANGLEP=	27.17	NSAMPL= 14	RANGEL=	403.87	RANGEN=	434.71
"PHV= 98	KD= 142	RANGEP=	435.01	ANGLEP=	26.97	NSAMPL= 16	RANGEL=	434.71	RANGEN=	437.66
"PHV= 99	KD= 143	RANGEP=	416.01	ANGLEP=	26.77	NSAMPL= 15	RANGEL=	437.66	RANGEN=	419.95
"PHV= 100	KD= 144	RANGEP=	390.89	ANGLEP=	26.57	NSAMPL= 15	RANGEL=	419.95	RANGEN=	393.70
"PHV= 101	KD= 145	RANGEP=	364.93	ANGLEP=	26.36	NSAMPL= 11	RANGEL=	393.70	RANGEN=	368.11
"PHV= 102	KD= 146	RANGEP=	332.39	ANGLEP=	25.98	NSAMPL= 10	RANGEL=	368.11	RANGEN=	336.29
					25.78	NSAMPL= 12	RANGEL=	336.29	RANGEN=	303.81

TIME OF SWEEP START = 57.474 SEC.  
 TIME OF SWEEP END = 58.655 SEC.  
 MID TIME OF SWEEP = 58.565 SEC.

IP	TIME	RANGE	ANGLE	YP	ZP	DELTA TIME	C WIND	SPEED	IFREQ	INTENSITY
1	57.474	285.8	62.6	68.4	260.7	1.091	.00	10.43	12	254
2	57.469	253.5	62.4	82.5	231.4	1.076	.00	10.43	12	240
3	57.504	218.9	62.1	97.7	200.4	1.061	.00	11.30	13	174
4	57.519	184.9	61.8	112.6	169.9	1.046	.00	10.43	12	128
5	57.574	210.4	60.8	97.3	190.4	.986	.00	11.30	13	318
6	57.594	238.9	60.6	82.6	215.1	.971	.00	9.56	11	320
7	57.609	271.4	60.4	65.6	243.4	.956	.00	10.43	12	318
8	57.624	299.8	60.2	50.9	267.1	.941	.00	12.17	14	192
9	57.639	331.1	59.9	34.2	293.4	.926	.00	11.30	13	320
10	57.668	386.6	59.4	3.1	339.7	.896	.00	9.56	11	158
11	57.683	412.3	59.2	-11.2	361.0	.881	.00	9.56	11	124
12	57.758	354.0	58.0	12.1	307.1	.807	.00	10.43	12	112
13	57.773	323.5	57.6	26.5	280.1	.792	.00	11.30	13	224
14	57.788	290.9	57.4	43.1	252.0	.777	.00	12.17	14	222
15	57.803	260.0	57.2	59.1	225.5	.762	.00	10.43	12	240
16	57.818	225.4	57.0	76.8	196.4	.747	.00	10.43	12	160
17	57.833	192.1	56.6	94.2	167.3	.732	.00	10.43	12	190
18	57.892	202.4	55.8	86.1	174.3	.672	.00	9.56	11	124
19	57.907	232.8	55.4	67.7	198.4	.657	.00	11.30	13	256
20	57.922	266.1	55.2	46.0	225.5	.642	.00	11.30	13	288
21	57.937	292.1	55.0	32.3	246.7	.627	.00	9.56	11	238
22	57.952	325.3	54.8	12.3	272.7	.613	.00	9.56	11	200
23	57.982	383.7	54.2	-24.6	318.1	.583	.00	9.56	11	128
24	58.072	362.4	52.8	-19.2	295.4	.493	.00	9.56	11	144
25	58.087	331.1	52.6	-1.3	269.9	.478	.00	9.56	11	188
26	58.102	298.7	52.2	16.8	243.0	.463	.00	9.56	11	256
27	58.117	267.4	52.0	35.3	217.4	.448	.00	9.56	11	190
28	58.132	234.1	51.8	55.2	190.9	.433	.00	9.56	11	374
29	58.146	200.0	51.6	75.7	163.4	.418	.00	9.56	11	172
30	58.206	195.6	50.6	75.7	158.1	.359	.00	8.69	10	126
31	58.221	226.5	50.2	55.0	180.9	.344	.00	9.56	11	256
32	58.236	259.8	50.0	32.9	206.0	.329	.00	11.30	13	278
33	58.251	285.7	49.8	15.4	225.7	.314	.00	10.43	12	176
34	58.266	316.4	49.6	-6.5	249.3	.299	.00	8.69	10	142
35	58.281	344.7	49.2	-25.4	267.8	.284	.00	11.30	13	180
36	58.296	378.0	49.0	-48.1	292.7	.269	.00	12.17	14	144
37	58.311	401.6	48.8	-64.6	309.1	.254	.00	8.69	10	112
38	58.341	435.6	48.3	-89.5	332.5	.224	.00	12.17	14	128
39	58.371	394.1	47.8	-64.9	296.4	.194	.00	16.52	19	164
40	58.386	369.5	47.6	-49.3	279.7	.179	.00	13.04	15	152
41	58.400	335.6	47.3	-27.4	253.4	.164	.00	13.04	15	148
42	58.415	305.1	47.0	-8.2	230.0	.149	.00	12.17	14	152
43	58.430	273.8	46.8	12.5	206.5	.134	.00	8.69	10	254
44	58.445	242.0	46.6	33.7	182.4	.120	.00	8.69	10	432
45	58.535	220.4	45.2	44.6	163.3	.030	.00	8.69	10	128
46	58.550	252.1	44.8	21.1	184.4	.015	.00	8.69	10	128
47	58.565	280.4	44.6	.3	203.4	.000	.00	9.56	11	192
48	58.580	311.5	44.4	-22.6	224.4	-.015	.00	9.56	11	172
49	58.595	340.7	44.1	-44.5	244.3	-.030	.00	12.17	14	126
50	58.610	371.2	43.8	-68.0	263.4	-.045	.00	10.43	12	128
51	58.639	425.0	43.4	-108.9	298.9	-.075	.00	10.43	12	124
52	58.664	425.3	42.8	-112.2	295.4	-.105	.00	11.30	13	128
53	58.684	401.4	42.6	-95.6	278.4	-.120	.00	9.56	11	152

ORDER	VELOCITY	INTENSITY
54	58.699	370.2
55	58.729	314.3
56	58.744	280.6
57	58.908	335.7
58	58.938	391.9
59	58.953	418.0
60	58.966	439.6
61	59.013	380.2
62	59.028	346.1
63	59.207	299.8
64	59.267	412.5
65	59.566	381.5
66	59.581	404.8
67	59.655	364.9
68		
69		
70		
71		
72		
73		
74		
75		
76		
77		
78		
79		
80		
81		
82		
83		
84		
85		
86		
87		
88		
89		
90		
91		
92		
93		
94		
95		
96		
97		
98		
99		
100		
101		
102		
103		
104		
105		
106		
107		
108		
109		
110		
111		
112		
113		
114		
115		
116		
117		
118		
119		
120		
121		
122		
123		
124		
125		
126		
127		
128		
129		
130		
131		
132		
133		
134		
135		
136		
137		
138		
139		
140		
141		
142		
143		
144		
145		
146		
147		
148		
149		
150		
151		
152		
153		
154		
155		
156		
157		
158		
159		
160		
161		
162		
163		
164		
165		
166		
167		
168		
169		
170		
171		
172		
173		
174		
175		
176		
177		
178		
179		
180		
181		
182		
183		
184		
185		
186		
187		
188		
189		
190		
191		
192		
193		
194		
195		
196		
197		
198		
199		
200		

42	21	36
43	22	57
44	23	34
45	24	59
46	25	4
47	26	23
48	27	38
49	28	45
50	29	46
51	31	50
52	47	52
53	48	55
54	53	56
55	60	62
56	30	65
57	34	30
58	37	49
59	43	58
60	44	60
61	45	63
62	46	11
63	55	18
64	57	51
65	65	12
66	66	37
67	67	66

11	113	N1	N2	R2
44	28	2	2	528.17
44	6	3	3	3443.30
44	20	4	4	2028.29
44	32	5	5	539.24
44	19	6	6	1408.77
44	31	7	7	456.58
44	43	8	8	1009.41
44	15	9	9	2470.52
44	47	10	10	1555.29
44	27	11	11	1216.85
44	33	12	12	2144.54
44	29	13	13	2129.46
44	16	14	14	2044.82
44	45	15	15	498.80
44	46	16	16	162.32
44	56	17	17	2007.23
44	30	18	18	2380.44
44	18	19	19	2824.32
44	18	19	19	46.4

KV = 1      JJJ = 44      YC =      ZC = 198.7

11	113	N1	N2	R2
61	54	2	2	1190.72
61	64	3	3	1888.51
61	53	4	4	1807.21
61	57	5	5	2106.69
61	59	6	6	1481.17
61	50	7	7	1952.76



NPAV=	4	KD=	219	RANGEP=	538.75	ANGLEP=	48.56	NSAMPL=	12	RANGEI=	411.75	RANGEM=	1970.14
NPAV=	5	KD=	226	RANGEP=	337.17	ANGLEP=	60.22	NSAMPL=	10	RANGEI=	340.22	RANGEM=	309.71
NPAV=	6	KD=	227	RANGEP=	305.62	ANGLEP=	60.42	NSAMPL=	12	RANGEI=	309.71	RANGEM=	275.59
NPAV=	7	KD=	228	RANGEP=	271.84	ANGLEP=	60.62	NSAMPL=	11	RANGEI=	275.59	RANGEM=	241.47
NPAV=	8	KD=	229	RANGEP=	237.20	ANGLEP=	60.85	NSAMPL=	13	RANGEI=	241.47	RANGEM=	208.66
NPAV=	9	KD=	230	RANGEP=	204.94	ANGLEP=	61.22	NSAMPL=	11	RANGEI=	208.66	RANGEM=	174.87
NPAV=	10	KD=	235	RANGEP=	222.18	ANGLEP=	62.42	NSAMPL=	10	RANGEI=	218.83	RANGEM=	282.30
NPAV=	11	KD=	236	RANGEP=	255.02	ANGLEP=	62.62	NSAMPL=	10	RANGEI=	252.30	RANGEM=	279.63
NPAV=	12	KD=	237	RANGEP=	283.21	ANGLEP=	62.80	NSAMPL=	11	RANGEI=	279.63	RANGEM=	312.99
NPAV=	13	KD=	238	RANGEP=	315.52	ANGLEP=	62.78	NSAMPL=	10	RANGEI=	312.99	RANGEM=	338.25

KOSAMOND DRY LAKE DAY 2      B747 12/03/75  
TIME IS 7:31:50  
KOSAMOND LAKE      HD270.      RUN NO. 4

STARBOARD VORTEX

TIME	Z	Y
4.05621	260.652	44.1498
8.27676	260.229	38.5139
13.85668	212.365	47.6868
15.5002	278.173	6.46237
18.7123	271.046	36.3668
20.6620	257.905	26.2682
24.3148	224.413	55.0379
26.2645	177.873	46.3209
29.8949	259.492	26.9209
31.6056	171.146	59.0845
34.7579	230.324	46.7477
37.0064	220.007	5.36603
40.5472	241.469	61.3459
42.5118	244.896	40.6397
45.4176	230.303	52.5408
47.4121	192.493	60.0888
51.1471	205.975	83.2493
53.0743	192.320	58.7777
63.6145	233.186	37.4797
69.2095	220.445	35.1234



PORT VORTEX

TIME	L	Y
4.05621	316.589	-81.6382
8.27676	357.333	-29.5650
13.8568	349.730	-34.7920
15.5002	258.296	-114.384
18.7123	323.249	-69.0965
20.6620	269.113	-123.139
24.3148	323.246	-60.4487
26.2645	273.360	14.0868
29.8949	323.499	-74.6053
31.6056	232.370	-37.9057
34.7579	334.106	-23.4391
37.0064	243.742	-125.949
40.5472	289.022	-84.2635
42.5118	258.368	-105.767
45.4176	318.621	-45.9242
47.4121	269.746	-97.0168
51.1471	354.548	-20.3668
53.0743	237.969	-126.092
63.6145	297.511	-90.3922
69.2095	308.295	-82.9007

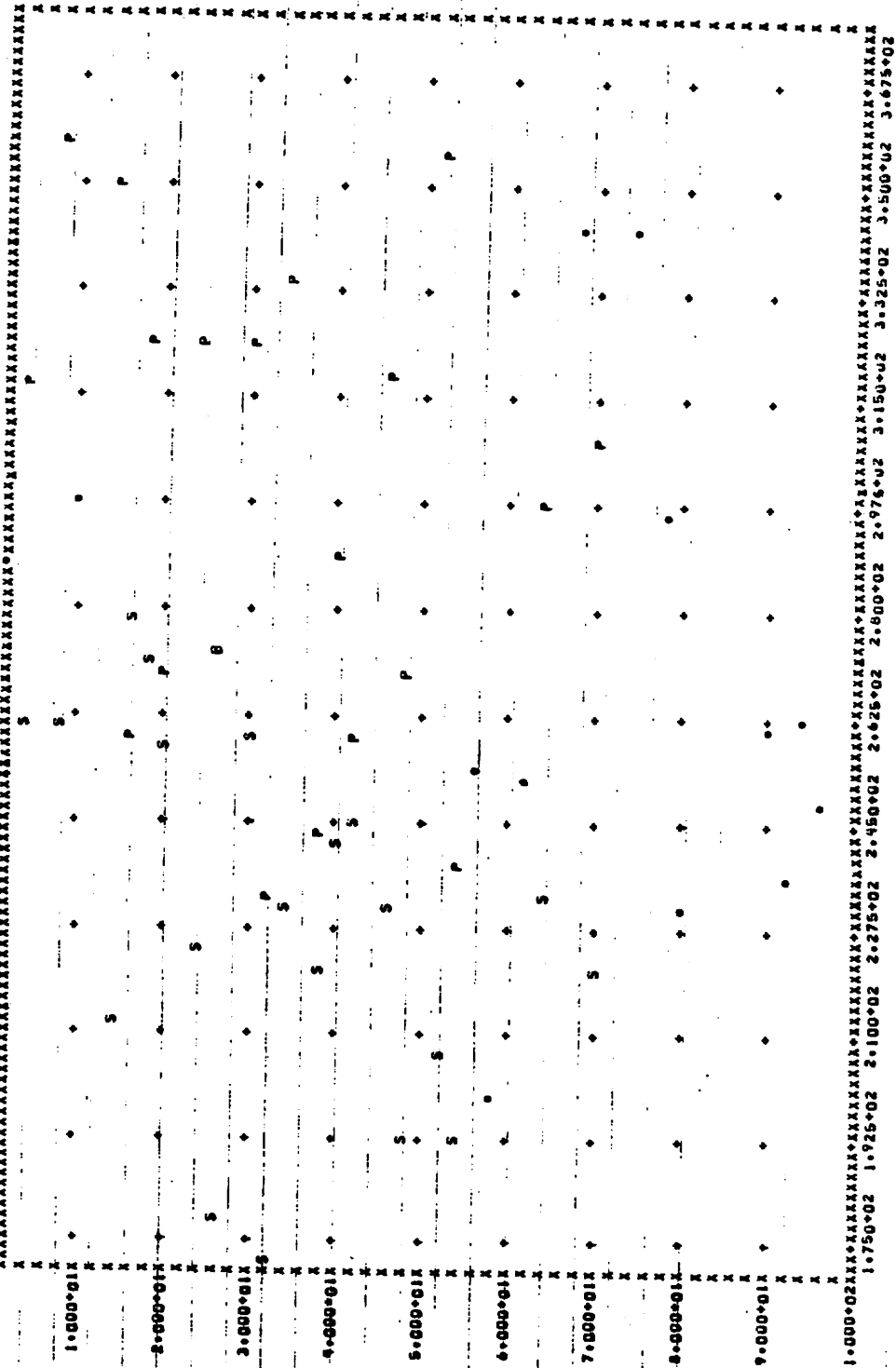
UNKNOWN TYPE OF VORTEX

TIME	Z	Y
2.89089	286.775	31.5946
9.94257	297.216	-87.3446
56.5852	253.098	45.4470
58.5648	198.678	46.4100
61.9412	252.638	67.2202
67.1926	342.761	-0.433675
73.0118	342.916	-59.9073
77.9868	296.564	-91.7344
80.8926	230.220	-141.526
89.0200	261.570	-43.6382
91.4552	235.385	-136.489
94.5179	262.498	-29.0438
96.8784	248.933	-124.571



ROSAMOND DRY LAKE DAY 2 8747 12/03/75 ROSAMOND LAKE MD27D. RUN NO. 4

PLOTTING T-VS Z



## Appendix C

### SAMPLE OUTPUT FROM NASA-MSFC LASER DOPPLER VELOCIMETER DATA PROCESSING ROUTINES FOR ROSAMOND FLYBY 47

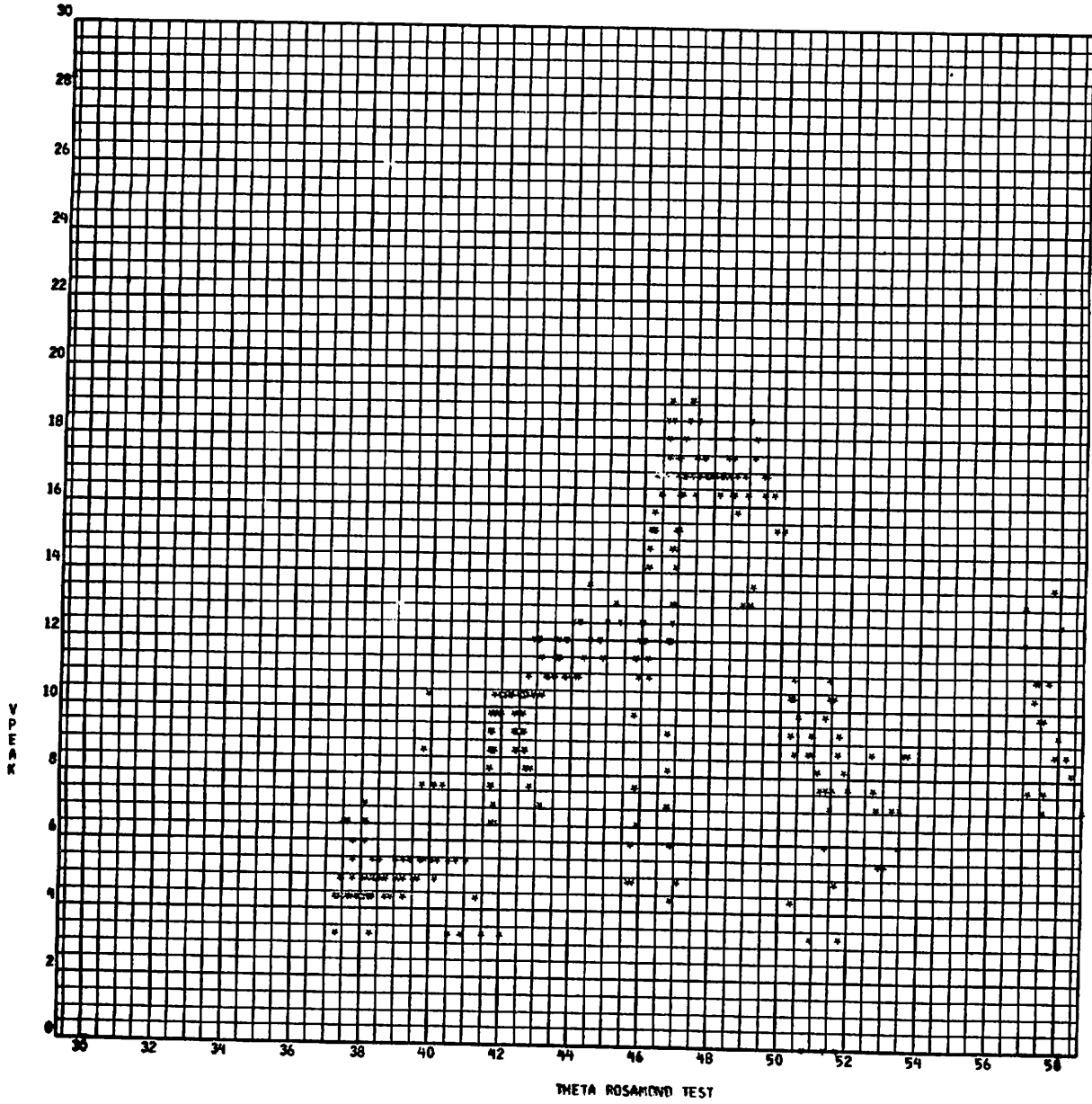
Results from the Rosamond high-speed data are given on page C-2 including a printout of the relative intensity of the LDV signal (IPEAK) and the frequency (or velocity) of the flow field including  $V_{ms}$  and  $V_{pk}$  in units of meters per second (VMAX and VPEAK, respectively). The sweep count from the start of the flyby is shown by the column labeled SCAN while the lateral and vertical location and range and elevation angle of the focal volume are given by X (m), Y (m), R (m), and T (deg), respectively. The time at which the LDV signal was sampled is contained in the frame count (1 FRAME = 1/500 sec).

From the array of LDV sample points illustrated on page C-2, plots of VPEAK versus the scan elevation angle in degrees, THETA, are generated as illustrated on pages C-3 through C-6. Note that the characteristic double peak signature of the wake vortex is evident in the sample plots.

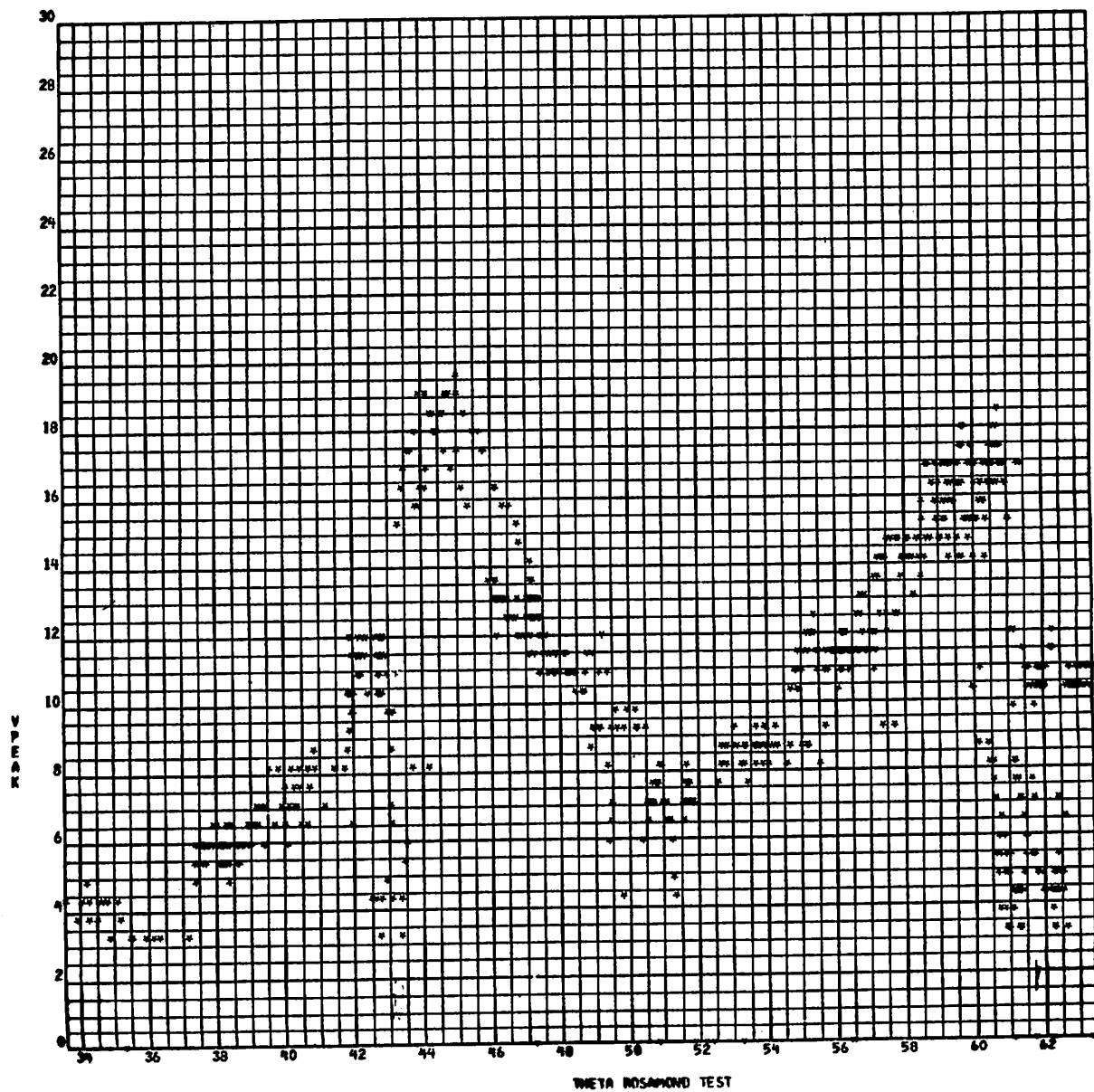
Applying the " $I_{pk}$ " algorithm (p. 4-7 of Ref. 7) to the threshold LDV spectrum illustrated above, the vortex location is determined. The vortex trajectory for flyby 47 as computed from the high speed data is shown on pages C-7 through C-9. On page C-7 the vertical and lateral motion of the vortices is given as a function of time, while page C-8 shows the altitude versus lateral position of the wake vortex. Page C-9 lists the vortex locations. For additional information regarding the vortex location, criteria, and coefficients used in the " $I_{pk}$ " algorithm and shown in the plots, refer to Ref. 7.

Note that the coordinate system used in the NASA-MSFC data processing routines is not the same as the coordinate system used in the text earlier. The runway centerline is located at  $y = -200$  ft in the NASA plots.

SCAN	FRAME	X	Y	R	T	IPEAK	VMAX	VPEAK	VAVG	VWIDTH
4	4150	219.4	245.0	328.9	48.2	127	9.8	10.9	9.0	8
4	4151	216.9	242.5	325.3	48.2	131	8.2	10.4	8.7	8
4	4152	218.8	240.0	324.7	47.7	134	8.2	10.9	8.8	8
4	4153	216.9	237.5	321.6	47.6	134	9.3	10.4	9.0	8
4	4154	208.7	235.0	314.3	48.4	123	10.4	10.9	9.1	8
4	4155	206.2	232.5	310.8	48.4	121	9.3	10.4	8.5	8
4	4156	208.1	229.4	309.7	47.8	121	10.4	10.4	8.8	8
4	4157	205.0	226.2	305.3	47.8	124	8.2	10.4	8.5	8
4	4158	196.9	223.7	298.0	48.7	118	8.2	10.4	8.2	8
4	4159	199.4	221.2	297.8	48.0	131	8.2	10.9	8.5	8
4	4160	196.9	217.5	293.4	47.8	136	7.1	10.4	8.0	9
4	4161	189.4	215.6	287.0	48.7	128	9.3	10.4	8.7	7
4	4162	186.2	212.5	282.6	48.8	125	9.3	10.9	9.4	8
4	4163	187.5	209.4	281.1	48.2	116	10.9	10.9	9.1	8
4	4164	185.6	206.9	277.9	48.1	123	8.7	10.9	8.8	5
4	4165	178.1	204.4	271.1	48.9	117	8.7	10.9	9.4	5
4	4166	179.4	201.2	269.4	48.3	111	7.1	10.4	7.8	4
4	4167	177.5	198.7	266.5	48.2	116	9.3	10.4	9.0	4
4	4168	169.4	195.6	258.8	49.1	118	9.3	9.8	8.8	5
4	4169	166.2	192.5	254.4	49.2	131	8.7	9.3	8.5	4
4	4170	169.4	190.6	255.0	48.4	119	8.7	10.9	8.8	4
4	4171	166.2	187.5	250.4	48.4	130	8.7	10.4	8.9	5
4	4172	158.7	185.0	243.8	49.4	126	8.7	8.7	8.3	3
4	4173	155.6	181.9	239.4	49.4	131	8.2	8.7	8.2	3
4	4174	158.1	179.4	239.1	48.6	136	8.2	10.4	8.5	5
4	4175	155.0	176.2	234.7	48.7	128	8.7	10.4	7.5	4
4	4176	147.5	173.1	227.4	49.6	129	8.7	9.8	8.1	5
4	4177	145.0	170.6	223.9	49.6	136	8.7	9.3	8.1	6
4	4178	146.9	168.1	223.2	48.9	120	8.2	8.7	7.5	5
4	4179	139.4	165.0	216.8	49.8	132	7.6	8.7	7.7	4
4	4180	136.2	161.9	211.6	49.9	134	8.2	9.3	8.0	5
4	4181	138.7	159.4	211.3	49.0	128	8.2	8.7	7.5	6
4	4182	136.2	156.3	207.3	48.9	130	8.2	8.7	8.4	2
4	4183	128.1	153.2	200.1	50.2	130	8.2	9.3	8.1	5
4	4184	126.2	151.2	197.0	50.1	117	9.3	9.3	8.5	5
4	4185	128.1	148.1	195.8	49.1	121	7.6	8.7	7.8	4
4	4186	125.6	145.0	191.9	49.1	116	6.0	9.3	7.3	5
4	4187	118.1	141.9	184.6	50.2	106	8.2	8.2	8.2	1
4	4188	115.0	139.4	180.7	50.5	115	8.2	8.7	8.2	2
4	4189	117.5	136.9	180.4	49.5					
4	4190	115.0	134.4	176.9	49.4					
4	4191	107.5	131.2	169.7	50.7					
4	4192	109.4	127.5	168.0	49.4					
4	4193	106.9	125.0	164.5	49.5					
4	4194	99.4	121.9	157.3	50.8					
4	4195	96.2	120.0	153.8	51.3					
4	4196	99.4	117.5	153.9	49.8					
4	4197	96.2	114.4	149.5	49.9					
4	4198	88.7	111.2	142.3	51.4					
4	4199	85.6	108.7	138.4	51.8					



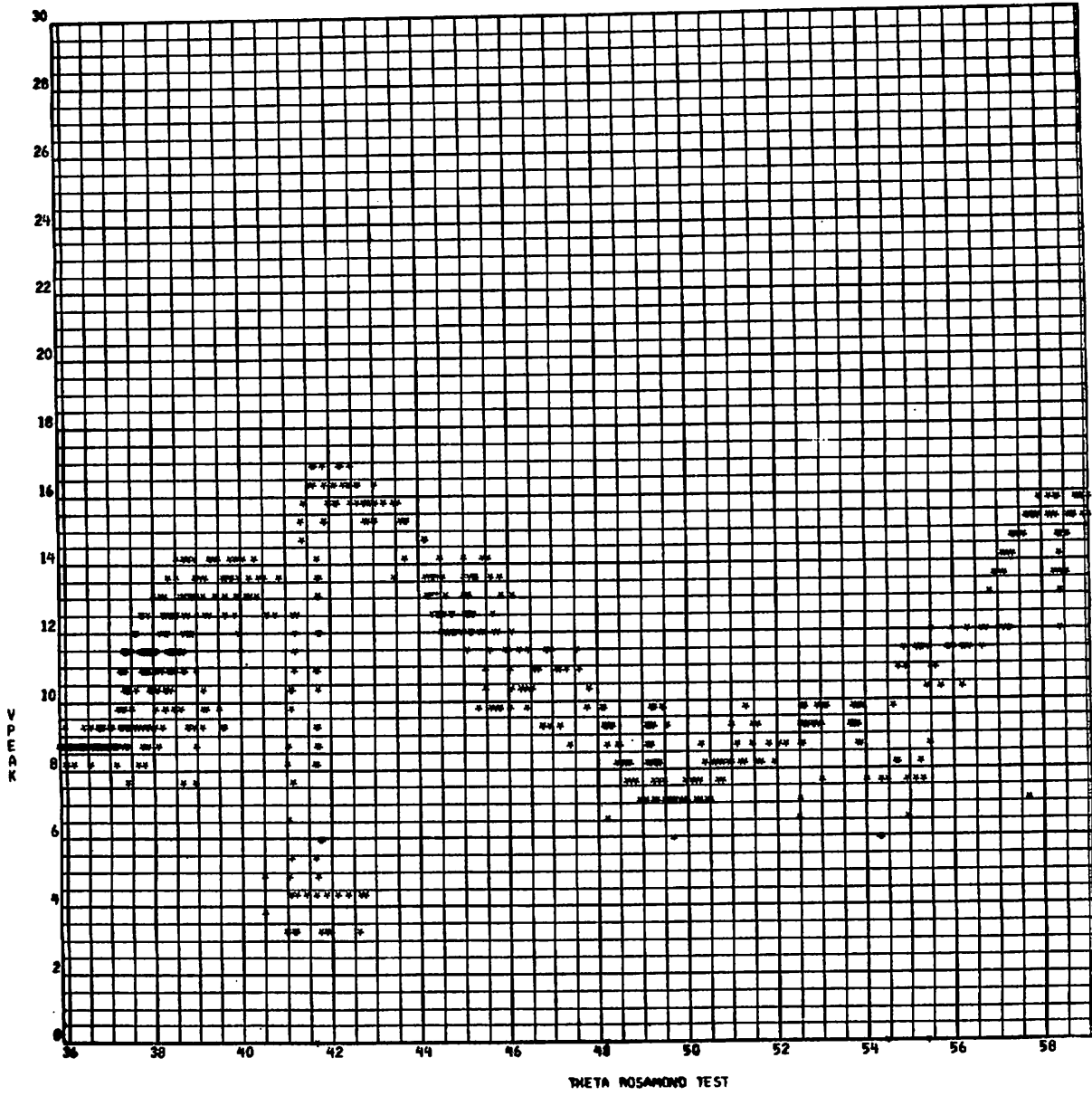
SCAN = 3

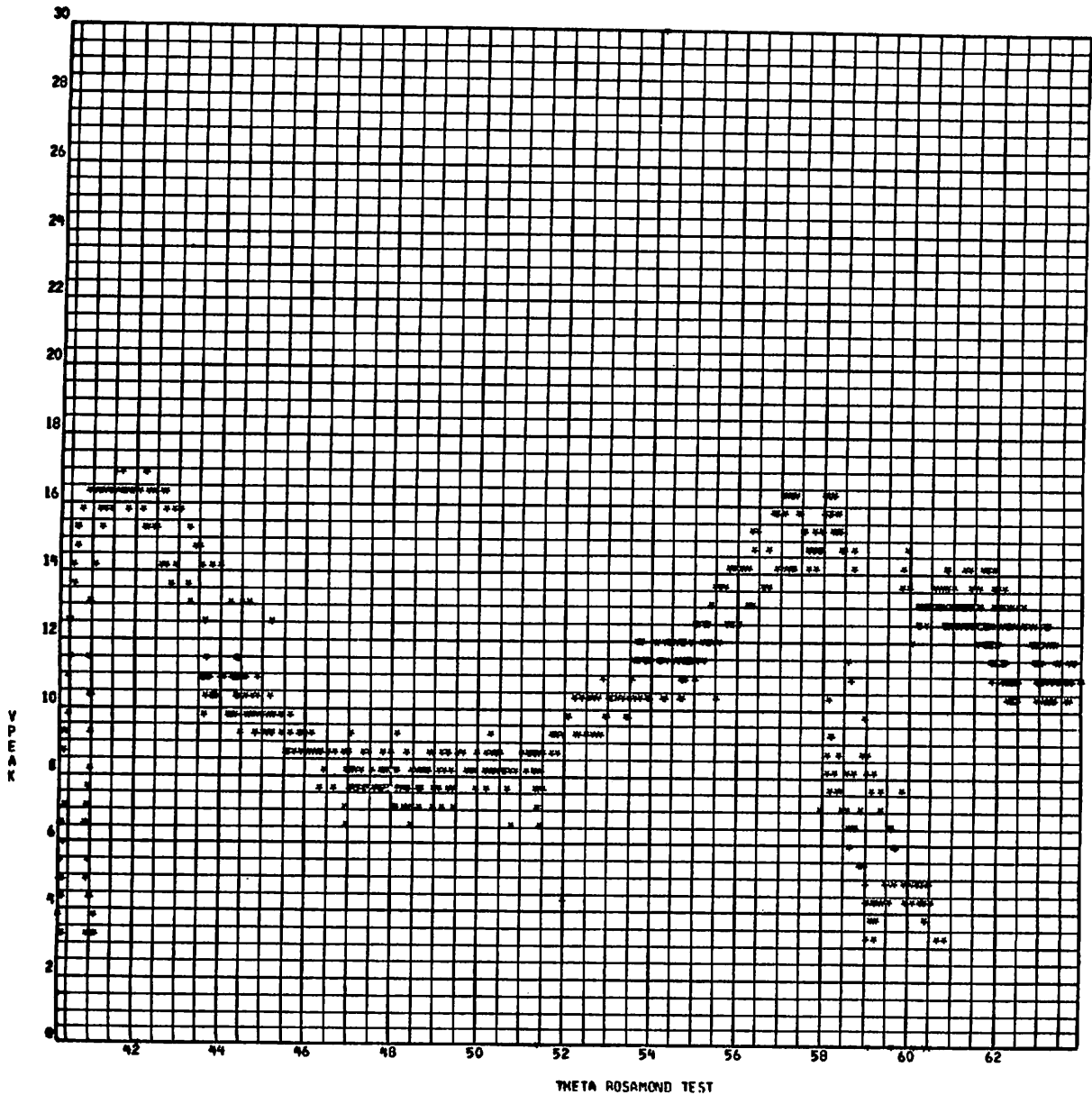


WETA ROSAMOND TEST

SCAN = 4

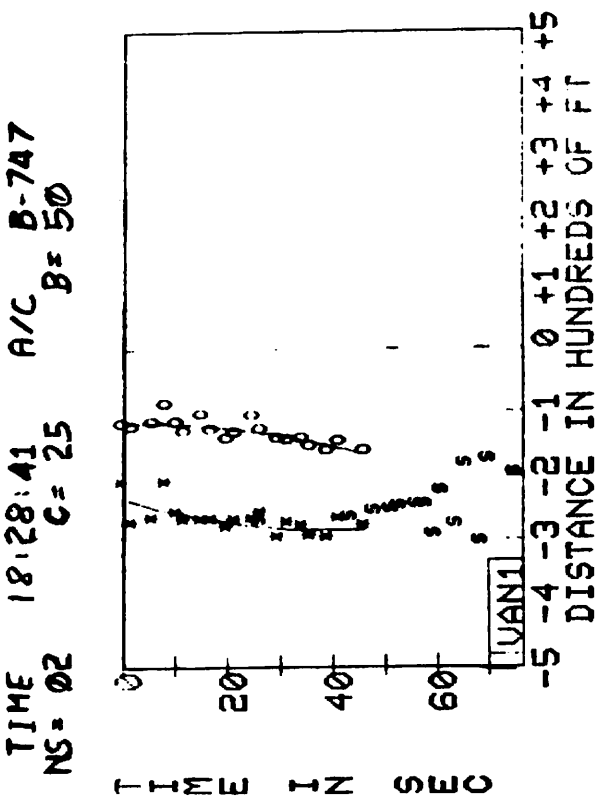
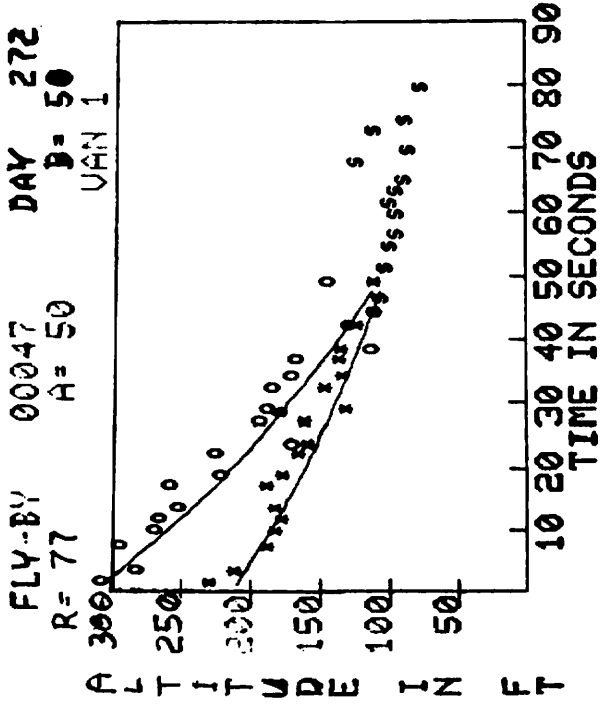




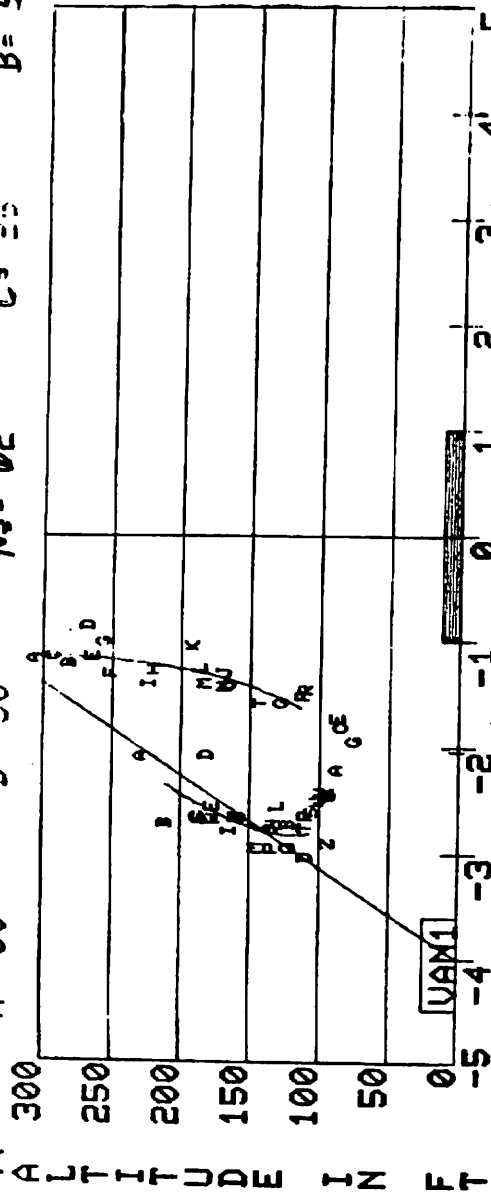


THETA ROSAMOND TEST

SCAN = 6



FLY-BY 00047      DAY 272      TIME 15:20:12      A/C B-747  
 R= 77      A= 50      NS= 02      C= 25      B= 50



FLY-BY 00047 DAY 272 TIME 15:28:32 A/C B-747  
 R=77 A=50 B=50 NS=02 C=25 D=50

FR DATA P'S	COR PT P S	NOISE P S	ANGLE MN MX	PK P	PAR TIME P S	PORT PCS X Y	STARB PCS X Y	FR DATA PTS	COR PT P S	MO:SE P S	ANGLE MN MX	PK B S	PAR TIME P S	PORT PCS X Y	STARB PCS X Y
01 270	151 055	00 00	41 61	230	200 000 0	211 225	-120 303								
02 251	128 099	00 00	37 62	230	200 002 8	214 207	-124 277								
03 253	150 146	00 00	33 60	241	210 006 8	224 207	-117 288								
04 253	250 238	00 00	37 61	222	208 009 4	210 173	-089 263								
05 253	250 238	00 00	37 61	257	225 011 4	220 173	-117 260								
06 253	250 238	00 00	37 61	257	225 013 2	220 173	-117 247								
07 253	250 238	00 00	37 61	257	225 014 0	220 173	-104 252								
08 253	233 222	00 00	38 60	249	220 018 3	220 171	-130 216								
09 253	186 135	00 00	29 60	248	185 021 6	221 160	-144 219								
10 253	200 224	00 00	29 60	248	186 023 2	220 153	-133 165								
11 253	250 238	00 00	29 60	248	186 025 0	220 153	-107 187								
12 253	250 238	00 00	29 60	248	186 027 8	220 153	-129 181								
13 253	151 108	00 00	31 62	255	193 031 6	228 141	-143 179								
14 253	151 108	00 00	31 62	255	172 033 3	226 128	-146 165								
15 253	111 111	00 00	30 61	255	170 036 0	220 131	-144 162								
16 253	111 111	00 00	30 61	273	176 041 7	227 118	-154 108								
17 253	077 077	00 00	20 63	273	176 043 4	228 118	-162 124								
18 253	057 025	00 00	18 62	237	145 047 0	228 105	-148 105								
19 253	062 019	00 00	18 62	237	145 048 7	228 105	-162 139								
20 253	043 019	00 00	19 62	212	144 048 9	228 106									
21 253	062 019	00 00	19 61	218	000 041 0	254 084									
22 253	051 051	00 00	18 51	220	000 041 0	248 090									
23 253	051 051	00 00	18 51	202	000 055 2	246 090									
24 253	083 040	00 00	21 50	188	000 059 8	246 094									
25 253	040 000	00 00	20 48	174	000 062 3	224 084									
26 253	040 000	00 00	37 42	198	000 064 7	224 084									
27 253	040 000	00 00	37 42	156	000 067 1	226 118									
28 253	040 000	00 00	37 42	000	186 069 1	-184 080									
29 253	040 000	00 00	23 32	000	186 072 3	-176 083									
30 253	040 000	00 00	24 25	000	186 073 8	-188 078									
31 253	040 000	00 00	19 21	000	186 079 1										
32 253	040 000	00 00	00 00	000											
33 253	040 000	00 00	00 00	000											
34 253	040 000	00 00	00 00	000											
35 253	040 000	00 00	00 00	000											

## Appendix D

### WAKE VORTEX TRACKS COMPUTED FROM LOW-SPEED MEASUREMENTS

The circles, triangles and diamond symbols represent the port, star-board and undefined vortex, respectively. For each flyby, the predicted wake vortex trajectory assuming zero crosswind is shown by the solid lines. The vortex tracks were computed from the predicted model described in Ref. 10 for a circulation strength of  $\Gamma = 662 \text{ m}^2/\text{sec}$  and an initial vortex spacing of  $b' = 41.8 \text{ m}$ . Available photographic and acoustic measurements also appear on the plots, the solid circles and triangles representing the former and the x's the latter measurements. The dashed line is a smooth curve drawn through the photographic vortex tracks.

<u>LDV Measurement</u>	<u>Photographic Measurement</u>	<u>MAVSS</u>	<u>Theory</u>
○ Port Vortex	● Port Vortex	□ Port Vortex	— Predictive Model
△ Starboard Vortex	▲ Starboard Vortex	× Starboard Vortex	

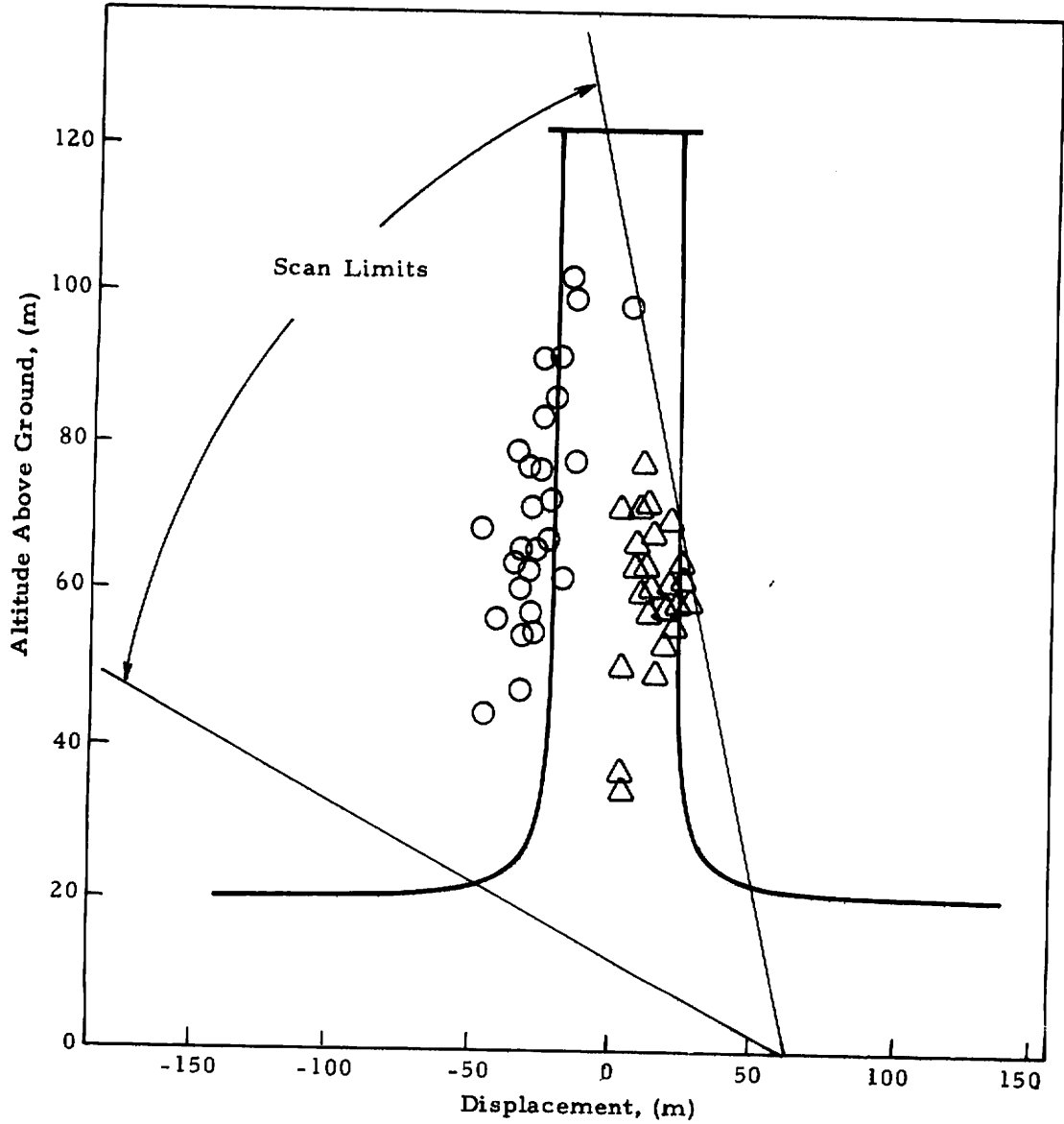


Fig.D-1 - Wake Vortex Trajectory for Rosamond Flyby 23

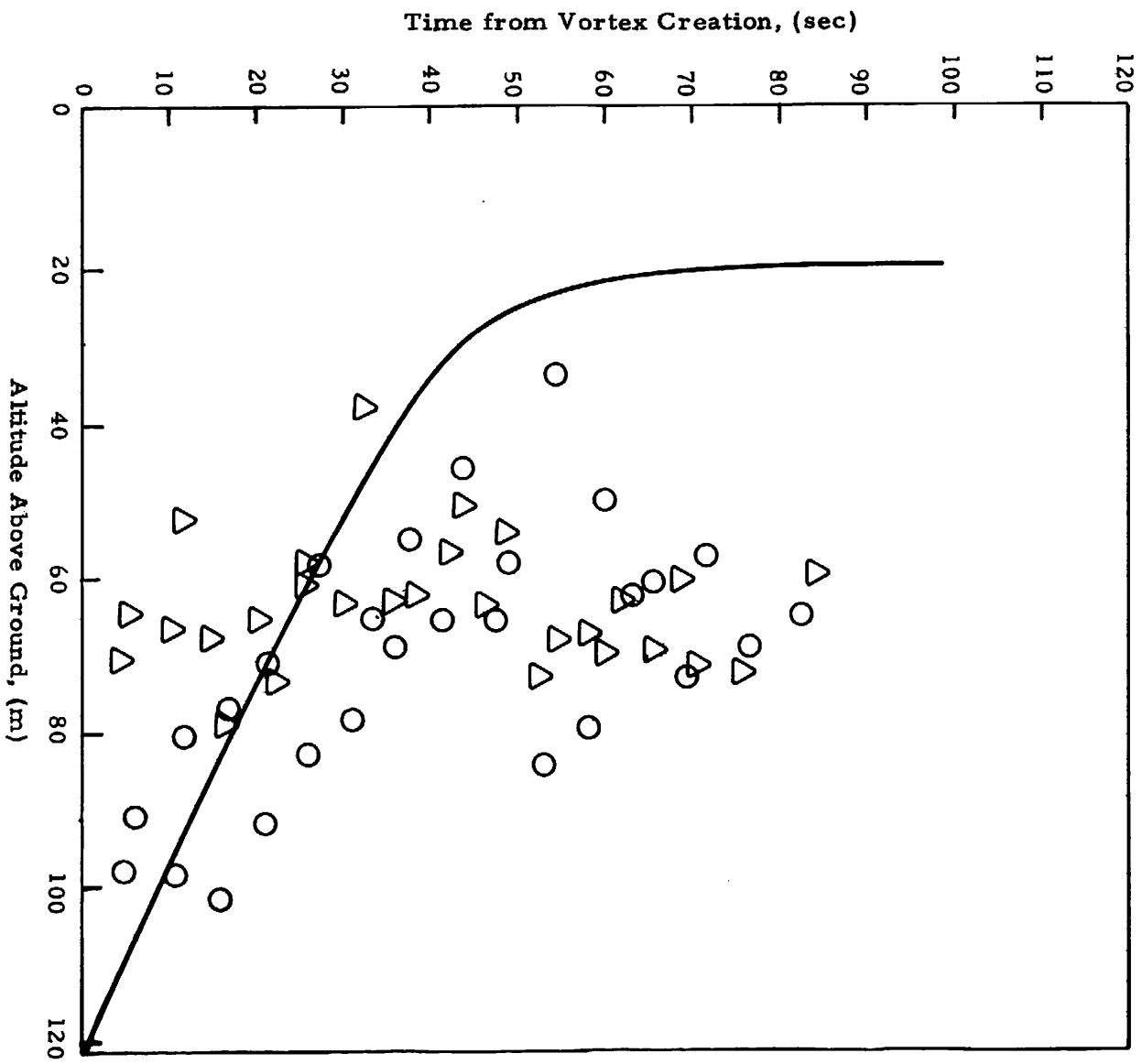


Fig. D-1 - (Concluded)



LDV Measurement

○ Port Vortex

△ Starboard Vortex

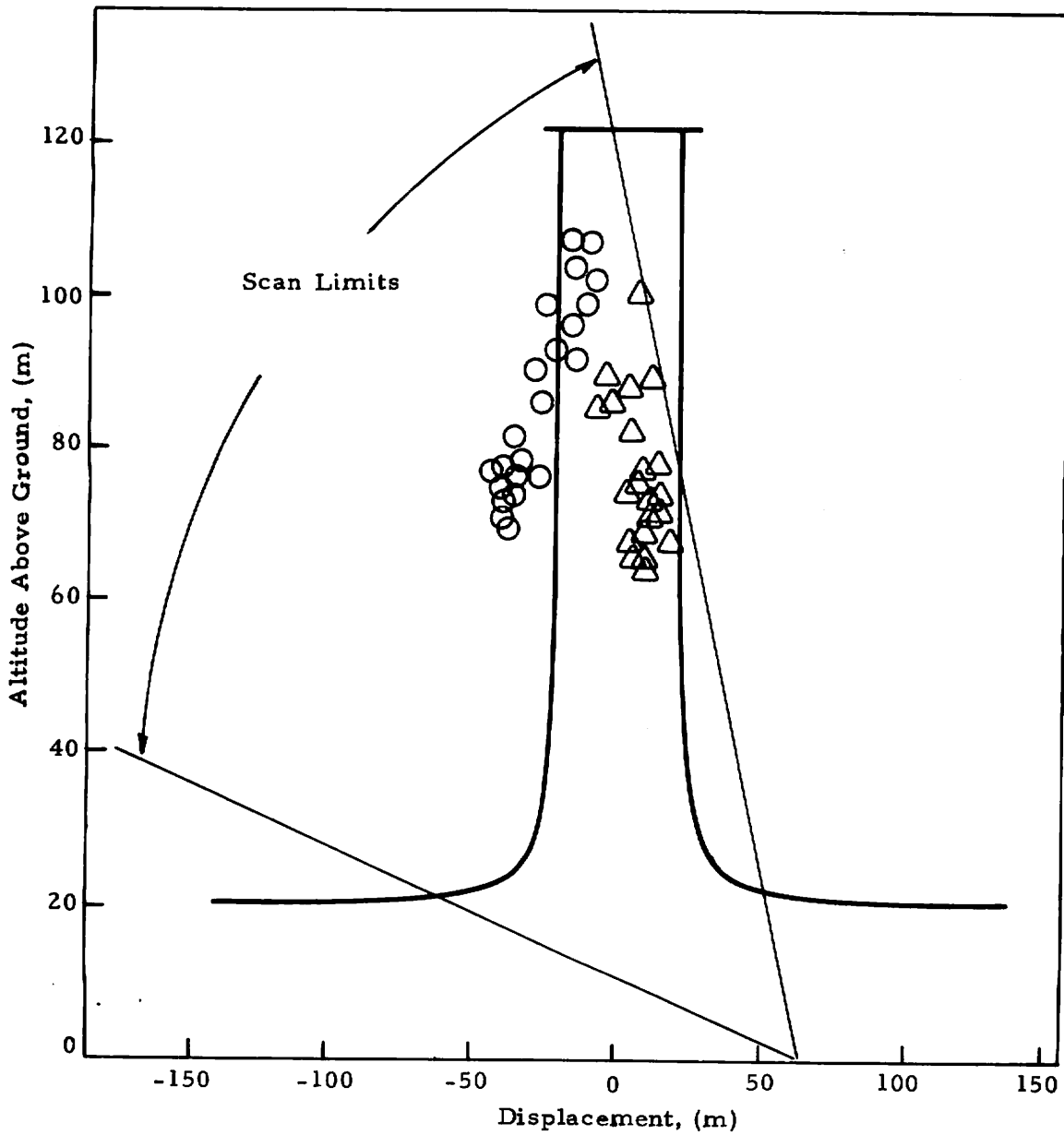


Fig.D-2 - Wake Vortex Trajectory for Rosamond Flyby 24

LDV Measurement

○ Port Vortex

△ Starboard Vortex

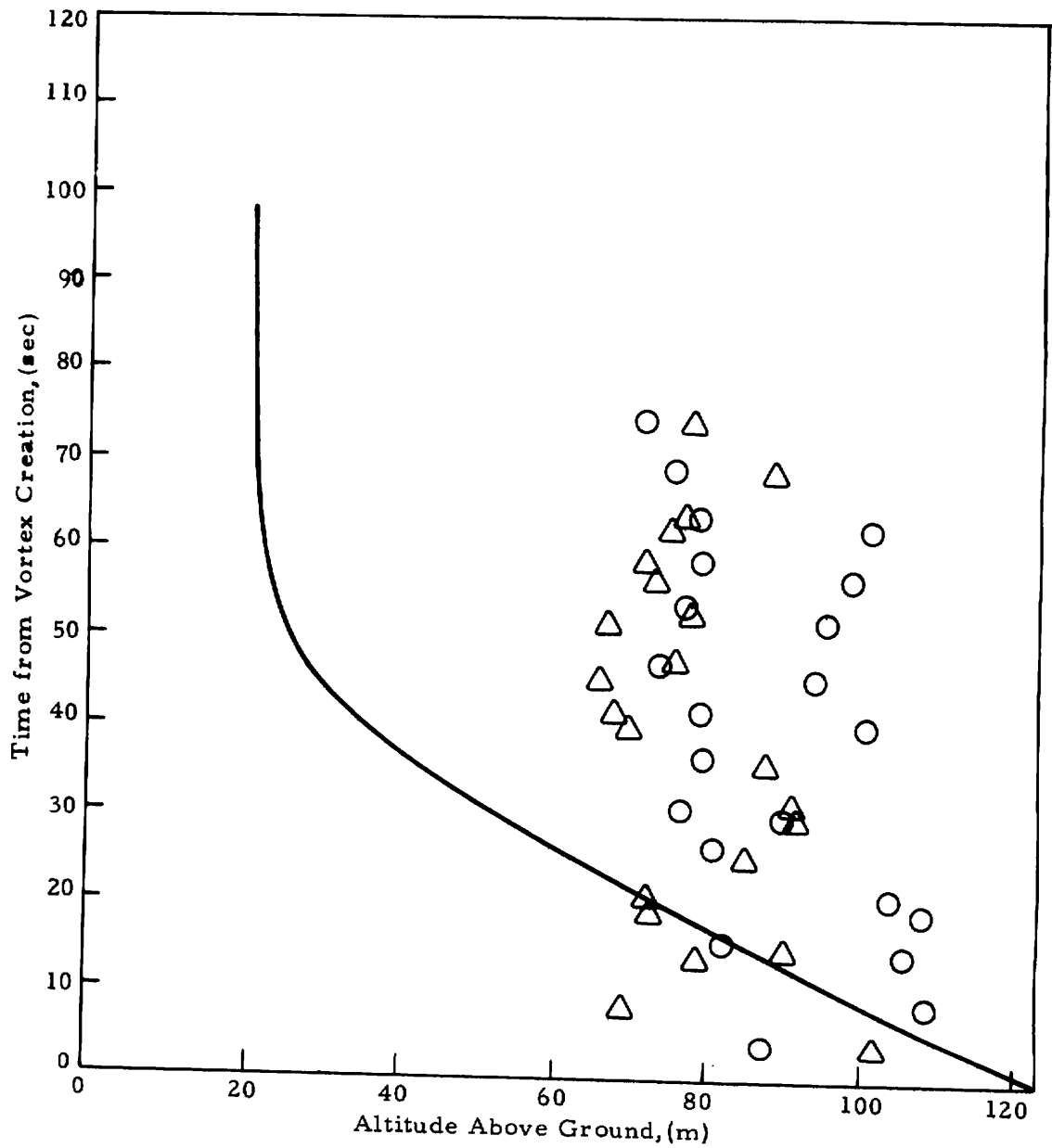


Fig. D-2 - (Concluded)

LDV Measurement

- Port Vortex
- △ Starboard Vortex

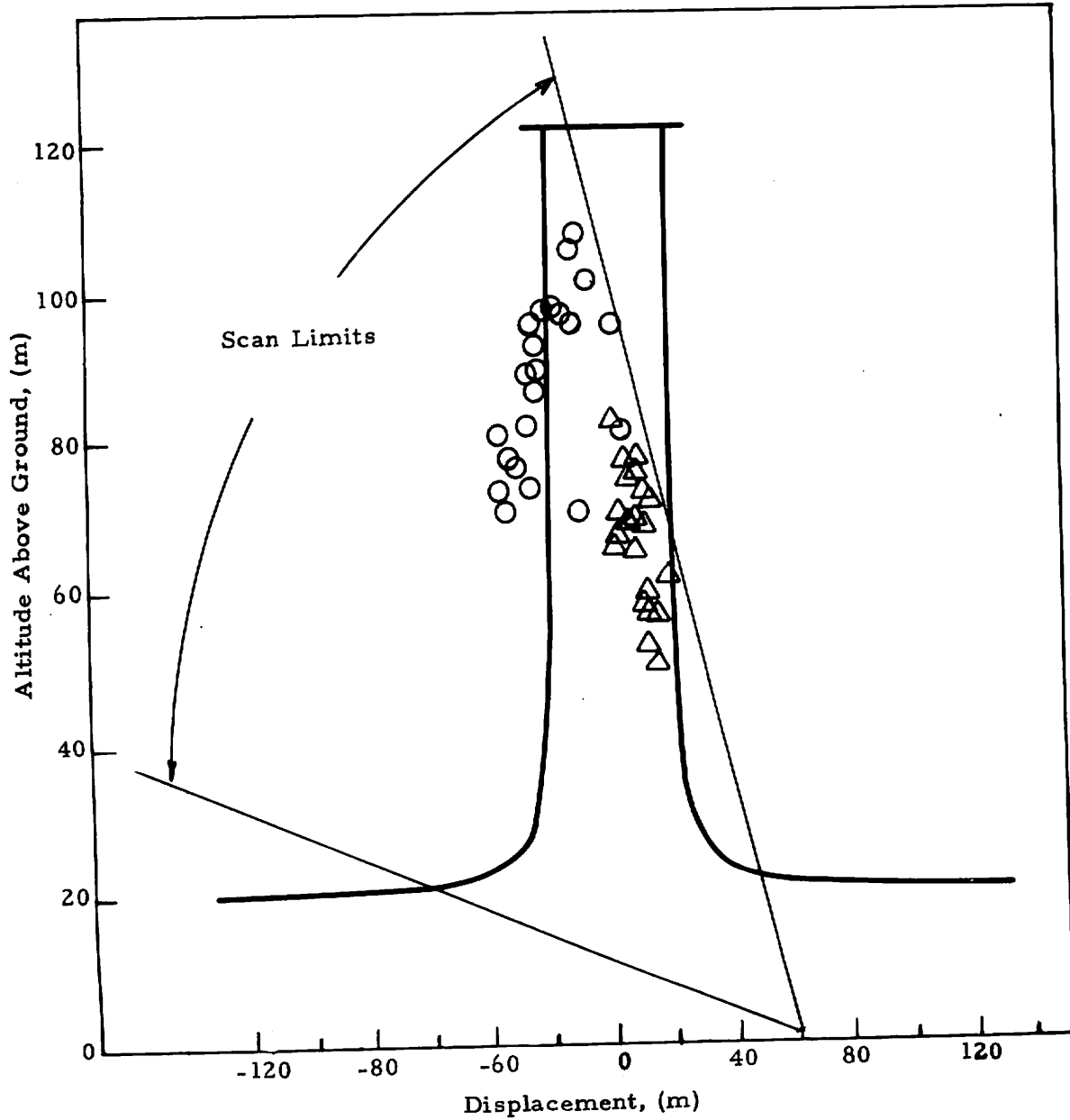


Fig. D-3 - Wake Vortex Trajectory for Rosamond Flyby 25

LDV Measurement

- Port Vortex
- △ Starboard Vortex

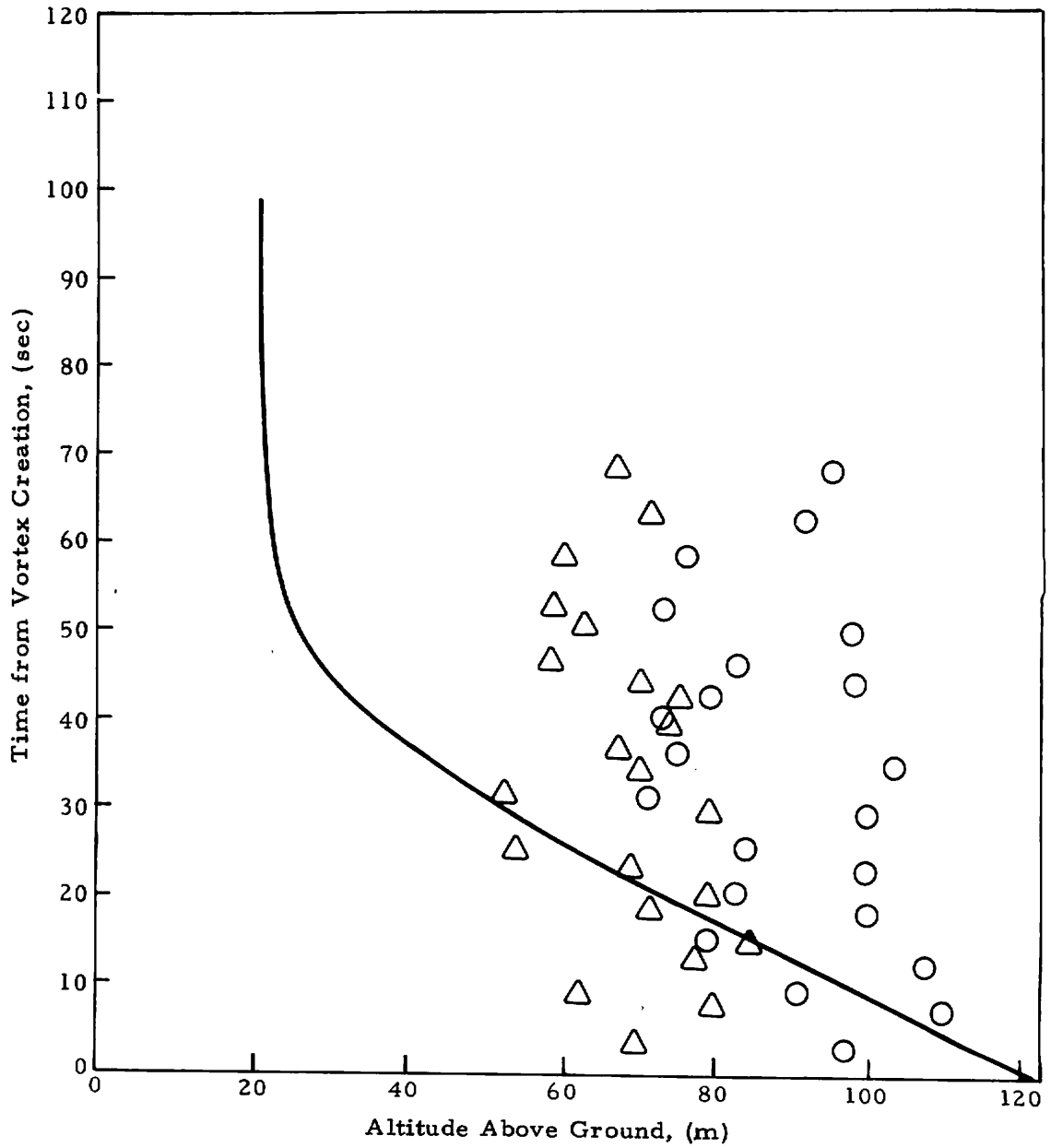


Fig. D-3 - (Concluded)

<u>LDV Measurement</u>	<u>Photographic Measurement</u>	<u>MAVSS</u>	<u>Theory</u>
○ Port Vortex	● Port Vortex	□ Port Vortex	— Predictive Model
△ Starboard Vortex	▲ Starboard Vortex	× Starboard Vortex	
		--- Curve Fit	

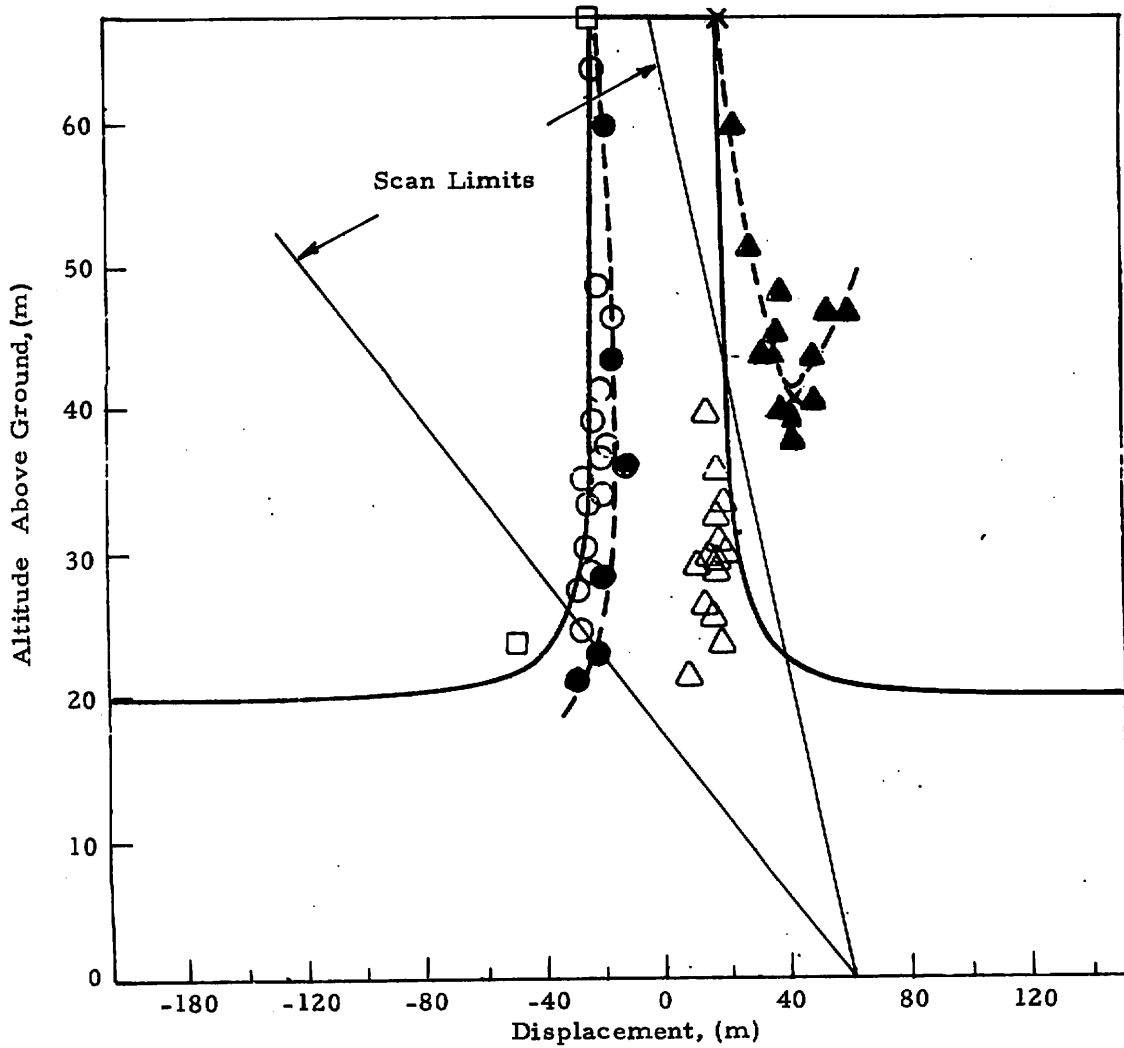


Fig. D-4 - Wake Vortex Trajectory for Rosamond Flyby 27

LDV Measurement	Photographic Measurement	MAVSS	Theory
○ Port Vortex	● Port Vortex	□ Port Vortex	— Predictive Model
△ Starboard Vortex	▲ Starboard Vortex	× Starboard Vortex	
	---	---	---
			Curve Fit

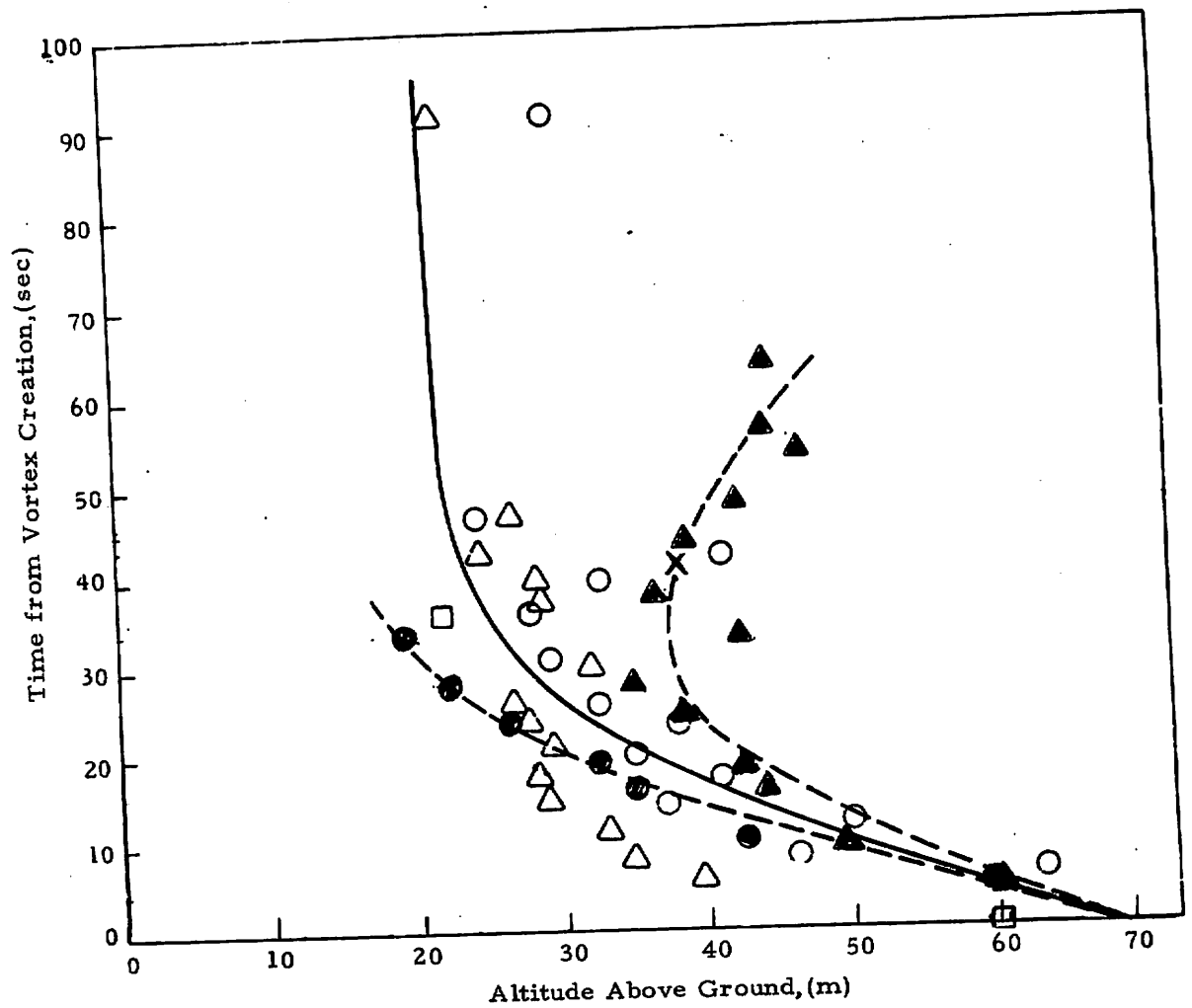


Fig. D-4 - (Concluded)

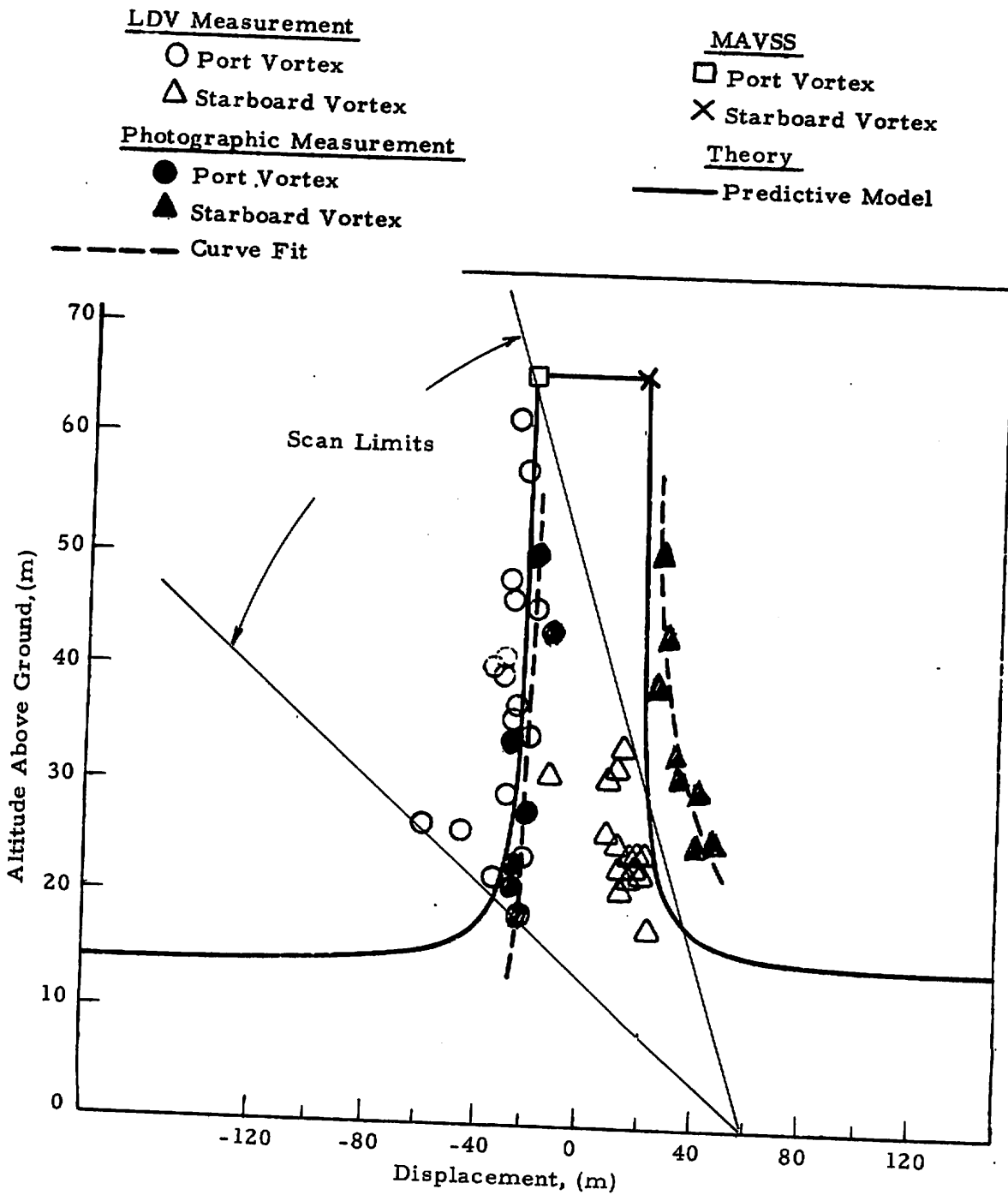


Fig. D-5 - Wake Vortex Trajectory for Rosamond Flyby 28

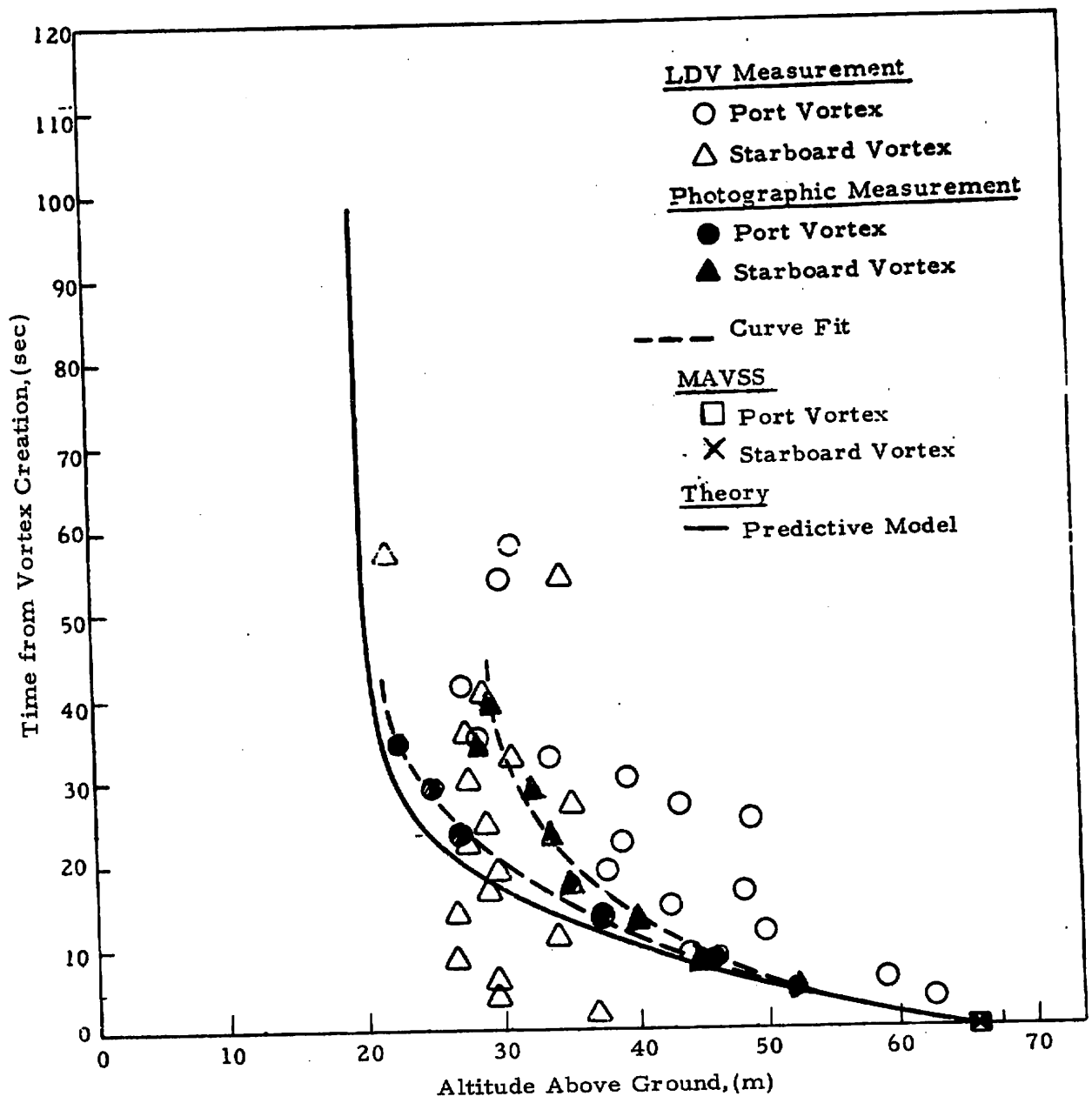


Fig. D-5 - (Concluded)



LDV Measurement

○ Port Vortex

△ Starboard Vortex

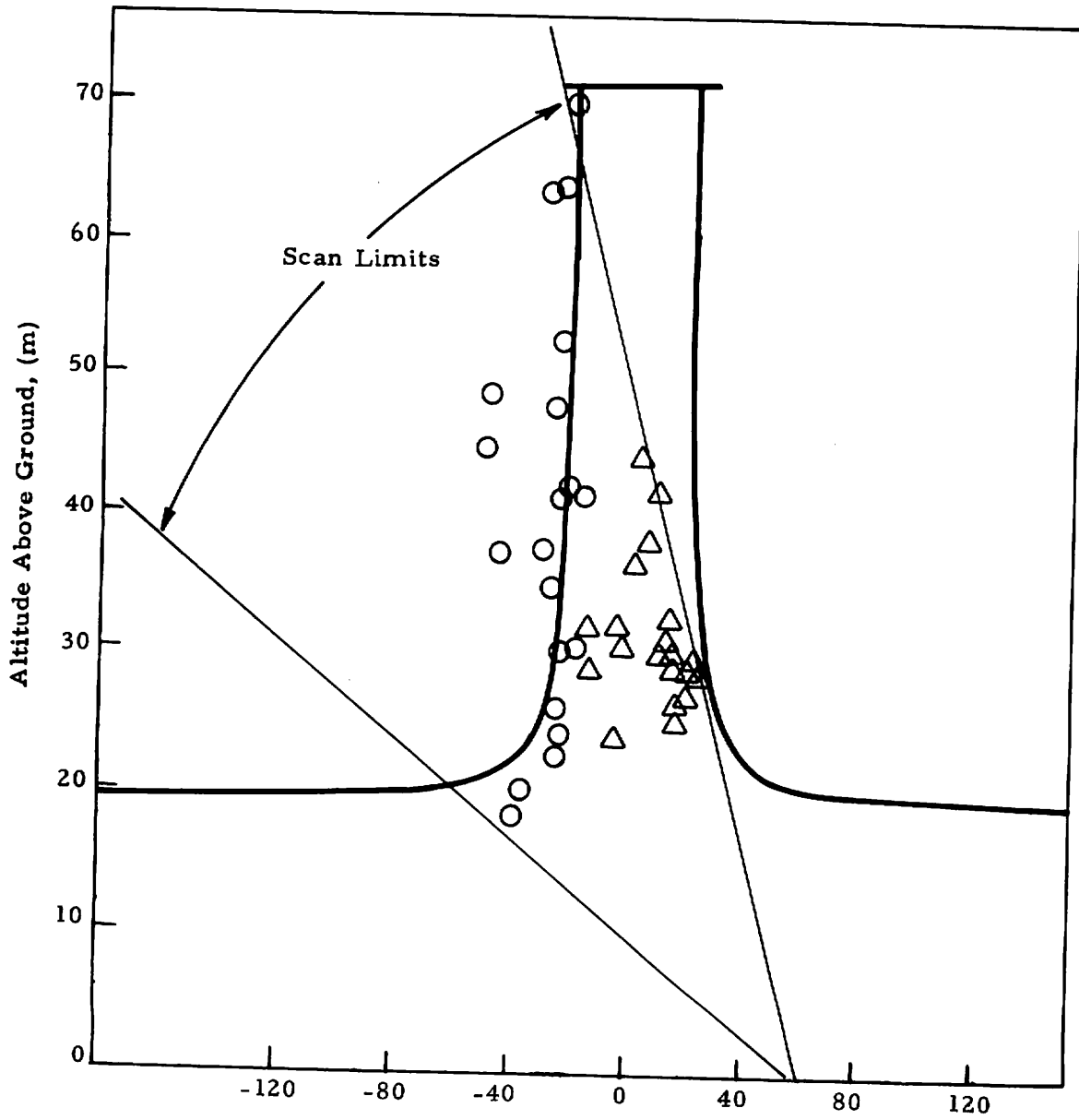


Fig. D-6 - Wake Vortex Trajectory for Rosamond Flyby 29

LDV Measurement

○ Port Vortex

△ Starboard Vortex

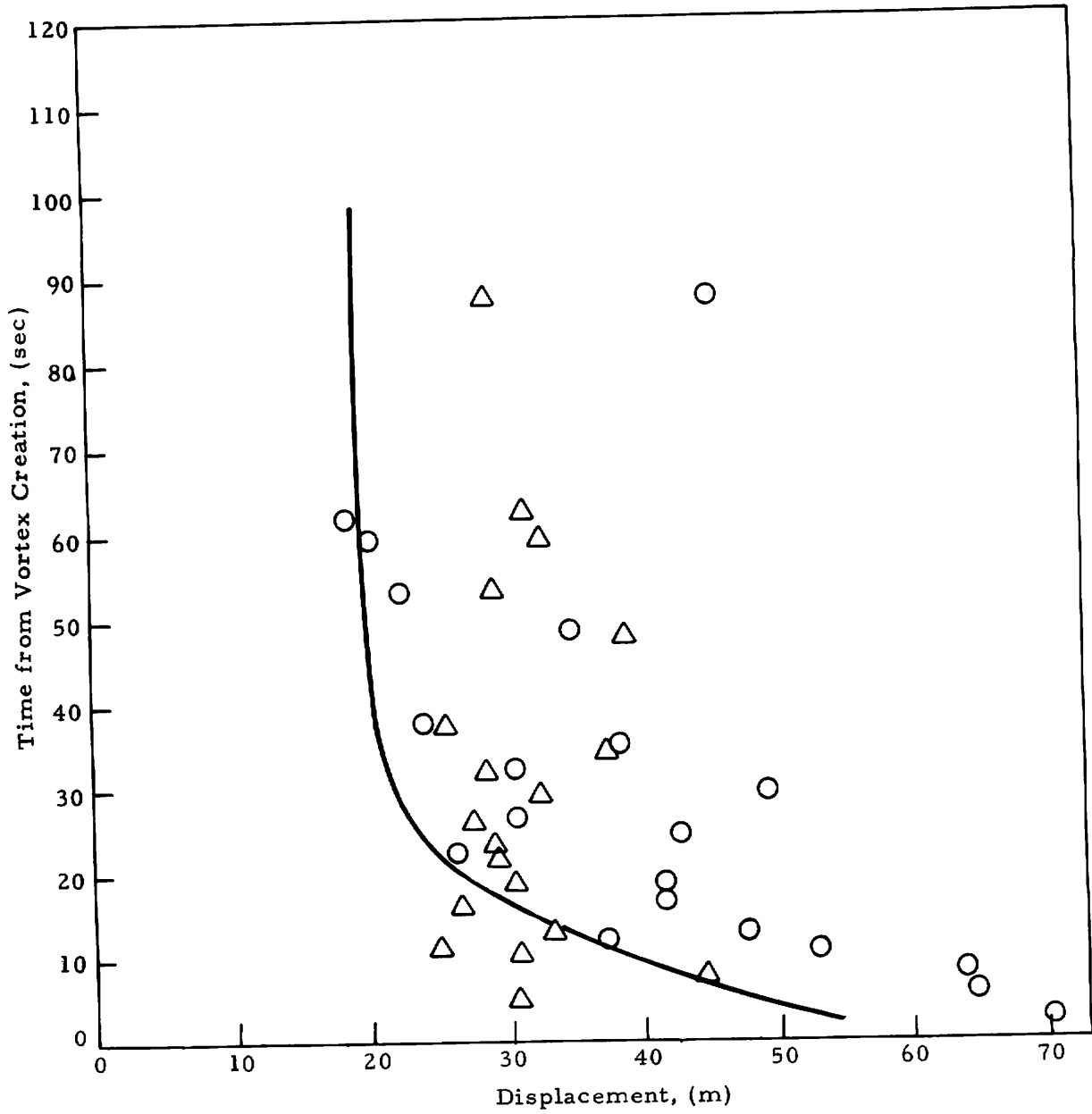


Fig.D-6 - (Concluded)

LDV Measurement

○ Port Vortex

△ Starboard Vortex

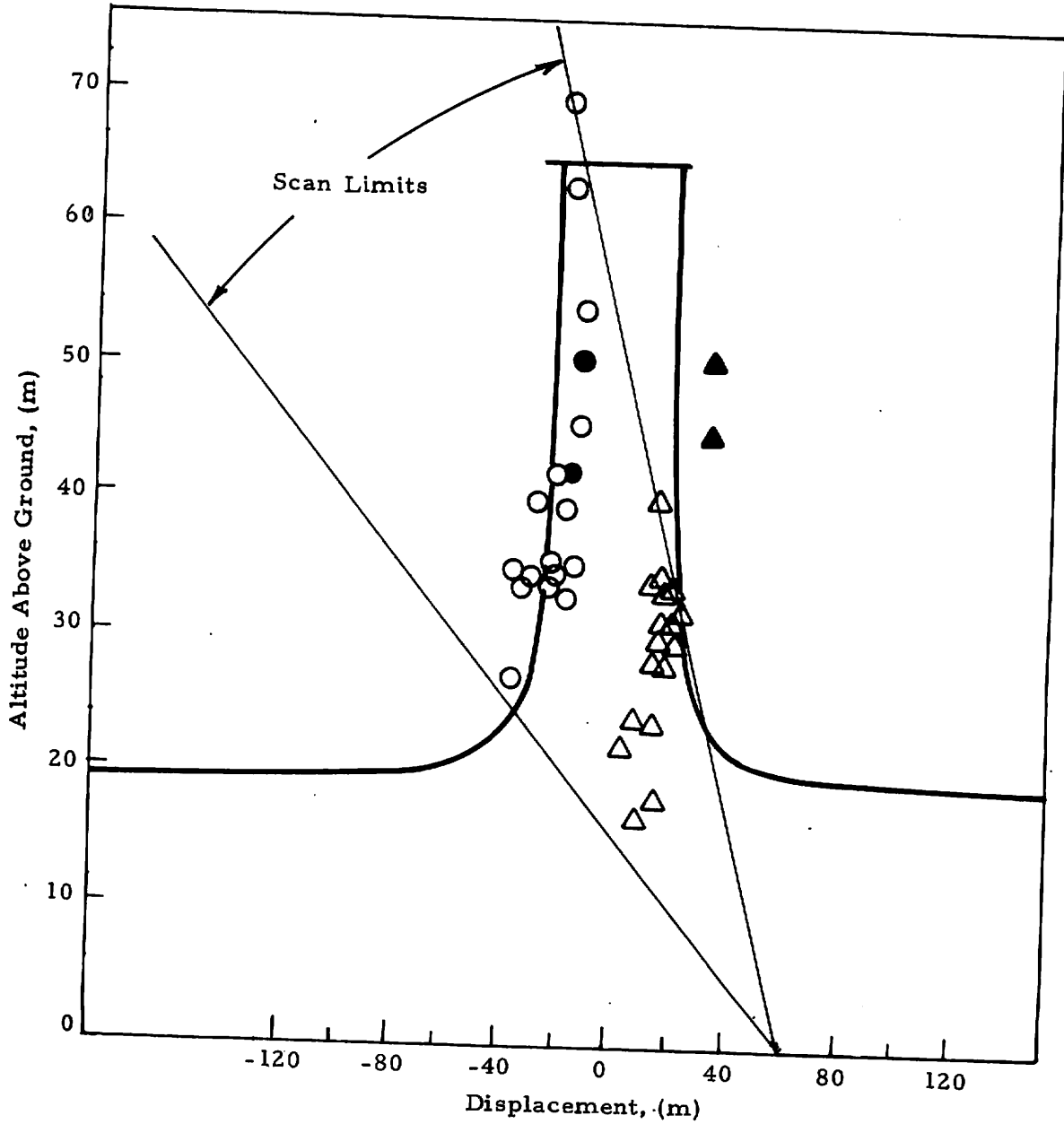


Fig. D-7 - Wake Vortex Trajectory for Rosamond Flyby 30

LDV Measurement

○ Port Vortex

△ Starboard Vortex

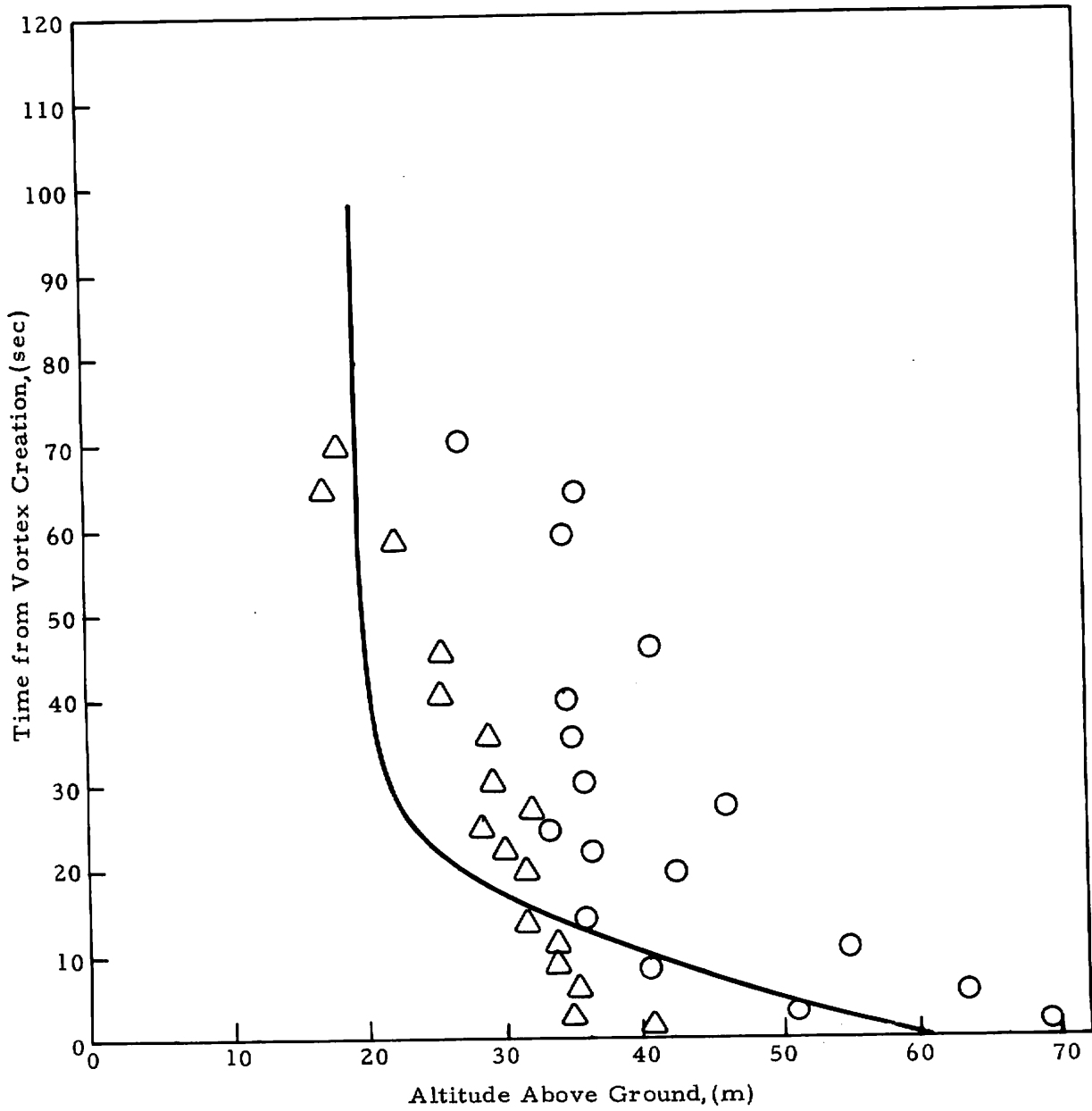


Fig. D-7 - (Concluded)

LDV Measurement

○ Port Vortex

△ Starboard Vortex

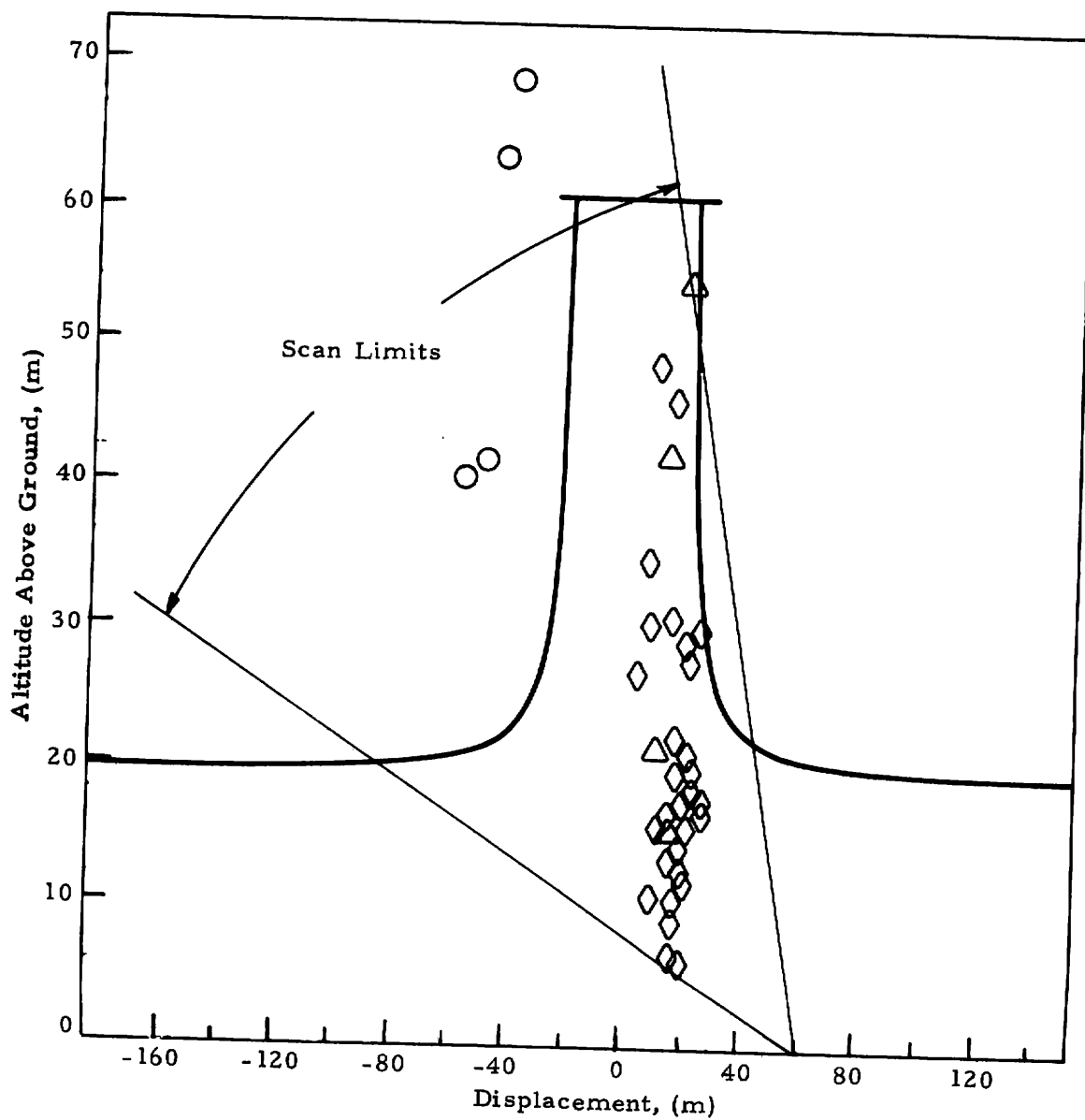


Fig. D-8 - Wake Vortex Trajectory for Rosamond Flyby 40

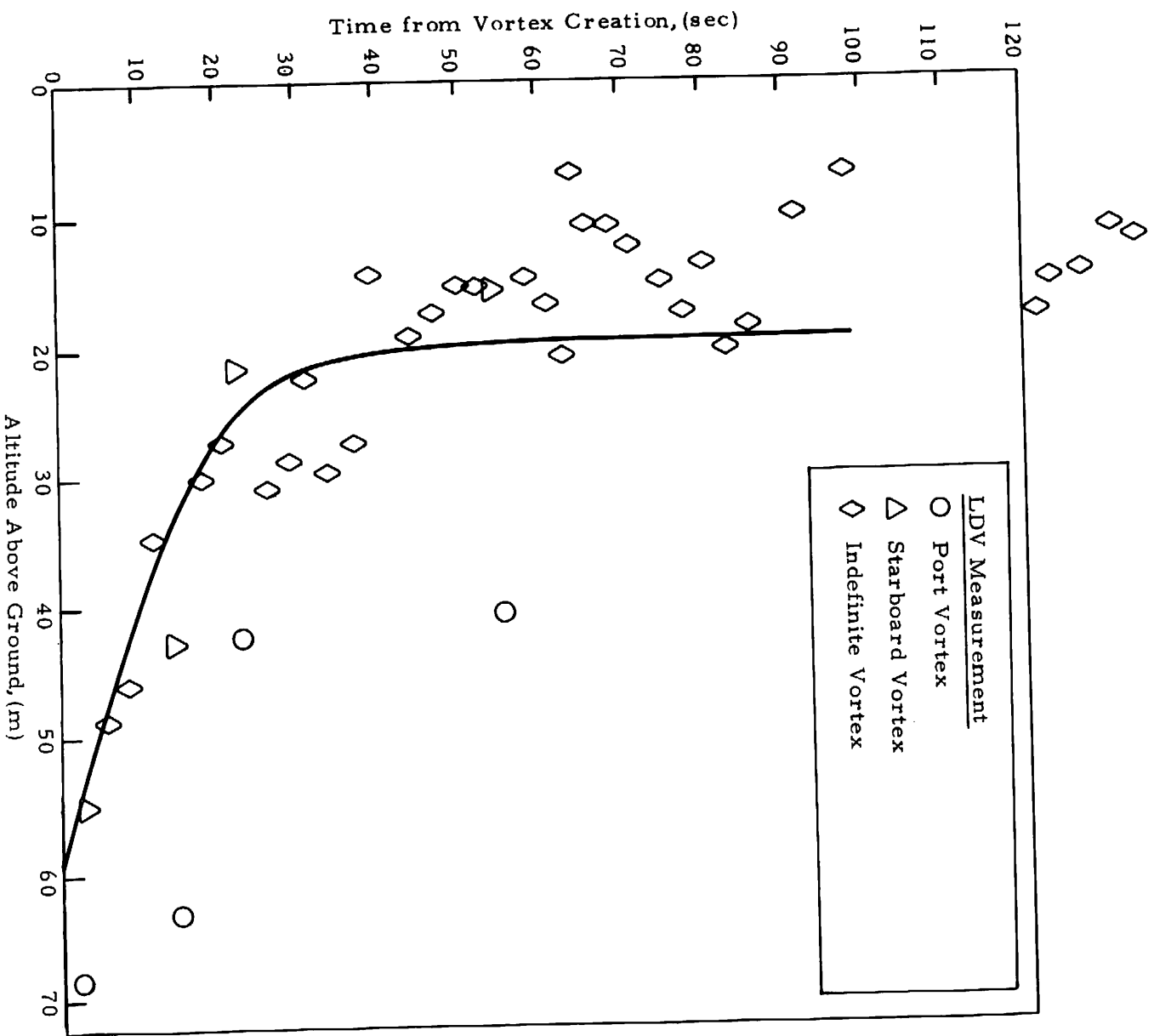


Fig. D-8 - (Concluded)

LDV Measurement

○ Port Vortex

△ Starboard Vortex

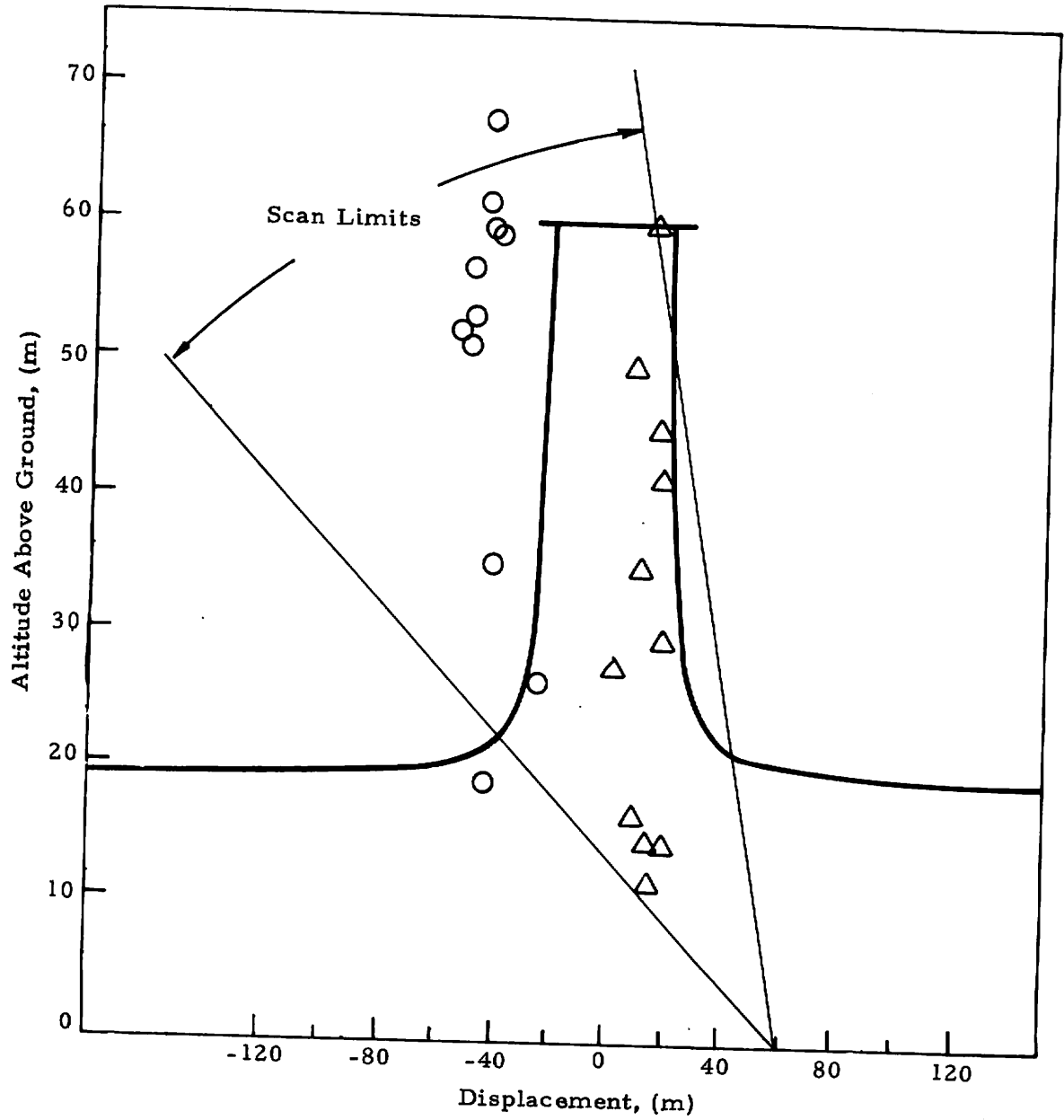


Fig. D-9 - Wake Vortex Trajectory for Rosamond Flyby 42

LDV Measurement

○ Port Vortex

△ Starboard Vortex

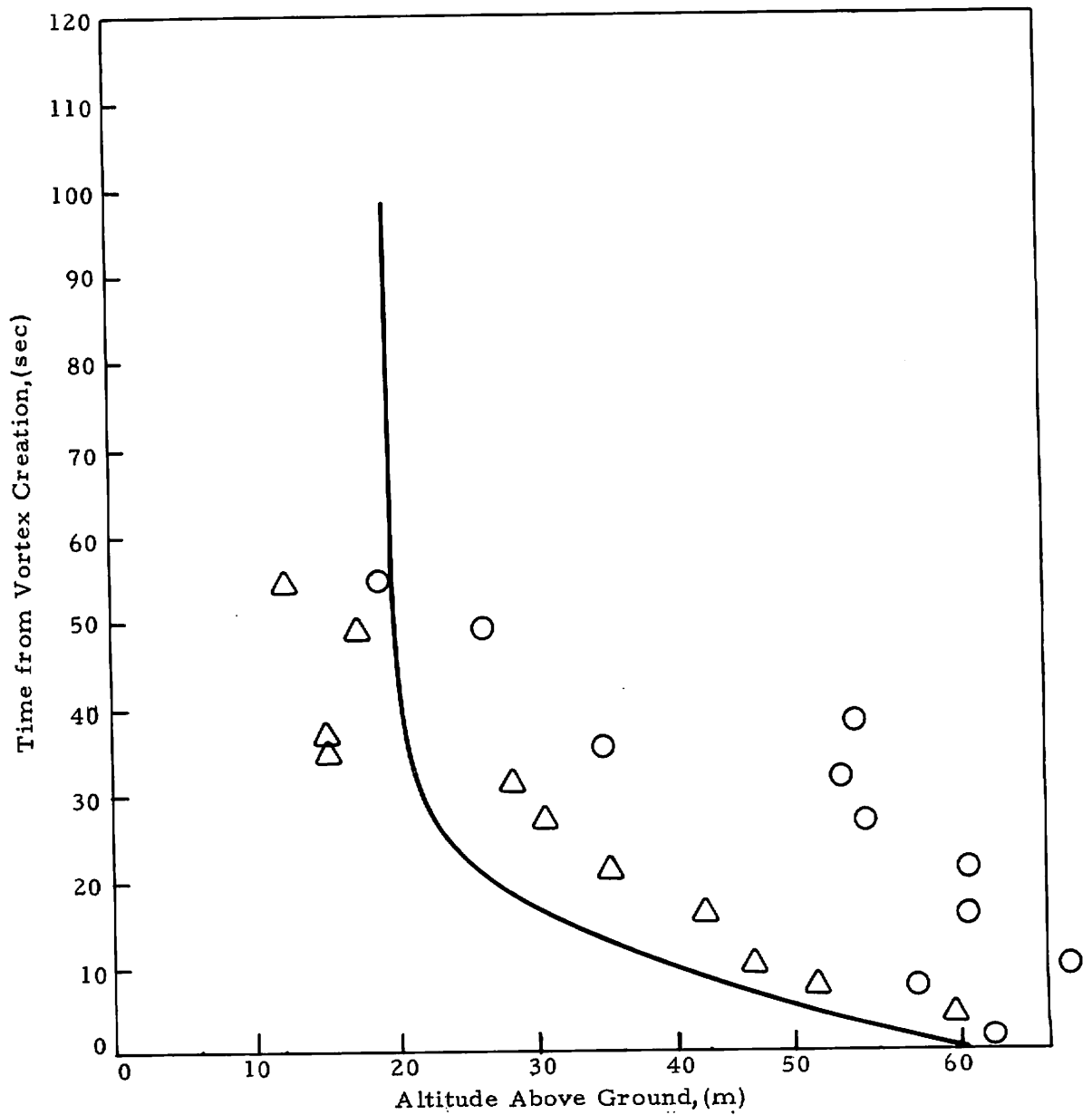


Fig. D-9 - (Concluded)



LDV Measurement

○ Port Vortex

△ Starboard Vortex

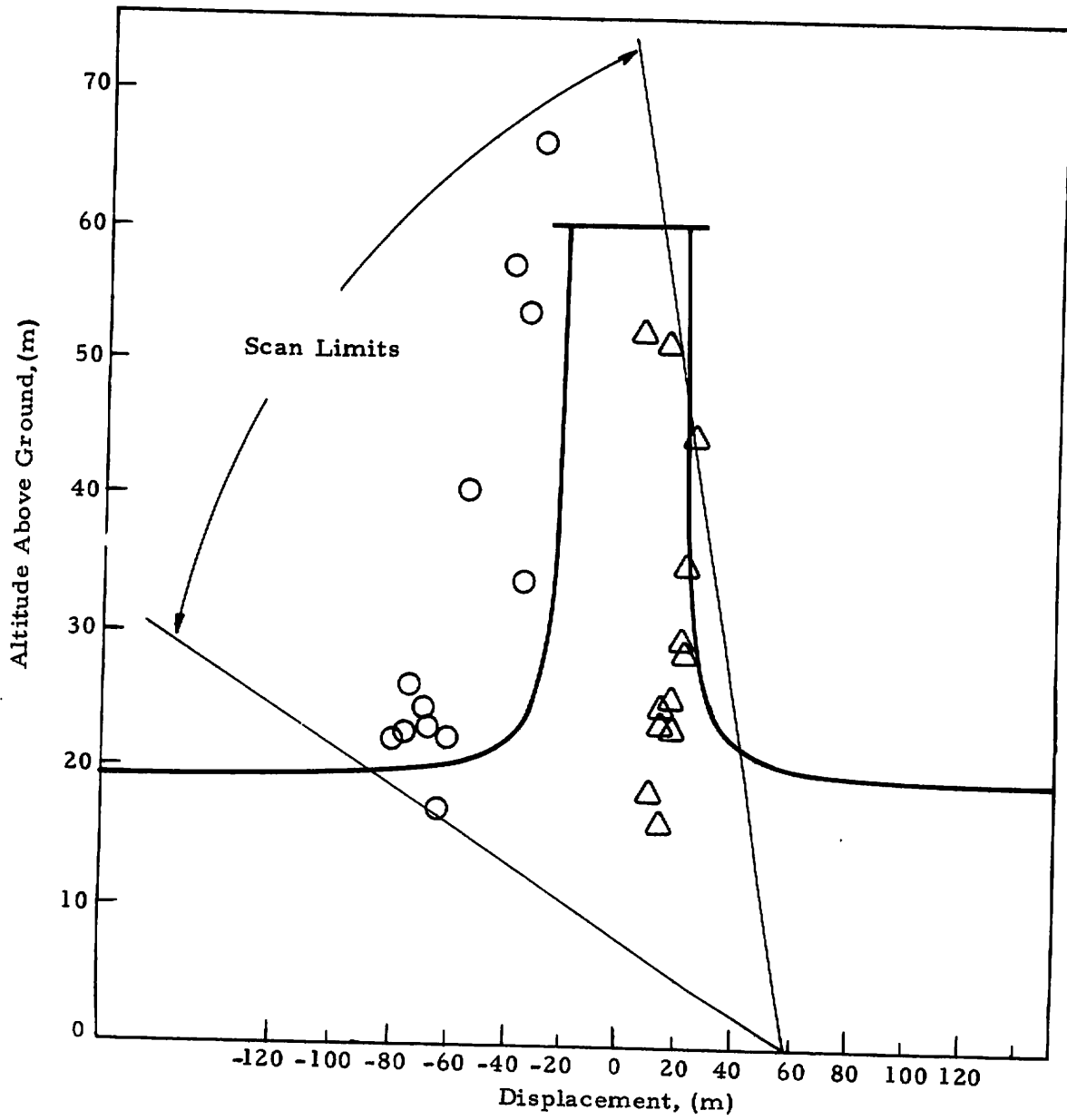


Fig. D-10 - Wake Vortex Trajectory for Rosamond Flyby 44

LDV Measurement

- Port Vortex
- △ Starboard Vortex

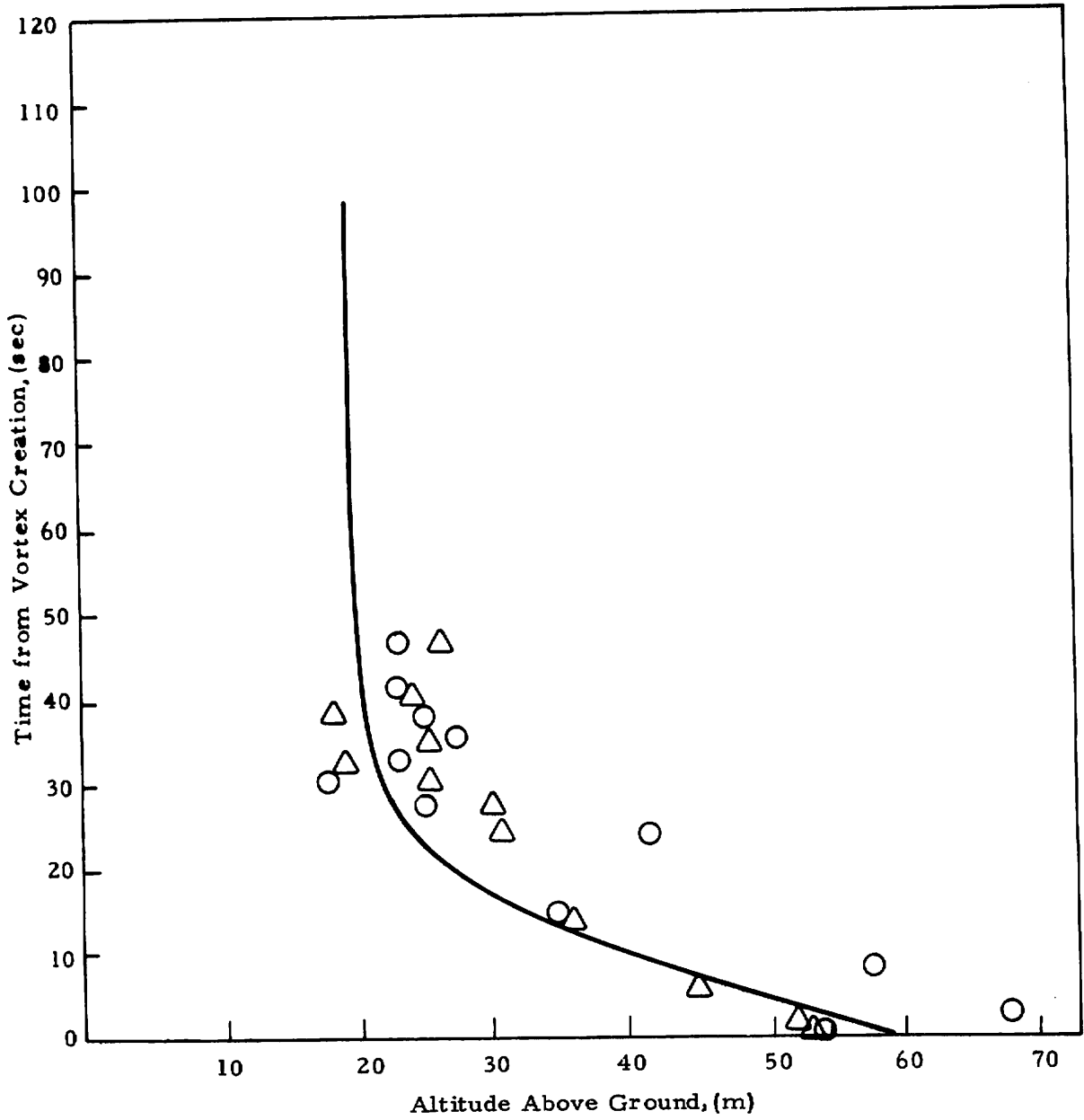


Fig. D-10 - (Concluded)

LDV Measurement

○ Port Vortex

△ Starboard Vortex

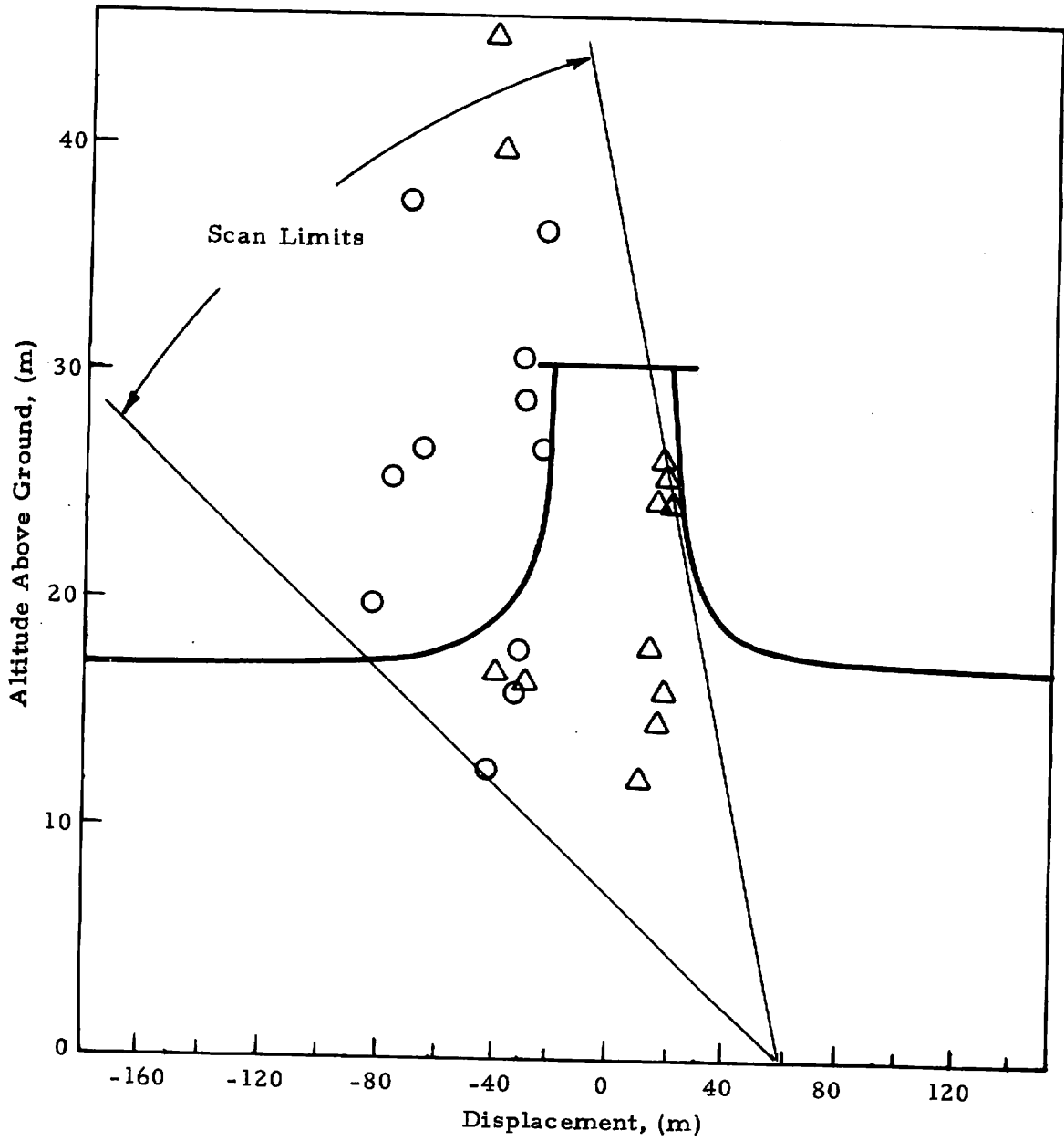


Fig. D-11 - Wake Vortex Trajectory for Rosamond Flyby 46

LDV Measurement

- Port Vortex
- △ Starboard Vortex

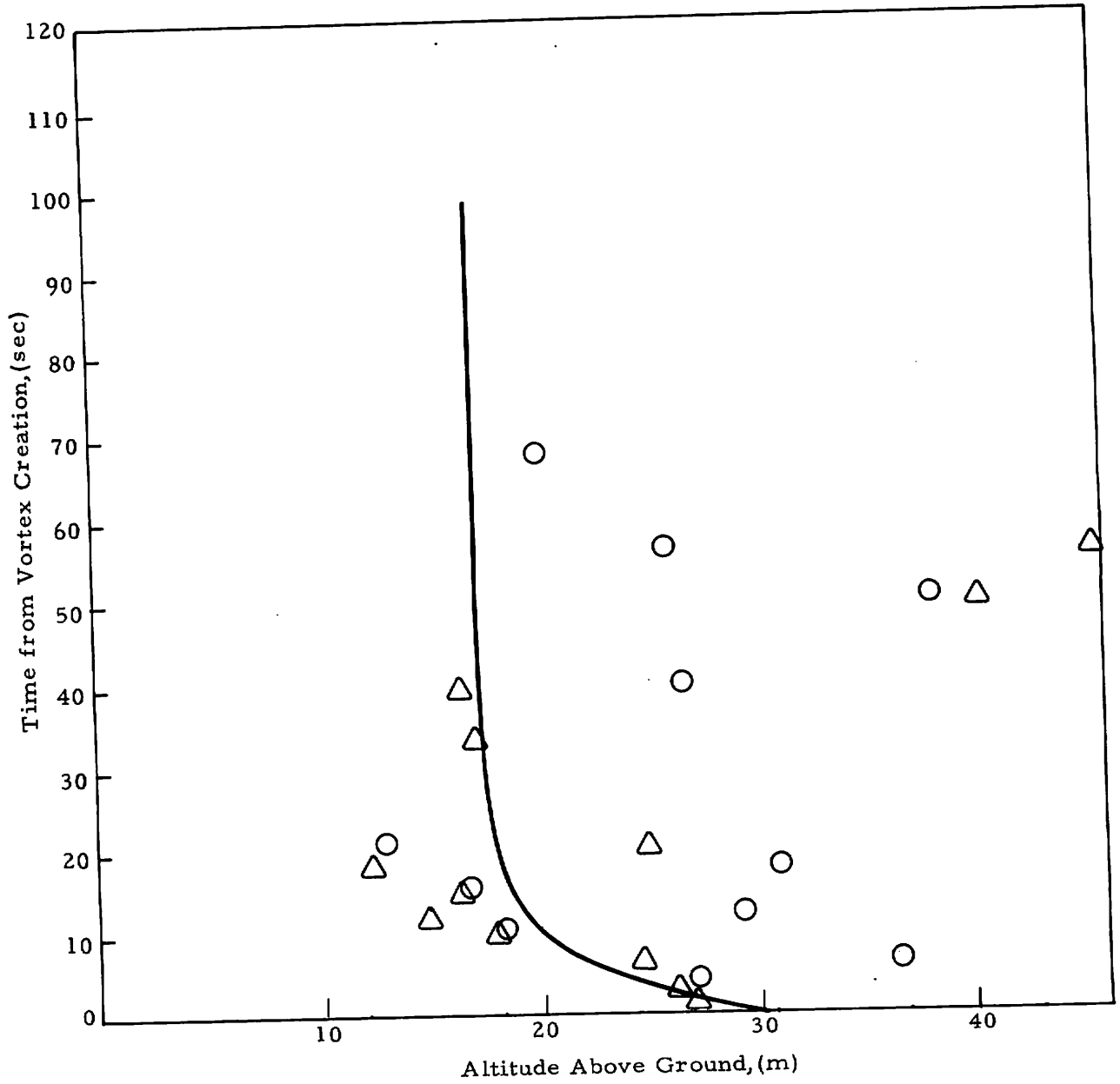


Fig. D-11 - (Concluded)

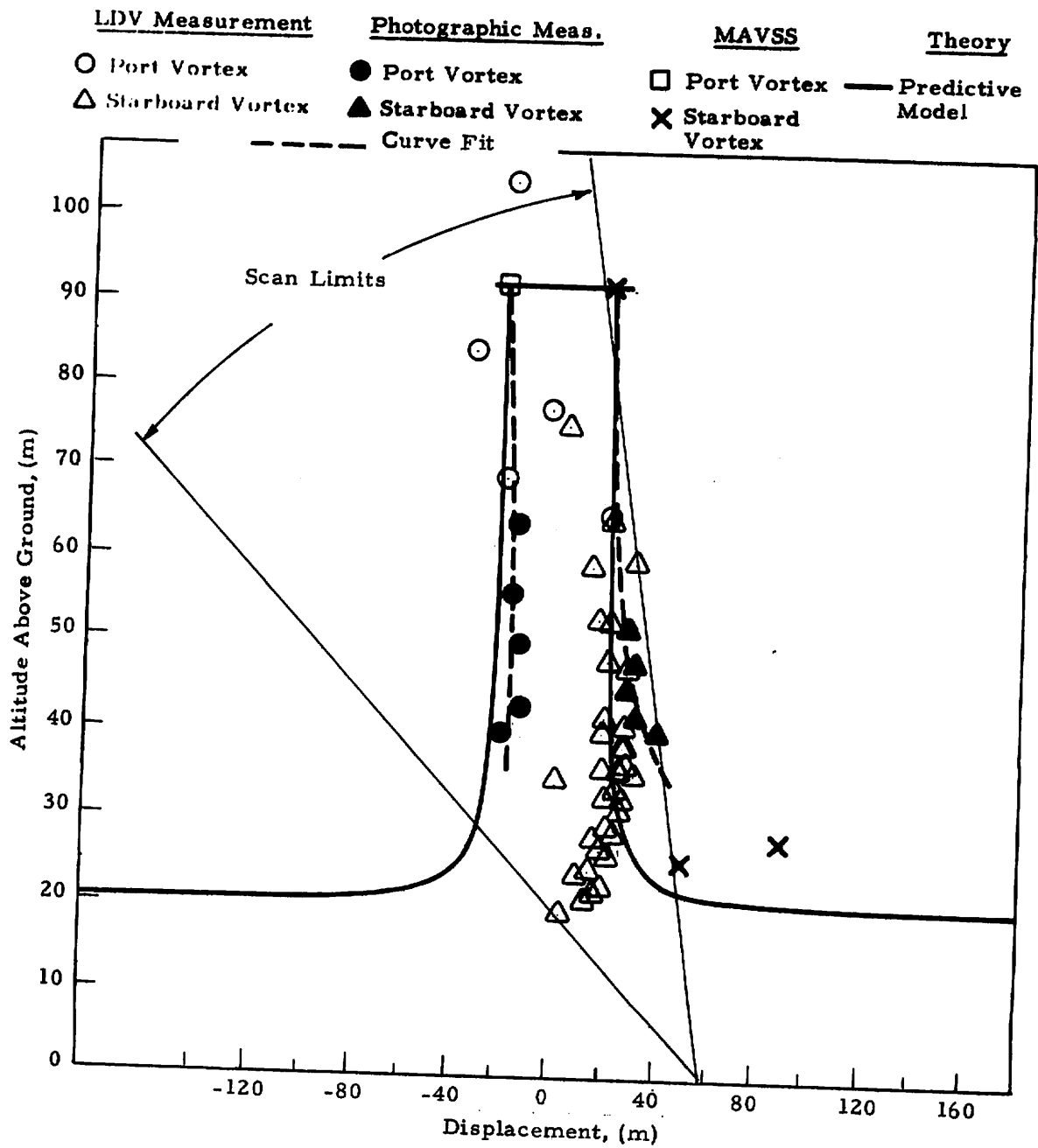


Fig. D-12 - Wake Vortex Trajectory for Rosamond Flyby 47

<u>LDV Measurement</u>	<u>Photographic Measurement</u>	<u>MAVSS</u>	<u>Theory</u>
○ Port Vortex	● Port Vortex	□ Port Vortex	— Predictive Model
△ Starboard Vortex	▲ Starboard Vortex	× Starboard Vortex	

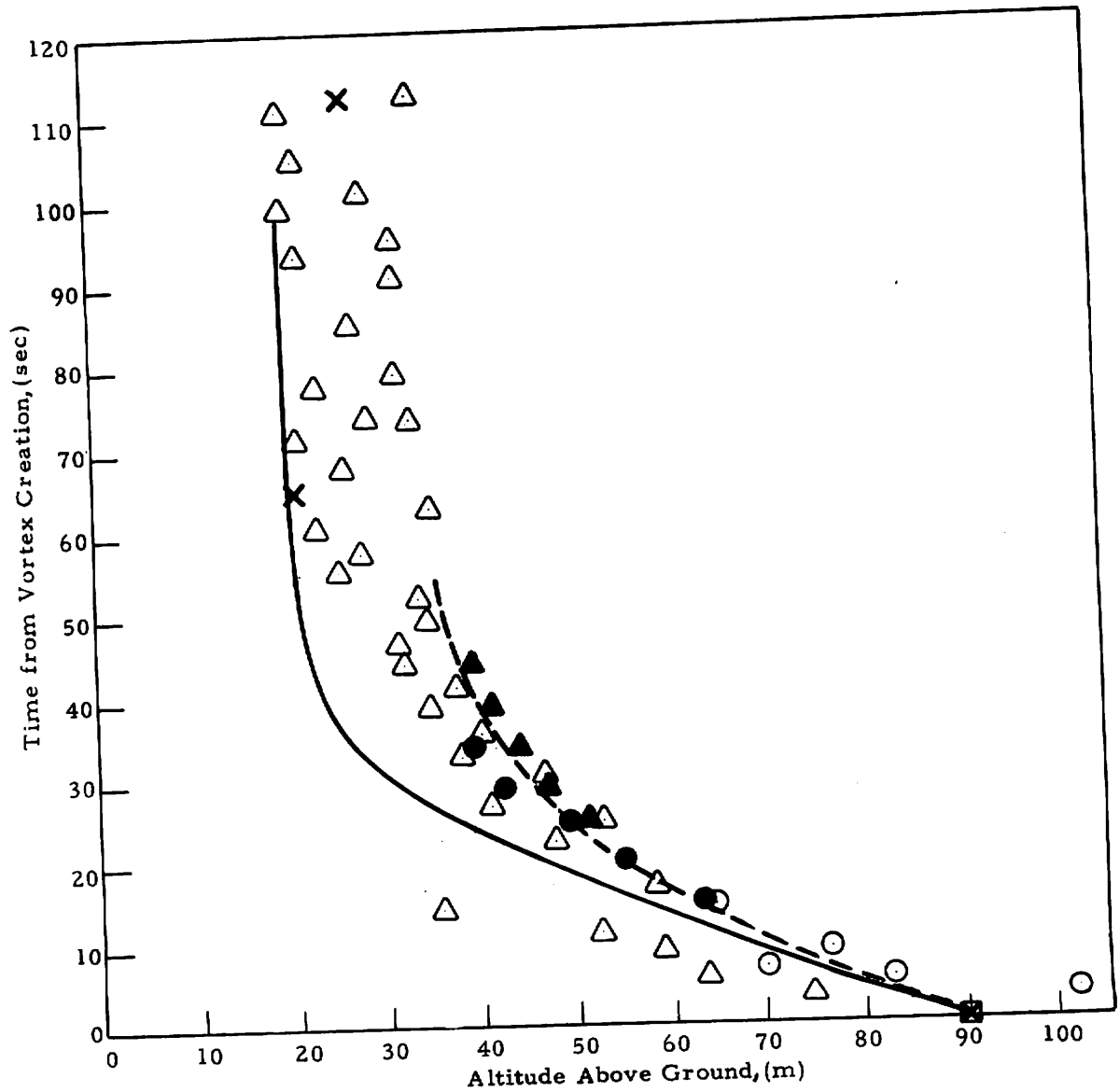


Fig. D-12 - (Concluded)

<u>LDV Measurement</u>	<u>Photographic Measurement</u>	<u>MAVSS</u>	<u>Theory</u>
○ Port Vortex	● Port Vortex	□ Port Vortex	— Predictive Model
△ Starboard Vortex	▲ Starboard Vortex	× Starboard Vortex	

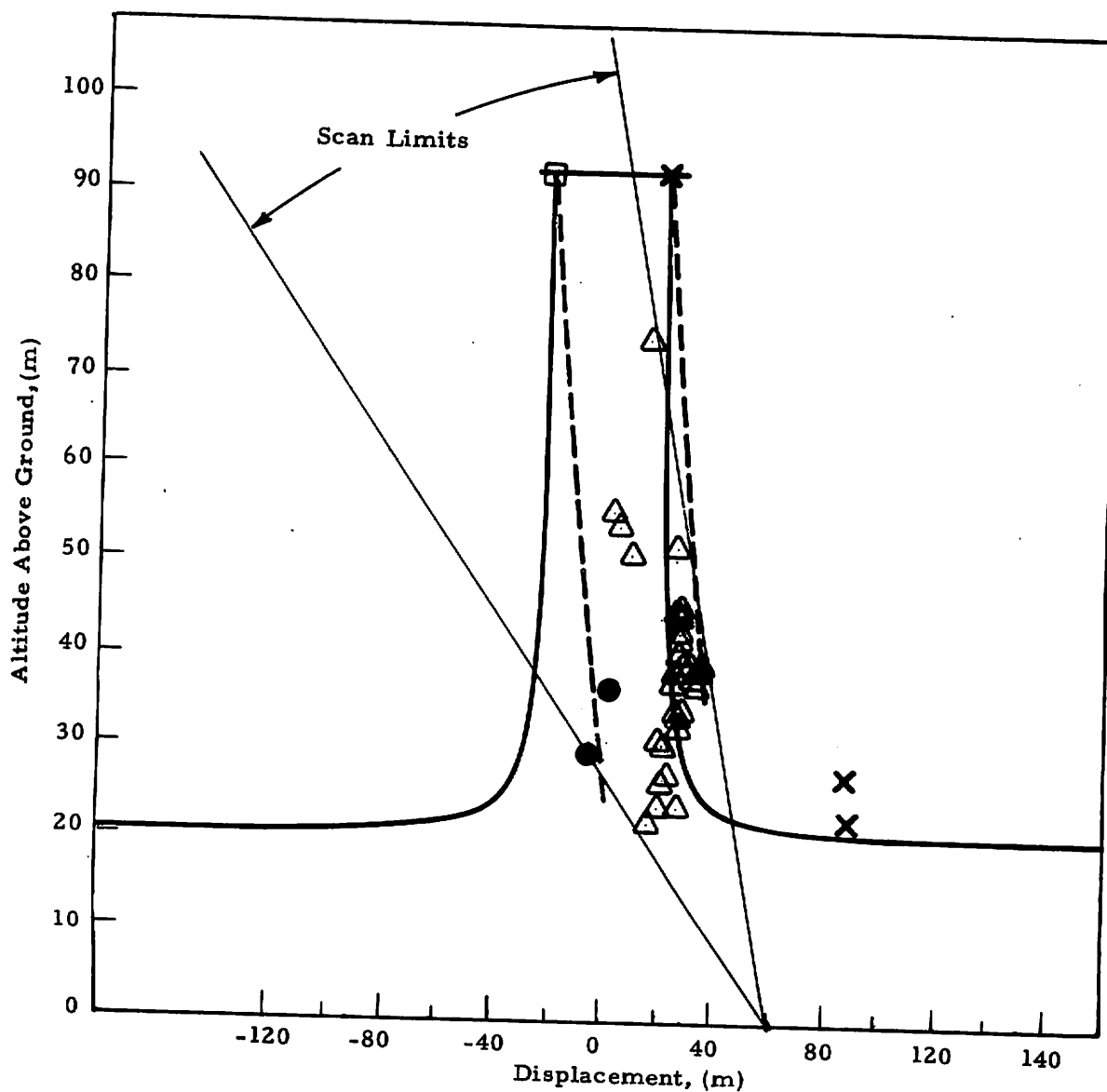


Fig. D-13 - Wake Vortex Trajectory for Rosamond Flyby 48

<u>LDV Measurement</u>	<u>Photographic Measurement</u>	<u>MAVSS</u>	<u>Theory</u>
○ Port Vortex	● Port Vortex	□ Port Vortex	— Predictive Model
△ Starboard Vortex	▲ Starboard Vortex	× Starboard Vortex	

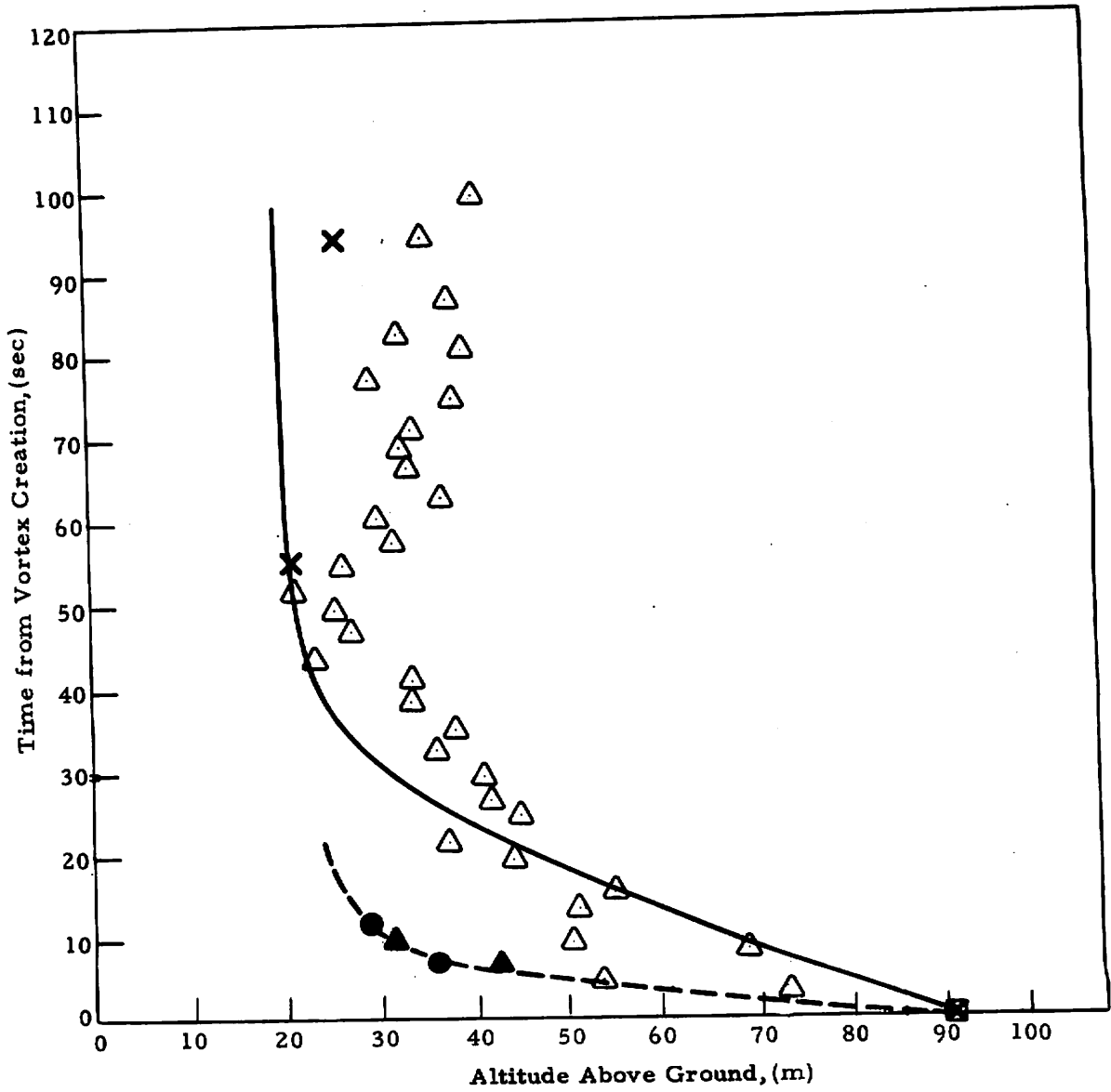


Fig. D-13 - (Concluded)



<u>LDV Measurement</u>	<u>Photographic Measurement</u>	<u>MAVSS</u>	<u>Theory</u>
○ Port Vortex	● Port Vortex	□ Port Vortex	— Predictive Model
△ Starboard Vortex	▲ Starboard Vortex	× Starboard Vortex	

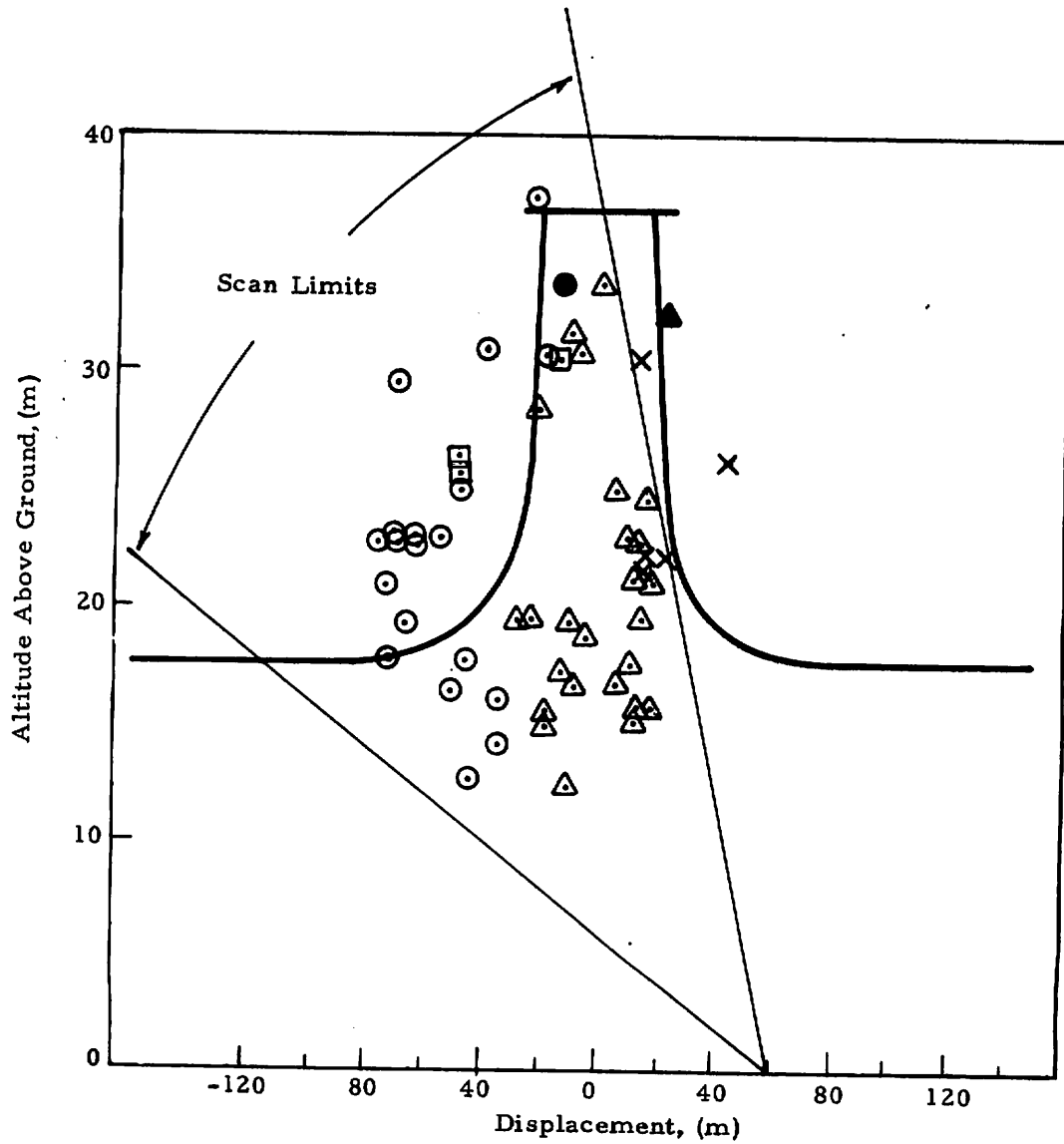


Fig. D-14 - Wake Vortex Trajectory for Rosamond Flyby 49

<u>LDV Measurement</u>	<u>Photographic Measurement</u>	<u>MAVSS</u>	<u>Theory</u>
○ Port Vortex	● Port Vortex	□ Port Vortex	— Predictive Model
△ Starboard Vortex	▲ Starboard Vortex	× Starboard Vortex	

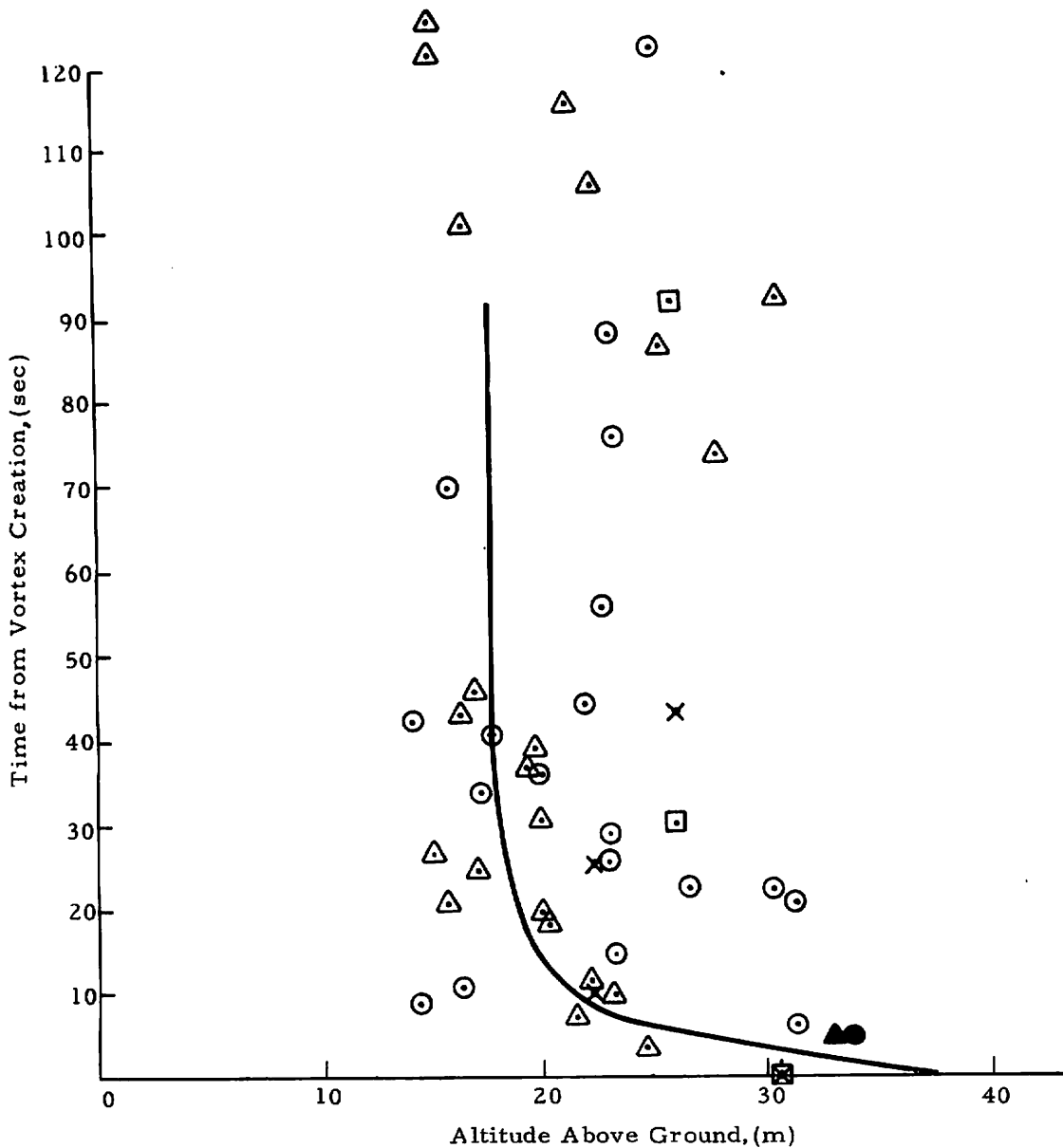
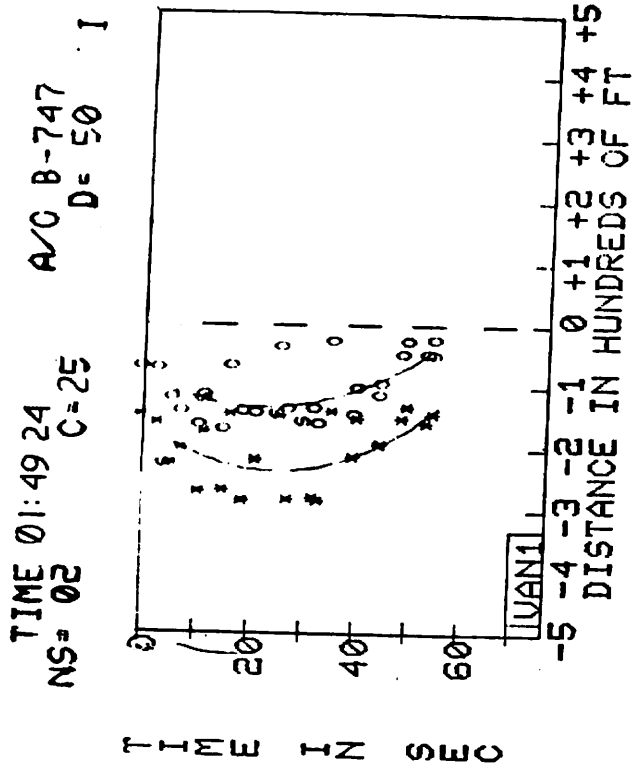
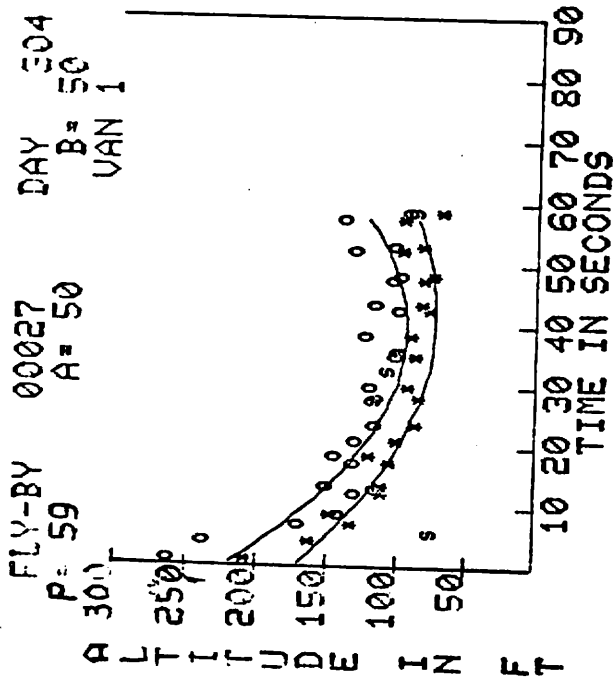


Fig. D-14 - (Concluded)

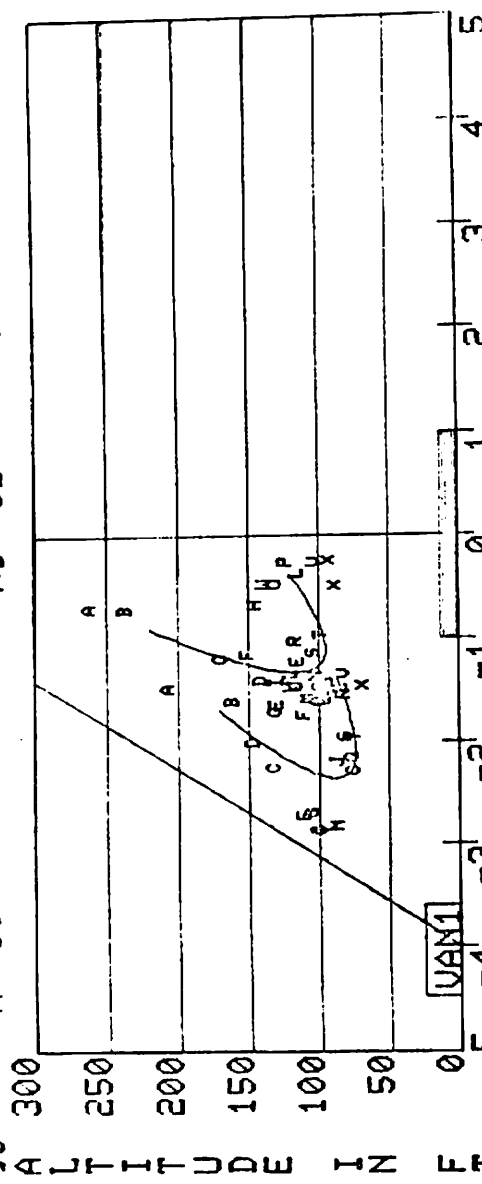
## Appendix E

### WAKE VORTEX TRACKS COMPUTED FROM HIGH-SPEED MEASUREMENTS

The measurements obtained with the NASA high-speed filter bank and processor and software system are summarized in this appendix. The output consists of three plots: (1) vortex altitude versus time; (2) lateral distance versus time; and (3) altitude versus lateral distance. A listing of the vortex locations is given in a table following the three plots. The port and starboard vortices are indicated by (0\*) and (\*) on the altitude and lateral distance versus time plots. The vortices are labeled by letters A to Z on the lateral distance plots (each pair of letters corresponds to a successive elevation scan frame).



FLY-BY 00027 DAY 304 TIME 01:49 24 A/O B-747  
 R: 59 ALTITUDE IN FT A= 50 B= 50 NS= 0E O= 5 D= 50



HORIZONTAL POSITION FROM CENTER OF RUNWAY IN HUNDREDS OF FT

FLY-BY 00027

DAY 304

TIME 01 49 24

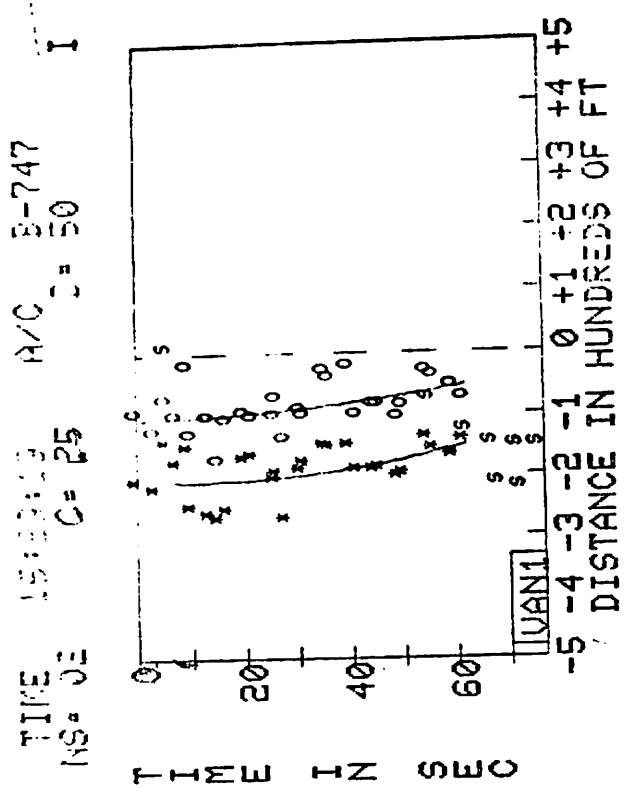
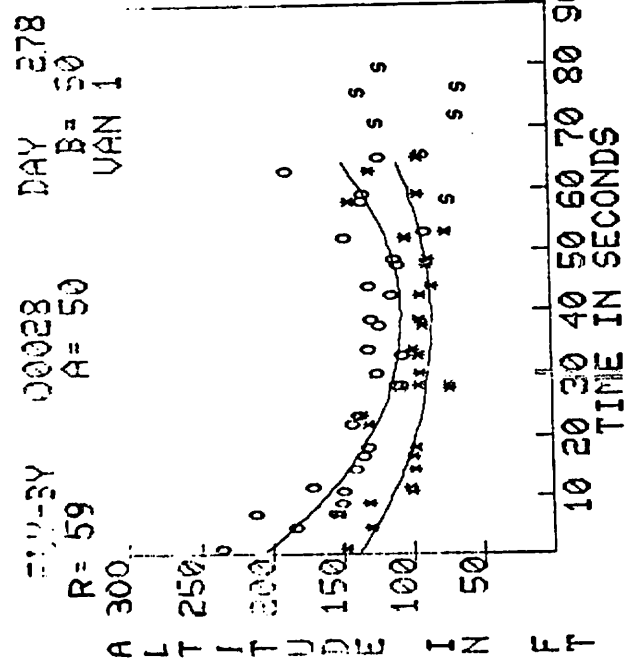
A/C B-747

C=25

D=50

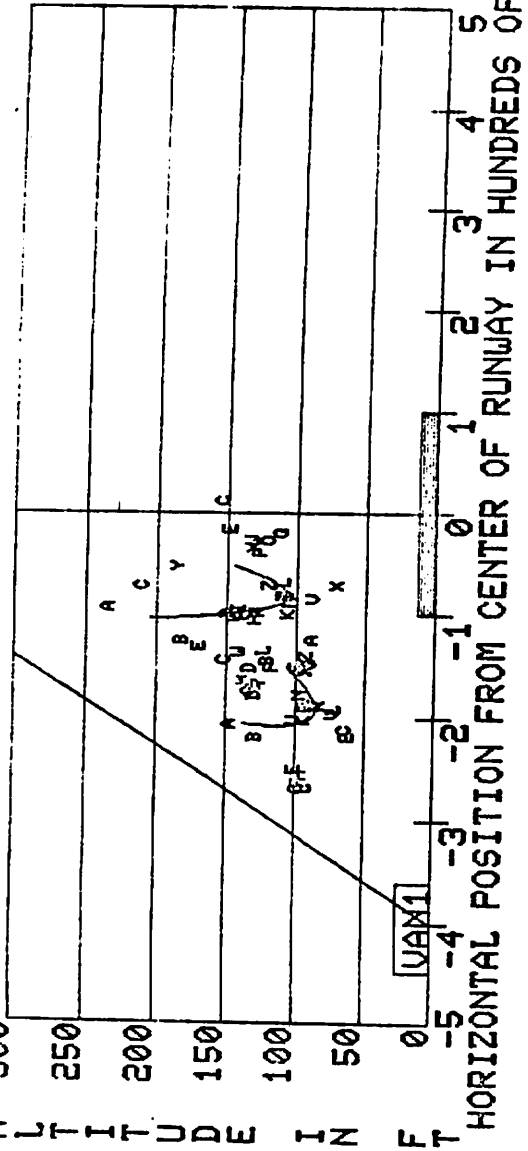
NS=02

FR	DATA	COR	PT	NOISE	ANGLE	PK	PAR	TIME	PORT	POS	STAR	POS	
PTS	P	P	S	P	IN	P	S		X	Y	X	Y	
01	074	250	090	00	00	273	216	000	6	-159	293	-074	258
02	075	250	141	00	00	273	218	000	5	-163	188	-074	237
03	076	250	200	01	00	280	218	000	5	-208	149	-121	186
04	077	250	200	01	00	280	225	000	4	-203	143	-133	138
05	078	250	193	00	01	277	225	000	4	-274	107	-186	188
06	079	250	200	00	01	277	225	000	4	-176	107	-117	147
07	080	250	200	00	01	245	225	000	7	-172	116	-117	128
08	081	250	200	00	01	261	225	000	8	-148	097	-071	141
09	082	250	155	00	00	222	225	000	9	-222	083	-144	126
10	083	250	155	00	00	210	225	000	9	-149	114	-147	113
11	084	250	155	00	00	235	225	000	9	-225	110	-123	110
12	085	250	155	00	00	235	224	000	9	-225	104	-160	097
13	086	250	155	00	00	235	224	000	9	-225	104	-160	097
14	087	250	155	00	00	235	224	000	9	-225	104	-160	097
15	088	250	155	00	00	235	224	000	9	-225	104	-160	097
16	089	250	155	00	00	235	224	000	9	-225	104	-160	097
17	090	250	155	00	00	235	224	000	9	-225	104	-160	097
18	091	250	155	00	00	235	224	000	9	-225	104	-160	097
19	092	250	155	00	00	235	224	000	9	-225	104	-160	097
20	093	250	155	00	00	235	224	000	9	-225	104	-160	097
21	094	250	155	00	00	235	224	000	9	-225	104	-160	097
22	095	250	155	00	00	235	224	000	9	-225	104	-160	097
23	096	250	155	00	00	235	224	000	9	-225	104	-160	097
24	097	250	155	00	00	235	224	000	9	-225	104	-160	097
25	098	250	155	00	00	235	224	000	9	-225	104	-160	097
26	099	250	155	00	00	235	224	000	9	-225	104	-160	097
27	100	250	155	00	00	235	224	000	9	-225	104	-160	097
28	101	250	155	00	00	235	224	000	9	-225	104	-160	097
29	102	250	155	00	00	235	224	000	9	-225	104	-160	097
30	103	250	155	00	00	235	224	000	9	-225	104	-160	097
31	104	250	155	00	00	235	224	000	9	-225	104	-160	097
32	105	250	155	00	00	235	224	000	9	-225	104	-160	097
33	106	250	155	00	00	235	224	000	9	-225	104	-160	097
34	107	250	155	00	00	235	224	000	9	-225	104	-160	097
35	108	250	155	00	00	235	224	000	9	-225	104	-160	097
36	109	250	155	00	00	235	224	000	9	-225	104	-160	097
37	110	250	155	00	00	235	224	000	9	-225	104	-160	097
38	111	250	155	00	00	235	224	000	9	-225	104	-160	097
39	112	250	155	00	00	235	224	000	9	-225	104	-160	097
40	113	250	155	00	00	235	224	000	9	-225	104	-160	097
41	114	250	155	00	00	235	224	000	9	-225	104	-160	097
42	115	250	155	00	00	235	224	000	9	-225	104	-160	097
43	116	250	155	00	00	235	224	000	9	-225	104	-160	097
44	117	250	155	00	00	235	224	000	9	-225	104	-160	097
45	118	250	155	00	00	235	224	000	9	-225	104	-160	097
46	119	250	155	00	00	235	224	000	9	-225	104	-160	097
47	120	250	155	00	00	235	224	000	9	-225	104	-160	097
48	121	250	155	00	00	235	224	000	9	-225	104	-160	097
49	122	250	155	00	00	235	224	000	9	-225	104	-160	097
50	123	250	155	00	00	235	224	000	9	-225	104	-160	097



FLV-BY 00028 DAY 278 TIME 15 26:05 A/C B-747  
 R: 59 A= 50 B= 50 NS= 0E C: 25 D= 50  
 ALTITUDE IN FT

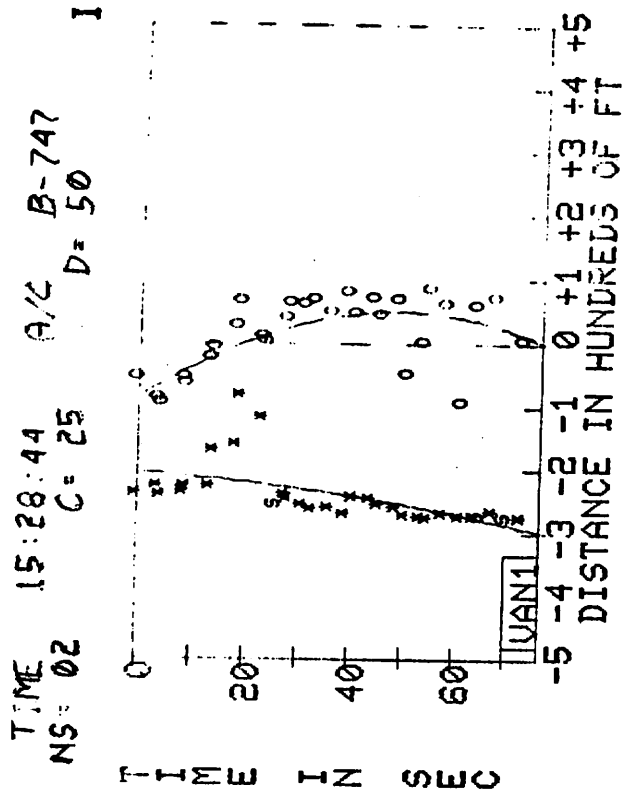
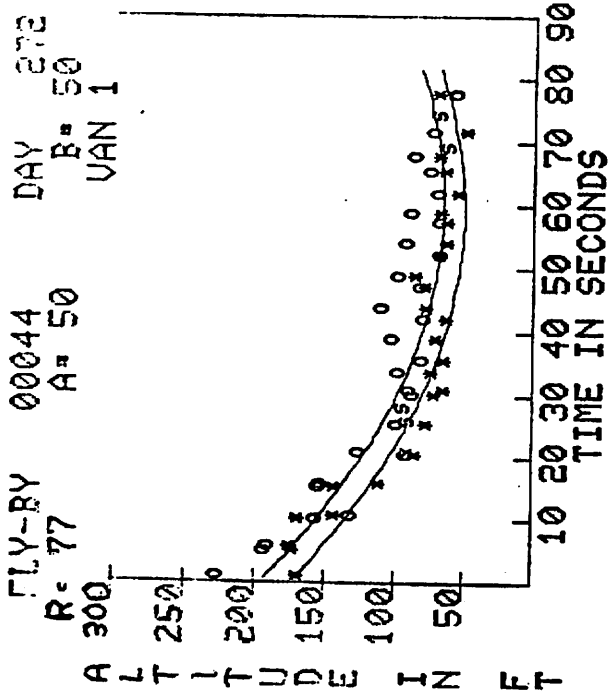
I



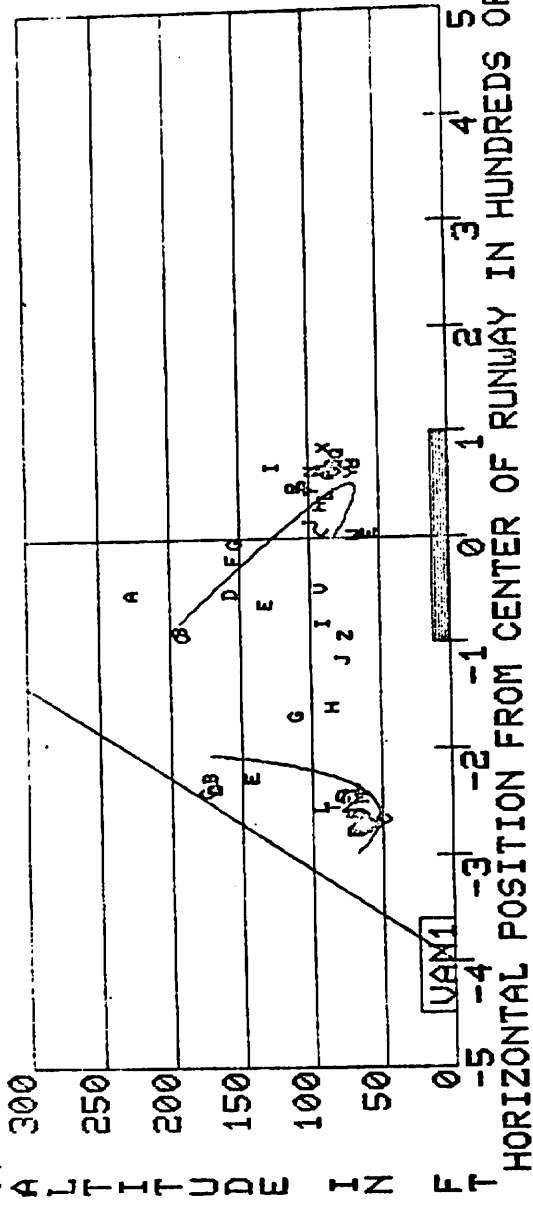


FLY-BY 00028 DAY 278 TIME 15:32:27 A/C B-747 I  
 R=59 A=50 B=50 C=25 NS=02

FR DATA PTS	COR PT P S	NOISE P S	ANGLE IN MX	PK P	PAR S	TIME S	PORT POS X Y	STARB POS X Y	FR DATA PTS	COR PT P S	NOISE P S	ANGLE IN MX	PK P S	PAR S	TIME S	PORT POS X Y	STARB POS X Y
01	0537	00	00	265	273	000	-209 144	-096 230	01	0537	00	00	265	273	000	-209 144	-096 230
02	0538	00	00	266	274	004	-221 125	-127 178	02	0538	00	00	266	274	004	-221 125	-127 178
03	0539	00	00	267	275	008	-146 148	023 289	03	0539	00	00	267	275	008	-146 148	023 289
04	0540	00	00	268	276	012	-180 126	-102 145	04	0540	00	00	268	276	012	-180 126	-102 145
05	0541	00	00	269	277	016	-153 093	-053 108	05	0541	00	00	269	277	016	-153 093	-053 108
06	0542	00	00	270	278	020	-266 034	-103 135	06	0542	00	00	270	278	020	-266 034	-103 135
07	0543	00	00	271	279	024	-271 032	-175 130	07	0543	00	00	271	279	024	-271 032	-175 130
08	0544	00	00	272	280	028	-172 126	-107 128	08	0544	00	00	272	280	028	-172 126	-107 128
09	0545	00	00	273	281	032	-167 130	-096 133	09	0545	00	00	273	281	032	-167 130	-096 133
10	0546	00	00	274	282	036	-255 033	-073 188	10	0546	00	00	274	282	036	-255 033	-073 188
11	0547	00	00	275	283	040	-192 030	-091 191	11	0547	00	00	275	283	040	-192 030	-091 191
12	0548	00	00	276	284	044	-150 037	-109 126	12	0548	00	00	276	284	044	-150 037	-109 126
13	0549	00	00	277	285	048	-154 033	-041 123	13	0549	00	00	277	285	048	-154 033	-041 123
14	0550	00	00	278	286	052	-150 037	-023 108	14	0550	00	00	278	286	052	-150 037	-023 108
15	0551	00	00	279	287	056	-191 033	-050 079	15	0551	00	00	279	287	056	-191 033	-050 079
16	0552	00	00	280	288	060	-182 034	-070 124	16	0552	00	00	280	288	060	-182 034	-070 124
17	0553	00	00	281	289	064	-133 031	-084 105	17	0553	00	00	281	289	064	-133 031	-084 105
18	0554	00	00	282	290	068	-134 031	-104 141	18	0554	00	00	282	290	068	-134 031	-104 141
19	0555	00	00	283	291	072	-137 030	-097 034	19	0555	00	00	283	291	072	-137 030	-097 034
20	0556	00	00	284	292	076	-157 033	-091 037	20	0556	00	00	284	292	076	-157 033	-091 037
21	0557	00	00	285	293	080	-142 033	-093 031	21	0557	00	00	285	293	080	-142 033	-093 031
22	0558	00	00	286	294	084	-143 033	-093 031	22	0558	00	00	286	294	084	-143 033	-093 031
23	0559	00	00	287	295	088	-143 033	-093 031	23	0559	00	00	287	295	088	-143 033	-093 031
24	0560	00	00	288	296	092	-143 033	-093 031	24	0560	00	00	288	296	092	-143 033	-093 031
25	0561	00	00	289	297	096	-143 033	-093 031	25	0561	00	00	289	297	096	-143 033	-093 031
26	0562	00	00	290	298	100	-143 033	-093 031	26	0562	00	00	290	298	100	-143 033	-093 031
27	0563	00	00	291	299	104	-143 033	-093 031	27	0563	00	00	291	299	104	-143 033	-093 031
28	0564	00	00	292	300	108	-143 033	-093 031	28	0564	00	00	292	300	108	-143 033	-093 031
29	0565	00	00	293	301	112	-143 033	-093 031	29	0565	00	00	293	301	112	-143 033	-093 031
30	0566	00	00	294	302	116	-143 033	-093 031	30	0566	00	00	294	302	116	-143 033	-093 031
31	0567	00	00	295	303	120	-143 033	-093 031	31	0567	00	00	295	303	120	-143 033	-093 031
32	0568	00	00	296	304	124	-143 033	-093 031	32	0568	00	00	296	304	124	-143 033	-093 031
33	0569	00	00	297	305	128	-143 033	-093 031	33	0569	00	00	297	305	128	-143 033	-093 031
34	0570	00	00	298	306	132	-143 033	-093 031	34	0570	00	00	298	306	132	-143 033	-093 031
35	0571	00	00	299	307	136	-143 033	-093 031	35	0571	00	00	299	307	136	-143 033	-093 031
36	0572	00	00	300	308	140	-143 033	-093 031	36	0572	00	00	300	308	140	-143 033	-093 031
37	0573	00	00	301	309	144	-143 033	-093 031	37	0573	00	00	301	309	144	-143 033	-093 031
38	0574	00	00	302	310	148	-143 033	-093 031	38	0574	00	00	302	310	148	-143 033	-093 031
39	0575	00	00	303	311	152	-143 033	-093 031	39	0575	00	00	303	311	152	-143 033	-093 031
40	0576	00	00	304	312	156	-143 033	-093 031	40	0576	00	00	304	312	156	-143 033	-093 031
41	0577	00	00	305	313	160	-143 033	-093 031	41	0577	00	00	305	313	160	-143 033	-093 031
42	0578	00	00	306	314	164	-143 033	-093 031	42	0578	00	00	306	314	164	-143 033	-093 031
43	0579	00	00	307	315	168	-143 033	-093 031	43	0579	00	00	307	315	168	-143 033	-093 031
44	0580	00	00	308	316	172	-143 033	-093 031	44	0580	00	00	308	316	172	-143 033	-093 031
45	0581	00	00	309	317	176	-143 033	-093 031	45	0581	00	00	309	317	176	-143 033	-093 031
46	0582	00	00	310	318	180	-143 033	-093 031	46	0582	00	00	310	318	180	-143 033	-093 031
47	0583	00	00	311	319	184	-143 033	-093 031	47	0583	00	00	311	319	184	-143 033	-093 031
48	0584	00	00	312	320	188	-143 033	-093 031	48	0584	00	00	312	320	188	-143 033	-093 031
49	0585	00	00	313	321	192	-143 033	-093 031	49	0585	00	00	313	321	192	-143 033	-093 031
50	0586	00	00	314	322	196	-143 033	-093 031	50	0586	00	00	314	322	196	-143 033	-093 031

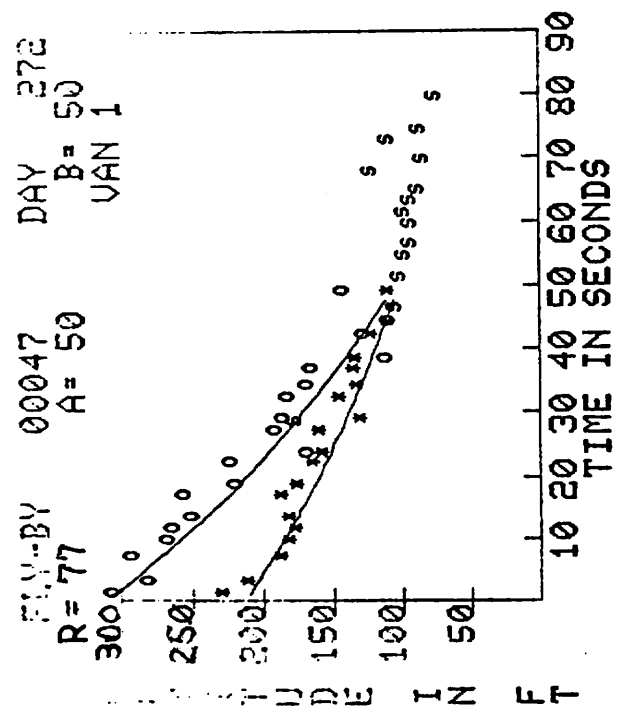
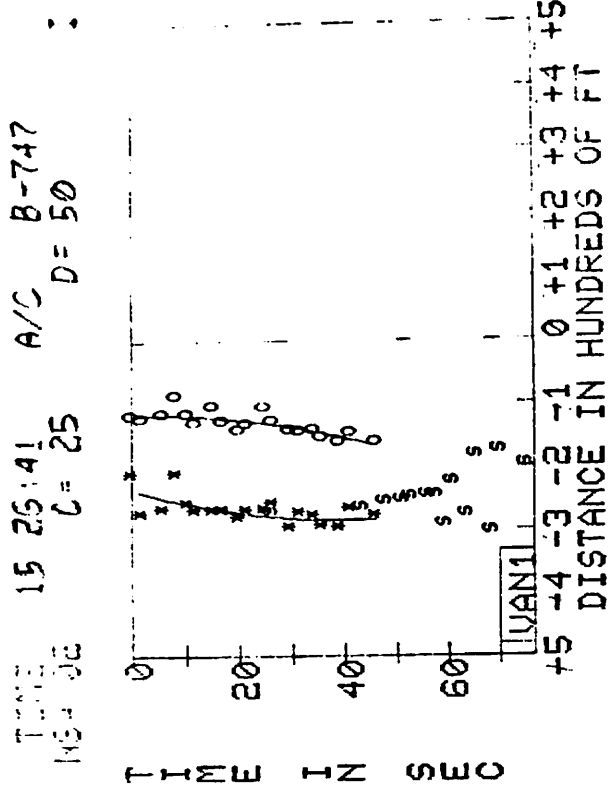


FLY-BY 00044 DAY 272 TIME 15:30:00 A/C B-747  
 R=77 A=50 B=50 NS=02 C=25 D=50

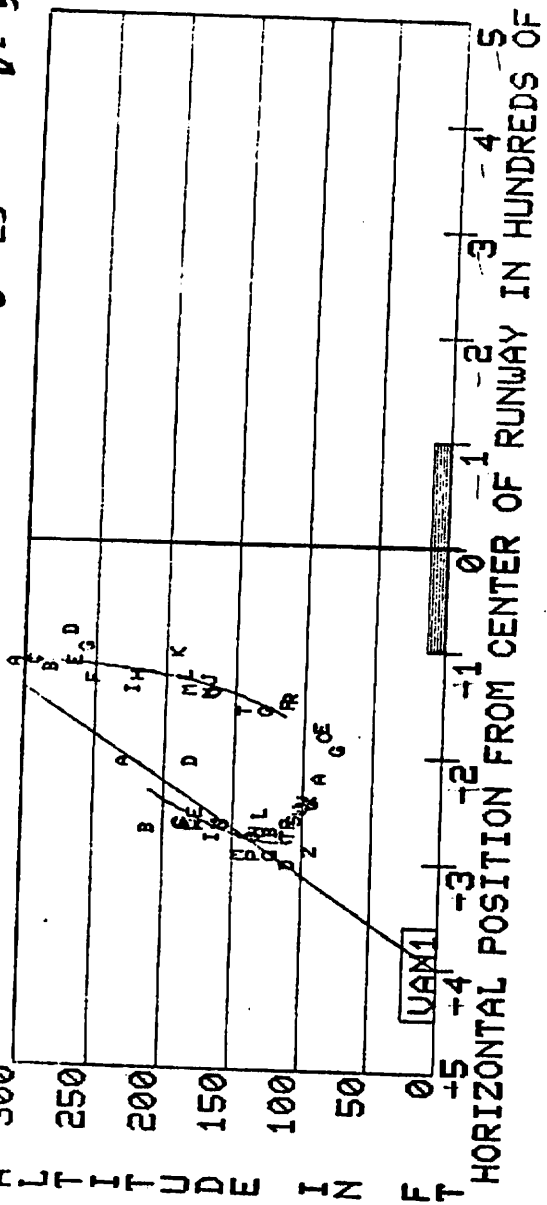


FLY-BY 00044 DAY 272  
 R=77 A=50 B=50  
 TIME 15:28:22 AOC B-747  
 NS=02 C=25 D=50

FR DATA PTS	CCR PT P S	NOISE P S	ANGLE MN MX	PK P	PAR TIME	PORT POS X Y	STARB POS X Y
01	094	220	27 54	263	5 5	240 165	-056 223
02	174	224	27 54	263	5 5	240 168	-090 189
03	174	187	27 54	263	5 5	240 170	-097 186
04	174	231	19 53	263	5 5	240 164	-055 157
05	178	154	19 53	263	5 5	240 130	-025 127
06	166	134	17 52	263	5 5	240 129	-024 150
07	133	141	17 52	263	5 5	240 107	-025 149
08	133	146	19 55	263	5 5	240 081	-023 121
09	119	122	19 55	263	5 5	240 073	-023 121
10	112	128	10 33	263	5 5	240 073	-023 087
11	112	128	10 33	263	5 5	240 073	-023 087
12	112	128	10 33	263	5 5	240 073	-023 087
13	112	128	10 33	263	5 5	240 073	-023 087
14	112	128	10 33	263	5 5	240 073	-023 087
15	112	128	10 33	263	5 5	240 073	-023 087
16	112	128	10 33	263	5 5	240 073	-023 087
17	112	128	10 33	263	5 5	240 073	-023 087
18	112	128	10 33	263	5 5	240 073	-023 087
19	112	128	10 33	263	5 5	240 073	-023 087
20	112	128	10 33	263	5 5	240 073	-023 087
21	112	128	10 33	263	5 5	240 073	-023 087
22	112	128	10 33	263	5 5	240 073	-023 087
23	112	128	10 33	263	5 5	240 073	-023 087
24	112	128	10 33	263	5 5	240 073	-023 087
25	112	128	10 33	263	5 5	240 073	-023 087
26	112	128	10 33	263	5 5	240 073	-023 087
27	112	128	10 33	263	5 5	240 073	-023 087
28	112	128	10 33	263	5 5	240 073	-023 087
29	112	128	10 33	263	5 5	240 073	-023 087
30	112	128	10 33	263	5 5	240 073	-023 087
31	112	128	10 33	263	5 5	240 073	-023 087
32	112	128	10 33	263	5 5	240 073	-023 087
33	112	128	10 33	263	5 5	240 073	-023 087
34	112	128	10 33	263	5 5	240 073	-023 087
35	112	128	10 33	263	5 5	240 073	-023 087
36	112	128	10 33	263	5 5	240 073	-023 087
37	112	128	10 33	263	5 5	240 073	-023 087
38	112	128	10 33	263	5 5	240 073	-023 087
39	112	128	10 33	263	5 5	240 073	-023 087
40	112	128	10 33	263	5 5	240 073	-023 087
41	112	128	10 33	263	5 5	240 073	-023 087
42	112	128	10 33	263	5 5	240 073	-023 087
43	112	128	10 33	263	5 5	240 073	-023 087
44	112	128	10 33	263	5 5	240 073	-023 087
45	112	128	10 33	263	5 5	240 073	-023 087
46	112	128	10 33	263	5 5	240 073	-023 087
47	112	128	10 33	263	5 5	240 073	-023 087
48	112	128	10 33	263	5 5	240 073	-023 087
49	112	128	10 33	263	5 5	240 073	-023 087
50	112	128	10 33	263	5 5	240 073	-023 087
51	112	128	10 33	263	5 5	240 073	-023 087
52	112	128	10 33	263	5 5	240 073	-023 087
53	112	128	10 33	263	5 5	240 073	-023 087
54	112	128	10 33	263	5 5	240 073	-023 087
55	112	128	10 33	263	5 5	240 073	-023 087
56	112	128	10 33	263	5 5	240 073	-023 087
57	112	128	10 33	263	5 5	240 073	-023 087
58	112	128	10 33	263	5 5	240 073	-023 087
59	112	128	10 33	263	5 5	240 073	-023 087
60	112	128	10 33	263	5 5	240 073	-023 087
61	112	128	10 33	263	5 5	240 073	-023 087
62	112	128	10 33	263	5 5	240 073	-023 087
63	112	128	10 33	263	5 5	240 073	-023 087
64	112	128	10 33	263	5 5	240 073	-023 087
65	112	128	10 33	263	5 5	240 073	-023 087
66	112	128	10 33	263	5 5	240 073	-023 087
67	112	128	10 33	263	5 5	240 073	-023 087
68	112	128	10 33	263	5 5	240 073	-023 087
69	112	128	10 33	263	5 5	240 073	-023 087
70	112	128	10 33	263	5 5	240 073	-023 087
71	112	128	10 33	263	5 5	240 073	-023 087
72	112	128	10 33	263	5 5	240 073	-023 087
73	112	128	10 33	263	5 5	240 073	-023 087
74	112	128	10 33	263	5 5	240 073	-023 087
75	112	128	10 33	263	5 5	240 073	-023 087
76	112	128	10 33	263	5 5	240 073	-023 087
77	112	128	10 33	263	5 5	240 073	-023 087
78	112	128	10 33	263	5 5	240 073	-023 087
79	112	128	10 33	263	5 5	240 073	-023 087
80	112	128	10 33	263	5 5	240 073	-023 087
81	112	128	10 33	263	5 5	240 073	-023 087
82	112	128	10 33	263	5 5	240 073	-023 087
83	112	128	10 33	263	5 5	240 073	-023 087
84	112	128	10 33	263	5 5	240 073	-023 087
85	112	128	10 33	263	5 5	240 073	-023 087
86	112	128	10 33	263	5 5	240 073	-023 087
87	112	128	10 33	263	5 5	240 073	-023 087
88	112	128	10 33	263	5 5	240 073	-023 087
89	112	128	10 33	263	5 5	240 073	-023 087
90	112	128	10 33	263	5 5	240 073	-023 087
91	112	128	10 33	263	5 5	240 073	-023 087
92	112	128	10 33	263	5 5	240 073	-023 087
93	112	128	10 33	263	5 5	240 073	-023 087
94	112	128	10 33	263	5 5	240 073	-023 087
95	112	128	10 33	263	5 5	240 073	-023 087
96	112	128	10 33	263	5 5	240 073	-023 087
97	112	128	10 33	263	5 5	240 073	-023 087
98	112	128	10 33	263	5 5	240 073	-023 087
99	112	128	10 33	263	5 5	240 073	-023 087
100	112	128	10 33	263	5 5	240 073	-023 087



FLY-BY 00047 DAY 272 TIME 15:30.12 A/C B-747  
 R: 77 A= 50 B= 50 NS= 02 C= 25 D= 50



FLY-BY  
R=77

00047  
A=50

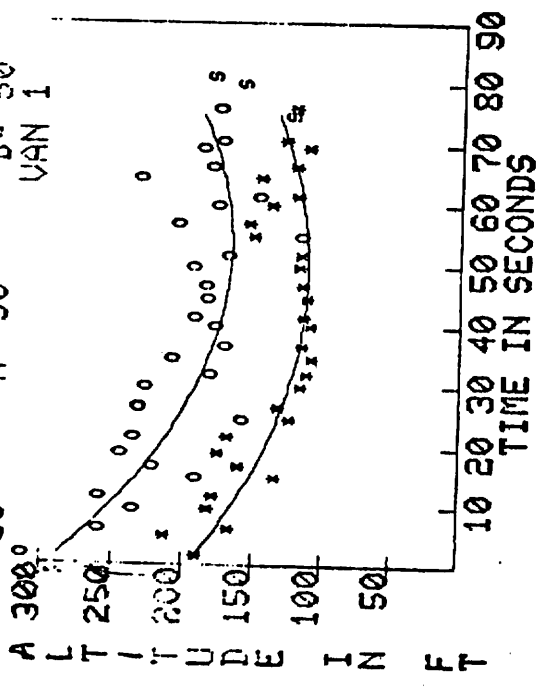
DAY 272  
B=50

TIME 15 23:32  
NS=02 C=25

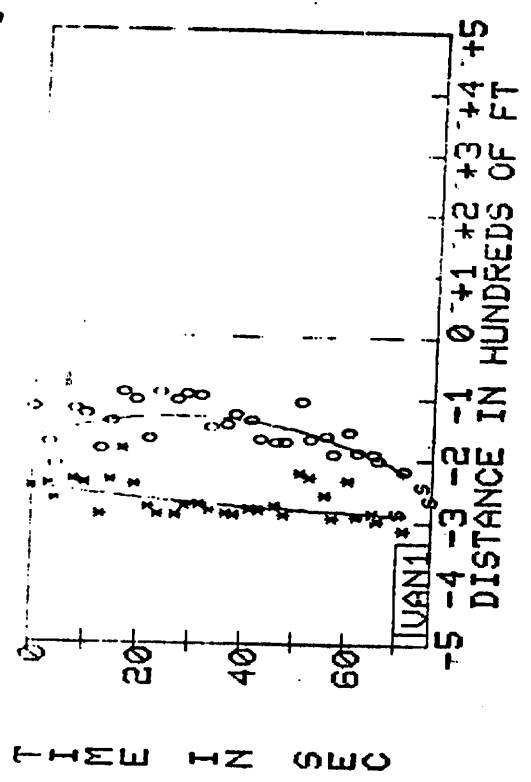
A/C B-747  
D=50

FR DATA	COR PT	NOISE	ANGLE	PK	PAR	TIME	PORT POS	STARB POS	FR DATA	COR PT	NOISE	ANGLE	PK	PAR	TIME	PORT POS	STARB POS	
PTS	P S	P S	MN MX	P	S		X Y	X Y	PTS	P S	P S	MN MX	P	S		X Y	X Y	
01	0270	151 055	00 00	44 61	230 200	000.8	-211 225	-120 309										
02	0491	128 128	00 00	37 62	230 221	002.8	-274 207	-124 277										
03	0509	150 099	00 00	33 60	241 210	006.8	-258 183	-117 288										
04	0753	250 146	00 00	37 61	222 208	009.4	-210 178	-089 263										
05	0931	250 238	00 00	37 61	257 225	011.4	-259 173	-117 260										
06	0817	238 250	00 00	36 61	258 209	013.2	-270 177	-133 247										
07	0665	250 112	00 00	37 63	248 214	016.7	-271 183	-104 252										
08	0719	233 222	00 00	38 61	260 220	018.3	-270 171	-130 216										
09	0569	186 135	00 00	38 60	249 185	021.6	-281 160	-144 219										
10	0680	209 224	00 00	29 69	248 196	023.2	-269 153	-139 165										
11	0577	250 125	00 00	29 62	262 189	026.5	-268 156	-107 187										
12	0486	090 089	00 00	88 89	250 090	028.8	-298 120	-129 181										
13	0494	151 179	00 00	31 62	265 189	031.8	-298 141	-143 179										
14	0401	158 098	00 00	29 60	272 172	033.6	-276 128	-146 165										
15	0286	111 098	00 00	30 61	265 170	036.3	-280 131	-144 162										
16	0311	056 114	00 00	18 61	276 176	038.0	-297 130	-154 108										
17	0187	036 077	00 00	20 63	273 176	041.7	-298 118	-162 124										
18	0178	057 025	00 00	18 62	237 145	043.8	-268 105	-148 105										
19	0167	062 000	00 00	18 62	238 000	046.0	-264 101											
20	0142	043 019	00 00	19 62	212 144	048.7	-278 106	-162 139										
21	0132	062 020	00 00	19 61	218 000	050.9	-254 098											
22	0116	054 000	00 00	19 54	220 000	054.0	-252 094											
23	0297	051 000	00 00	18 51	232 000	055.9	-248 090											
24	0232	039 000	00 00	07 57	171 000	059.2	-246 090											
25	0232	040 000	00 00	20 45	188 000	060.8	-246 094											
26	0232	002 000	00 00	37 42	174 000	062.8	-293 089											
27	0290	048 000	00 00	30 36	198 000	064.3	-224 084											
28	0236	006 000	00 00	39 45	166 000	067.1	-276 118											
29	0200	000 078	00 00	23 32	000 185	069.1		-184 080										
30	0202	002 000	00 00	47 49	174 000	072.3	-306 106											
31	0208	020 068	00 00	24 25	000 176	073.8		-176 083										
32	0200	000	00 00	00 00	000													
33	0333	000 024	00 00	19 21	000 196	079.1		-198 072										
34	0300	000	00 00	00 00	000													
35	0000	000	00 00	00 00	000													
36	0000	000	00 00	00 00	000													

FLYBY 00048 DAY 288  
 R = 59 A = 50 B = 50  
 VAN 1

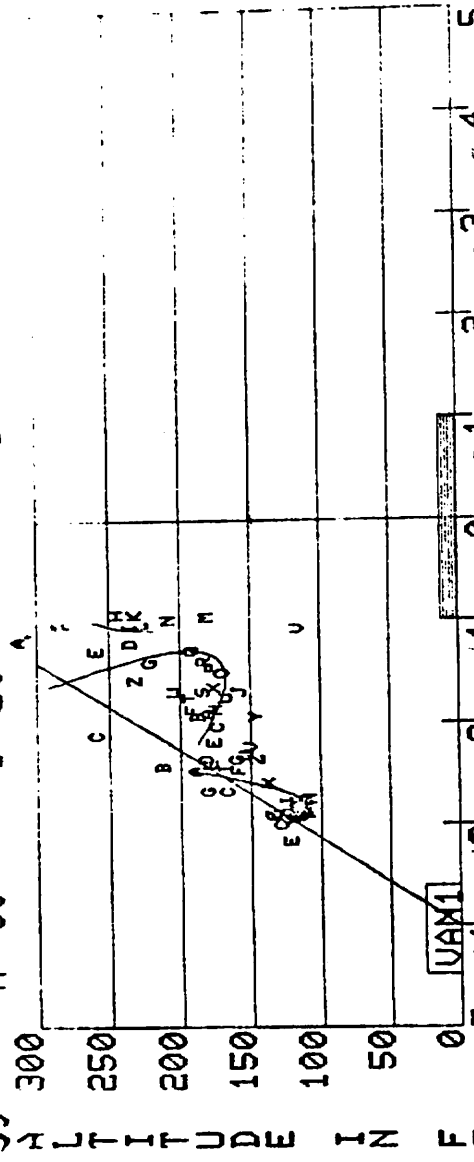


TIME IS 42 35 A/C B-747  
 NS= 22 C= 25 D= 50





R= 59    A= 50    DAY 233    TIME 15 41 28    A/C B-747  
 MS 02    C=25    D= 50



HORIZONTAL POSITION FROM CENTER OF RUNWAY IN HUNDREDS OF FT

FLY-BY  
R = 59

00048  
A = 50

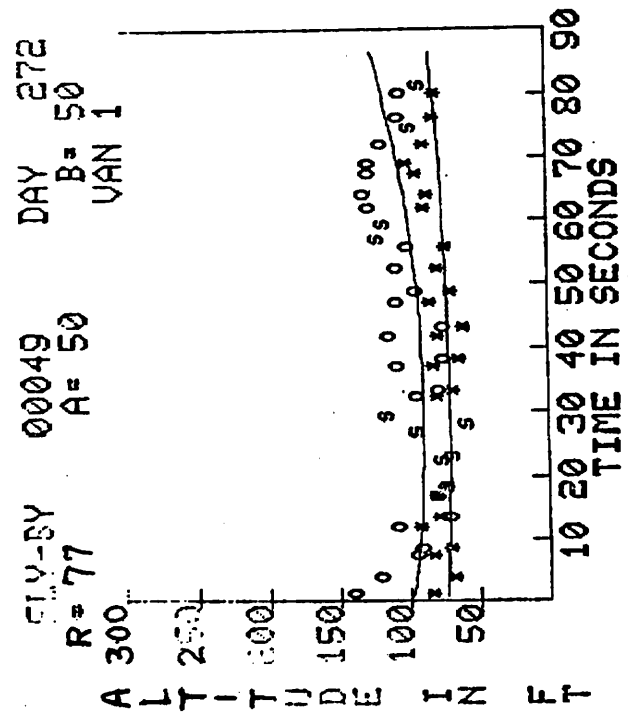
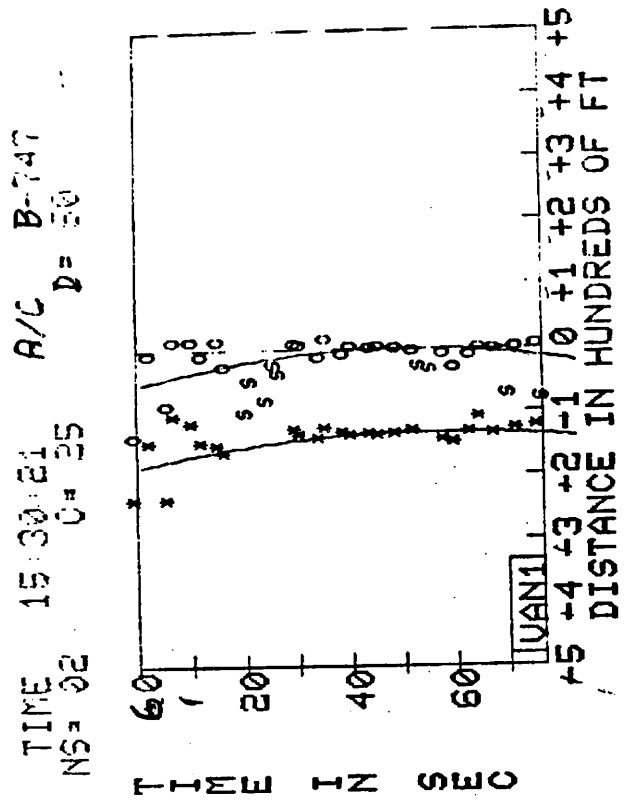
DAY 288  
B = 50

TIME 15:44:12  
NB = 02

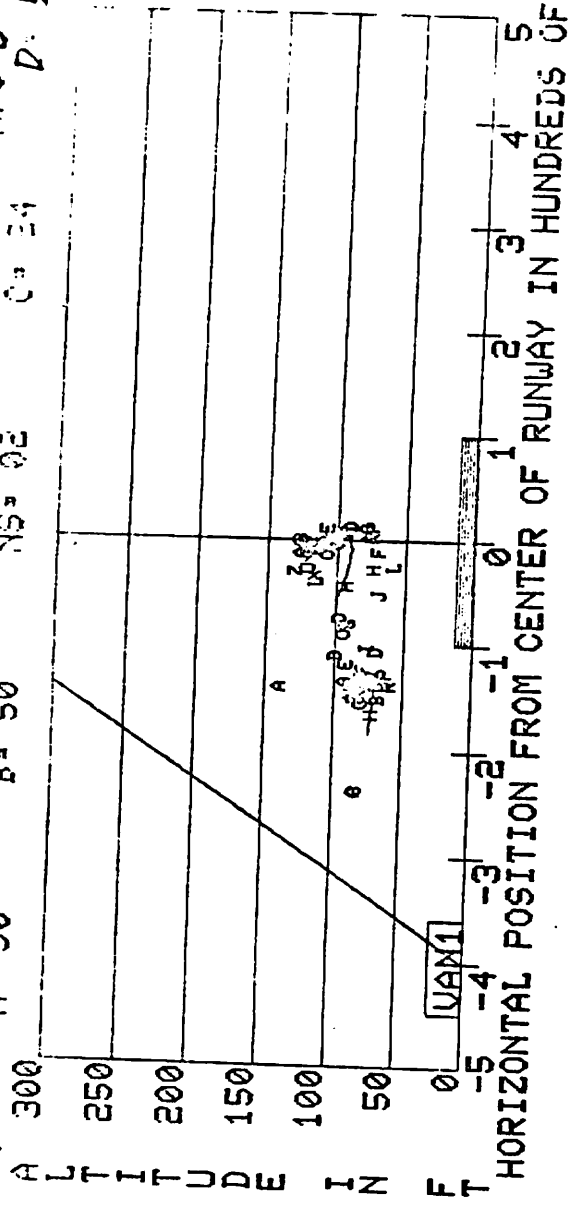
A/C B = 7457  
D = 50

I

FR DATA PTS	COR PT P S	NOISE P S	ANGLE MN TH	PK P S	PAR TIME	PORT POS X Y	STARB POS X Y
01 0489	088 079	00 00	35 30	24 28	0 26	150 186	121 308
02 0673	154 073	00 00	33 30	21 29	00 00	154 208	-180 326
03 0602	159 108	00 00	33 30	22 28	00 00	159 177	-214 254
04 0644	148 110	00 00	33 30	22 28	00 00	174 174	-242 255
05 0625	148 110	00 00	33 30	22 28	00 00	174 174	-242 255
06 0694	148 110	00 00	33 30	22 28	00 00	174 174	-242 255
07 0625	148 110	00 00	33 30	22 28	00 00	174 174	-242 255
08 0650	133 084	00 00	33 30	22 28	00 00	156 156	-189 187
09 0620	129 084	00 00	33 30	22 28	00 00	156 156	-189 187
10 0637	129 084	00 00	33 30	22 28	00 00	156 156	-189 187
11 0650	129 084	00 00	33 30	22 28	00 00	156 156	-189 187
12 0650	129 084	00 00	33 30	22 28	00 00	156 156	-189 187
13 0450	088 095	00 00	33 30	22 28	00 00	170 170	-198 230
14 0472	043 057	00 00	33 30	22 28	00 00	184 184	-171 153
15 0424	043 057	00 00	33 30	22 28	00 00	184 184	-171 153
16 0424	043 057	00 00	33 30	22 28	00 00	184 184	-171 153
17 0424	043 057	00 00	33 30	22 28	00 00	184 184	-171 153
18 0424	043 057	00 00	33 30	22 28	00 00	184 184	-171 153
19 0424	043 057	00 00	33 30	22 28	00 00	184 184	-171 153
20 0424	043 057	00 00	33 30	22 28	00 00	184 184	-171 153
21 0424	043 057	00 00	33 30	22 28	00 00	184 184	-171 153
22 0424	043 057	00 00	33 30	22 28	00 00	184 184	-171 153
23 0424	043 057	00 00	33 30	22 28	00 00	184 184	-171 153
24 0424	043 057	00 00	33 30	22 28	00 00	184 184	-171 153
25 0424	043 057	00 00	33 30	22 28	00 00	184 184	-171 153
26 0424	043 057	00 00	33 30	22 28	00 00	184 184	-171 153
27 0424	043 057	00 00	33 30	22 28	00 00	184 184	-171 153
28 0424	043 057	00 00	33 30	22 28	00 00	184 184	-171 153
29 0424	043 057	00 00	33 30	22 28	00 00	184 184	-171 153
30 0424	043 057	00 00	33 30	22 28	00 00	184 184	-171 153
31 0424	043 057	00 00	33 30	22 28	00 00	184 184	-171 153
32 0424	043 057	00 00	33 30	22 28	00 00	184 184	-171 153
33 0424	043 057	00 00	33 30	22 28	00 00	184 184	-171 153
34 0424	043 057	00 00	33 30	22 28	00 00	184 184	-171 153
35 0424	043 057	00 00	33 30	22 28	00 00	184 184	-171 153



CITY-BY 00049 DAY 272 TIME 15:50 52 A/C B-7-7  
 R=77 A= 50 B= 50 NS= 02 C= 34 D= 50



TIME 15:51:55 A/C-- B-747  
 NS# 02 C= 24 D= 50 I

FLY-BY 00049 DAY 272  
 R=77 A= 50 B= 50

FR DATA PYS	COR PT P S	NOISE P S	ANGLE MN MX	PX P	PAR TIME S	PORT POS X Y	STARB POS X Y	FR DATA PYS	CCR PT P S	NOISE P S	ANGLE MN MX	PX P	PAR TIME S	PORT POS X Y	STARB POS X Y
01	0903	050	07 35	220	262	060 6	-241 080	01	0903	050	07 35	220	262	060 6	-144 135
02	0909	050	07 34	220	262	063 7	-154 054	02	0909	050	07 34	220	262	063 7	-013 116
03	0917	050	08 33	266	240	007 9	-240 079	03	0917	050	08 33	266	240	007 9	-093 090
04	0928	050	08 33	261	214	011 5	-110 066	04	0928	050	08 33	261	214	011 5	0009 086
05	0930	050	08 33	261	214	011 5	-122 087	05	0930	050	08 33	261	214	011 5	0007 103
06	0939	050	07 33	261	250	015 3	-153 074	06	0939	050	07 33	261	250	015 3	-014 066
07	0949	050	07 28	252	276	017 9	-158 076	07	0949	050	07 28	252	276	017 9	0007 075
08	0957	050	09 28	170	240	022 0	-169 068	08	0957	050	09 28	170	240	022 0	-031 069
09	0958	050	08 22	170	240	022 0	-106 073	09	0958	050	08 22	170	240	022 0	-056 065
10	0958	050	08 23	080	250	023 0		10	0958	050	08 23	080	250	023 0	-085 090
11	0958	050	08 23	080	250	023 0		11	0958	050	08 23	080	250	023 0	-089 058
12	0958	050	08 23	080	250	023 0		12	0958	050	08 23	080	250	023 0	0004 089
13	0958	050	08 23	080	250	023 0		13	0958	050	08 23	080	250	023 0	-017 104
14	0958	050	08 23	214	242	036 6	132 064	14	0958	050	08 23	214	242	036 6	0002 074
15	0971	050	10 23	214	242	037 6	-145 059	15	0971	050	10 23	214	242	037 6	-017 071
16	0970	050	09 23	214	242	041 1	-137 074	16	0970	050	09 23	214	242	041 1	0009 071
17	0977	050	09 23	214	242	041 1	-142 056	17	0977	050	09 23	214	242	041 1	0000 071
18	0977	050	09 23	214	242	041 1	-139 085	18	0977	050	09 23	214	242	041 1	-093 103
19	0915	050	10 22	184	225	048 1	-139 065	19	0915	050	10 22	184	225	048 1	0000 099
20	0945	050	12 21	200	225	051 8	-139 074	20	0945	050	12 21	200	225	051 8	-034 103
21	0945	050	09 22	200	225	051 8	-134 068	21	0945	050	09 22	200	225	051 8	-037 117
22	0945	050	09 22	200	225	051 8		22	0945	050	09 22	200	225	051 8	-037 117
23	0945	050	09 22	200	225	051 8		23	0945	050	09 22	200	225	051 8	-011 123
24	0945	050	09 22	200	225	051 8		24	0945	050	09 22	200	225	051 8	-015 123
25	0945	050	09 22	200	225	051 8		25	0945	050	09 22	200	225	051 8	-033 123
26	0945	050	09 22	200	225	051 8		26	0945	050	09 22	200	225	051 8	-033 123
27	0945	050	09 22	200	225	051 8		27	0945	050	09 22	200	225	051 8	-033 123
28	0945	050	09 22	200	225	051 8		28	0945	050	09 22	200	225	051 8	-033 123
29	0945	050	09 22	200	225	051 8		29	0945	050	09 22	200	225	051 8	-033 123
30	0945	050	09 22	200	225	051 8		30	0945	050	09 22	200	225	051 8	-033 123
31	0945	050	09 22	200	225	051 8		31	0945	050	09 22	200	225	051 8	-033 123
32	0945	050	09 22	200	225	051 8		32	0945	050	09 22	200	225	051 8	-033 123
33	0945	050	09 22	200	225	051 8		33	0945	050	09 22	200	225	051 8	-033 123
34	0945	050	09 22	200	225	051 8		34	0945	050	09 22	200	225	051 8	-033 123
35	0945	050	09 22	200	225	051 8		35	0945	050	09 22	200	225	051 8	-033 123

Appendix F  
TIME HISTORY OF VORTEX ROTATIONAL VELOCITY

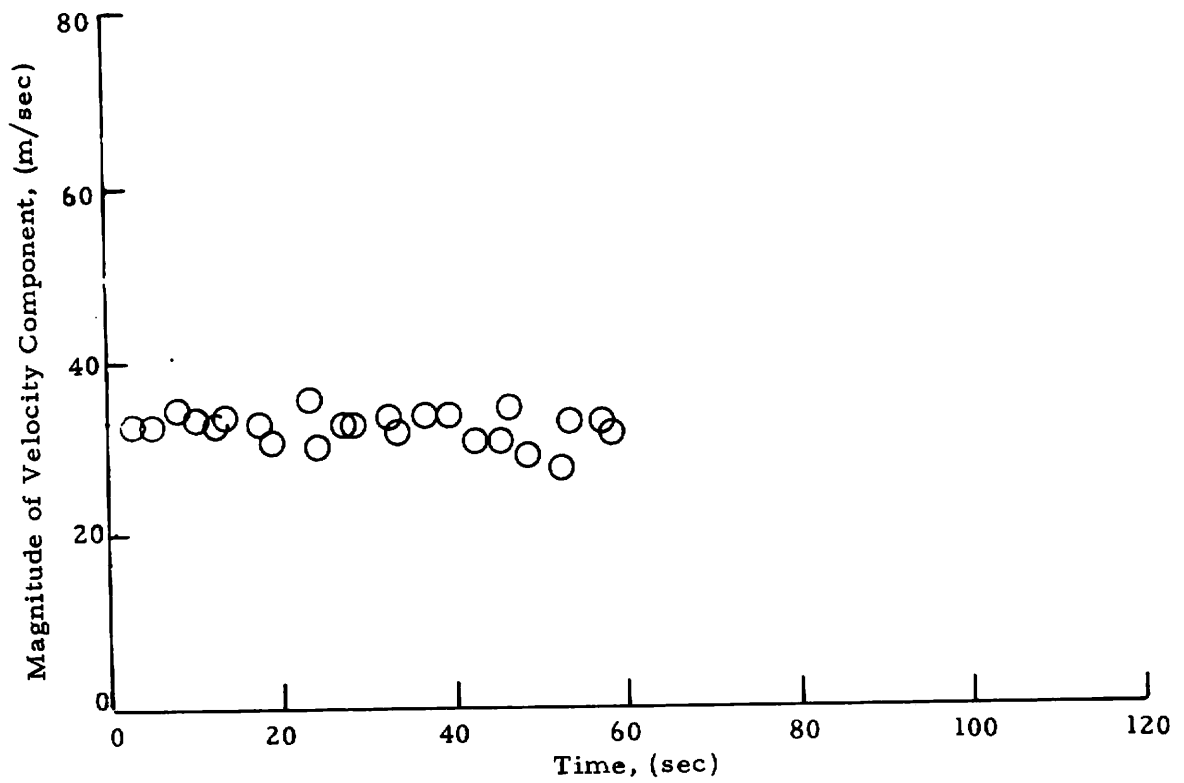


Fig. F-1  $-|V_{pk}|$  as a Function of Time for Rosamond B-747 Flyby 24  
(from High-Speed Data)

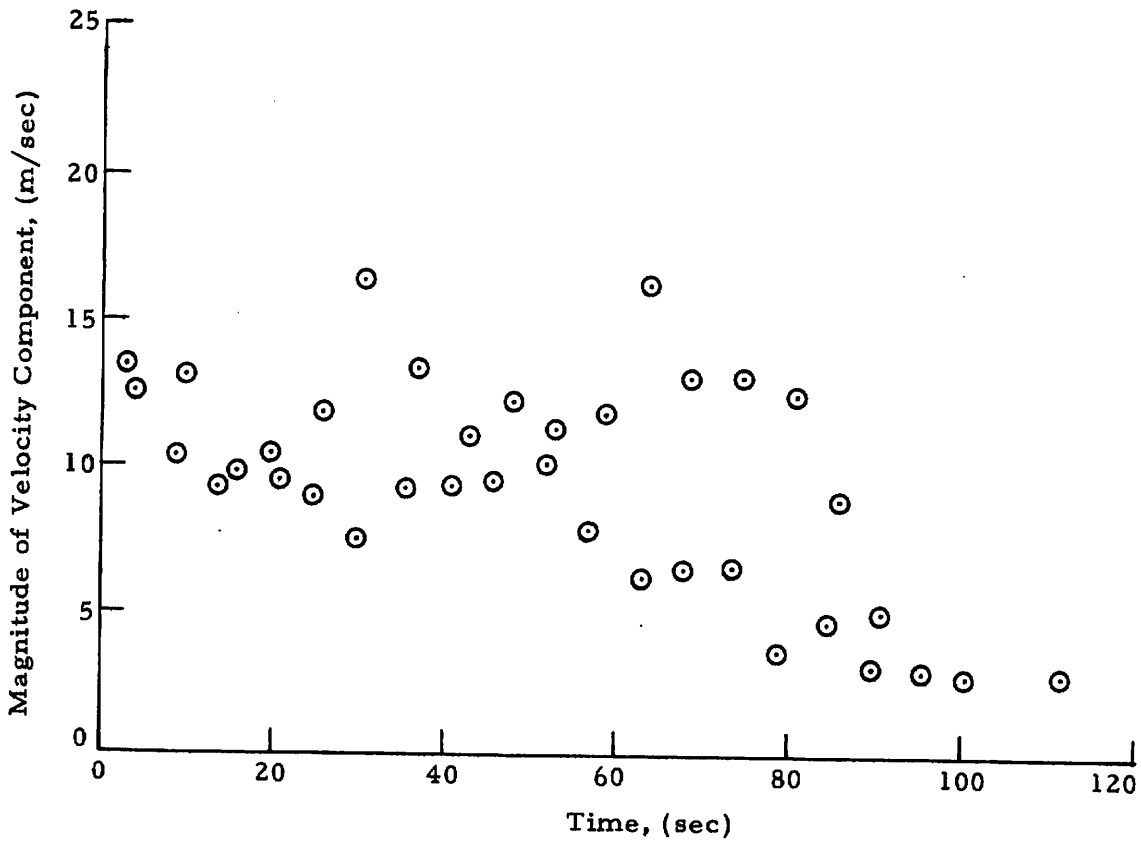


Fig. F-2  $|V_{ms}|$  as a Function of Time for Rosamond B-747 Flyby 24  
(from Low-Speed Data)

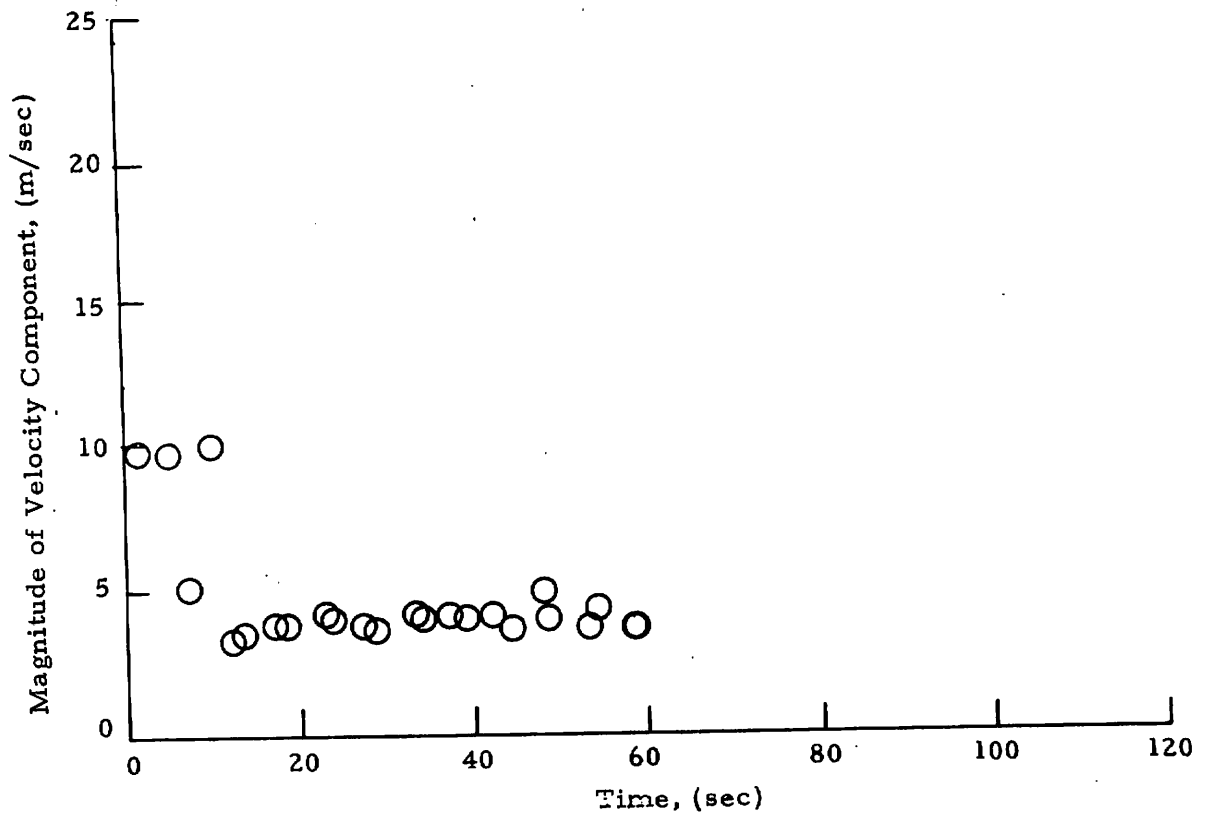


Fig. F-3  $|V_{ms}|$  as a Function of Time for Rosamond B-747 Flyby 24  
(from High-Speed Data)



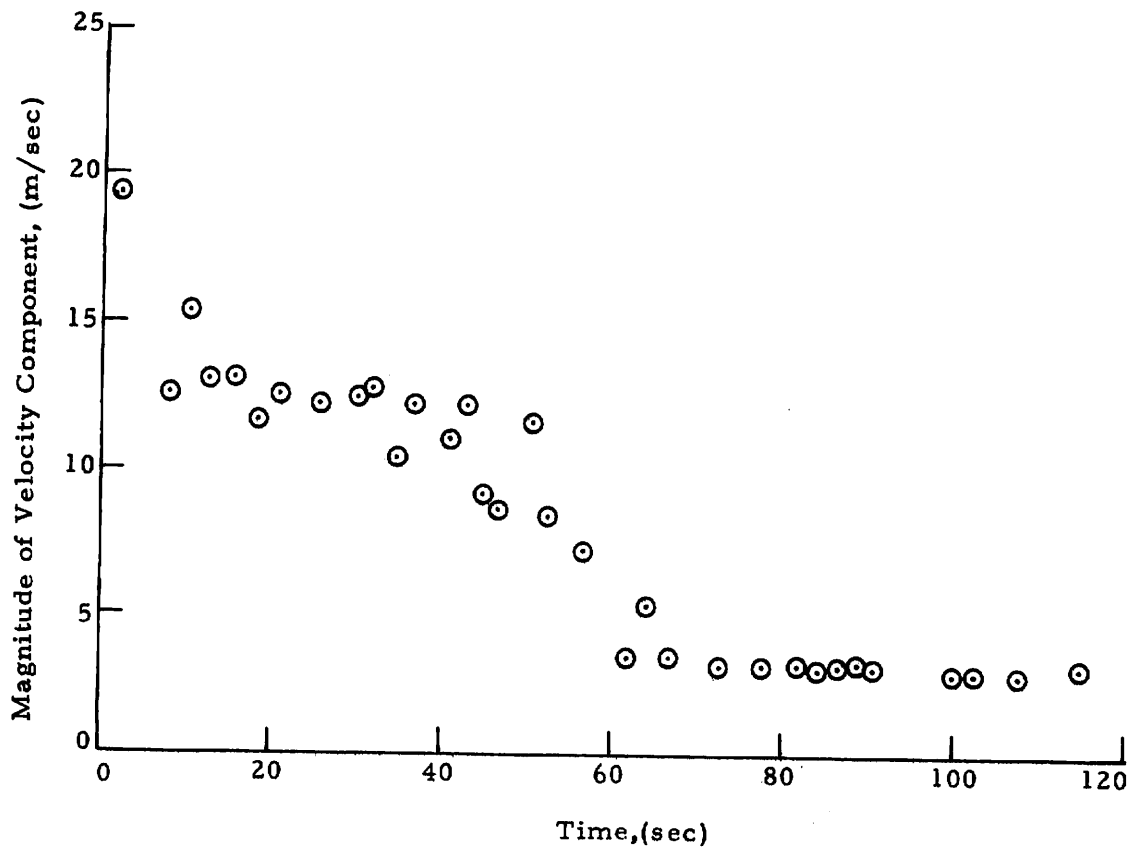


Fig. F-4 -  $|V_{ms}|$  as a Function of Time for Rosamond B-747 Flyby 25  
 (from Low-Speed Data)

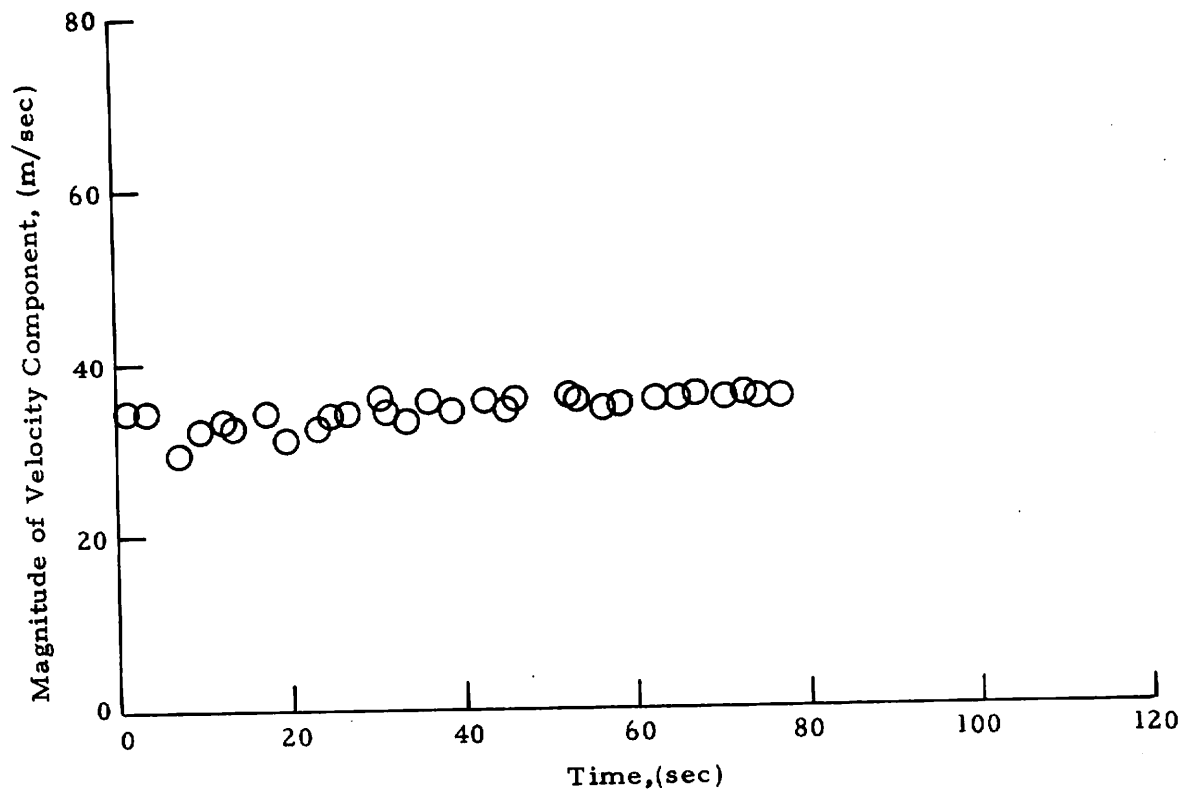


Fig. F-5 -  $|V_{pk}|$  as a Function of Time for Rosamond B-747 Flyby 27  
 (from high speed data)

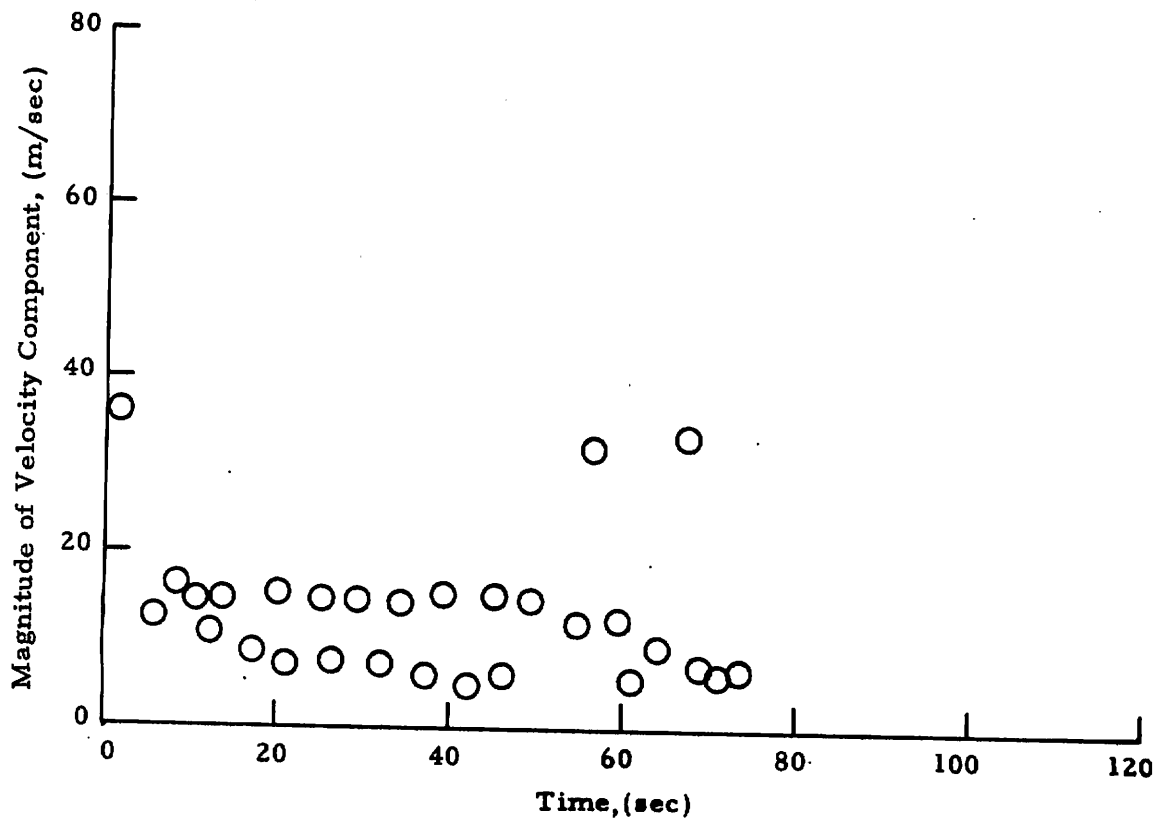


Fig. F-6 -  $|V_{ms}|$  as a Function of Time for Rosamond B-747 Flyby 27  
(from High-Speed Data)

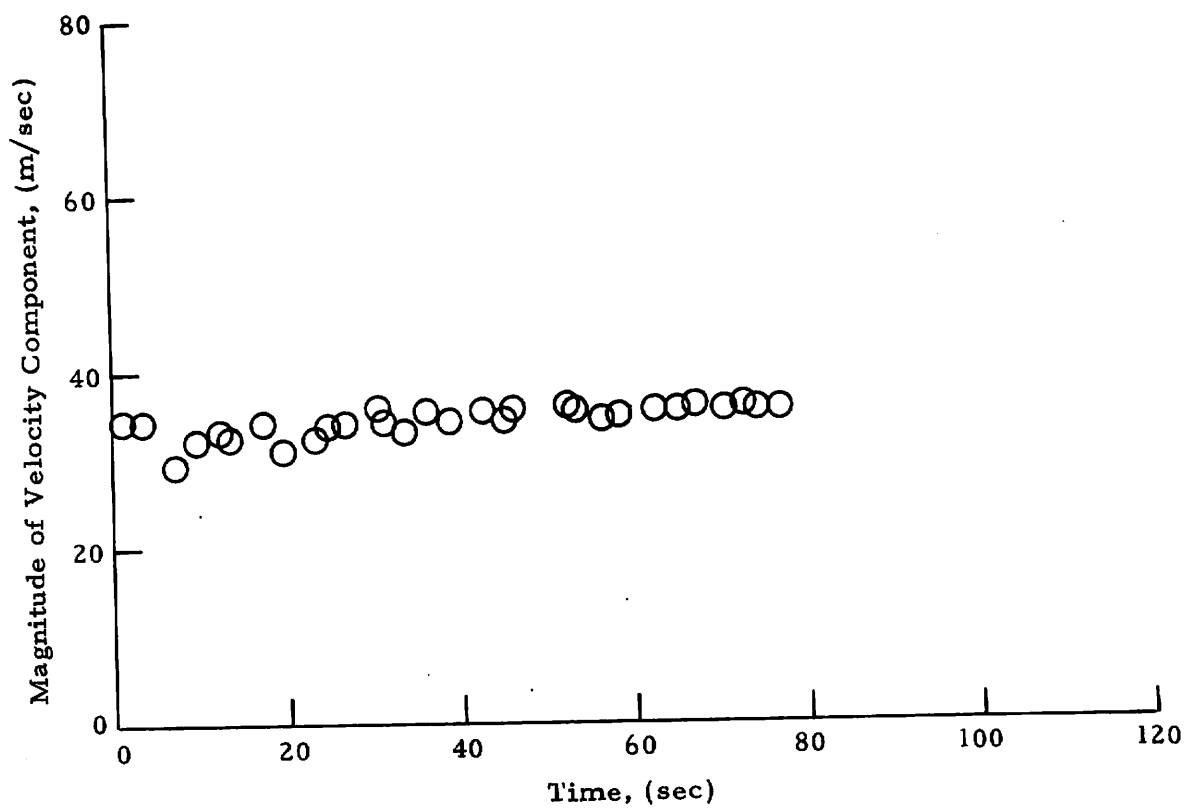


Fig. F-7 -  $|V_{pk}|$  as a Function of Time for Rosamond B-747 Flyby 28  
(from High-Speed Data)

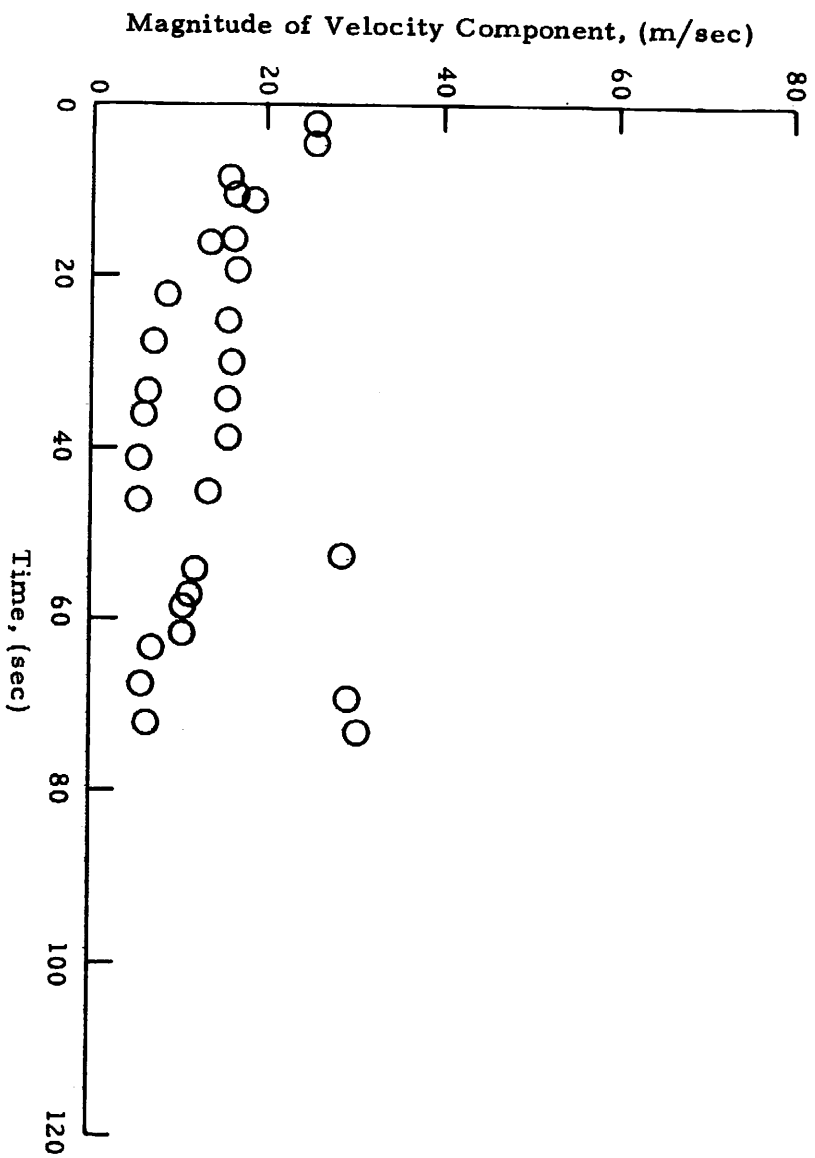


Fig. F-8 -  $|V_{ms}|$  as a Function of Time for Rosamond B-747 F1yby 28  
 (from High-Speed Data)

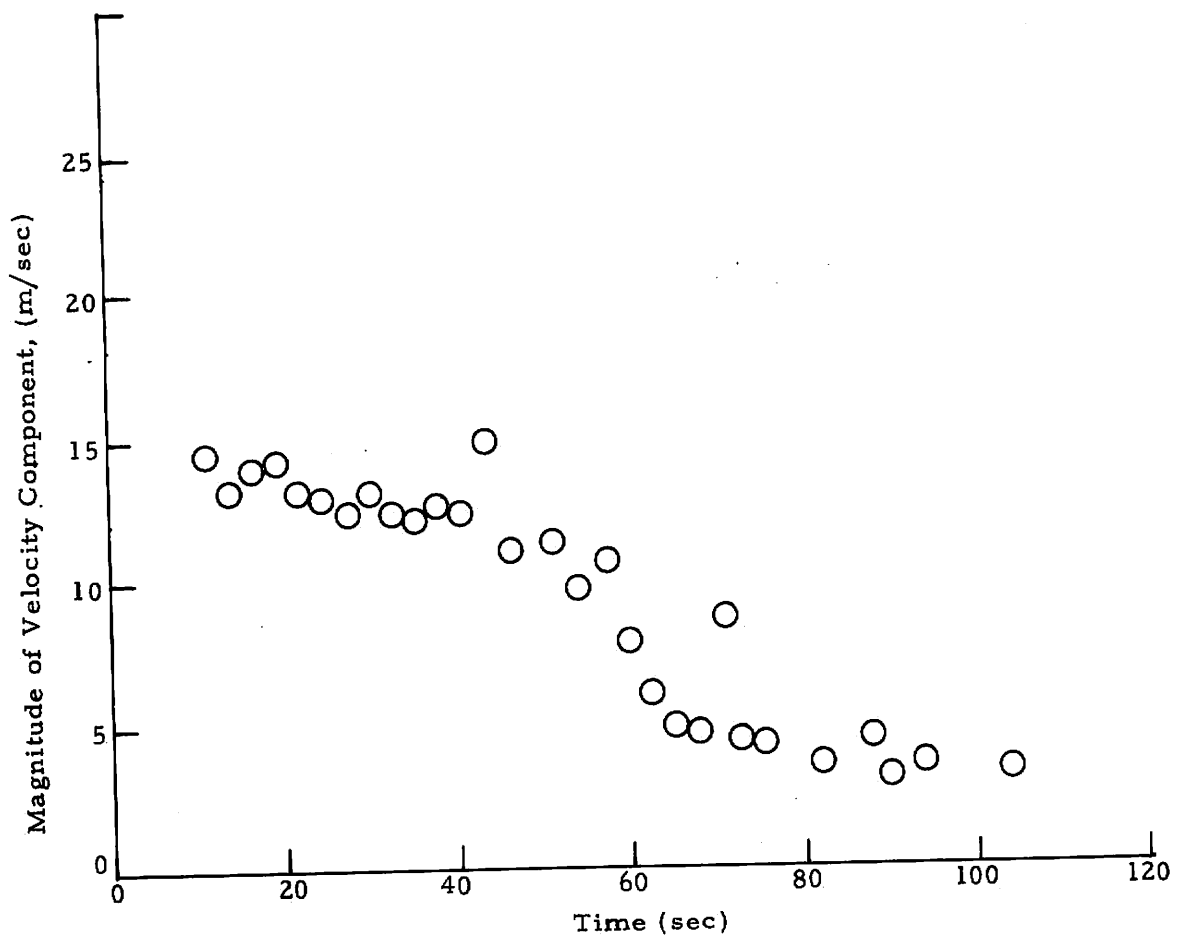


Fig. F-9  $-|V_{ms}|$  as a Function of Time for Rosamond Flyby 29  
(from Low-Speed Data)

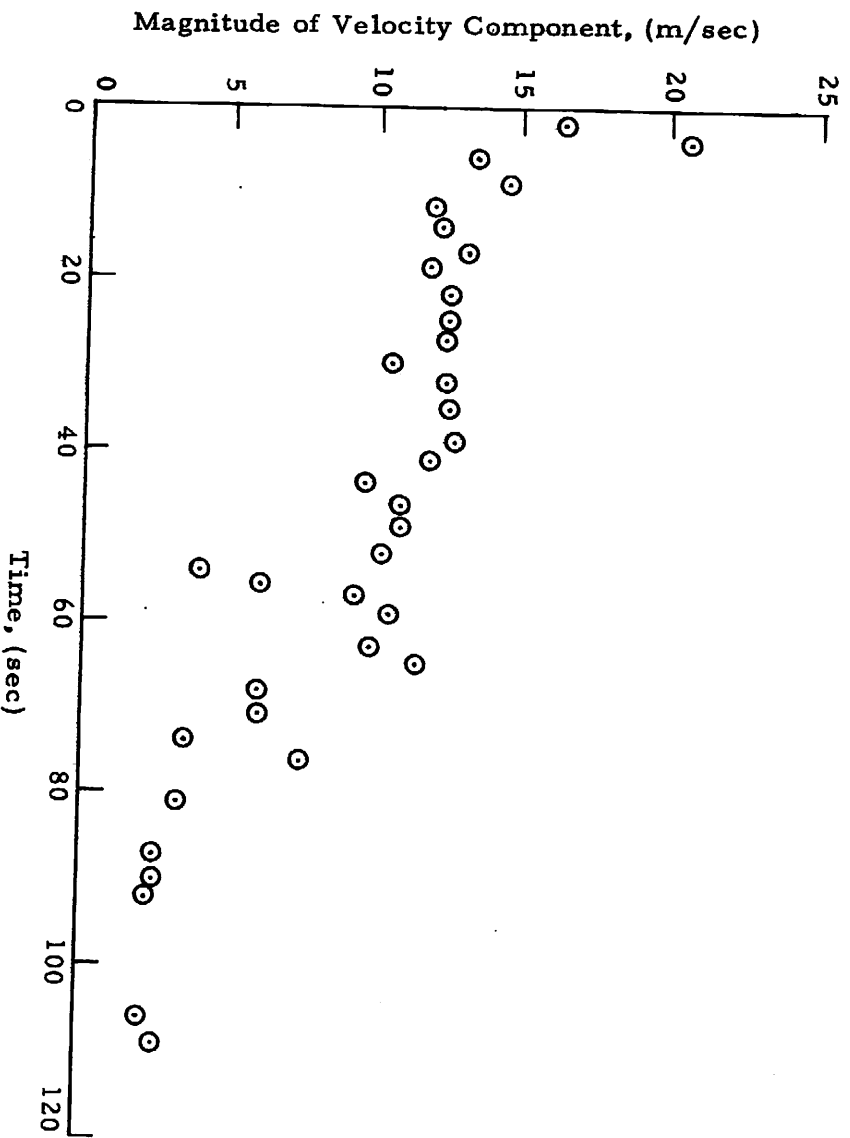


Fig. F-10  $|V|_{ms}$  as a Function of Time for Rosamond B-747 Flyby 30  
 (from Low-Speed Data)

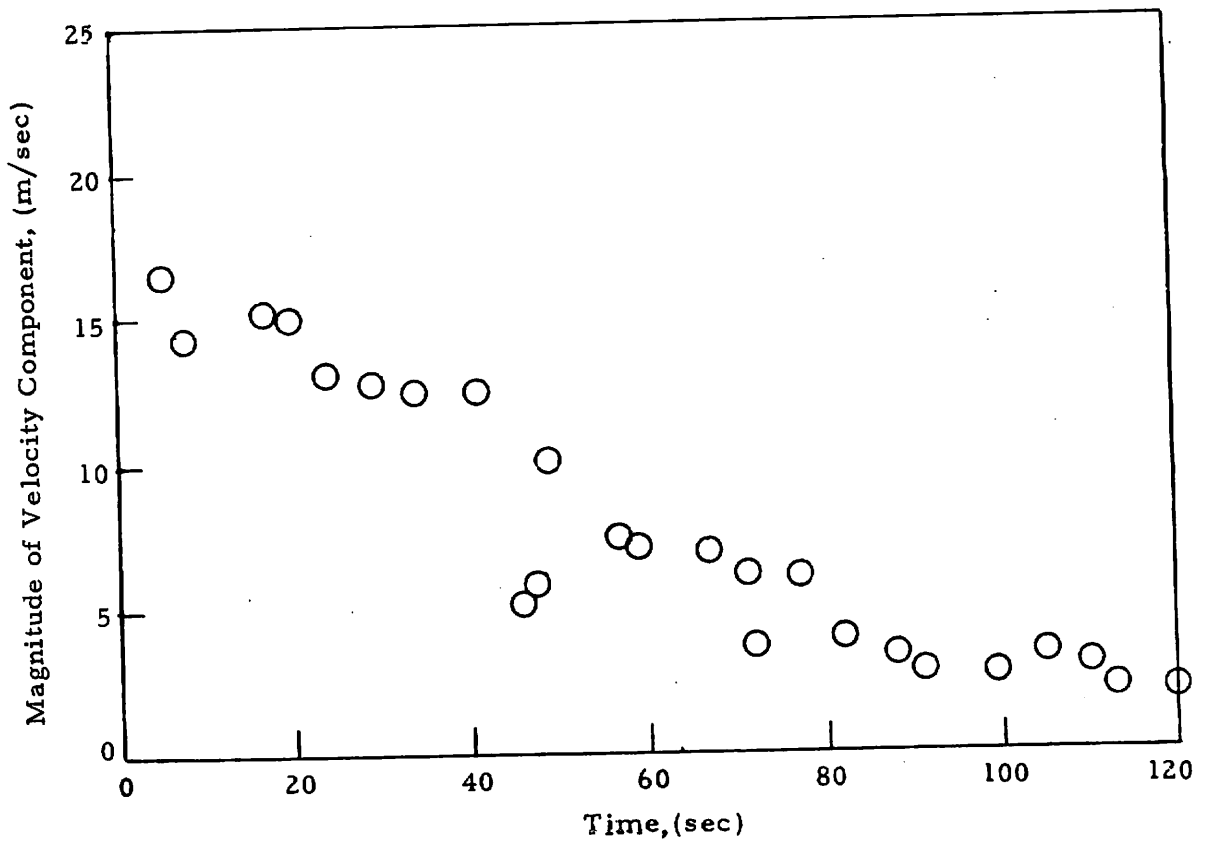


Fig. F-11 -  $|V_{ms}|$  as a Function of Time for Rosamond B-747 Flyby 35  
(from Low-Speed Data)



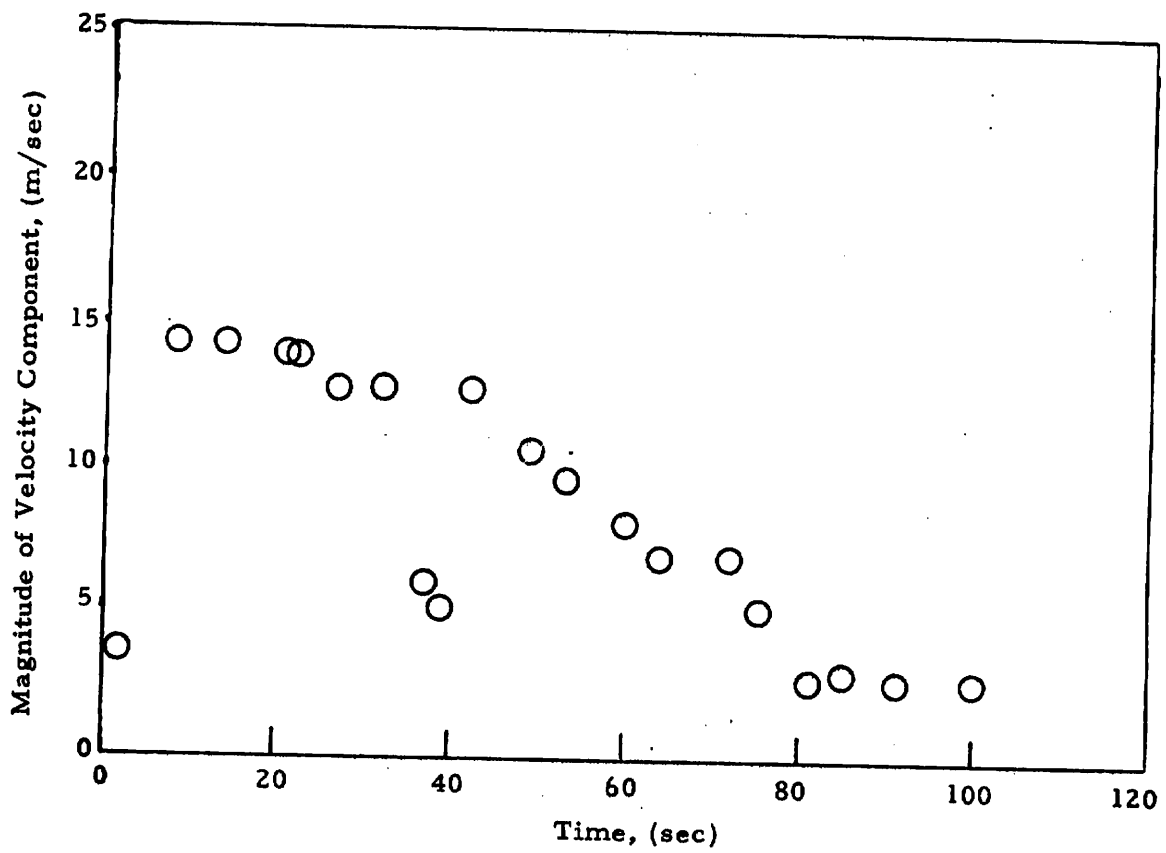


Fig. F-12 -  $|V_{ms}|$  as a Function of Time for Rosamond B-747 Flyby 38  
(from Low-Speed Data)

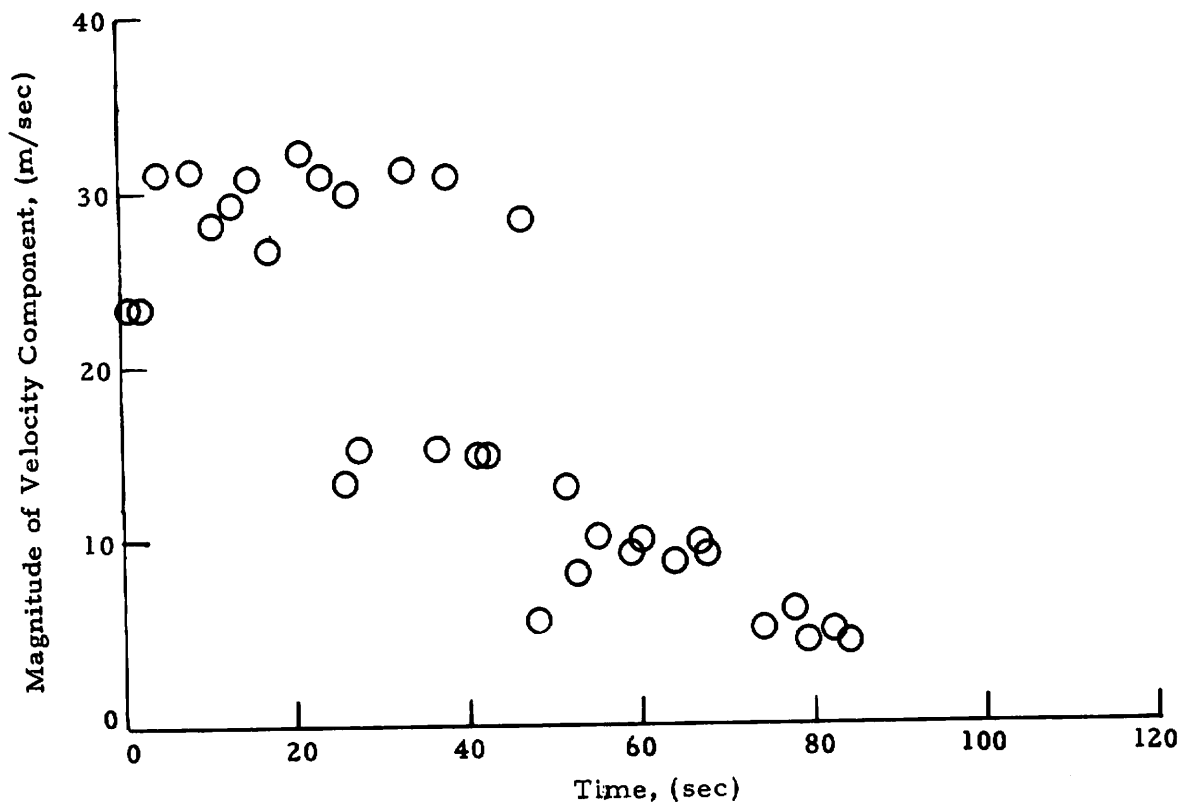


Fig. F-13 -  $|V_{pk}|$  as a Function of Time for Rosamond B-747 Flyby 44  
(from High Speed Data)

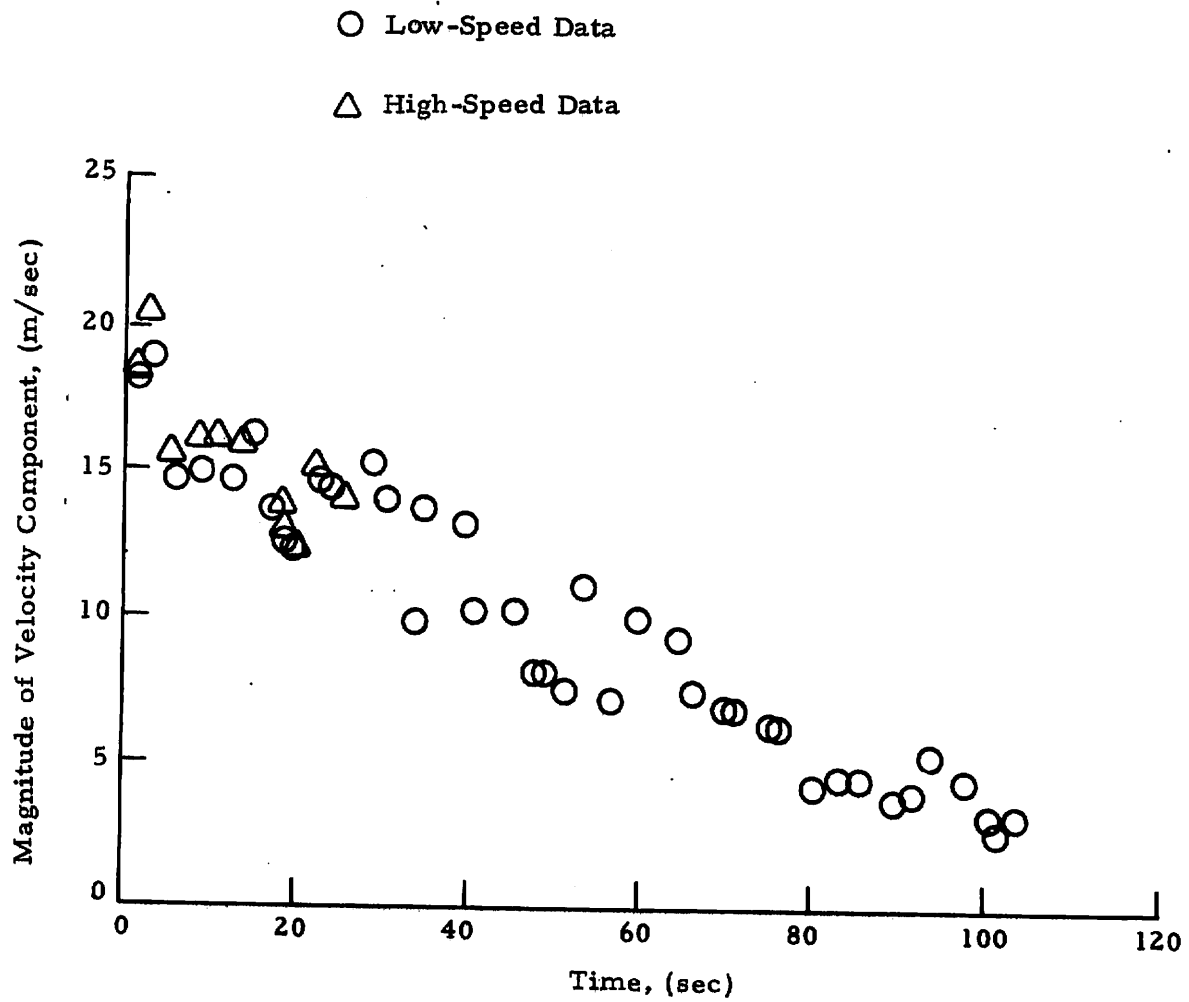


Fig. F-14  $-|V_{ms}|$  as a Function of Time for Rosamond B-747 Flyby 44

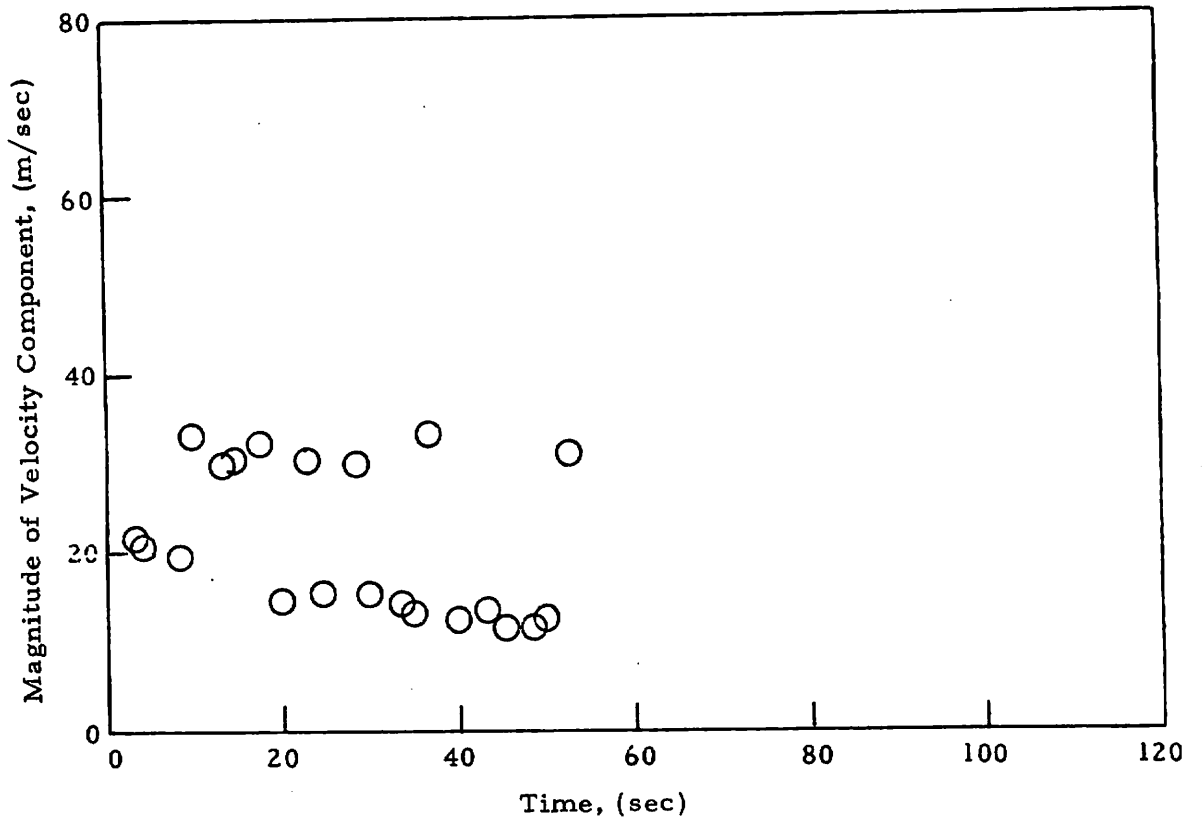


Fig. F-15 -  $|V_{pk}|$  as a Function of Time for Rosamond B-747 Flyby 47  
 (from High-Speed Data)

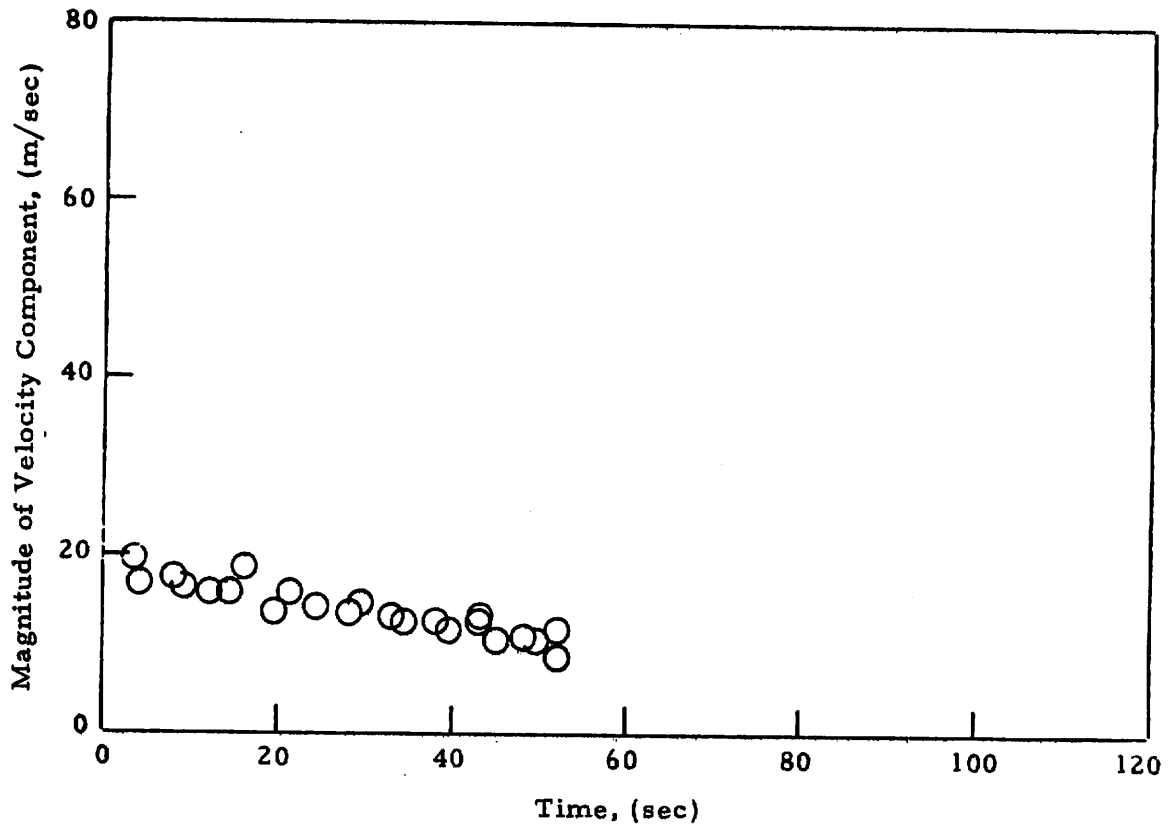


Fig. F-16 -  $|V_{ms}|$  as a Function of Time for Rosamond B-747 Flyby 47  
 (from High-Speed Data)

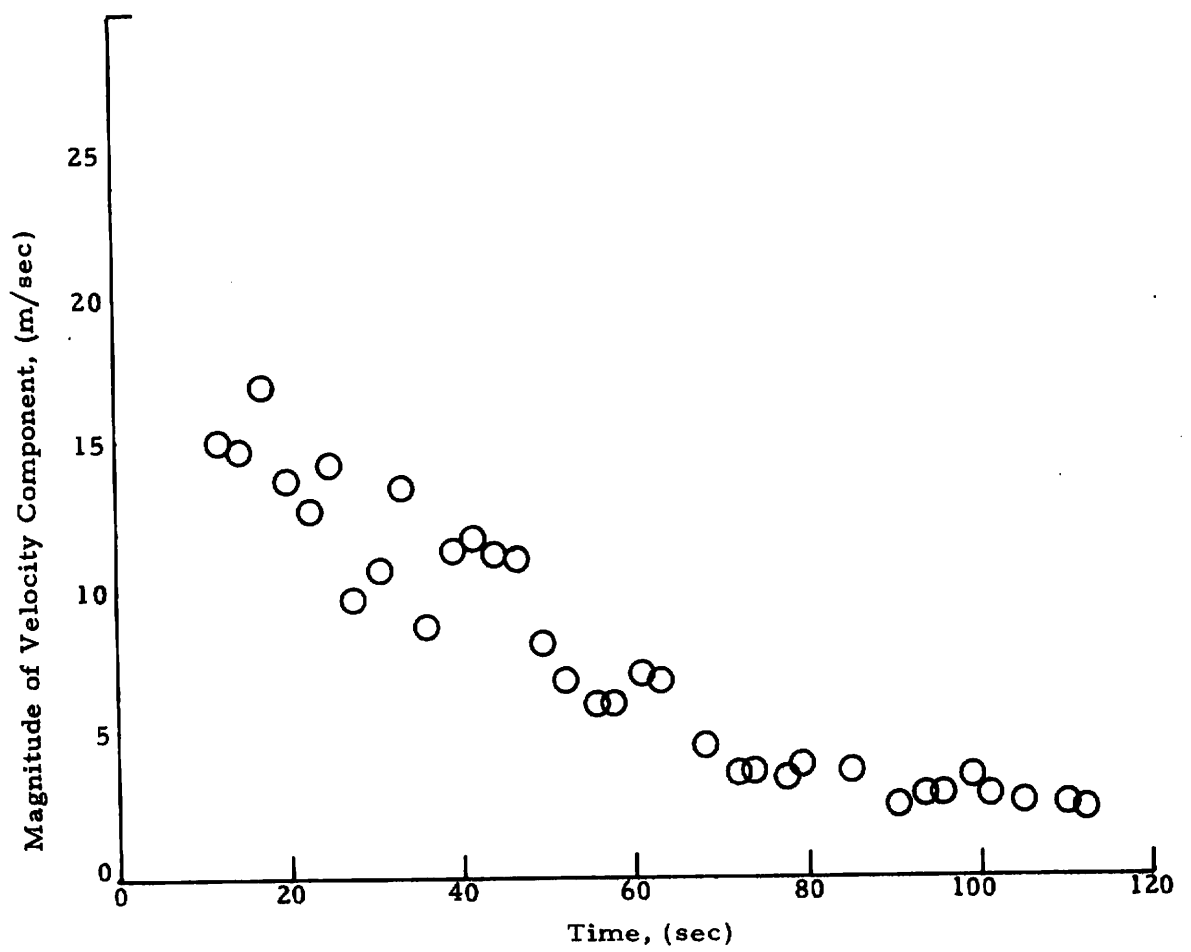


Fig. F-17 -  $|V_{ms}|$  as a Function of Time for Rosamond B-747 Flyby 47  
(from Low-Speed Data)

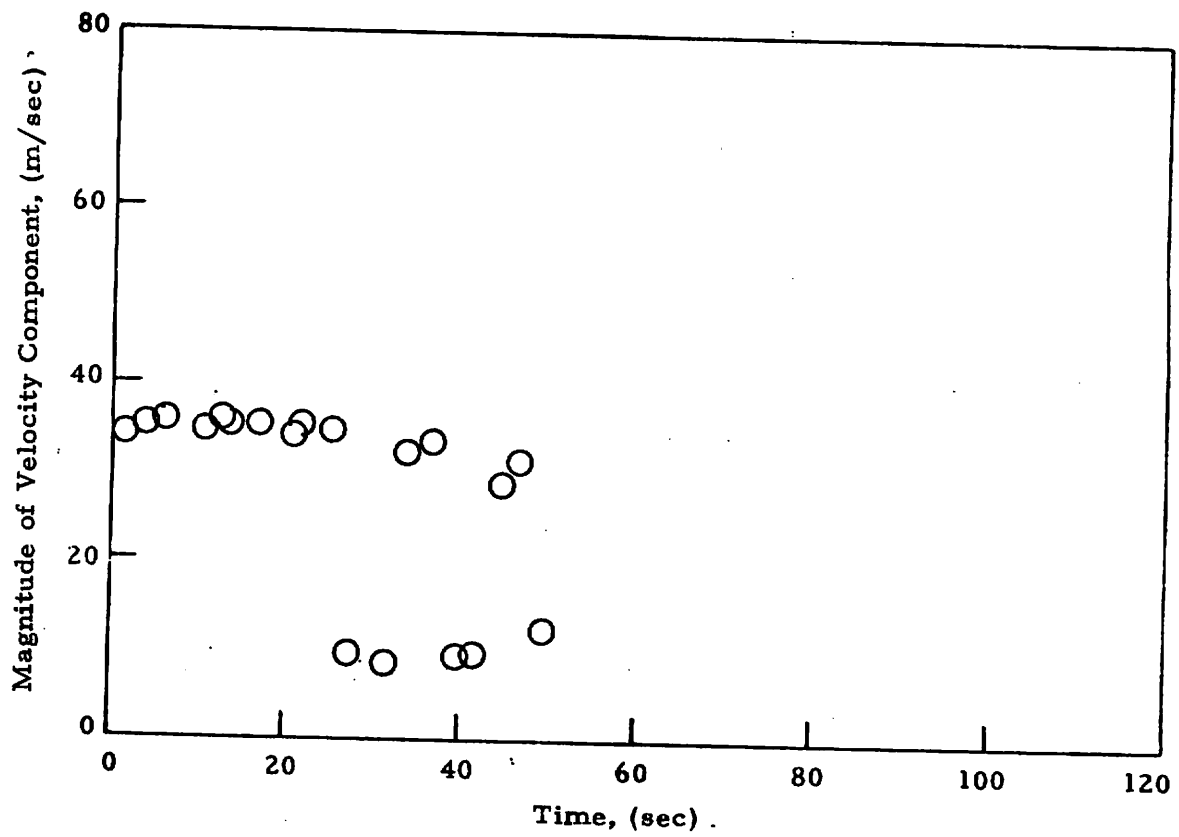


Fig. F-18 -  $|V_{pk}|$  as a Function of Time for Rosamond B-747 Flyby 48  
 (from High-Speed Data)

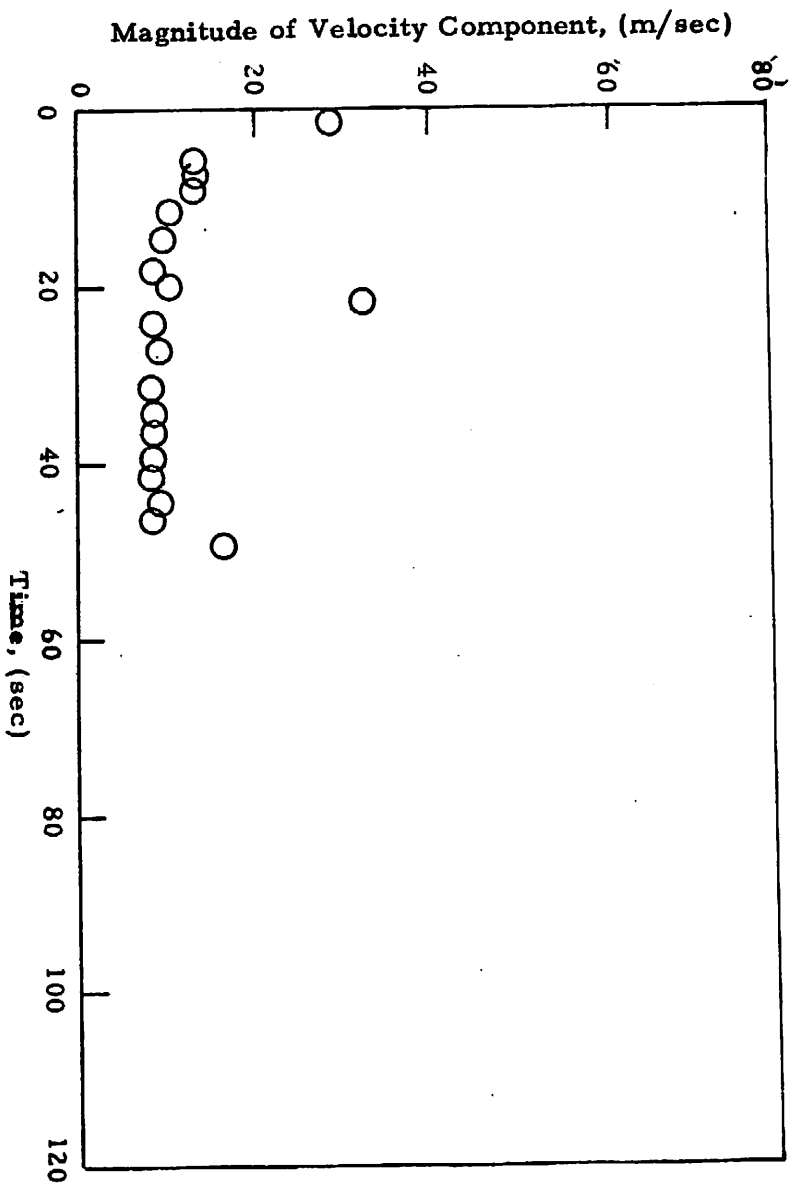


Fig. F-19 -  $|V_{ms}|$  as a Function of Time for Rosamond B-747 F1yby 48  
 (from High-Speed Data)



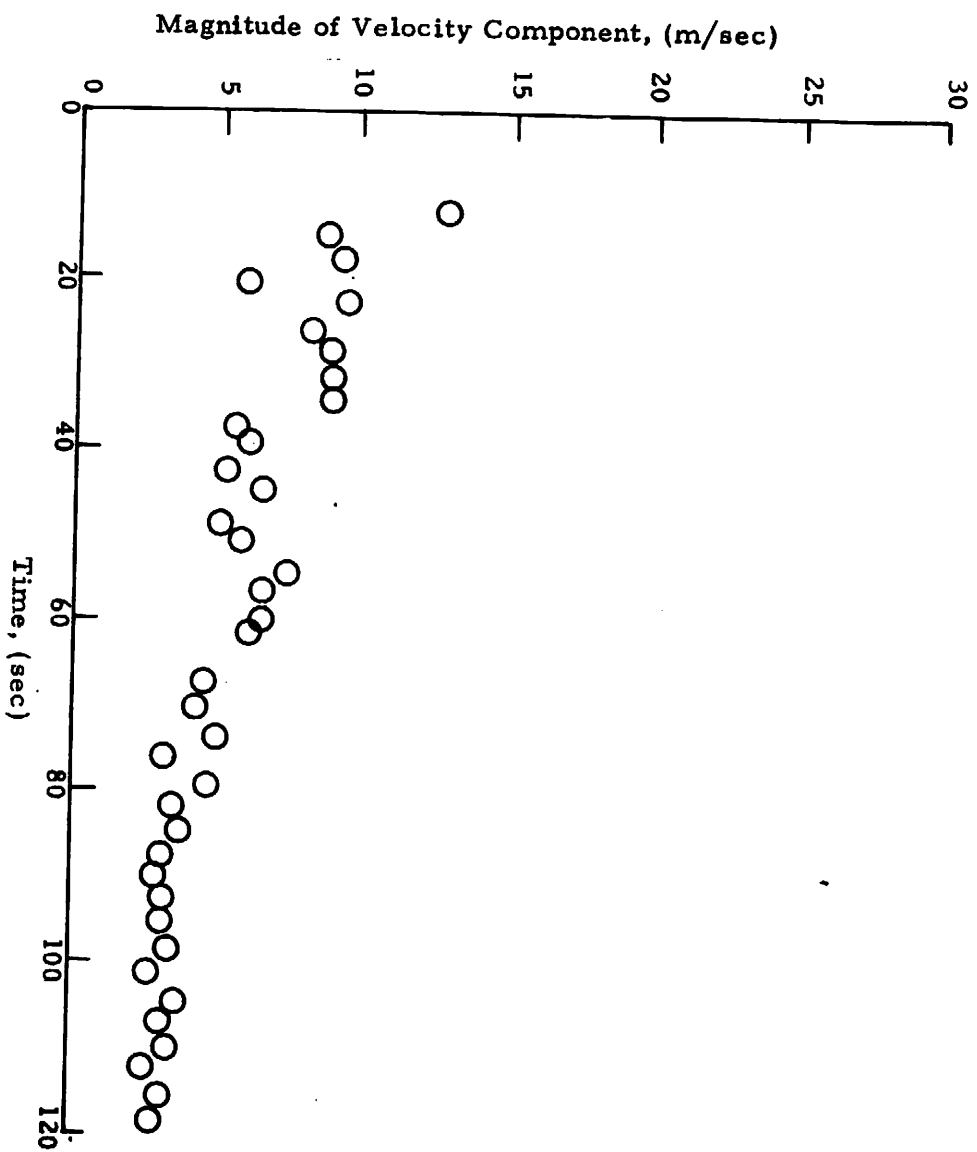


Fig. F-20- $|V_{ms}|$  as a Function of Time for Rosamond B-747 Flyby 48  
 (from Low-Speed Data)

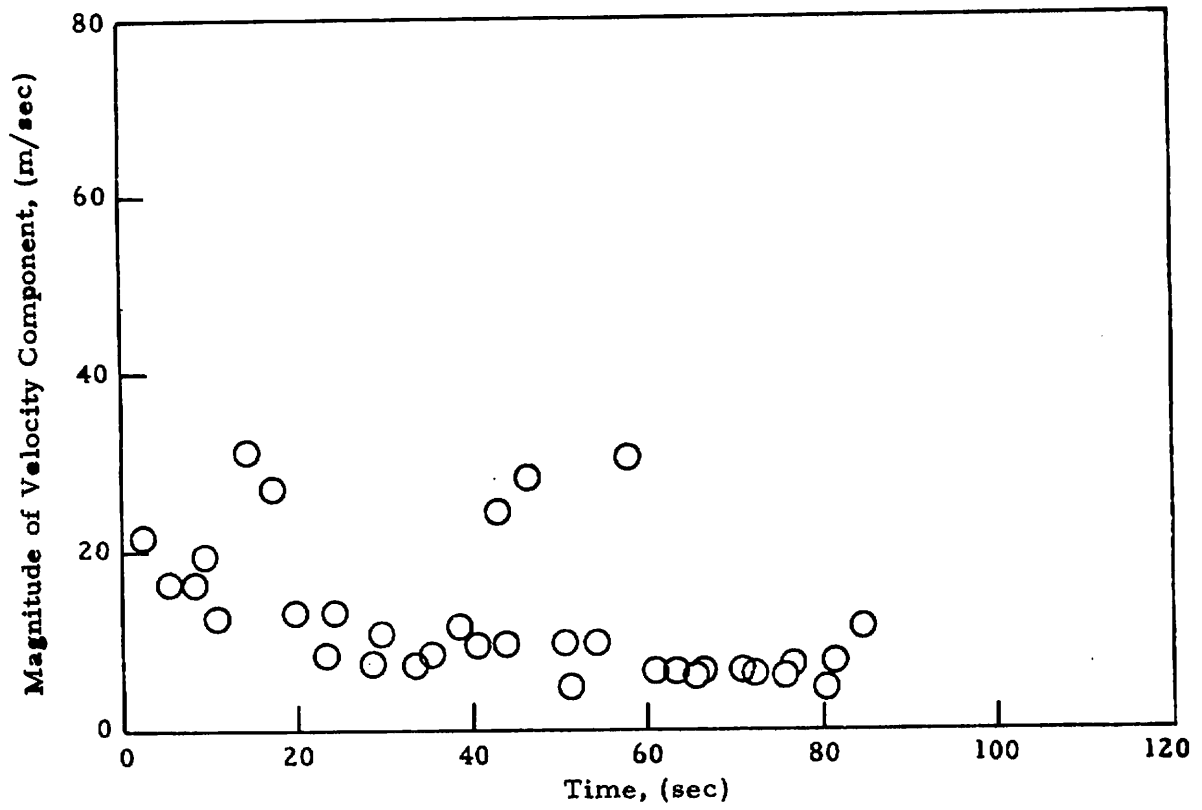


Fig. F-21 -  $|V_{pk}|$  as a Function of Time for Rosamond B-747 Flyby 49  
(from High-Speed Data)

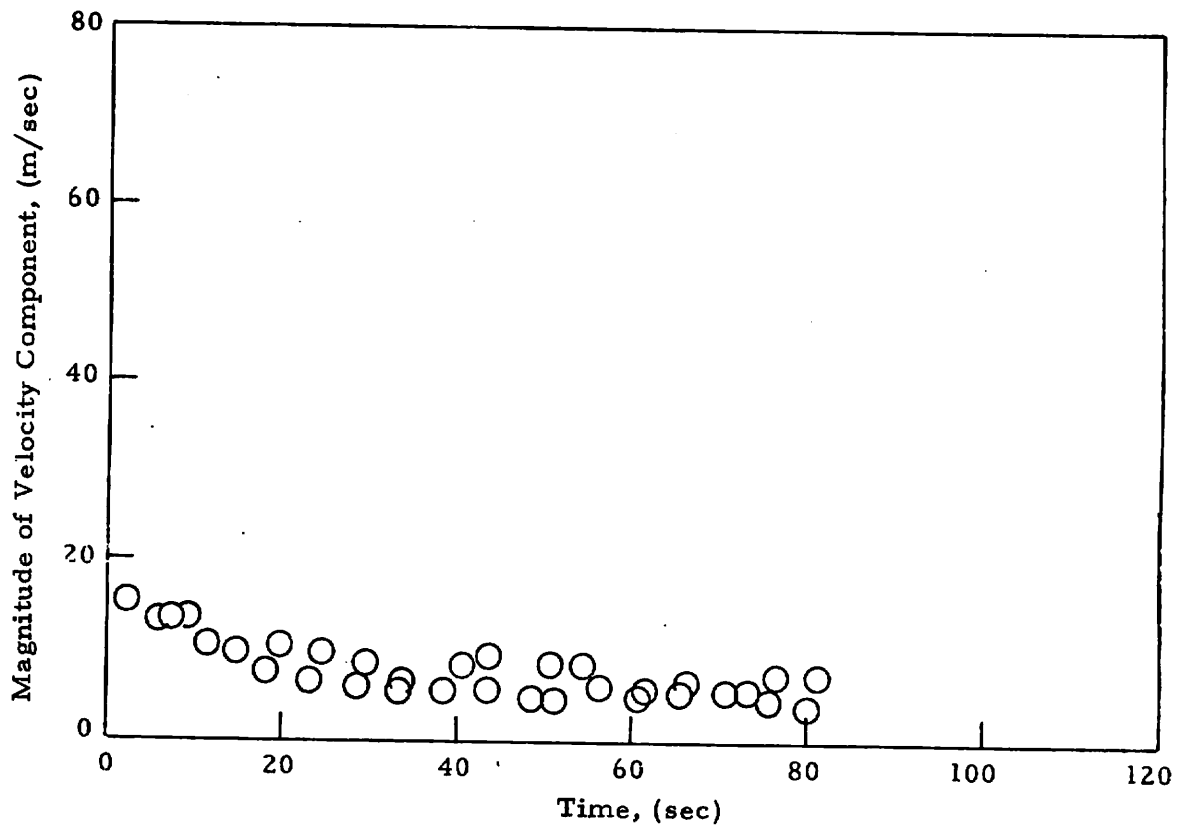


Fig. F-22  $-|V_{ms}|$  as a Function of Time for Rosamond B-747 Flyby 49  
 (from High-Speed Data)

Appendix G  
TIME HISTORY OF VORTEX  
CIRCULATION

○ Port  
△ Starboard

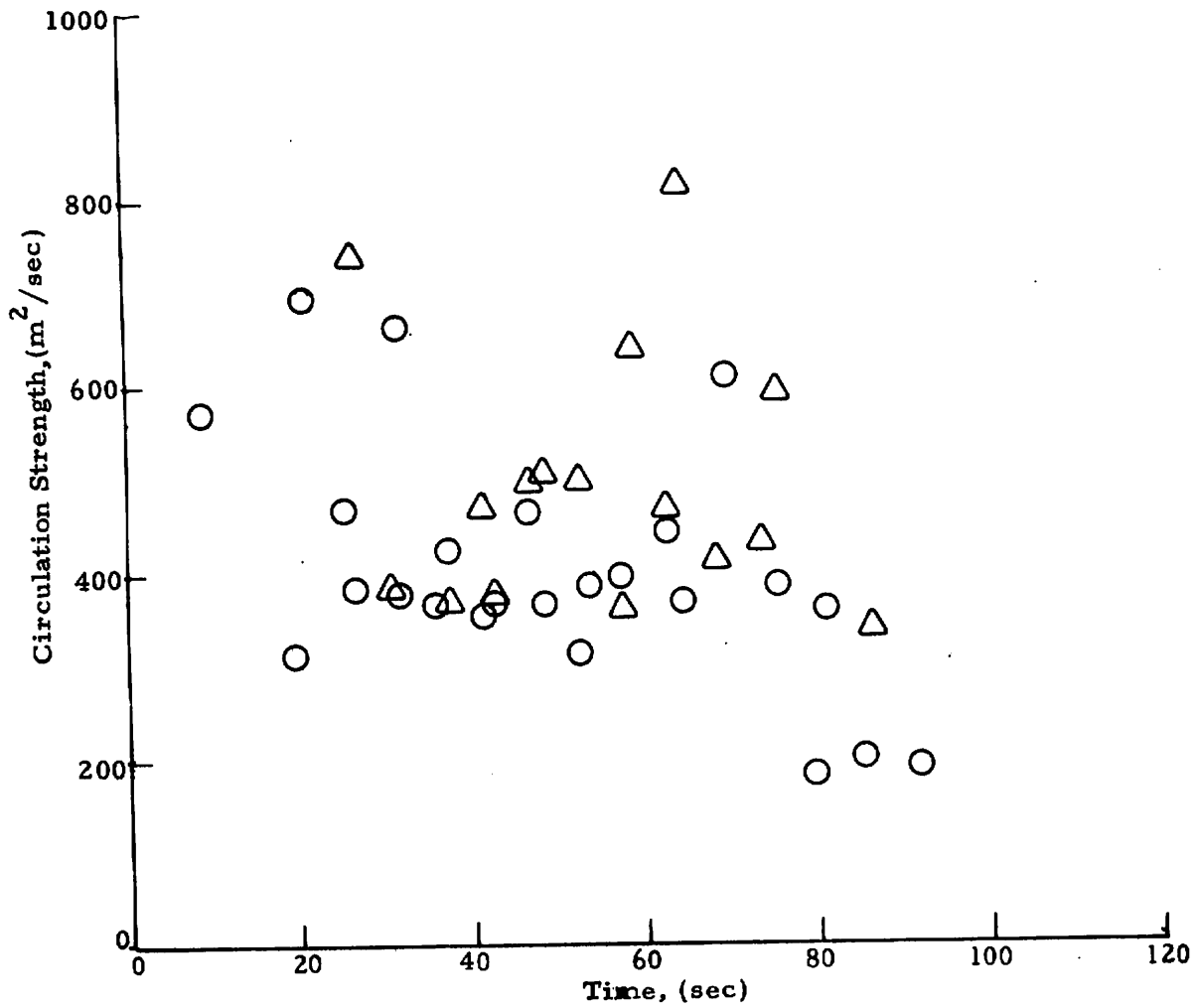


Fig. G-1 - Observed Circulation Time History for Rosamond B-747 Flyby 24

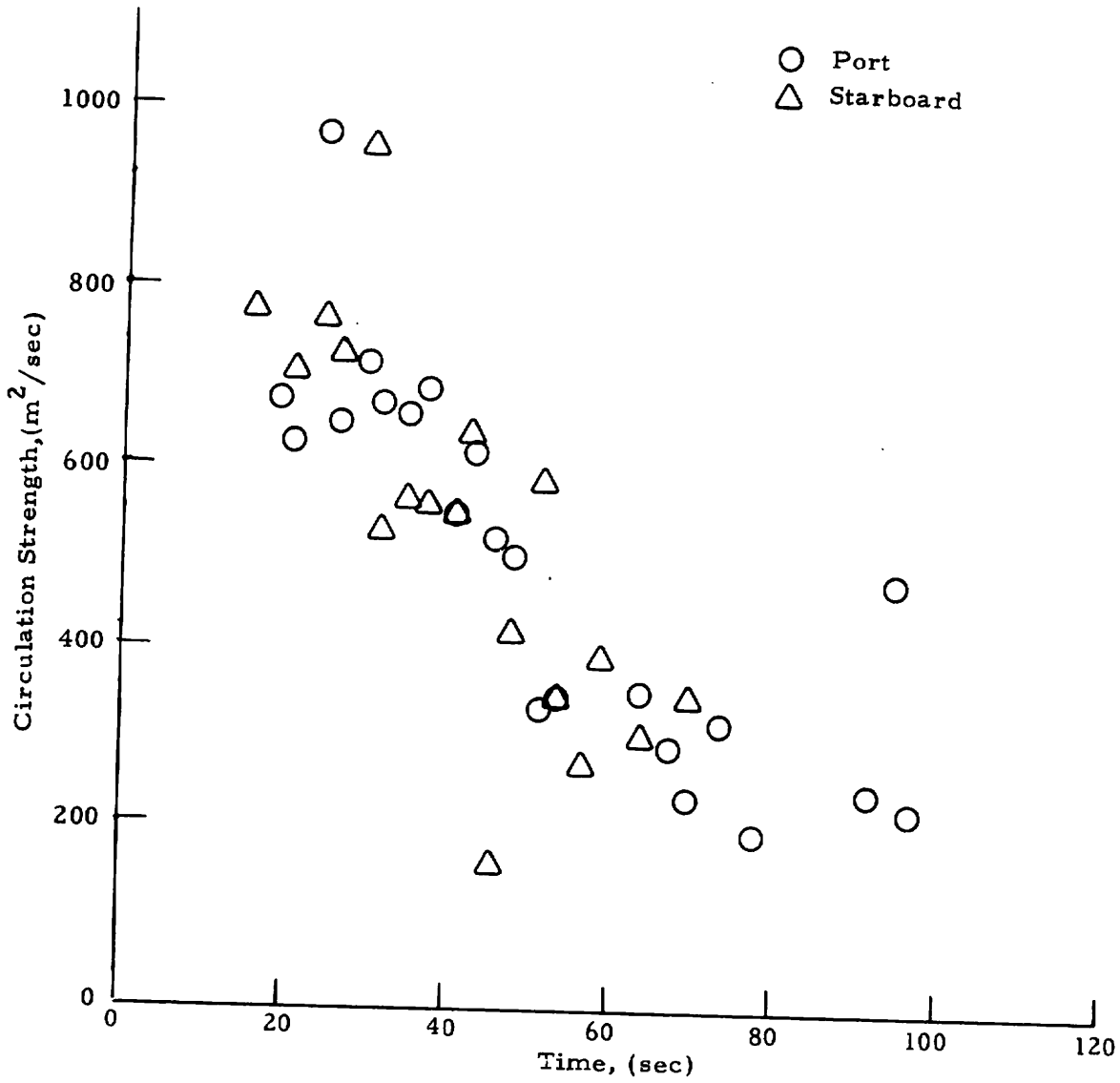


Fig.G-2 - Observed Circulation Time History for Rosamond B-747 Flyby 25

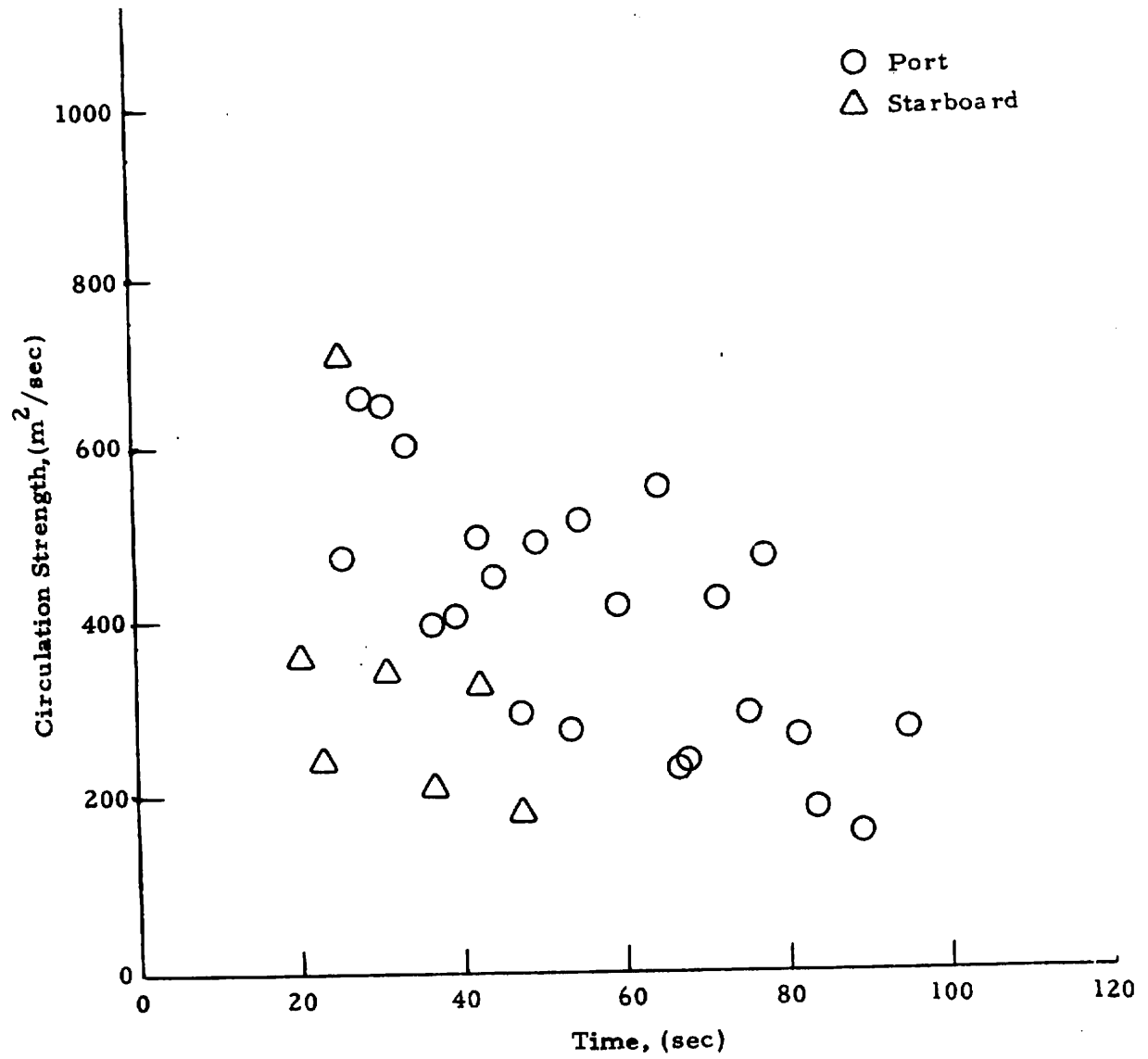


Fig.G-3 - Observed Circulation Time History for Rosamond B-747 Flyby 27

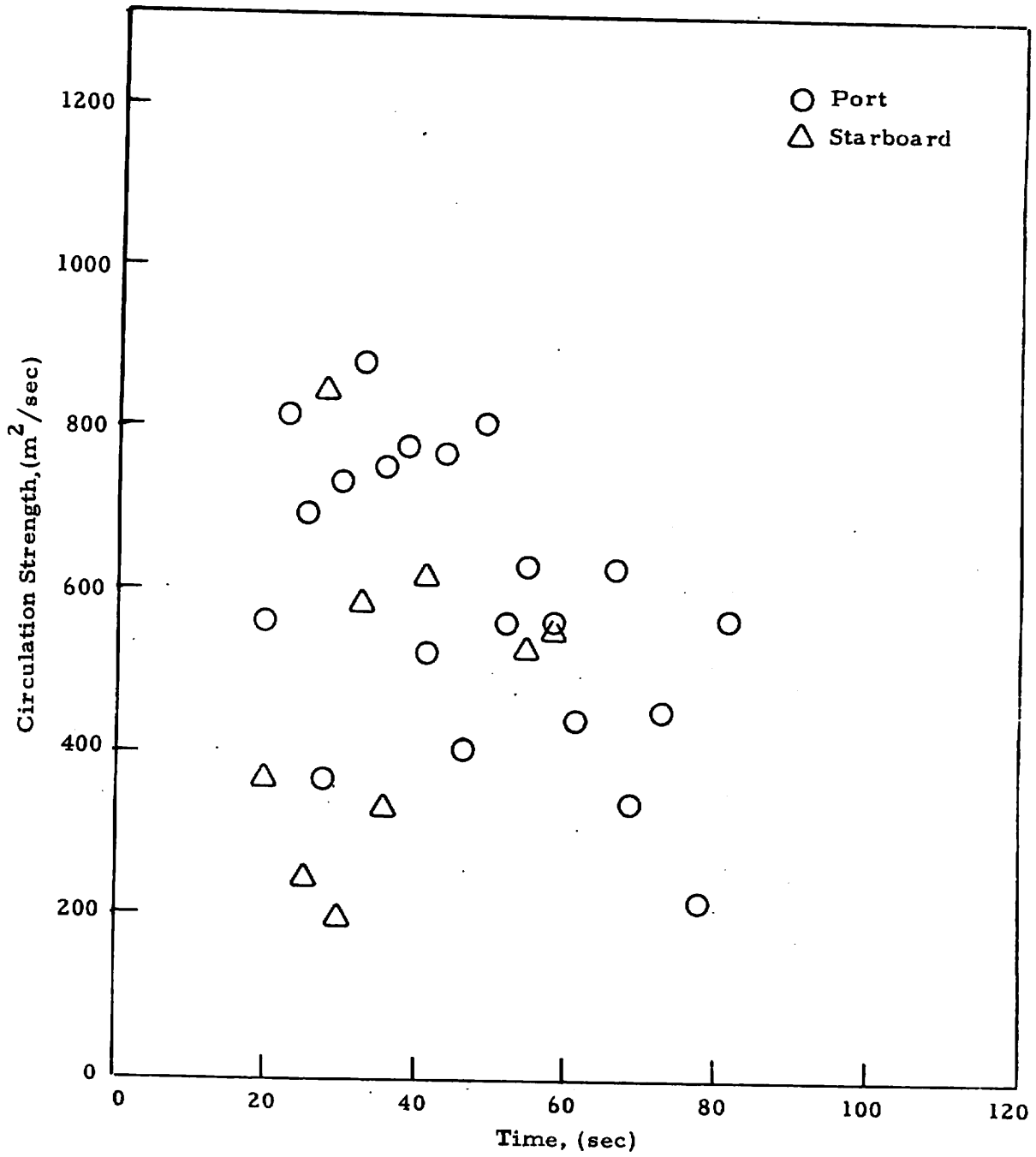


Fig. G-4 - Observed Circulation Time History for Rosamond B-747 Flyby 28

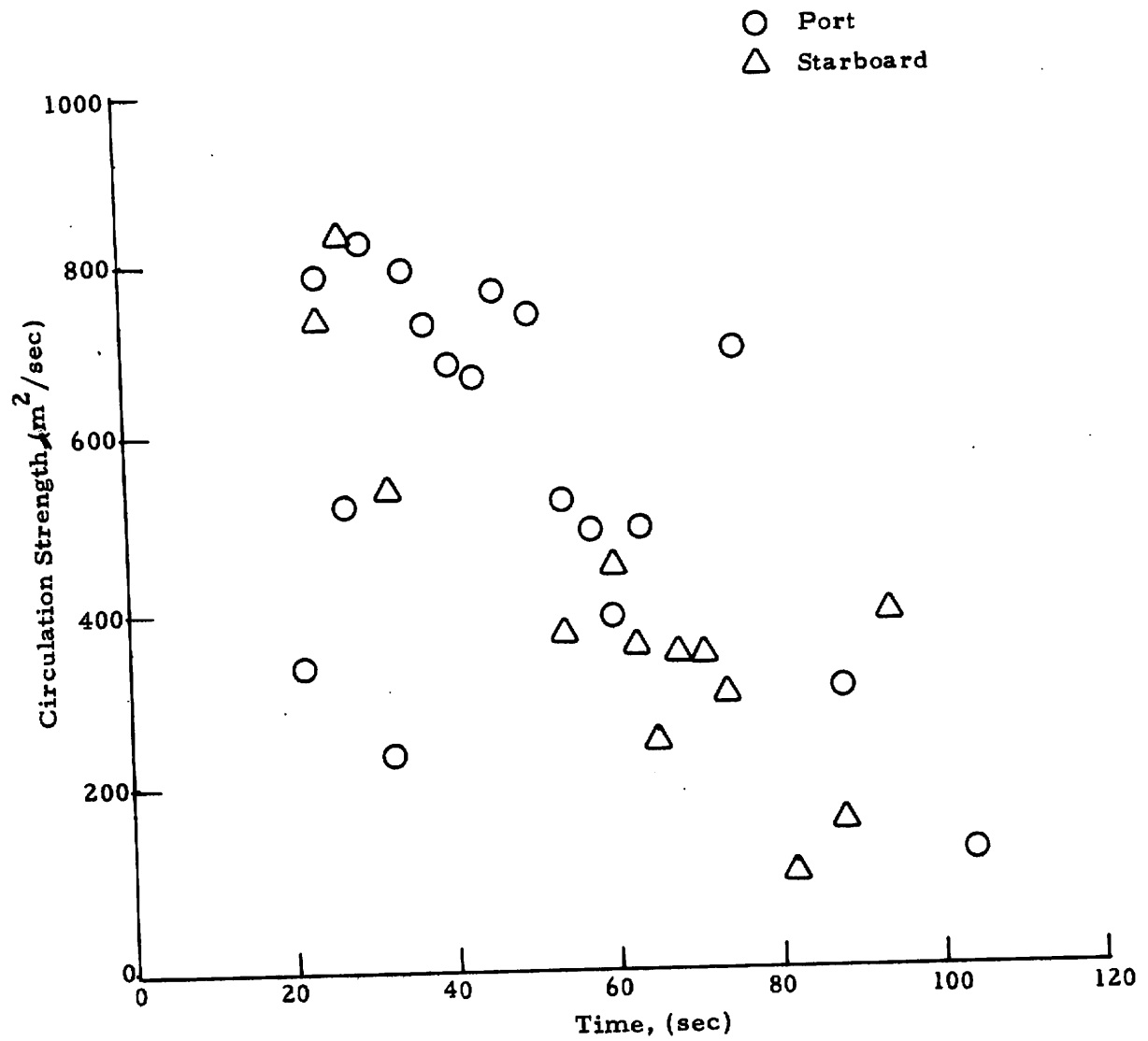


Fig. G-5 - Observed Circulation Time History for Rosamond B-747 Flyby 29



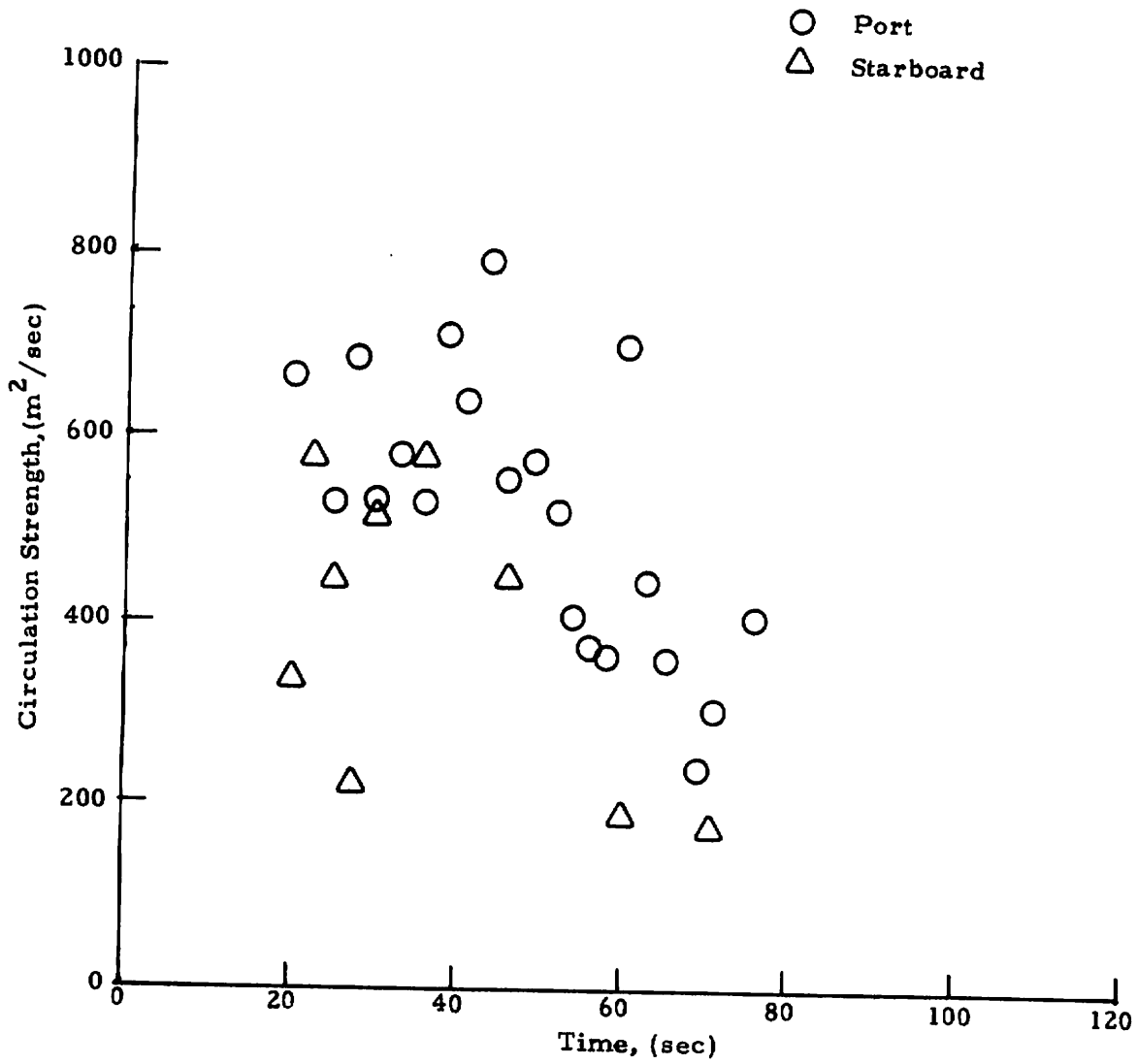


Fig. G-6 - Observed Circulation Time History for Rosamond B-747 Flyby 30

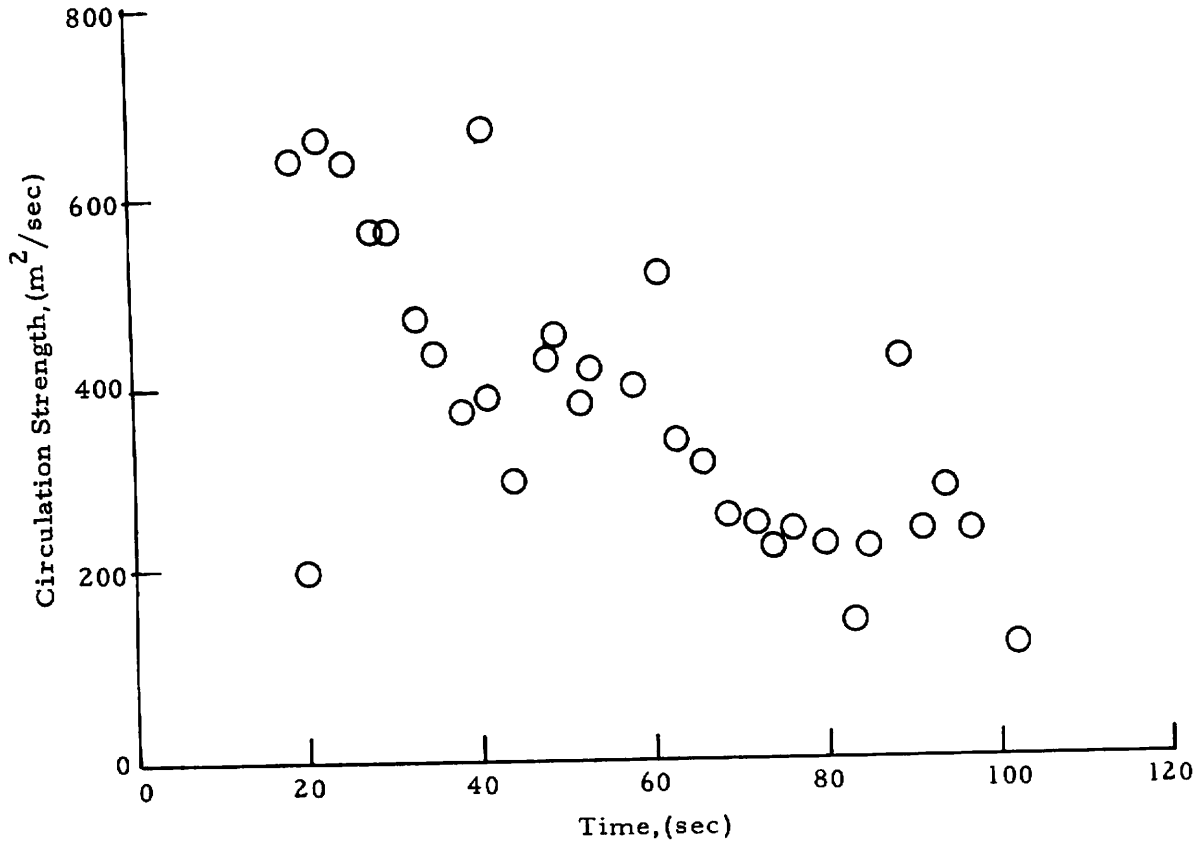


Fig. G-7 - Observed Circulation Time History for Rosamond B-747  
Flyby 44, Starboard Vortex

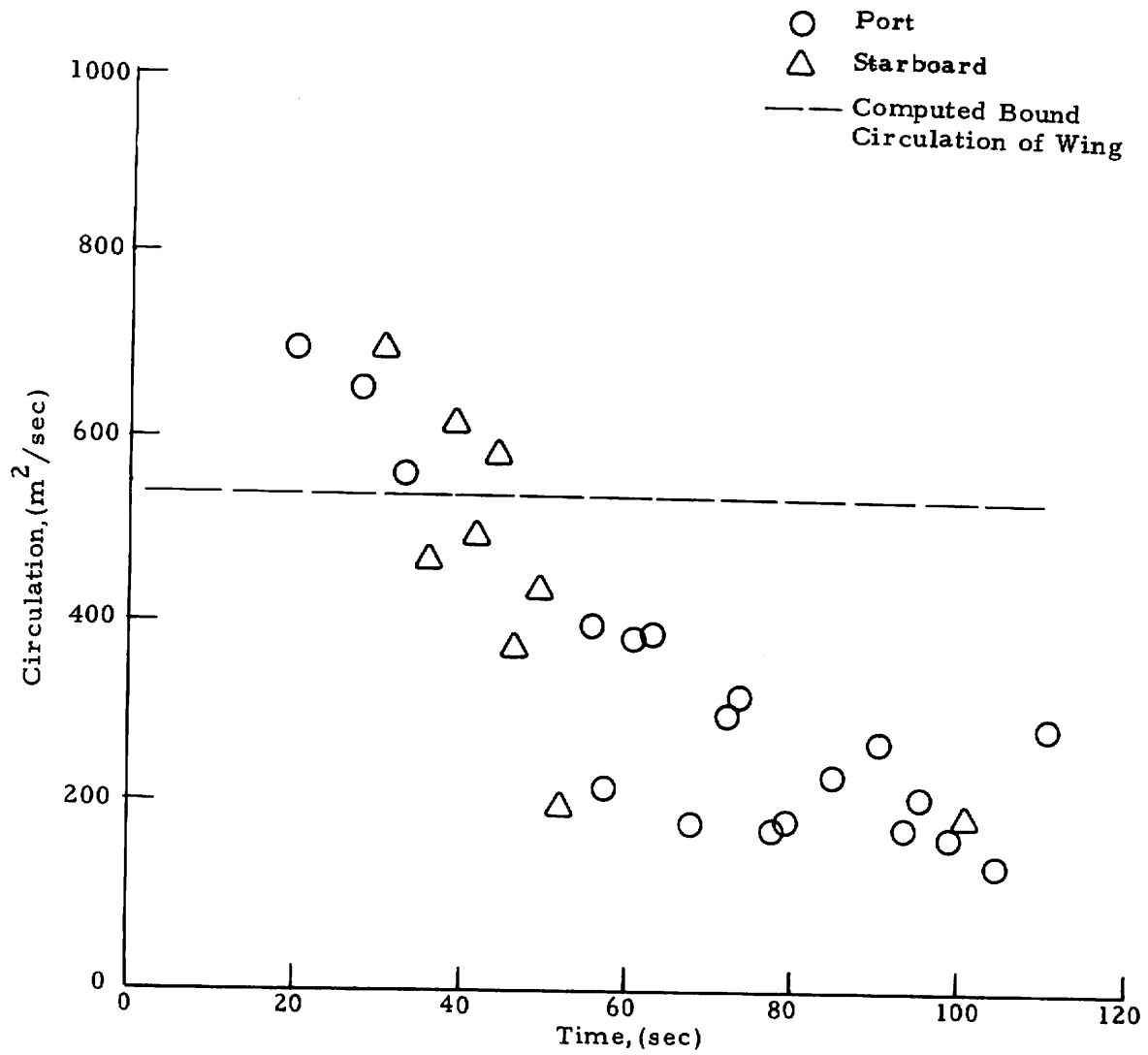


Fig.G-8 - Observed Circulation Time History for Rosamond B-747 Flyby 47

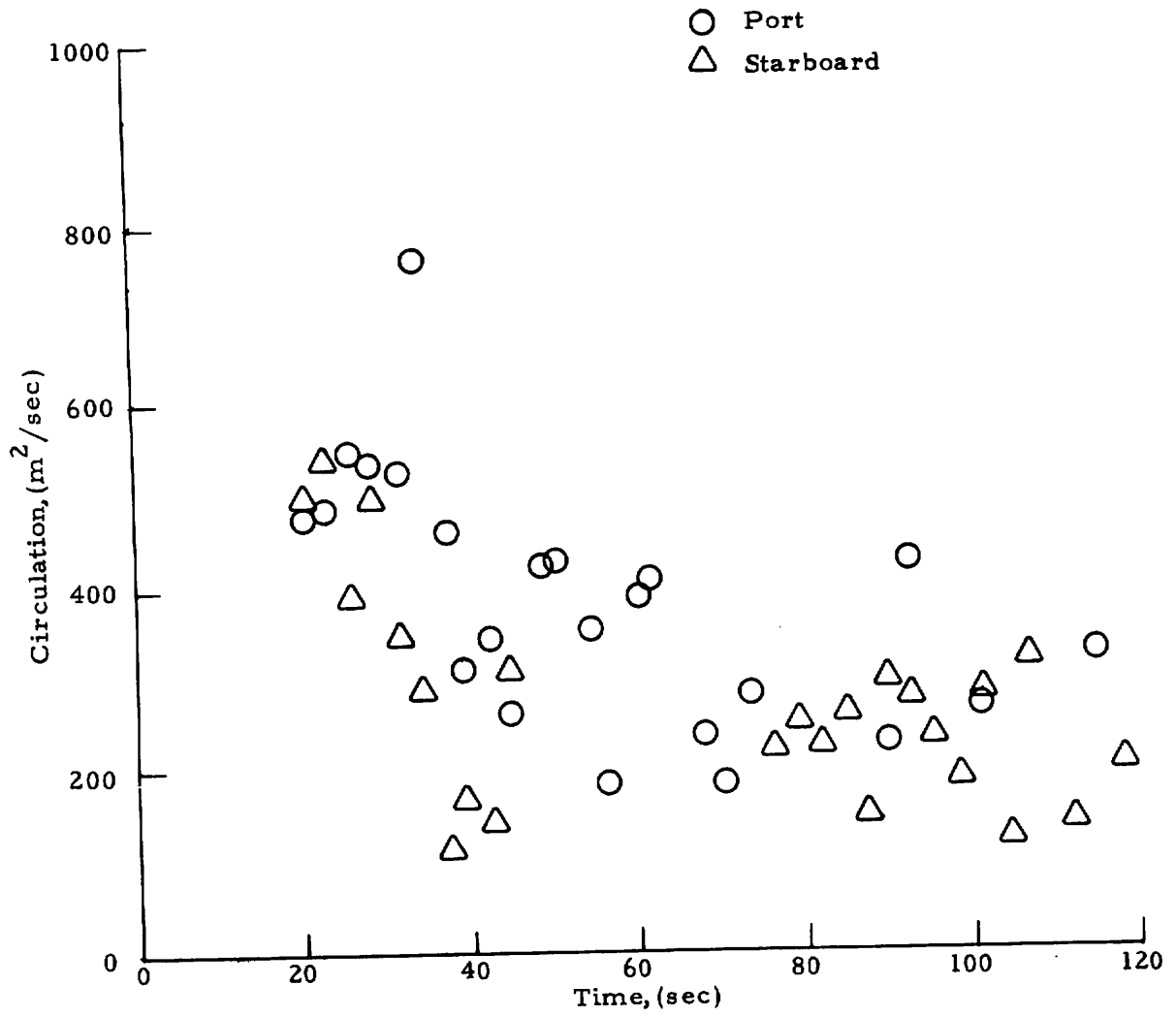


Fig.G-9 - Observed Circulation Time History for Rosamond B-747 Flyby 48

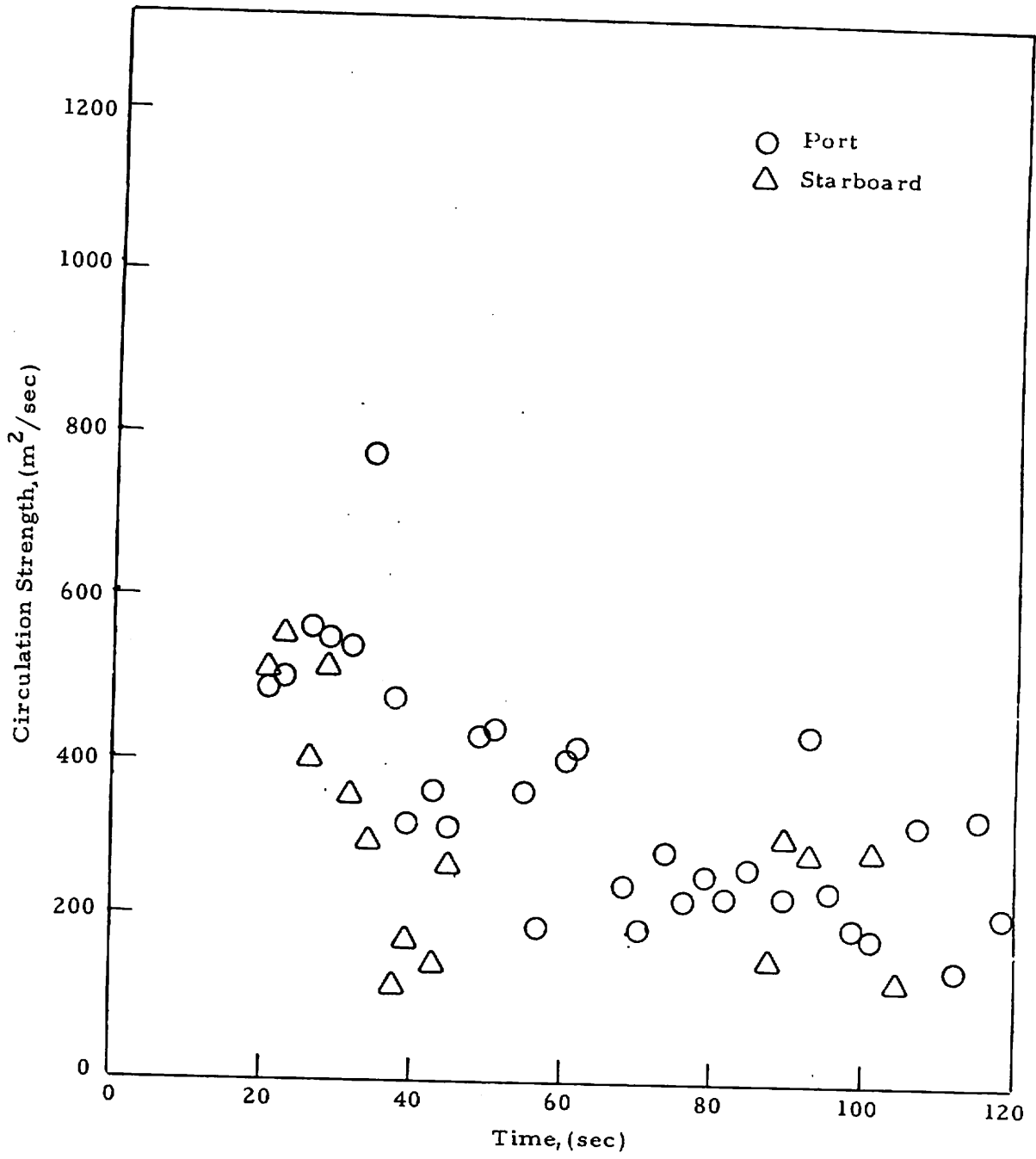


Fig. G-10 - Observed Circulation Time History for Rosamond B-747 Flyby 49

Appendix H  
REPORT OF INVENTIONS

In accordance with the objectives of the contract, wake vortex and wind measurements were carried out at the Rosamond, California, test site with a scanning laser Doppler velocimeter system, and the LDV measurements were processed, reduced, and analyzed. The contract objectives were met, and no invention, discovery, or innovation was found.

\*U.S. GOVERNMENT PRINTING OFFICE: 1977-701-663/179